2024

VOLCANIC DEBRIS AVALANCHE PROPAGATION AND EMPLACEMENT MECHANISMS: SEDIMENTOLOGICAL FIELD EVIDENCE AND BIDISPERSE GRANULAR FLOW EXPERIMENTS

Makris, Symeon

UNIVERSITY OF
PLYMOUTH

VOLCANIC DEBRIS AVALANCHE PROPAGATION AND EMPLACEMENT MECHANISMS: SEDIMENTOLOGICAL FIELD EVIDENCE AND BIDISPERSE GRANULAR FLOW EXPERIMENTS

by

Symeon Makris

A thesis submitted to the University of Plymouth
in partial fulfilment for the degree of

DOCTOR OF PHILOSOPHY

School of Geography, Earth and Environmental Sciences

December 1, 2023

Acknowledgements

Before considering the academic aspect, I would like to thank my parents and sister: George Makris, Maria Makri and Christina Makri. Without their financial and emotional support, guidance and encouragement I would not have been in the position to even start a PhD, or successfully carry out this challenging work. My privilege is a direct result of the sacrifices my parents have made. They have motivated me throughout my studies, joined me in the field, and maybe even became interested in my research. Living and working with them during the COVID-19 pandemic made a challenging time undeniably enjoyable. The confidence of having a home unconditionally waiting for me to go back to and find a family has allowed me to focus on my studies and research. It's a privilege that I appreciate and not everyone is lucky to have. I would also like to express my heartfelt appreciation to my partner, Dr Chrystala Fakonti, for her support and understanding throughout my PhD journey. Her encouragement, patience, and constant belief in me have been invaluable. I am truly grateful.

This research is the product of over four years of research that would not have been possible without the contribution and support of an academic team. Firstly, I would like to express my utmost gratitude to my supervisory team for their invaluable support and guidance: Dr Irene Manzella, Dr Matteo Roverato and Dr Paul Cole. Above their academic contribution, their motivation, encouragement and inspiration have made this project possible. Paul's experience and expertise in volcanic processes were vital to the research. His guidance in planning fieldwork and discussion and analysis of findings was invaluable, as well as his supervisory support. Matteo joined the team later after being a collaborator and generously contributing data and knowledge. Since the project examined volcanic debris avalanches, Matteo's expertise would have been impossible to replace. I am grateful for his readiness to support me and the project. The fieldwork we carried out in the Canary Islands was an academic privilege for me, and I thoroughly enjoyed the exposure hunting and discussions we had. Irene's support and encouragement since the first day I started working on this project made me confident in the work and welcome in the department. Without Irene's advice, constant support and encouragement, especially during the pandemic, the project would not have been possible. Her encouragement to create a research network, publish research outcomes, and attend stimulating conferences were essential not only to the project but also to my development as a researcher. I am grateful to Irene, Matteo and Paul and content to have had the fortune to work with them. I would also like to express my gratitude to the collaborators that contributed to the project: Prof. Pablo Dávila Harris, Prof. Alejandro Lomoschitz Mora-Figueroa and Dr Alessandro Sgarabotto. Facilitating this project to build on their previous work and generously contributing their expertise made the project much more effective. Meeting and working with them has been a pleasure. I hope that we will continue to enjoy working together in the future on interesting and exciting projects. I am also grateful to the University of Plymouth for funding this project through a University of Plymouth Studentship (URS).

My experience at the School of Geography, Earth and Environmental Sciences would not

have been the same without Alessandro Sgarabotto and Josh Jones. Discussing research and learning from each other was a fundamental and enjoyable part of my PhD. Discussing research and climbing with Alessandro and the hiking and climbing adventures with him, Michael Wakefield, and Will Mortimer were a highlight of these years.

I would also like to thank the former students, Amelia Dunn, Georgina White, Jack Collingbridge and Taylor Wood for their contribution to the experiments carried out for this project.

Finally, I would like to thank my friends Andreas Christoforou, Stefanos Konstantinou, Michalis Michael, Lambros Geropapas and Charalambos Gregoras for their support, interest, and even help with the project.

To the people mentioned, and the many more that have played a role in this project, thank you.

Author's declaration

At no time during the registration for the degree of Doctor of Philosophy has the author been registered for any other University award without prior agreement of the Doctoral College Quality Sub-Committee. Work submitted for this research degree at University of Plymouth has not formed part of any other degree either at University of Plymouth or at another establishment.

Relevant scientific seminars and conferences were regularly attended at which work was often presented:

Publications:

Makris, S., Roverato, M., Dávila-Harris, P., Cole, P. and Manzella, I., 2023. **Distributed stress fluidisation: Insights into the propagation mechanisms of the Abona debris avalanche (Tenerife) through a novel method for indurated deposit sedimentological analysis**. Frontiers in Earth Science, 11:659. [doi: 10.3389/feart.2023.1177507] (*The publishing cost of USD 2,902.50 was covered by funding allocated from the University of Plymouth Frontiers Open Access publishing external funding*.)

Makris, S., Roverato, M., Lomoschitz, A., Cole, P. and Manzella, I., 2023. **The propagation and emplacement mechanisms of the Tenteniguada volcanic debris avalanche (Gran Canaria): Field evidence for brittle fault-accommodated spreading.** Journal of Volcanology and Geothermal Research, 435:107773. [doi: 10.1016/j.jvolgeores.2023.107773]

Makris S, Roverato M, Lomoschitz M, Cole P, Manzella I (2022). **Evidencias sobre la dinámica de propagación de los debris avalanches de Tenteniguada y Abona, Islas Canarias, a partir del análisis sedimentológico.** Hürlimann M and Pinyol N., X Simposio Nacional sobre Taludes y Laderas Inestables, Granada, September 2022. [ISBN: 978-84-123222-7-9]

Makris S, Manzella I, Cole P, Roverato M (2020). **Grain size distribution and sedimentology in volcanic mass-wasting flows: implications for propagation and mobility.** International Journal of Earth Sciences. [doi: 10.1007/s00531-020-01907-8]

Presentations and conferences attended:

International Association of Volcanology and Chemistry of the Earth's Interior - Rotorua 2023 (upcoming): Volcanic debris avalanche propagation mechanisms and dynamics: field evidence and analogue experiments. (Awarded a travel grant of €700 by the International Association of Volcanology and Chemistry of the Earth's Interior for participation in the Association's conference, in Rotorua, New Zealand)

UK Volcanic and Magmatic Studies Group Conference - London 2023: Volcanic debris avalanche propagation dynamics and the importance of lithological properties:

evidence from sedimentological analysis.

Cities on Volcanoes conference - Crete 2022: Evidence of volcanic debris avalanche propagation dynamics from sedimentological analysis of the Tenteniguada and Abona deposits, Canary Islands.

European Geosciences Union General Assembly - Vienna 2022: Evidence of volcanic debris avalanche propagation dynamics from sedimentological analysis of the Tenteniguada and Abona deposits, Canary Islands.

*__American Geophysical Union Meeting__ - 2021: Bimodality of the Grain Size Distribution as a Potential Factor for the High Mobility of Rock/Debris Avalanches: Small-Scale Analogue Experiments Examination.

*__European Geosciences Union General Assembly__ - 2021: The role of sedimentology in the mobility of debris avalanches: Evidence from their deposits and granular flow experiments.

*__American Geophysical Union Meeting__ - 2020: What Grain Size Distribution And Sedimentology Can Tell Us About The Propagation Of Volcanic Mass Wasting Flows.

The Geological Society Early Careers Geoscientists Evening (Southwest Regional Group) - 2020: Understanding the mobility of volcanic landslides through sedimentology and grain size distribution.

UK Volcanic and Magmatic Studies Group Conference - Plymouth 2020: Propagation and mobility of lahars and debris avalanches: evidence from sedimentology.

**online attendance*

Word count for the main body of this thesis: **47,058**

Signed: 

Date: January 30, 2024

VOLCANIC DEBRIS AVALANCHE PROPAGATION AND EMPLACEMENT MECHANISMS: SEDIMENTOLOGICAL FIELD EVIDENCE AND BIDISPERSE GRANULAR FLOW EXPERIMENTS

Symeon Makris

Volcanic debris avalanches mobilise large volumes and achieve long runouts with high destructive potential. Although many theories have been proposed regarding the mechanisms that enable their long runouts, the processes remain unknown. Theoretical and numerical models are unable to account for their long runout while being consistent with deposit observations. Therefore, evaluation of their dynamics in reference to deposit structure and sedimentology is fundamental for constraining such models.

This thesis explores volcanic debris avalanche propagation dynamics and evaluates potential factors contributing to their long runouts. A systematic comparison of volcanic debris avalanches and lahars allows the evaluation of water as a factor in mass flow propagation. The structure and sedimentology of two deposits from the Canary Islands (Spain) with different properties, and composed of distinct lithologies, are examined and their propagation processes evaluated. A novel technique using structure from motion photogrammetry is developed and proposed for the clast size analysis of indurated/lithified deposits. Finally, analogue granular avalanche experiments are employed to evaluate grain size bidispersity as a factor for enhanced runout. The potential and limitations of analogue experiments are evaluated.

Findings suggest that water does not play a major role in the propagation mechanisms of volcanic debris avalanches and is not a factor contributing to their long runouts. The two studied deposits constitute endmembers consisting of homogenous competent lava lithologies in one case, and less competent pyroclastic products in the other. Consequently, they result in end-member propagation models: (1) brittle fault-accommodated spreading and (2) distributed stress fluidisation respectively. Their comparison suggests that lithological properties are a principal factor for the structural evolution, dynamics and kinematics of volcanic debris avalanches.

Although enhanced runouts are achieved in the analogue experiments with bidisperse grain size distributions, this is the result of scale-dependent processes, dissimilar to real events, generating a collisional flow regime. Consequently, the importance of dynamic scaling for the effective simulation of avalanche dynamics is highlighted.

Contents

List of Figures

List of Tables

Chapter 1

Introduction

Volcanic debris avalanches (VDAs) are large mass movement events generated by the collapse of unstable volcanic edifice flanks (Ui, 1983; Siebert, 1984; Pierson and Costa, 1987; Shea and van Wyk de Vries, 2008; Roverato and Dufresne, 2021) and are a common occurrence in the history of most stratovolcanoes (Siebert and Roverato, 2021). They propagate as volcanic landslides (Bernard et al., 2021) immediately after the initial collapse and usually progressively partially evolve towards flows (Voight et al., 1983; Siebert, 1984; Glicken, 1991; Scott et al., 2001; Thompson et al., 2009; Hungr et al., 2013). Although the majority of VDAs occur in active volcanoes (Siebert, 1984; Voight, 2000), they are not necessarily triggered by volcanic activity, and can also be initiated by rainfall, seismic activity or other destabilizing factors such as over-steepened slopes, hydrothermal activity and climate fluctuations among others (Belousov et al., 1999; Capra et al., 2002; Lomoschitz et al., 2008; Roverato et al., 2021). These events can attain velocities over 300 km/h, with runout distances up to 100 km (Dufresne et al., 2010b). They mobilise volumes up to tens of km^3, and less often up to hundreds of km^3, while deposits cover hundreds, even up to thousands of km^2 for some VDAs (Dufresne, 2009). The high energy generated by such voluminous and far-reaching mass movements constitutes a hazard to communities close to volcanoes and infrastructure. Additionally, they can trigger secondary hazards such as volcanic eruptions, debris flows, and tsunamis on ocean island volcanoes (Siebert, 1984; Leyrit, 2000; van Wyk de Vries and Delcamp, 2015; Di Traglia et al., 2018), making them one of the most destructive phenomena (Hürlimann et al., 1999) and a potential threat at a more global scale. In the past 400 years VDAs are estimated to have caused 20,000 casualties (Siebert et al., 1987, 2006), while the tsunami triggered by the flank failure of the Anak Krakatau volcano (Indonesia) in December 2018 highlights the potential of

cascading hazards stemming from VDAs (Walter et al., 2019).

The propagation of VDAs achieves much greater horizontal runout component distance compared to their fall height (Davies, 1982; Hungr, 2002; Legros, 2002), far greater than predicted by simple frictional models of a coherent sliding mass (Rait and Bowman, 2016). This is a characteristic VDAs share with their non-volcanic equivalent, rock avalanches (RAs) in mountainous environments (Scott et al., 2001; Dufresne, 2009; Hungr et al., 2013). Due to similarities in their physical processes, studies examining RAs are also considered in this thesis in association with VDAs. Long runout in large mass movements was first observed in RAs by Heim (1882). The long runout of both VDAs and RAs (hereafter referred to as VDA/RAs collectively) is commonly expressed by small apparent friction coefficients (e.g. Shreve, 1968; Erismann, 1979; Hürlimann and Ledesma, 2003), often expressed as the H/L ratio, initially introduced by Heim (1932), between height fallen (H) and horizontal component of the runout in the direction of propagation (L) (fig. 1.1) (Scheidegger, 1973; Hsü, 1975). Simple frictional models would predict values of ~ 0.5-0.6

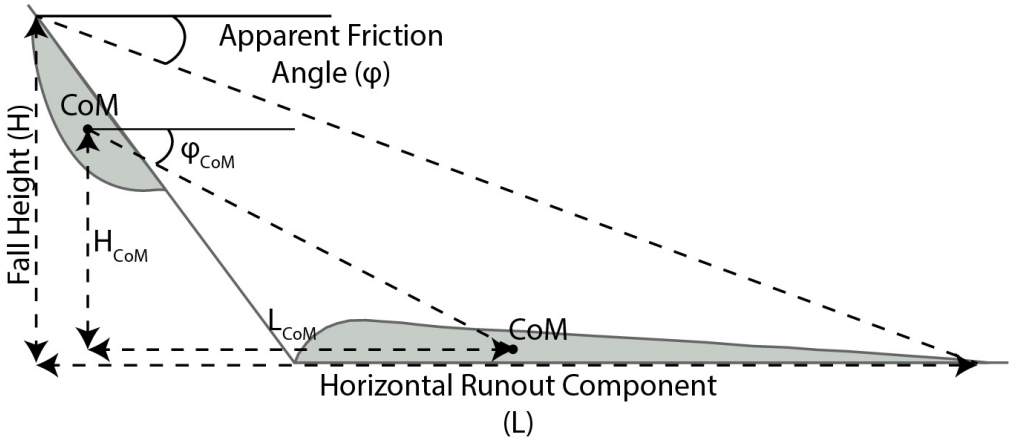

Figure 1.1: Schematic representation of the definitions of the fall height (H), horizontal runout (L) and apparent friction angle ϕ; with their equivalents for the centre of mass (L_{CoM}, H_{CoM} and ϕ_{CoM}). CoM indicates the centre of mass of the destabilised mass and the deposit (modified after Legros, 2002 and Manzella and Labiouse, 2013).

for VDA/RAs, however, it is typical that they exhibit H/L values of 0.1-0.2, or even lower (fig. 1.2) (Scheidegger, 1973; Hsü, 1975; Davies, 1982; Ui, 1983; Legros, 2002; Dufresne, 2009). After the observation of Heim (1882), long runout mass flows have been further studied in diverse settings, even extraterrestrial, by several authors (including but not limited to: Hsü 1975; Davies 1982; Siebert 1984; Glicken 1991; Corominas 1996; Legros 2002; Hungr and Evans 2004; Davies and McSaveney 2012; Manzella and Labiouse 2013; van Wyk de Vries and Delcamp 2015). However, it is only after the 1980 Mount St. Helens

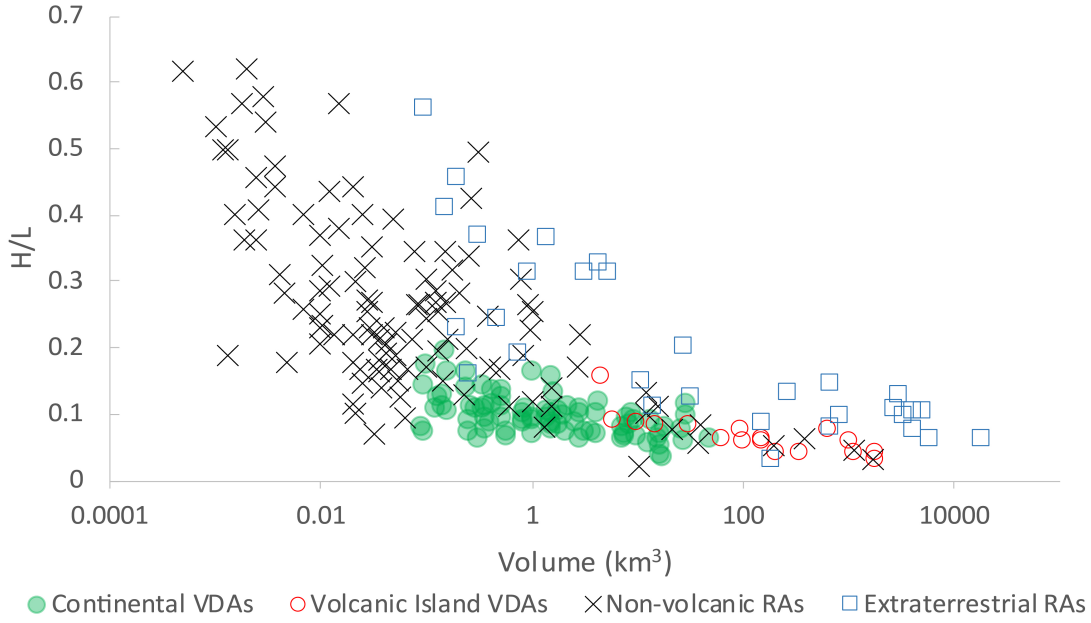

Figure 1.2: Apparent coefficient of friction (H/L) versus volume for continental volcanic debris avalanches (VDAs), VDAs on volcanic islands, non-volcanic rock avalanches (RAs) and extraterrestrial RAs (modified after van Wyk de Vries and Delcamp (2015), Hürlimann and Ledesma (2003).

lateral collapse (Voight et al., 1983; Siebert, 1992; Glicken, 1996) that scientific interest towards volcanic slope stability and VDAs increased (Hürlimann et al., 1999), with more studies examining their dynamics.

Even though it is useful to associate VDAs and RAs in the study of large mass movements, it is important to be aware of the differences between them, as their comparison can be a tool in evaluating their dynamics. VDAs statistically mobilise higher volumes and are capable of longer runouts and higher mobility of their centre of mass than volume-equivalent RAs (Siebert, 1984; Ui and Glicken, 1986; Hürlimann et al., 2000; van Wyk de Vries and Delcamp, 2015; Dufresne et al., 2021b). The higher runouts of VDAs, illustrated in fig. 1.2, are at least partly, the effect of the higher volumes mobilised. This is in line with the size effect, first identified and named by Scheidegger (1973) and that suggests that more voluminous mass flows achieve higher runouts (Ui, 1983; Davies and McSaveney, 2012). Davies (1982) suggested that the observed size effect is the result of the greater spreading of more voluminous VDA/RAs. However, Campbell et al. (1995), and more recently Legros (2002), performed a more precise calculation of the effective coefficient of friction, using the fall height and displacement of the centre of mass (instead of the distance travelled by the front of a VDA/RA - difference illustrated in fig. 1.1), and

their findings support that the effective coefficient of friction in this case also decreases monotonically with the volume of the VDA/RAs. Thus, they suggest that friction is reduced by physical mechanisms and not as a result of spreading and the geometry of deposits (reviews Legros 2002; Davies and McSaveney 2012). Earlier, Ui (1983) and Voight et al. (1985), with separate evidence, also reached the conclusion that VDAs are more mobile than RAs, and that the size effect could not be the only reason. Nonetheless, results derived from calculations by Smyth (1991) oppose this suggestion and illustrate that VDAs and RAs have similar mobilities once the volume effect is removed and that their mobility has the same relationship with volume. However, RAs have a stronger correlation to this relationship. VDAs and RAs also generally differ in the material involved and in the initial conditions as mass movements in volcanic settings occur on slopes constructed of rocks accumulated from eruptions, containing volcanic and hydrothermally altered material (Siebert, 1984; van Wyk de Vries and Delcamp, 2015) which generally strongly differ from non-volcanic material in terms of geotechnical and sedimentary properties.

Davies and McSaveney (2009) suggest that the porosity and water content and tephra-mantled weak substrates surrounding volcanoes act as factors increasing their mobility. Given the nature of the generation of these volcanic rocks, they are generally more fractured and granular prior to mobilisation (Roverato et al., 2015; van Wyk de Vries and Delcamp, 2015). Thus, differences in initial conditions and material properties such as the amount of unconsolidated material, percentage of finer material, steepness of volcanic terrain, water content and the presence of hydrothermally altered minerals in volcanic environments have all been identified as potential factors contributing to a potential divergence in mobility (Ui, 1983; Hayashi and Self, 1992; Hürlimann et al., 1999; Robinson et al., 2015). Hence evaluation of the similarities and differences in material properties and resultant geometry and structure is important as it enables the assessment of similarities and divergence in their dynamics. At the same time, constraining the dynamics and runout of both VDAs and RAs is fundamental for the related hazard assessment and hence it plays a significant role in limiting economic and life loss caused by such events (Di Luzio et al., 2004; Iverson et al., 2011; Yang et al., 2011; Fan et al., 2016; Zhou and Sun, 2017; Duan et al., 2020, 2022).

Since the 1960s many theories, hypotheses and models have been proposed regarding the mechanisms that enable the long runouts of VDA/RAs based on morphology, internal

architecture, sedimentology, theoretical approaches, and numerical and analogue models (for reviews, see Chapter 2 of this thesis and Davies, 1982; Erismann and Abele, 2001; Hungr, 2002; Legros, 2002; Collins and Melosh, 2003; Friedmann et al., 2006; Manzella and Labiouse, 2008; Davies and McSaveney, 2012). Nonetheless, no single proposed model can account for the runout while being consistent with field observations of the deposits of all events. VDA deposits (VDADs) exhibit a set of common characteristic features such as jigsaw-fractured clasts, block and matrix-rich facies, remnant stratigraphy, textural and sedimentological heterogeneity and hummocky surfaces (e.g. Siebert, 1984; Glicken, 1991; Roverato et al., 2015; Dufresne et al., 2021b). However, the variability they exhibit in the proportion and sedimentological composition of each facies, internal structure and longitudinal evolution is unattainable by a single conceptual, analogue or numerical model due to the lack of understanding of VDA/RA propagation mechanisms and the factors dictating their dynamics. For example, conceptual models such as those proposed by Campbell (1989) and Takarada et al. (1999) which suggest a plug flow over an agitated basal layer, find support in VDADs such as Iwasegawa (Japan) and Kaida (Japan) (Takarada et al., 1999) which preserve such a basal layer. However, the observation of sheared material in the body of VDA/RAs such as the Pungarehu VDAD (New Zealand) (Roverato et al., 2015) and Tschirgant RA (Austria) (Dufresne and Dunning, 2017) implies that a hypothesis based entirely on stresses accommodated in a basal layer cannot be the primary explanation for the runout of all VDA/RAs. Some researchers have argued that something more than the fractured rock mass itself is required to explain the behaviour of VDA/RAs and their runout (reviewed and discussed in Erismann and Abele, 2001; Hungr, 2002; Legros, 2002; Collins and Melosh, 2003; Friedmann et al., 2006; Manzella and Labiouse, 2008; Davies and McSaveney, 2012; Perinotto et al., 2015). Many of the mechanisms proposed suggest intergranular mediums such as water (Katayama, 1974), steam (Goguel, 1978) or dust (Hsü, 1975) to account for the long runouts, however many of the deposits do not exhibit any such evidence (Hewitt et al., 2008). Others include other auxiliary mechanisms such as a frictional heat-generated basal frictionite/pseudotachylyte layer (Erismann, 1979), which are only exhibited by a few specific events, or only locally. Today, propagating VDA/RAs are considered to behave as dense granular avalanches where grain interactions are the most important energy dissipation process (Voight et al., 1983; Campbell, 1990; Schneider and Fisher, 1998; Davies and McSaveney, 1999; Roverato and Dufresne, 2021). However, the mechanisms enabling long runouts remain

controversial and unresolved (Legros, 2002; Pollet and Schneider, 2004; Banton et al., 2009; Davies and McSaveney, 2012; Perinotto et al., 2015; Cabrera and Estrada, 2021), demanding an evaluation of theoretical models in comparison to real events and their deposits.

1.1 Motivation

1.1.1 Field sudies

A major factor for the lack of understanding of VDA/RAs dynamics results from the difficulty of developing models and theoretical concepts that are able to interpret and represent field observations of the sedimentology and structure of VDA/RA deposits (Perinotto et al., 2015; Johnson et al., 2016). Nonetheless, any model representing propagation and emplacement dynamics of these processes needs to be able to replicate not only their long runouts, but at the same time be consistent with the sedimentological, internal structure and geomorphological features of deposits (Cruden and Varnes, 1996; Pudasaini and Hutter, 2007; Shea and van Wyk de Vries, 2008; Dufresne, 2009). Therefore, a better understanding of VDA/RA deposits and the processes they represent is required, in order to contribute to the development of models regarding their kinematics and dynamics. Although VDA/RA deposits are complex (Roverato and Dufresne, 2021), detailed examination of their morphology, internal architecture, substrate interactions and sedimentology provides fundamental information regarding their dynamics (Dufresne and Dunning, 2017) as demonstrated by field studies (including but not limited to Smyth, 1991; Glicken, 1996; Belousov et al., 1999; van Wyk De Vries et al., 2001; Clavero et al., 2002; Kelfoun and Druitt, 2005; Roverato and Capra, 2013; Roverato et al., 2015; Dufresne et al., 2016b; Dufresne and Dunning, 2017; Paguican et al., 2021). In accordance, these studies have highlighted the importance of dedicated field investigations to better identify structural and sedimentological features such as facies and feature distribution, and clast-size distribution patterns in evaluating VDA dynamics, energetics and propagation and emplacement processes. Systematic comparison studies of the sedimentology of deposits from different types of mass flows, such as saturated lahars and pyroclastic density currents, are also scarce in the literature (Dufresne et al., 2016a). In the same way as the comparison between RAs and VDAs, such studies have the potential of constraining the factors that are different in each (e.g. presence of water, difference in temperature,

presence of gas) and how these can contribute to divergence in the dynamics and runout of different mass movements.

One of the main reasons for the lack of such studies and comparisons is that although highly variable, the frequency of VDA reoccurrence is on average in the timescale of thousands to tens of thousands of years on individual volcanoes (Mcguire, 1996; Capra et al., 2002; Zernack et al., 2012). Owing to the rarity of recent events, there is a lack of well-preserved deposits. In addition to that, older deposits are commonly indurated, prohibiting the detailed study of sedimentology, and especially clast-size analysis of VDA/RA deposits with conventional sedimentological methods (Tost et al., 2014).

1.1.2 Analogue experiments

The scarcity, inaccessibility, induration and complexity of VDADs encourage alternative study methods such as analogue experiments (e.g. Iverson et al., 2004; Manzella and Labiouse, 2008; Dufresne, 2012; Yang et al., 2015; Manzella et al., 2016; Hu et al., 2020) and numerical modelling (e.g. Campbell et al., 1995; Thompson et al., 2009, 2010; Davies et al., 2010; Cuomo, 2020) to be employed to support or complement field investigations. Analogue lab experiments can also provide evidence to evaluate theoretical and numerical propagation models. They do not aim to mimic reality but rather to simplify the conditions of a mass flow to examine a specific aspect (Manzella, 2008; Manzella and Labiouse, 2010; Longchamp et al., 2016) and reproduce their major features (Davies and McSaveney, 2009). In fact, Davies and McSaveney (1999, 2003) state that in small-scale granular flow experiments ($<10^5$ m^3), the behaviour diverges significantly from the case studies they used for comparison. They suggest that this is the result of conditions that cannot be imitated in the lab, like pore pressure, rock fragmentation and saturated strata. However, the reduced complexity of laboratory experiments allows for the parameterisation of specific factors in isolation. Such experiments seek to explore propagation and emplacement, sometimes to validate and calibrate models (e.g. Denlinger and Iverson, 2001) and sometimes to explore the influence of specific parameters at the scale of the experiments (Davies and McSaveney, 1999; Manzella, 2008; Manzella and Labiouse, 2009). After careful consideration of the scaling and the constraints given by a laboratory setting, observations can then be verified through field observations and numerical simulations to evaluate hypotheses. The effect of individual parameters observed in the lab can also be evaluated with respect to their

importance in real events (Manzella, 2008; Kelfoun, 2011).

Numerical simulations are a powerful tool in the exploration of VDA/RAs and their dynamics. However, numerical models need to be constrained by field and analogue observations and evaluated for their effectiveness in reproducing them. Currently, existing models are not able to fully reflect the complexities of VDA/RA propagation and emplacement dynamics (Roverato and Dufresne, 2021). In fact, few events have been modelled in detail (e.g. Heinrich et al., 2001; Le Friant et al., 2003; Sheridan et al., 2003; Kelfoun and Druitt, 2005; Capra et al., 2008). Nonetheless, numerical simulations and simplified analytical models can provide valuable information on the physical processes. More complex models of VDA/RAs need to be developed alongside, and with constraints from, field observations (Procter et al., 2021; Roverato and Dufresne, 2021) so that they can effectively simulate both the dynamics of VDAs and the structure and sedimentology. Although numerical modelling was not carried out for this thesis, such models are discussed throughout this study in comparison to field or analogue experimental findings that are fundamental to correctly validate models.

1.2 Aims and objectives

The present thesis examines the mechanisms and dynamics of VDAs during their propagation and emplacement. The aim is to provide evidence for these dynamics in order to evaluate and provide constraints for the further development of theoretical models of VDA propagation and emplacement. This overarching aim has been achieved through different objectives and methods:

1. The identification of the role of water by the systematic and detailed comparison of different types of volcanic mass flows.

2. The assessment of the influence of the lithological material characteristics in determining the propagation mechanisms by the detailed field characterisation of VDADs.

3. The development of a method for the sedimentological examination of indurated VDADs.

4. The evaluation of the effect of bidispersity in high mobility of granular flows by

using analogue granular avalanche experiments.

5. The critical analysis of laboratory experimental conditions, scaling and interpretation.

This overall content has been distributed in eight chapters, including the present introduction and the conclusions (Chapter 7) and a brief overview of identified future works (Chapter 8). The remaining chapters are detailed in the following.

Chapter 2 presents and discusses the theories, models and mechanisms that have been submitted in the literature to explain the long runouts of VDA/RAs.

In Chapter 3 the assessment of the potential role of fluids in the propagation of VDAs is evaluated, for the first objective, through a systematic comparison of the sedimentological data of nine VDADs and eight lahar deposits obtained from the literature. The sedimentological differences between the two mass flow types occurring in volcanic environments illustrate the role of water in their dynamics. These findings have been published as an original article in the International *Journal of Earth Sciences* under the title "Grain size distribution and sedimentology in volcanic mass-wasting flows: implications for propagation and mobility" (Makris et al., 2020).

Chapters 4 and 5 present the second objective of the thesis, to assess the role of the properties of the material involved in VDAs in determining their propagation dynamics and also to evaluate how field studies can be used to examine these. Therefore, this thesis provides an analysis of two deposits with very different lithological properties. These are the Tenteniguada VDAD (Gran Canaria, Spain) in Chapter 4, and the Abona VDAD (Tenerife, Spain) in Chapter 5. Field evidence is evaluated with the aim of constraining their propagation dynamics. This thesis component contributes towards assessing the mechanisms that enable long runouts and high mobility. Conceptual models regarding their propagation and emplacement mechanisms and dynamics according to the observations are presented. Since a large portion of VDADs is indurated, a new tool is developed for their examination and is proposed in Chapter 5 for the third objective. The novel technique utilising structure from motion photogrammetry and photographic sampling was developed for clast-size analysis of the Abona VDAD. The technique employs a novel combination of methods and sample strategies for clast-size analysis. This would increase

the capacity for collecting field evidence and to further investigating VDA/RAs and the hazards these complex and hazardous phenomena pose. The study of the Tenteniguada VDAD has been published in the *Journal of Volcanology and Geothermal Research* under the title "The propagation and emplacement mechanisms of the Tenteniguada volcanic debris avalanche (Gran Canaria): Field evidence for brittle fault-accommodated spreading" (Makris et al., 2023a). The study of the Abona VDAD has been published in the journal *Frontiers in Earth Science* under the title "Distributed stress fluidisation: Insights into the propagation mechanisms of the Abona debris avalanche (Tenerife) through a novel method for indurated deposit sedimentological analysis" (Makris et al., 2023b). Chapter 5 also presents conclusions drawn from the comparison of the Abona and Tenteniguada VDADs.

For the fourth objective (Chapter 6) of evaluating the potential of grain-size distribution bidispersity on VDA dynamics, mechanisms and runout; a series of analogue experiments have been carried out. VDA/RA deposits are characterised by bidisperse to polydisperse grain-size distributions (e.g. Scott et al., 1995; Glicken, 1996; Vallance, 2000; Pollet and Schneider, 2004; Vallance and Iverson, 2015; Bernard et al., 2017). Bidispersity implies the existence of two dominant sizes or size ranges in the grain-size distribution. Bidispersity is exhibited in VDADs, at least locally (Ui and Glicken, 1986; Siebert et al., 1989; Glicken, 1996; Siebert, 2002; Bernard and van Wyk de Vries, 2017); while in the case of RA deposits, bidispersity develops especially in zones of concentrated shear stresses (Dufresne and Dunning, 2017). Recent analogue experimental studies have examined the potential of a bidisperse grain-size distribution for providing a more energy-efficient shear accommodation arrangement reducing frictional losses at the base of VDA/RAs. An evolution towards bidisperse distributions is also supported by the findings of Chapter 3. Therefore, Chapter 6 presents analogue bidisperse granular avalanche experiments examining the potential of grain-size distribution bidispersity in increasing the runout and mobility of granular avalanches in general, and VDAs in particular. For the fifth objective, this chapter discusses the potential and limitations of analogue experiments. The scaling requirements for the effective examination of VDA dynamics in analogue experiments are also evaluated.

The different sections of this thesis contribute to the understanding of the propagation mechanisms of VDAs through different approaches, while proposing new and evaluating

existing methods which are fundamental for the progress of the field.

Chapter 2

Mobility mechanisms review

Many theories and models have been proposed regarding the mechanisms that enable the enhanced runouts of volcanic debris avalanches (VDAs)/rock avalanches (RAs). These are based on morphology, internal architecture, sedimentology, theoretical approaches, and numerical and analogue models (for reviews, see Davies, 1982; Erismann and Abele, 2001; Hungr, 2002; Legros, 2002; Collins and Melosh, 2003; Friedmann et al., 2006; Manzella and Labiouse, 2008; Davies and McSaveney, 2012). A list of the more relevant mechanisms for the present work is provided in Table 2.1.

Long runout landslides were first recognised by Heim (1932) with the analysis of the Elm RA event (Switzerland). Long runouts mass flow deposits have since been identified on various terrestrial settings as well as other planets, moons and asteroids (Howard, 1973; Lucchitta, 1979; Singer et al., 2012; Schmidt et al., 2017; Beddingfield et al., 2020; Magnarini et al., 2021). The long runouts and high mobility suggest an apparent reduction of friction during propagation. The following section is a more comprehensive review of the main mechanisms proposed for VDA/RAs including critiques that followed their publication. The proposed models can be categorised into those not requiring a fluid or lubrication, those implying basal lubrication, those implying fluidisation by a fluid within the body of the avalanche, and those related to active volcanic processes. The distinction is also made in table 2.1, which serves as a key for the mechanisms for the rest of the thesis.

Table 2.1: Mechanisms proposed for the low apparent friction of volcanic debris/rock avalanches (adapted after Smyth 1991).

Mechanism Proposed	Author
Flow behaviour	Hsü, 1975
Sliding behaviour	Ui, 1983
Fluid-absent	
Highly energetic collisions among individual grains maintaining the original kinetic energy	Heim, 1932
Acoustic/vibratory fluidisation – high-frequency vibration which momentarily relieves overburden pressure locally, allowing sliding to occur in the unloaded regions	Melosh, 1979, 2015
Dry acoustically and seismically fluidised flow	Francis and Wells, 1988
Spreading of a rapid granular mass	Davies, 1982
Dynamic rock fragmentation	Davies and McSaveney, 2002
Plug flow over an **agitated basal layer**	Campbell, 1989; Takarada et al., 1999
Bidisperse grain-size distribution accommodating shear stress as a more efficient shearing arrangement	Linares-Guerrero et al., 2007; Yang et al., 2015; Lai et al., 2017; Hu et al., 2021; Duan et al., 2022
Air lubricated or fluidised	
Trapped layer of compressed air beneath the mass, supporting it	Shreve, 1968
Fluidisation by air: dilated upward flow of air within the mass maintains a low coefficient of friction **between particles**	Kent, 1966; Wilson, 1984
Lubricated or fluidised by the presence of a fluid	
Water-saturated slide	Katayama, 1974
Small amounts of water in the basal layer accommodating shear in a **wet basal zone** with reduced friction	Goguel, 1978b; Johnson, 1978; Voight and Sousa, 1994
High-pressure steam generated by frictional heat at the base of the flow	Goguel, 1978a
Highly energetic interstitial dust acting as intergranular fluid	Hsü, 1975
A layer of molten rock generated at the base by frictional heat	Erismann, 1979
Gravitational sliding fractured and mobility enhanced by steam explosions	Ui, 1983
Boiling of interstitial fluid by frictional heat - vaporised in the mass	Habib, 1975; Voight et al., 1983
Specific to volcanic environments	
Volcanic gases injected along the slip plane	Prostka, 1978
Hydrothermal fluids - allowing incomplete fluidisation of weak rocks	Siebert, 1984
Fluidisation by volcanic gases	Voight et al., 1983
Magmatic Blast	Gorshkov and Dubik, 1970

2.1 Fluid-absent

Heim (1932) hypothesised that the motion of the Elm RA was the result of numerous **highly energetic collisions** between the grains maintaining the original kinetic energy of the fall and driving the propagation. Bagnold (1954) also supported the idea of a dispersive grain flow with agitated particle-particle collisions supporting the weight of the matrix of the mass. However, grain-flow type movements were not often connected to VDAs, possibly because it is hard to envisage a large dry granular flow of this scale as Smyth (1991) suggests. It is now also believed that VDA/RAs do not propagate under a collisional regime and therefore this type of energy exchange at the scale inferred by the authors is unlikely. It is no longer believed that this type of flows is dominated by chaotic particle collisions and high granular temperatures that would support the weight of the material in the way implied (e.g. Dunning, 2006; Dufresne et al., 2016a; Paguican et al., 2021).

Hsü (1975), adding to the theory of Bagnold (1954) proposed that **highly energetic interstitial dust** could act as an intergranular fluid fluidising a RA. McSaveney (1978) disagreed with this theory and suggested that an intergranular fluid is not required. They instead suggested that **vibrational energy produced by an earthquake** is sufficient to allow fluidisation of the Sherman RA (Alaska) which, however, had moved over Sherman glacier, making it an even more complex case.

Melosh (1979) and Collins and Melosh (2003) proposed **acoustic fluidisation (vibratory fluidisation)** as the mechanism fluidising VDA/RAs. According to Melosh (2015), the passing of high-frequency vibrations creates transient, high-frequency pressure fluctuations (or acoustic waves), that fluidise the homogenous debris mass through local variations in contact forces. These pressure fluctuations instantaneously locally relieve the overburden weight on individual clasts that become free to slip. This process creates an agitated laminar flow with low mixing between units and is capable of enhancing the mobility of granular flows (Collins and Melosh, 2003). The numerical modelling of Collins and Melosh (2003) suggests that under high-frequency pressure vibrations, a granular mass will develop into a fluid-like flow with uniform viscosity. Numerical modelling by Johnson et al. (2014) offers support for the theory by suggesting that sliding preferentially occurs in a granular flow when normal stress is reduced. Francis and Wells (1988) and Francis and

Self (1987) similarly support that seismic energy can have a similar effect on the motion of VDA/RAs, especially where intensified and prolonged by the subsurface structure of the geology by substituting the kinetic decreasing energy (Francis and Self 1987, p78).

Mechanical fluidisation has been proposed by McSaveney (1978) and Davies (1982) as a process where the high energy in a granular mass generates high impulsive contact pressures between particles, causing the dilation of the mass. In this case, internal resistance to shear stress is reduced (Bagnold, 1954) and the mass may flow under gravity (Davies, 1982).

Campbell (1989) suggested **self-lubrication** could occur by an avalanche flowing like a solid sheet over a dilute layer of highly agitated particles that should form naturally in high-speed granular flows. They proposed that only a small portion of the mass would be dissipating energy, and this also complies with the size effect where mass flows of larger volume are capable of greater mobility.

According to the theory of **spreading of a rapid granular flow**, Davies (1982) suggested that the observed size effect was the result of the greater spreading of more voluminous mass flows. However, Campbell et al (1995) performed a more precise calculation of the effective coefficient of friction using the fall height and displacement of the centre of mass and their findings support that the effective coefficient of friction is in this case also decreases monotonically with the volume of the mass flows, and thus suggest that friction is reduced by a physical mechanism and not as a result of spreading and the geometry of deposits as suggested by other authors (Davies 1982; Johnson et al. 2014 and references therein). The calculations of Campbell et al. (1995) suggest that spreading is not the factor imposing the low apparent coefficient of friction in the geometry of VDA/RA deposits; and that a physical mechanism is reducing the effective coefficient of friction. Measurements of the travel distance of the centre of mass rather than the runout of the deposit have confirmed that spreading is not enough explanation for high mobility (Legros, 2002).

Dynamic rock fragmentation has more recently been proposed (Davies and McSaveney, 2002; Pollet and Schneider, 2004) as the effect generated by the fracturing of intact rock under rapid strain and confining pressure and can preserve the dilated state in a granular

material as supported by studies such as Davies et al. (2010) and Zhang and McSaveney (2017). Prior to fracturing, particles deform plastically under the shearing motion around them. When these forces exceed the local strength of a particle, it breaks and generates fractures. A proportion of the stored elastic energy is then released with the fractures radiating from the centre of mass of the clast. The elastic energy released during disintegration could contribute to the enhanced mobility of VDAs/RAs by generating pressure which supports some of the force on the shear layer so that the effective stress in the shear layer is reduced. Because frictional resistance is proportional to effective stress, this reduces the overall frictional resistance to shear (Davies and McSaveney, 2009). This theory is disputed by Rait and Bowman (2016) who observed that the kinetic energy produced in dedicated shear tests is quickly dissipated in the matrix with no long-lasting impact.

A number of studies (Linares-Guerrero et al., 2007; Yang et al., 2015; Lai et al., 2017; Hu et al., 2021; Duan et al., 2022) have proposed the **grain-size distribution bidispersity** observed locally in VDA/RA deposits as a potential factor enhancing their mobility. These studies suggest that fine particles migrate to the base, where they act to lubricate the flow. It has been observed in analogue experiments and numerical models that fine particles reduce the frictional areas between the coarse particles and the substrate by acting as 'ball-bearings' (Roche et al., 2006; Linares-Guerrero et al., 2007), while they simultaneously act as 'rollers' to encourage rolling as opposed to frictional sliding (Phillips et al., 2006; Hu et al., 2021). The studies of Linares-Guerrero et al. (2007), Yang et al. (2015), Lai et al. (2017), Hu et al. (2021) and Duan et al. (2022) propose that fine particles migrate and lubricate the base, in a process identical to the described lab experiments. However, the applicability of this process at the scale of VDA/RAs has not been evaluated, and graded deposits with fines at the base deposits are not often observed. Analogue (e.g. Phillips et al. 2006; Moro et al. 2010; Yang et al. 2015) and numerical experiments (e.g Linares-Guerrero et al. 2007) also support that the bidisperse grain-size distribution that is observed in shear zones (Dufresne and Dunning, 2017) is more efficient in accommodating shear and potentially enables longer runouts and greater mobility in granular avalanches. This controversial aspect of the role of bidispersity in VDA/RA runout and the validity of experimental observations is discussed in detail in Chapter 6.

2.2 Basal lubrication by fluid or air

Shreve (1968) proposed that a layer of compressed air, trapped beneath a VDA/RA (air cushion) could support its weight and thus lubricate its flow. Erismann (1979), however, disputed this hypothesis by theoretically calculating the unrealistic conditions that would be required for it to be true. They calculated that a "bouncing height" over 100 metres would be required to generate the air compression that would allow this cushion to move over even slightly uneven topography. They also illustrated that the marginal rim that the original hypothesis suggested would limit the air cushion (Shreve, 1968) would need to resist a lateral air-jet of 450m/s that the weight of a 62.5 m thick VDA would produce, and thus would not remain in place. This theory also assumes low leakage rates through the mass. The required low permeability has been calculated as theoretically possible for VDA/RA poorly sorted material (Iverson, 1997), however, fluidisation experiments suggest a dramatic increase in permeability with fluidisation (Wilson, 1984). Similarly, Prostka (1978) proposed that **volcanic gasses injected in the slip plane** could lubricate the flow. The blast surge from the Mt St Helens eruption was indeed gas-rich at temperatures >100°C (Banks and Hoblitt, 1981). However, Glicken (1996) supports that the uneven topography of the valley could not have enabled this process. Also, the permeability arguments (Erismann, 1979) outlined above suggest that the confinement of the fluid to the base of the flow is unlikely (Smyth, 1991). Additionally, the recognition of long runout landslides on the Moon, where the is no air, by Guest (1971) and Howard (1973) supported the argument that hypotheses attributing mobility to the effect of air were less likely to be responsible, at least for all, long runout mass flows and that therefore there must also be other mechanisms.

Basal lubrication by a **formed or injected fluid** has been hypothesised by various studies (e.g. Marangunic 1972; Ui 1983). These hypotheses can be divided into three types: a. injection of a lubricant, b. hypotheses that frictional heat at the base of the mass causes a phase change (melting of rock or ice, evaporation of water to steam), and c. mechanical lubrication (Smyth, 1991).

Some authors have suggested that small amounts of water located in the basal layer can lubricate the propagation of VDA/RAs by accommodating shear in **a wet basal zone** (e.g. Goguel 1978; Johnson 1978; Voight and Sousa 1994). Similarly, other authors have

proposed the lubrication being a result of undrained loading of saturated substrates (Abele, 1974; Sassa, 1989; Legros, 2002).

Gliding long distances on the surface of glaciers has also been proposed for some VDA/RAs; with the smooth surface of the ice and a layer of frictionally melted water-reducing friction at a basal shear plane. This mode of lubrication has been proposed by McSaveney (1978) for the Sherman RA (Alaska). However, most of the long-runout VDA/RAs do not occur on glaciers, therefore this theory does not offer a universal explanation.

Erismann (1979) suggested that a **layer of frictionally generated molten rock** (friction-ite/pseudotachylyte) could lubricate the flow. However, this layer would solidify as glass which has rarely been found at the base of a VDA/RA and could not occur in carbonate rocks (Smyth, 1991). Many long runout RAs have been reported in limestone terrains (e.g. Flims, Switzerland). The combination of this evidence suggests that this process is unlikely to occur in all but some exceptional slides like the Koefels RA (Austria) (Smyth, 1991) where glass was found at its base. Basal sliding on a dissociated or melted rock has also been supported as plausible by other authors (Erismann, 1979; Masch et al., 1985; Legros, 2002; De Blasio and Elverhøi, 2008) even though rarely and only locally observed.

The observation of sheared material in the body of VDA/RAs indicates that a hypothesis based entirely on a low-friction basal layer cannot be the primary explanation for their mobility (Johnson et al., 2016). Also, the presence of shear zones that accommodate shear within the body of VDA/RAs (Roverato et al., 2015; Dufresne and Dunning, 2017) suggest that the mass is not ravelling as a plug on a single basal layer; although it is likely that the material above these internal shear zones experiences less shear than the shear zones that concentrate shear.

2.3 Lubricated/fluidised by the presence of fluid or air within the body of volcanic debris/rock avalanches

The ability of VDA/RAs to travel longer than predicted by simple frictional models has been attributed by many authors to the action of a **fluid significantly reducing solid friction** (e.g. Kent 1966; Shreve 1968; Goguel 1978; Johnson 1978; Voight et al. 1983;

Voight and Sousa 1994). Modified or lubricated grain flow occurs when the presence of an interstitial fluid, liquid, or gas, builds up pressure gradients in the gas with collisions. In this case, particles are affected by the fluid pressure in addition to the momentum and interaction with other clasts (Smyth, 1991). This leads to the conservation of frictional energy dissipation. Legros (2002) also explains how an interstitial fluid could reduce the effective coefficient of solid friction by partly supporting particles, reducing the normal granular stress (Bagnold, 1954). However, as mentioned above, the importance of fluids in the mobility of VDA/RAs has been questioned by the discovery of long runout deposits on the Moon and Mars (Howard, 1973; McEwen, 1989).

Habib (1975) proposed that frictional heat might cause any **water vapour** to expand to steam at the base of the flow and support the mass by gaseous pore pressure. Expanding on this, Goguel (1978) suggested smaller particles within the body of the VDA/RA can be supported by the steam, while larger would be supported by **turbulent suspended dust**. Voight et al. (1981) similarly proposed the **boiling of interstitial fluid** by frictional heat steam had the effect of lubricating or fluidising the Mt St Helens VDA. However, Francis and Wells (1988) concluded that this is not necessary for all VDA/RAs, after examining the Socompa VDA (Chile), where insufficient water quantities would have been available at the time of the event for this process. The combination of the required unrealistic impermeability (Erismann, 1979), the existence of long runout landslides on the waterless Moon, and disagreement with sedimentological observations at the Rio Pita VDA (Ecuador), Smyth (1991) suggest that these hypotheses are unlikely.

Kent (1966) proposed **fluidisation by air extrusion**, that flow of air upwards through the body of the VDA/RA is capable of maintaining a low coefficient of friction between particles. This kind of gas fluidisation requires the rapid propulsion of air or magmatic or hydrothermal gases through the material (Smyth, 1991). Such fluidisation is incomplete in VDA and occurs where gas bubbles make their way through the mass to the surface (Wilson, 1984).

2.4 Related to eruptive volcanism

Glicken (1996) express the conviction that the **blast explosion** from the eruption of Mount St. Helens may have increased the mobility of the matrix-rich facies, through the reduction

of intergranular friction as the explosion promoted a dilated flow. However, they did not believe that complete fluidisation occurred.

Hydrothermal fluids have been proposed by Siebert (1984) to help lubricate the flow and they have also been suggested to weaken hydrothermally altered volcanic material (e.g. Vallance and Scott 1997; van Wyk de Vries and Delcamp 2015).

Although many of these explanations appear plausible in some specific case studies many are unlikely to offer a comprehensive explanation for the mobility of VDA/RAs. If there is indeed a single universal explanation, it is more likely an explanation that does not require exotic emplacement mechanisms (such as air-layer lubrication or fluidised substrates) (Davies and McSaveney, 2012; Dufresne and Dunning, 2017). Models for the mobility that encompass the features of VDA/RAs deposits but only require simple heterogeneous fragmentation of an initially intact source rock are both possible and more likely (Dufresne and Dunning, 2017).

Chapter 3

Grain size distribution and sedimentology in volcanic mass-wasting flows: water as a factor for propagation and mobility

Note, the content of this chapter comparing the deposit sedimentology and propagation mechanisms of volcanic debris avalanches and lahars has been published in the International Journal of Earth Sciences under the title "Grain size distribution and sedimentology in volcanic mass-wasting flows: implications for propagation and mobility" (Makris et al., 2020). A pre-print version of the publication is included in the supplementary material (as it was not published open access). Symeon Makris wrote the text, prepared all of the figures and developed the arguments therein. All authors discussed the science and commented on the manuscript. The format of this chapter is not the same as the publication, as different sections have been integrated in different parts of this thesis.

3.1 Introduction

The sedimentological characteristics of mass-wasting flow deposits are important for assessing the differences between phenomena and their propagation and emplacement mechanisms. The term volcanic mass-wasting flow, in this study, refers to the propagation of volcanic material downslope under gravity. The term makes no distinction as to their water content and sediment concentration. The mass-wasting flows considered are volcanic debris avalanches (VDAs) and lahars. VDAs (as well as non-volcanic rock

avalanches) are extremely rapid flows of fragmented rock derived from a slope failure (Sharpe 1938; Schuster and Crandell 1984; Hungr 2001) or a volcanic flank collapse (Siebert 1984); and may evolve from an initial rockfall or rockslide (Hungr and Evans 2004; Clague and Stead 2013). Although they may contain water, VDAs are not water-saturated (Iverson 1997; Legros 2002) as the majority of pore spaces are occupied by air so that the mass is mostly supported by particle-to-particle contacts (Siebert et al. 2006; Vallance and Iverson 2015). Lahars are defined as rapidly flowing, gravity-driven mixtures of rock, debris and water from a volcano (Vallance and Iverson 2015). Large quantities of unconsolidated material is required for their initiation (Lavigne and Thouret 2002). In contrast to VDAs, in lahars, the material is water-saturated with pore spaces filled with water (Iverson 1997; Scott et al. 2001; Legros 2002; Griswold and Iverson 2007). In the literature, lahars typically include sediment concentrations >60% by volume, whereas hyperconcentrated flows have sediment concentrations 20-60% (Fisher et al. 1984; Vallance 2000). Lahars can be closely associated with VDAs as they can evolve from the propagating VDA mass with the incorporation of water, or originate from the remobilisation of VDA deposits (VDADs) (Crandell 1971; Glicken 1991). However, even if they have a similar initial composition, they show fundamental differences in runouts and deposit characteristics (Crandell 1971; Pierson and Scott 1985; Glicken 1991; Iverson 1997; Scott et al. 2001; Legros 2002; Vallance and Iverson 2015).

While water can affect VDA propagation as a lubricating or fluidising medium (Bagnold 1954; Voight et al. 1983, 1985; Legros 2002; Roverato et al. 2015); there are fundamental differences between not fully saturated or even dry VDAs and saturated lahars (Smyth 1991; Iverson 1997; Scott et al. 2001). However, the effect on propagation of both the water content and material differences are still unclear (Hürlimann and Ledesma 2000; Legros 2002).

Following the approach used by Dunning (2004), the present study analyses and compares the grain size distribution (GSD) of VDAs and lahar deposits and offers a comparison to allow the evaluation of the effect of water and the extent of its contribution to high mobility in VDAs, as well as revealing similarities or differences in the mode of propagation of the two mass-wasting flows.

3.2 Sedimentary and structural characteristics of volcanic debris avalanche deposits

Material mobilised by VDAs can be heterogeneous in origin and thus size distribution and strength. However, there have been several studies regarding their sedimentology (e.g. Siebert, 1984; Ui and Glicken, 1986; Glicken, 1991; Smyth, 1991; Caballero and Capra, 2011; Roverato et al., 2015; Dufresne et al., 2021; Roverato and Dufresne, 2021); reporting a set of common characteristic features:

1. In the source area, the collapse typically leaves a horseshoe-shaped scar where the material collapsed (e.g. Roverato and Dufresne, 2021).

2. The most frequently reported feature of VDADs themselves is their jigsaw-fractured clasts and blocks (fig. 3.1). These are characterised by a fabric of a chaotic fracture network where fragments experience little relative displacement in the lack of disaggregation of the rock unit (Ui, 1983; Glicken, 1996; Bernard et al., 2021). Such jigsaw-fragmented sections of the source edifice are preserved as blocks up to hundreds of meters in size (Glicken, 1991), that nonetheless remain coherent and preserve their outline (e.g. Ui and Glicken 1986; Ui 1989; Glicken 1991; Palmer et al. 1991; Tost et al. 2014).

3. The interior of VDADs is composed of fragmented debris produced by the fracturing, disaggregation and comminution of the original material (Roverato et al., 2015), and jigsaw-fractured but relatively coherent blocks (Shreve, 1968; Glicken, 1991). Their component parts are usually angular to very angular (Glicken, 1991; Roverato et al., 2011).

4. Poor mixing of the incorporated lithologies and sedimentary units often leads to the preservation of original stratigraphy (remnant stratigraphy) and areas of distinct lithologies within the deposit (e.g. Shreve, 1968; Siebert, 1984; Ui and Glicken, 1986; Glicken, 1996; Belousov et al., 1999; Voight et al., 2002; Roverato et al., 2015). Source stratigraphic sequence is locally retained despite long runout distances (further discussed in Chapters 4 and 5), and shear bands, faults, and block-in-matrix fabrics being common features (Siebert, 1984; Glicken, 1991; Davies and McSaveney, 2009).

5. Due to the poor mixing and its uneven distribution, VDADs exhibit a high hetero-

geneity in terms of lithology, texture, sedimentology and degree of disintegration even at the small scale of a single block (Glicken, 1996; Bernard et al., 2008).

6. The surface of VDADs displays hummocky topography and longitudinal and transverse ridges (Siebert, 1984; Glicken, 1991; Bernard et al., 2008; Paguican et al., 2014). Levees sometimes form on the sides of the flow, as is the case for the Mount St. Helens (USA) 1980 VDAD (Voight et al., 1983) and Socompa (Chile) (Francis et al., 1985). The surface hummocks in the topography of VDADs is a characteristic feature (Ui, 1989). The size of the hummocks tends to decrease away from the axis of the deposit, however, their density increases towards the margins (Siebert, 1984). The hummocks often, but not always, contain blocks, and some of them are only composed of one block (fig. 3.1) (Siebert, 1984; Paguican et al., 2014; Procter et al., 2021).

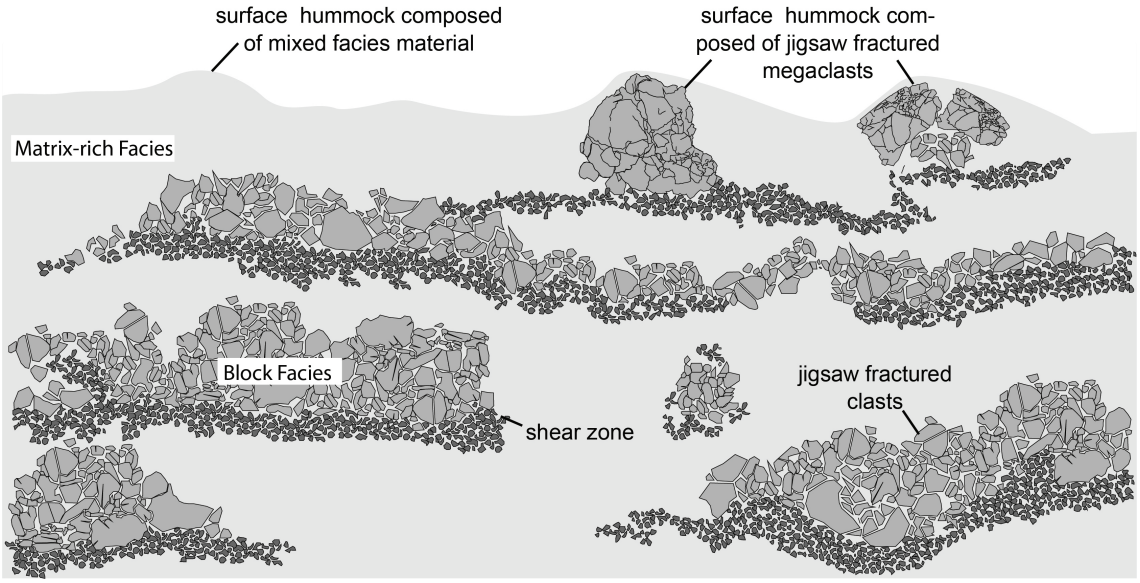

Figure 3.1: Schematic representation of debris avalanche deposit (modified after Roverato et al., 2015; Dufresne et al., 2016a; Bernard et al., 2008).

Other than these general features, lithology has a major control on the structure and sedimentology of the VDADs (and RAs - Dufresne et al., 2017), as further discussed in this thesis in Chaptre 4 and 5.

Moreover, using a first-order classification, VDADs can be divided into two distinct facies. A facies is typically characterised by a property that is common among its members, but unique among other areas of the deposit (Cas and Wright, 1987). The main body of

VDADs is subdivided into the end member block facies (after Ui, 1989; Glicken, 1991) and the matrix-rich facies (after Roverato et al., 2011; matrix/mixed facies in previous VDA literature after Glicken, 1991) (Ui, 1983; Ui and Glicken, 1986; Glicken, 1991; Siebert et al., 1995). However, distinction into these facies is not always simple due to the variable degree of disaggregation and shearing, producing a chaotic architecture that is difficult to categorise. The block and matrix-rich facies are not horizontally continuous or homogenously distributed; but rather characterise the location of different lithologies, blocks, and matrix within the body of a VDAD. Thus they can be present in proximity to each other (fig. 3.1). The two facies are described below:

3.2.1 Matrix-rich facies

The matrix-rich facies (mixed facies prior to Roverato et al., 2011, matrix facies prior to Glicken 1991) consists of a very poorly sorted, heterolithic mixture of clasts and a fine interblock matrix. The matrix is derived from different material of the source volcano as well as juvenile material and material incorporated during propagation from the path (Ui, 1989; Glicken, 1991) forming a heterogeneous matrix of sand-silt grain sizes. The facies also includes some matrix-rich facies blocks (Bernard et al., 2008). A clast refers to any rock which would not break if passed through a sieve or was immersed in water, after the definition by Glicken (1991). However, a block in a portion of the original edifice transported and deposited within the matrix wihtoug becoming disaggregated, even though it is composed of multiple clasts and potentially matrix. Particle sizes (including clasts and matrix) range from micrometres to metres in size (Glicken, 1991). The material in this facies lacks grading and stratification (Ui, 1989). Laminations, stretched clasts and injections in cataclased blocks in the matrix-rich facies indicate its motion during the propagation (Bernard et al., 2008).

3.2.2 Block facies

The block facies is composed of monolithological/polylithlogical unconsolidated, or poorly consolidated, portions of the original edifice (referred to as blocks) that collapse, propagate within the VDA and become emplaced to their position in the deposit (Glicken, 1991) unmixed with the surrounding material, thus retaining lithological distinctness (Bernard et al., 2021). Such blocks are composed of better-preserved, more intact material

(Glicken, 1991, 1996; Bernard et al., 2021) which might preserve original stratification, intrusive contacts or other features (Ui, 1989; Roverato et al., 2015). The material originates from the source edifice or is incorporated from the substrate during propagation. Blocks can be up to hundreds of meters in size (Glicken, 1991) and are often partially deformed and jigsaw fractured (Ui and Glicken, 1986). For typical metre-sized blocks, few clasts preserve their original texture (Glicken, 1991). There are few intrablock features such as incomplete mixture material (Bernard et al., 2008). Blocks greater than one metre in diameter are common in most VDADs, however, they are lacking in some, such as the VDADs of Mount St. Helens (USA) (Glicken, 1996) and Chimborazo (Ecuador) (Bernard et al., 2008).

Other than the relatively well-preserved block component, fracturing, partial disaggregation and mixing of the material within a block can generate an intrablock matrix (e.g. Roverato et al., 2015; Bernard et al., 2021). Like the interblock matrix of the matrix-rich facies, the intrablock matrix is composed of heterolithic clasts within a heterolithic matrix. Although the degree of mixing within the intrablock matrix exhibits some variability it is always lower than the interblock matrix, which is completely mixed. The lithology of the clasts and matrix represents the lithologies in the vicinity, within each block, as will be discussed in Chapters 4 and 5. The intrablock matrix (as well as the intrablock) exhibits no internal structures or features.

In addition to the two facies, VDADs exhibit shear zones (fig. 3.1) with finer particles but with the same lithology as neighbouring blocks (Smyth, 1991; Roverato et al., 2015; Roberti et al., 2017). The easier pulverisation of weak volcanic material like vesicular scoria is likely to encourage the formation of a sand-rich matrix as Roverato et al. (2015) suggest is the case for the Pungurehu VDA (New Zealand). This fine matrix allows the formation of irregular shear zones. These are thought to act as corridors of shear accommodation around more coherent domains that are less exposed to shear, as illustrated in fig. 3.1, thus dictating where particle disaggregation is concentrated and any present fluids are focused. The protected sections are consequently deposited as the observed block facies (fig. 3.1) (Roverato et al., 2015).

Jigsaw-fractured blocks and source stratigraphy are also retained in rock avalanche (RA)

deposits despite long runout distances, and shear bands, faults, and block-in-matrix fabrics are also common features (Davies and McSaveney, 2009; Weidinger et al., 2014; Dufresne et al., 2016b; Crosta et al., 2017). However, VDADs appear to contain larger proportions of matrix and areas of mixing, with preservation of source stratigraphy generally restricted to the large blocks (Dufresne et al., 2021). Clast-size distribution bidispersity has been reported, at least locally, for VDADs as well as RA deposits (Yarnold, 1993; Dufresne and Dunning, 2017) as will be discussed in this thesis. RA deposits additionally exhibit a carapace surface facies not observed in VDADs. The carapace is a top armouring of the deposit that is composed of large boulders. This layer is relatively thin and often exhibits inverse grading (Dufresne et al., 2018). Nonetheless, the most notable sedimentological difference between VDA and RA deposits is their lithological composition. Volcanic slopes contain large proportions of unconsolidated pyroclastic products and hydrothermally altered material, which are less competent and more likely to disaggregate towards a granular mass (Dufresne et al., 2021). This is a theme that will be evaluated in this thesis in Chapters 4 and 5.

3.3 Sedimentary and structural characteristics of lahars

Lahar deposits are characteristically flat-topped (Crandell 1971; Glicken 1991; Palmer et al. 1991). The marginal edges of the deposit grade into the substrate without forming steep slopes (Ui 1989). In terms of internal structure, lahar deposits are massive, compact and consist of very poorly sorted fragments of the original mass (Vallance and Iverson 2015). More dilute lahar deposits are more similar to fluvial sand and gravel deposits (Crandell 1971). Lahar deposits are very homogenous (Vallance 2000; Vallance and Iverson 2015), lacking fractures and fault surfaces (Ui 1989). This lack of internal features is a diagnostic characteristic along with an abundance of air spaces in their matrix (Crandell 1971; Vallance and Iverson 2015). They may contain structurally intact boulders (unfractured compact single clasts) surrounded by the finer-grained material, but not fractured (or jigsaw-fractured) blocks (Ui 1989). Lahar deposits can be graded, especially if less dense material like pumice is present, which are concentrated at the top to form a lower density carapace (Vallance 2000). Also, larger boulders are concentrated at the top of the deposit, contributing to the reverse-grading (e.g. Pierson and Scott 1985; Ui 1989; Saucedo et al. 2008). However, normal grading with coarse material at the base and finer at the top has

also been observed, at least locally, in some lahars (e.g. Crandell 1971; Pierson and Scott 1985b; Vallance and Scott 1997; Saucedo et al. 2008).

3.4 Data sources and method

This study provides a semiquantitative assessment of the GSD of VDA and lahar deposits, through the examination of nine VDADs and eight lahar deposits through data assembled from published studies. These volcanic mass-wasting flows were selected because detailed studies of their sedimentology are available. All the events present long runouts and low H/L ratios (table 3.1). Other case studies were also considered but could not be included as the desired statistical descriptors or the raw sedimentological data for their calculation were not available. For the Cotopaxi VDAD, raw sedimentological data were kindly provided directly by the authors (Vezzoli et al. 2017). Data included for VDADs are from both the matrix-rich and the block facies and are labelled appropriately where fitting. The events, their authors and their properties are listed in table 3.1.

Table 3.1: Events considered in this study. Note that some are related either geographically (bold, enclosed in thicker border), or both geographically and temporally (same shade colour).

Type	Location	Sampling	Age	Runout	Volume	Water content	H/L	Source
DA	Pungarehu, Taranaki Volcano, NZ	several samples from each locality to cover all lithofacies, 13km length covered	25 ka	>27km	>7 km^3	incorporated snow, ice and substantial groundwater	<0.09	*Roverato et al., 2015*
DA	Shiveluch Volcano, Kamchatka, RS	samples from block facies, 10km length covered	multiple DADs	>15km	1.5 km^3	high	0.133	*Belousov et al., 1999; Hayashi and Self, 1992*
DA	Cubilche, EC	outcrops few and concentrated	>30 ka	>20km	>3–3.5 km^3	initial low content <10%, increasing during propagation	0.063	*Roverato et al., 2018; Pierson and Costa, 1987*
DA	San Marcos, Colima, MX	sampled along the deposit	>28 ka	22.55km	~1.3 km^3	<10%		*Roverato et al., 2011*
DA	Tonila, Colima, MX	sampled along the deposit	15–16 ka	23.01km	~1 km^3	high		
Lahar	Montegrande ravine, Colima, MX	sampled along the deposit	15/09/2012					*Vàzquez et al., 2014*
DA	Acajutla, Santa Ana Volcano, SV	sampled along the deposit	<57 ka	~50 km	16 ± 5 km^3	very high - some areas classified as a cohesive debris flow	>0.05	*Siebert et al., 2004*
DA	Rio Pita, Cotopaxi, EC		4 ka	21km	2.1 km^3	local partial saturation	0.12	*Smyth, 1991*
DA	**Cotopaxi**, EC	data from different facies in the same area	4.5 ka	20km	~2 km^3	not significant		*Vezzoli et al., 2017*
Lahar	Chillos Valley, **Cotopaxi**, EC **(evolved from Cotopaxi DA)**	sampled along northern and southern flow paths		326km	3.8 km^3	melted icecap saturated the material to generate the lahar		*Mothes et al., 1998*
Lahar	**Cotopaxi**, EC	one sample location, samples from different events	multiple, post-1150 AD			water released from summit glaciers with different mechanisms		*Pistolesi et al., 2013*
DA	**Mt St Helens**, USA	sampled along the deposit, different facies	18/05/1980	29km	2.9 km^3	0.31 km^3, 11%	0.106	*Glicken, 1996*
Lahar	Toutle River, North Fork, **Mt St Helens (evolved from Mt St Helens DA)**	sampled along the deposit						*Scott, 1988*
Lahar	Toutle River, South Fork, **Mt St Helens (evolved from Mt St Helens DA)**							
Lahar	Toutle River, **Mt St Helens**, USA	sampled along the deposit	19/03/1982	83km		Eruption of the volcano released a flood of water from the cater, 4x$10^6$$m^3$	0.06	*Pierson and Scott, 1985*
Lahar	Popocatépetl, MX	sampled along the deposit	2001	>15km		<25%		*Capra et al., 2003*
		sampled along the deposit	1997		3.3 x$10^5$$m^3$			

Sample strategies and analyses vary in these studies since the examination of the evolution of GSD was not the original aim of the data collection campaigns of the published works, however, trends can be extracted for each event independently. In particular, events in Cotopaxi, Colima and Mount St. Helens are significant as, lahars and VDA are available

representing different types of mass-wasting flows composed of similar material. The Cotopaxi lahar data are not used for longitudinal evolution analyses because they are all collected from the same location. In other cases, where a specific statistical descriptor is used that could not be obtained for some events, these events are not included in that specific analysis. It should also be noted that in the paper of Glicken (1996) describing the Mount St. Helens VDAD, the distances of the sampling sites from the source are overestimated by a factor of 1.6 throughout the paper (probably due to an error in conversion from miles to kilometres). This is evident by the location of the sampling sites on the map in plate 4 of that publication. This is mentioned so that the valuable findings of the study are correctly interpreted.

The parameters used for the characterisation of the deposits are the statistical descriptors: median grain size, sand, gravel and silt and clay particle fractions, skewness and sorting. Grain size fractions are chosen because comparison of their distribution and abundance can allow the evaluation of the comminution processes and any preferential comminution of size classes. The sizes of each class are defined according to the Wentworth (1922) classification. In particular, the sand range coincides with the size of interest for the fine material commonly used in relevant studies of VDA and lahars deposits (e.g. Scott, 1988; Vallance and Iverson, 2015). Inclusive graphic sorting (σ) and skewness (sk_1) of Folk (Folk and Ward 1957; Folk 1968) are used for all events except Shiveluch VDA (Belousov et al. 1999) and Acajutla VDA (Siebert et al. 2004), where they were not available. In these two cases, Inman (1952) statistics are used instead, which although might not be directly comparable, can still reveal trend within the same deposit. The sorting coefficient (σ) describes the range in size required to encompass a given majority of the population around the mean. A low sorting coefficient thus describes a population with little spread around the mean. A higher sorting coefficient indicates that the population is spread over a larger range of sizes. A verbal classification from very well sorted to extremely poorly sorted was introduced by Folk (1968) and is presented in table 3.4. Folk skewness (sk_1) measures the degree to which the population approaches symmetry, and (in contrast to Inman) includes a measure of the "tail" (material outside the mode of the distribution) of the population. Positive skewness describes populations with large proportions of fine material (fine-skewed) and a tail in the coarser range of sizes; and negative skewness the opposite (coarse-skewed). A skewness of zero would describe a symmetrical distribution. Higher values describe progressively more fine-skewed

Table 3.2: Sorting classification (Folk 1968)

Sorting value (ϕ)	Sorting classification
$0.00 - 0.35$	Very well sorted
$0.35 - 0.50$	Well sorted
$0.50 - 0.71$	Moderately well sorted
$0.71 - 1.00$	Moderately sorted
$1.00 - 2.00$	Poorly sorted
$2.00 - 4.00$	Very poorly sorted
> 4.00	Extremely poorly sorted

distributions. A verbal classification of skewness by Folk (1968) suggests sk_1 values from +0.1 to -0.1 as nearly symmetrical, -0.1 to -0.3, fine-skewed and -0.3 to -1.0 as strongly coarse-skewed, and the opposite for fine-skewed populations.

3.5 Results - Grain Size Analysis:

3.5.1 Median grain size

Comparison of both median grain sizes of VDADs and lahar deposits demonstrates that the average grain size for lahars is consistently lower than VDADs, after the most proximal (~5-6km) parts of the deposits (fig. 3.2). The median grain size of lahars demonstrates a rapid decline at these initial stage, and then slowly becomes finer. Although there is some overlap, lahars are consistently at the finer-grained end of the overall population. In the Mount St. Helens VDAD and lahars originating from the same event and material, the GSD of the lahars is always finer.

Analysis of the longitudinal evolution of the median grain size in VDADs shows a constant grain size with no obvious trend. Lahars, on the other hand, show a fining (previously identified by Pierson and Scott 1985; Scott 1988) both individually as well as in the combined population in fig. 3.2.

3.5.2 Silt and clay, sand and gravel particle content

With decrease in median grain size, there is a decrease in the gravel content of the mass, and an equivalent increase in the sand component, both in lahars and VDADs (fig. 3.3a and b). Conversely, there is only a minor increase of the silt and clay component in both lahars and VDADs (fig. 3.3c). The silt and clay content only reaches percentages greater than 20% in a few very fine samples.

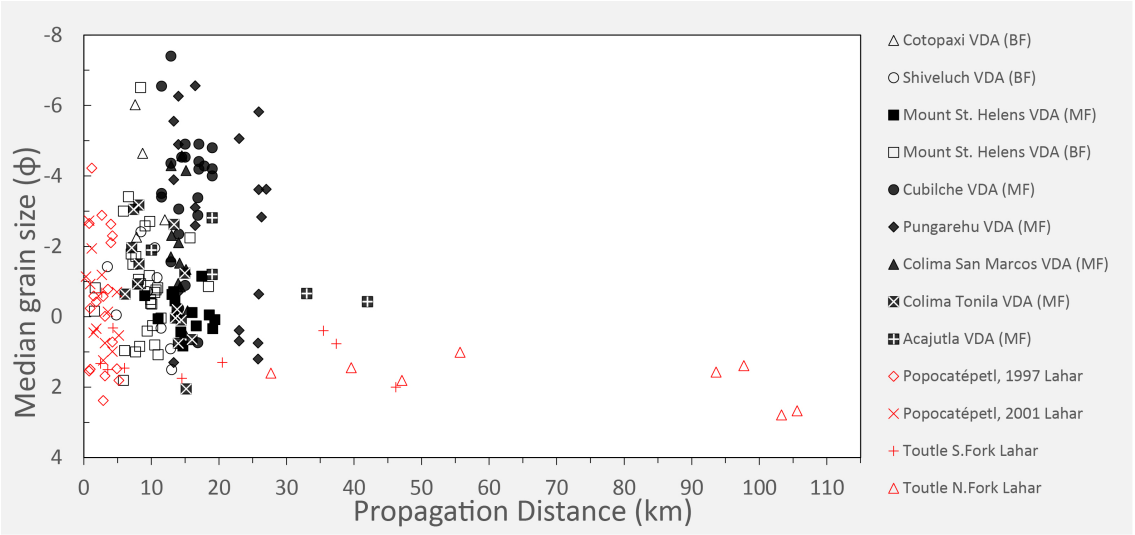

Figure 3.2: Evolution of the grain size distribution of volcanic debris avalanches (VDAs) and lahars with propagation distance. Note that the x-axis is inverted so that size increases up the axis. (MF: Matrix-rich facies; BF: Block facies)

3.5.3 Sorting

The majority of both VDAD and lahar samples are very poorly sorted (σ= 2 to 4). Several VDAD samples are extremely poorly sorted (σ>4), and very few are poorly sorted only from the Rio Pita VDA (fig. 3.4b). With decreasing grain size the sorting of lahars improves and thus a decrease of the sorting coefficient is observed (fig. 3.4a). This implies that their GSD becomes more concentrated around the mean and is less spread in terms of the grain size range. For lahars, this trend is consistent in all the lahars where data was available. This trend is not exhibited by the VDADs (fig. 3.4b).

3.5.4 Skewness

Skewness data for VDADs exhibits a consistent decrease of skewness from positive to negative with decreasing median grain size (fig. 3.5b). This signifies that initially, coarser material composes the majority of the mass with the finer particles generating a 'tail' in the GSD. Progressively, comminution generates more fines that become the majority of the GSD; however, a significant coarse component is preserved as a tail. This evolution is common in all VDADs (fig. 3.5b). In lahars, an evolution towards negative skewness is not consistent in all events examined (fig. 3.5a), indicating that a coarse tail is not generated in the GSD.

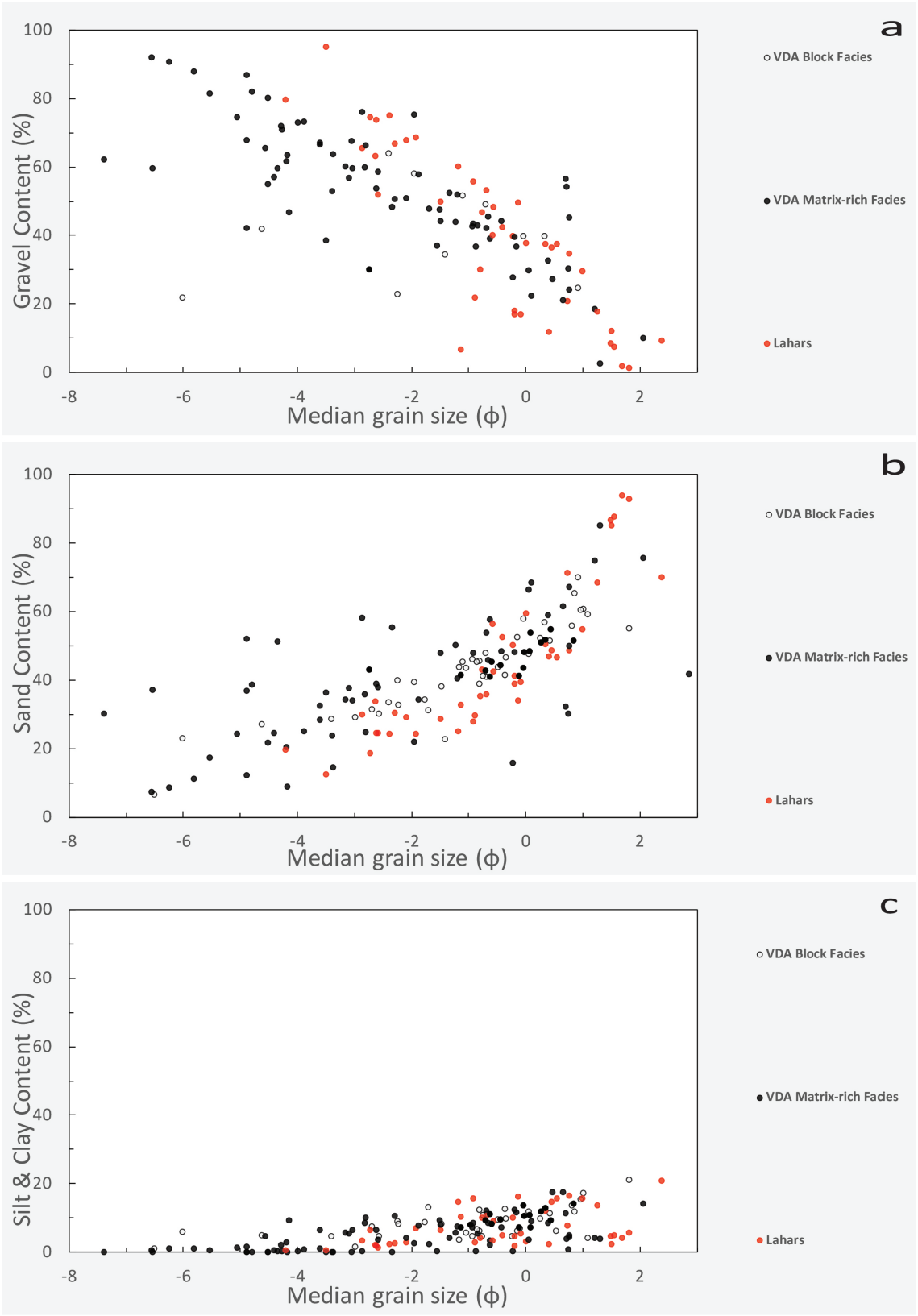

Figure 3.3: The evolution of specific grain size range component of the mass with decreasing median grain size: **A** gravel, **B** sand, **C** silt and clay in volcanic debris avalanche (VDA) deposits and lahar deposits.

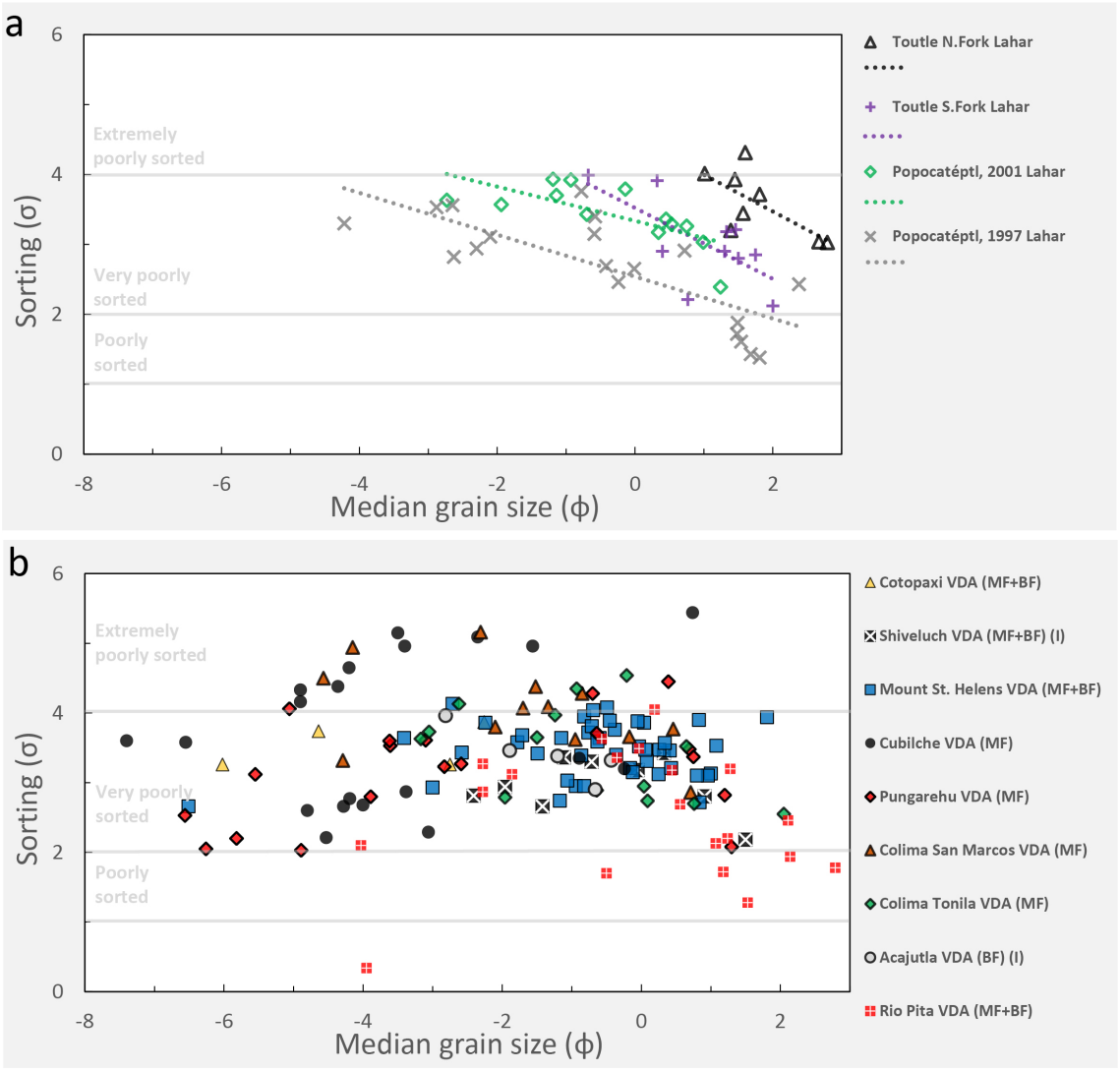

Figure 3.4: Median grain size versus sorting for: **A** lahars, and **B** volcanic debris avalanches (VDA) (MF: matrix-rich facies, BF: block facies, I: Indicates where Inman (Inman 1952) statistics were used; in all other cases Folk and Ward (Folk and Ward 1957; Folk 1968) statistics are used.

3.6 Discussion

3.6.1 Volcanic Debris Avalanche Deposits (VDADs)

The GSD data for VDADs show that as the median grain size decreases, the sorting remains largely unaffected in the very poorly sorted range (fig. 3.4c), skewness decreases and progressively becomes negative (fig. 3.5b), and there is an exchange between the gravel and sand component with very little increase in finer particles (fig. 3.3). The VDAD GSD evolution of the skewness from positive to negative, that has been previously identified by Dunning (2004), suggests that although progressive comminution reduces the size of the coarse gravel that is initially the majority of the material, a substantial amount of the coarse

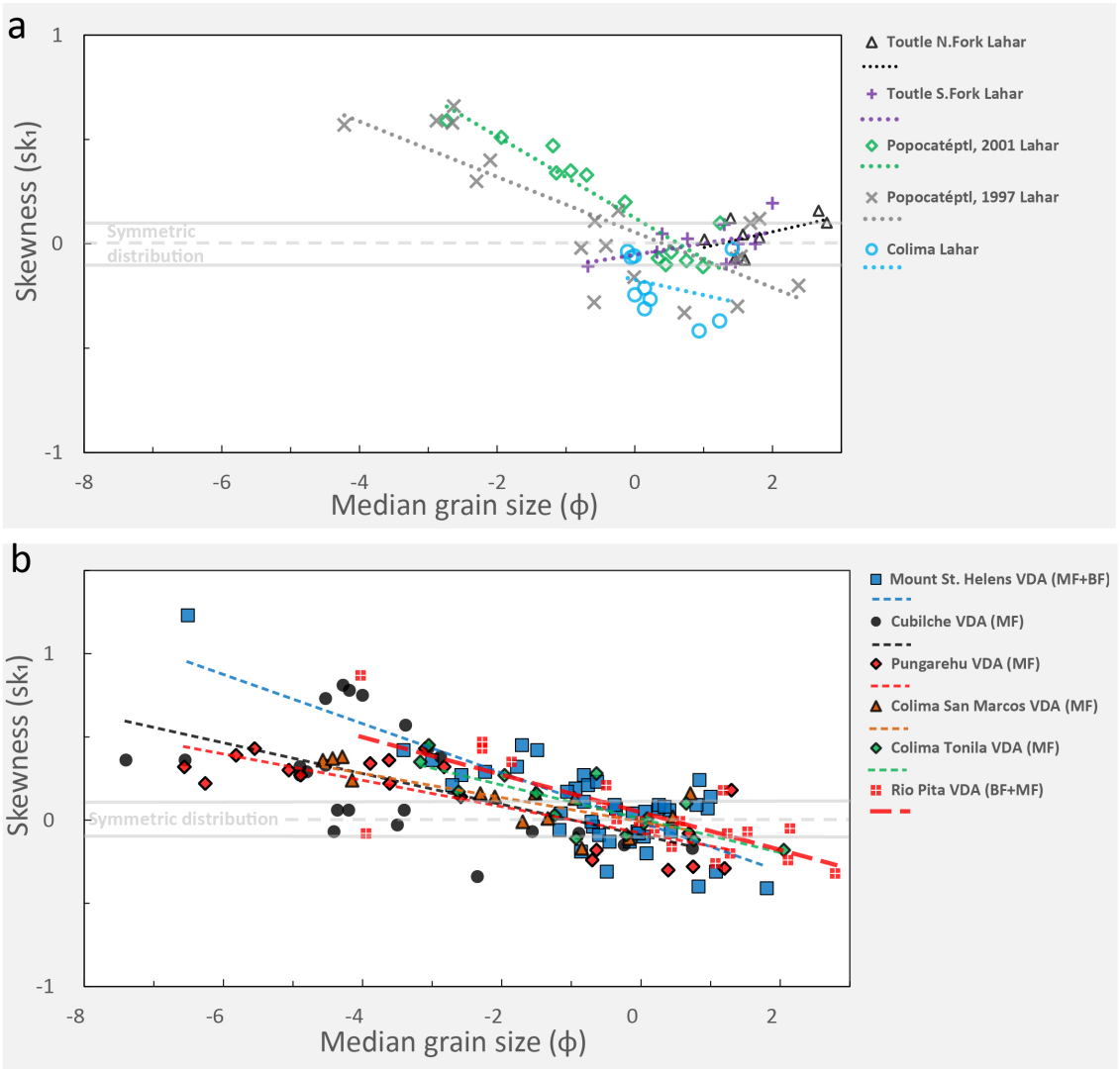

Figure 3.5: Median grain size versus skewness for: **A** lahar deposit, and **B** volcanic debris avalanche (VDA) deposits (MF: matrix-rich facies, BF: block facies).

particles is preserved. This is confirmed by the GSD histograms of VDADs as presented in fig. 3.6a that suggests that a coarse mode is preserved as a second mode develops in the sand size range with fining. This supports that there is preferential comminution of the finer grains because fragmentation of larger particles requires collision with grains of equal or larger size, assuming equal strength, as previously proposed by Davies and McSaveney (2009). The lack of a trend in sorting is also in agreement as sorting which describes the spread of the data around the mean of the population cannot represent the two modes generated. This phenomenon is also supported by the experimental findings of Hörz et al. (1984) who observed the evolution of the GSD of a rock sample after repeated impacts that caused comminution to the original rock mass. The authors observed the evolution of their particle population from positive to negative skewness with more impacts and comminution; meaning that more fines were produced with time while coarser particles

were preserved in the mass, in agreement with the data present study. The analogue experiments of Caballero et al. (2014) further explore this relationship in granular flows generally and suggest that while coarse particles develop small fractures, contributing sharp edges as fine particles to the overall population, medium-sized particles can develop through-fractures, thus contributing fines and depleting the medium-size range with their comminution. This results in the observed bimodality, as well as the peak in the GSD, observed for many of the deposits in correspondence of the sand-size range. The preference for further fragmentation of medium size particles into finer ones, because they require less energy, leads to the preservation of the larger particles throughout the length of DAD, which is also consistent with geomorphic observation (e.g. Glicken, 1996; Roverato et al., 2015). Roverato et al. (2018) suggest that in the case of the Cubilche VDA, the matrix was generated by the continuous disintegration of existing fractures into finer particles whereas coarse ones were preserved. Such facies development was also documented in non-volcanic RAs by Dufresne et al. (2016a), who identified this evolution from proximal to distal sample locations including the progressive fining of smaller clasts and preservation of large 'survivor clasts'. Also, in experiments of crushing granular materials, large sizes are always preserved and are never lost despite continued shearing and crushing (Lade et al. 1996; Einav 2007).

The combined data from the studies illustrate an exchange between the gravel and sand content of the samples as they become finer (median grain size), while there is only a minor increase in the silt and clay content (fig. 3.3). Other studies also report high proportions of particles in this size range in volcaniclastic deposits of intermediate and silicic composition from different parts of the world (Glicken, 1996 and references therein); as well as the lack of silt grade material or finer observed in VDADs (Roverato et al. 2018). These offer support that the preferential fracturing and comminution stop when the particles reach a sand size (-1ϕ to 4ϕ). This is because in volcanic environments at this size they are often composed of a single crystals of plagioclase, amphibole, and pyroxene in the -1ϕ to 3ϕ range (Davies et al. 1978). Particles and fragments produced by comminution just larger than -1ϕ likely consist of more than one crystal and are thus more easily broken than individual crystals. Therefore, particles classified in the sand-size range are often preserved.

The GSD data also suggest an evolution towards negative skewness (fig. 3.5b) and a

bimodality is observed in GSD histograms as also recognised in literature (Ui and Glicken 1986; Siebert 2002)(fig. 3.6a). Glicken (1996) state that the matrix facies of the Mount

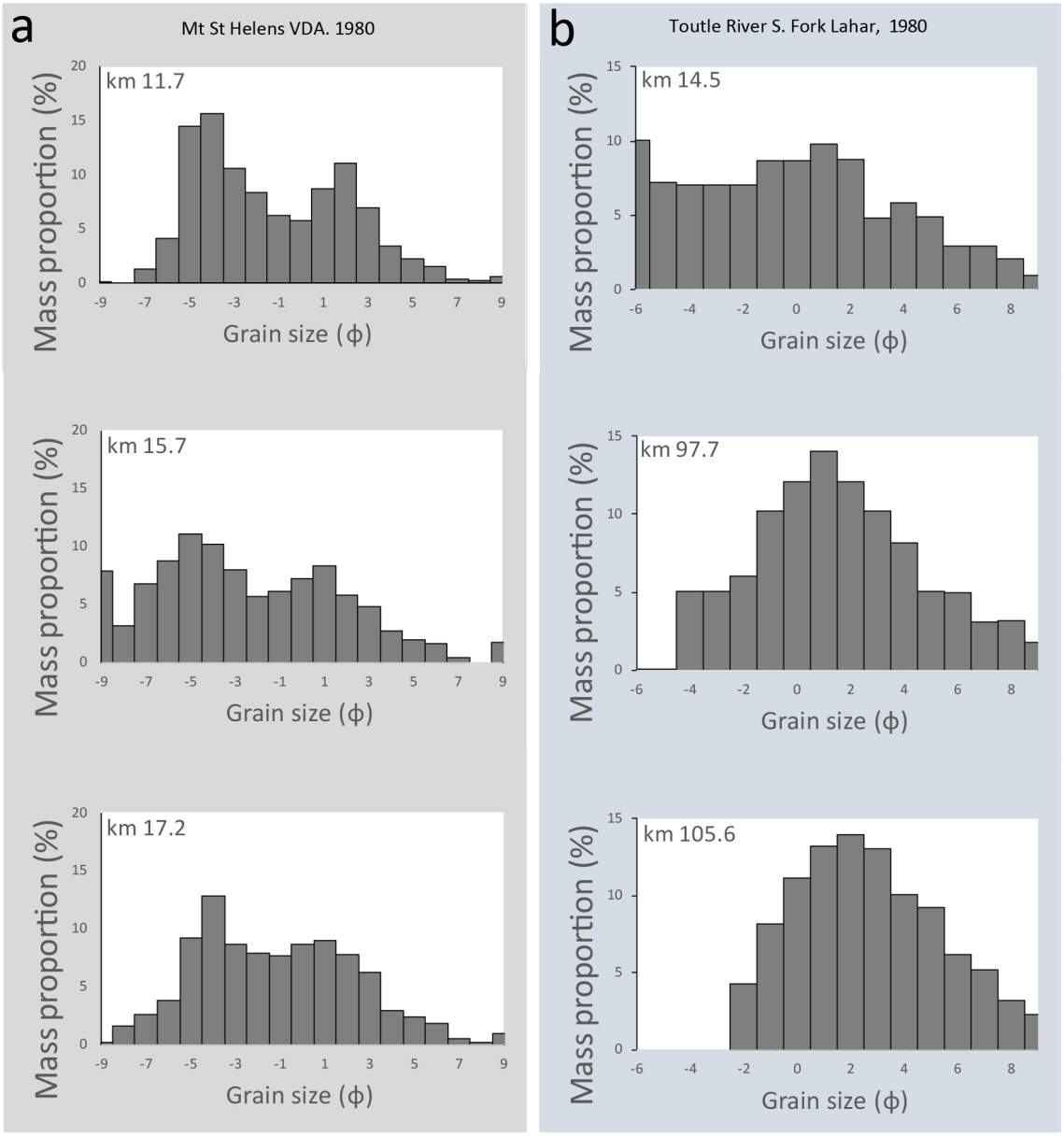

Figure 3.6: Grain size distributions from: **A** Mount St. Helens 1980 volcanic debris avalanche (VDA) (Glicken 1996), and **B** South Fork Toutle River Lahar (Scott 1988). Data are from different locations indicated by the distance from the source (in km) at the top left of each plot.

St. Helens VDAD is in most areas characterised by a bimodal distribution with the fine-grained peak in the histogram between -1ϕ and 3ϕ (gravel); and the maxima of this peak typically lying between 0ϕ and 2ϕ (sand). The Cubilche VDAD was divided into different lithological units for analysis by Roverato et al. (2018) and bimodal distributions are generally exhibited in all the units. The less fragmented sections exhibit the coarse mode between -8ϕ and 7ϕ (gravel), while the fine mode is between -3ϕ and -1ϕ (gravel).

However, when also considering the interclast matrix, the highest percentage of the samples is gravel (-8ϕ to -2ϕ) and sand (-1ϕ and +4ϕ). The increase of the sand to generate a mode and bimodality in the GSD of the samples that have experienced more fragmentation agrees with the hypothesis that the propagating mass will progressively evolve towards a larger sand-sized component during propagation (Glicken 1996). As the interclast matrix experiences more shear, and therefore comminution, sand particles increase disproportionally to finer particles. The simultaneous increase in the sand-size component and preservation of the coarsest particles generates the bimodality in such deposits with the finer mode of the distribution in the sand-size range. The coarse mode is likely to be a function of the source material and lithology as the size of the larger clasts that will be preserved is likely to be a function of the original lithology. The observed negative skewness represents this preservation of a significant component of coarse particles as a tail to the population.

For the VDADs the longitudinal evolution of the median grain size appears to not follow a trend; even though progressive comminution of particles is typically observed and reported downslope along VDADs in the literature (e.g. Perinotto et al. 2015; Roverato et al. 2015) (fig. 3.2). The record of this process will theoretically be the progressive grain size reduction, within each facies, with increasing distance from source (Dunning 2004). The lack of a trend might reflect the heterogeneity of the deposits and the fact that the sampling strategies were not designed to reveal this fining. Glicken (1996) interprets the lack of fining to signify the lack of major fracturing of the clasts progressively during transport, and that fracturing occurs mainly near the source. The author suggests that since the trend is not visible in the data, clast-to-clast interactions that resulted in fracturing must have not been a major occurrence during transport. This could also be the impact of a high water content filling pores, increasing pore pressure and limiting particle interactions. However, sampling each facies individually is necessary to confirm these hypotheses as also suggested by Dunning (2004), Dufresne et al. (2016) and Dufresne and Dunning (2017). Moreover, bulldozing and incorporation of material along the flow path can interfere with these processes and affect the GSD, especially with samples from basal facies (Bernard et al. 2008) (although no samples from basal facies are included in this study).

3.6.2 Lahar deposits

The lahar GSD data from the literature presented show a decrease of the median grain size with propagation distance and an improvement in the sorting of lahars with decreasing median grain size (fig. 3.5a), as is also reported by Pierson and Scott (1985) and Scott (1988). This is perhaps easier for the sampling strategies to expose because of the higher homogeneity of lahar deposits (Vallance 2000) owing to greater mixing during propagation compared to VDAs (Pierson and Scott 1985; Glicken 1991; Siebert 2002). GSD histograms of lahars illustrated in fig. 3.6b and 3.7 show a progressive removal of the coarsest particles; a process described by Pierson and Scott (1985). The deposition of the coarsest particles eliminates any initial bimodality in the material if they were previously deposited by VDAs as illustrated in fig. 3.7 with gradual loss of the bimodality of the Toutle River N. Fork Lahar (Scott, 1988). This evidence suggests the process of debulking and progressive deposition of the coarsest particles in the mass (Pierson and Scott 1985). Debulking is the process where as the lahar becomes progressively more dilute, it becomes less capable to transport the coarsest particles which are preferentially deposited, resulting in decreasing sediment concentrations, and median grain size with propagation distance (Fisher et al. 1984; Pierson and Scott 1985; Vallance 2000). The water content increases and sediment concentration decreases as lahars evolve from debris flow to a more hyperconcentrated flow. And in the distal phases, they can approach more alluvial-type processes (Vallance 2000). Although there is abundant evidence of cataclasis in lahar deposits, debulking is the process more likely to be responsible for the fining observed in their depositional phase when they become more dilute (Pierson and Scott 1985; Vallance 2000). The improvement of sorting is the result of the narrowing of the distribution of the histogram as the coarsest particles are removed. The improvement in sorting of the Mount St. Helens North and South Fork, Toutle River lahars by the narrowing of the range of the GSD can be observed in fig. 3.6b and fig. 3.7 and described by Pierson and Scott (1985). However, Vallance and Iverson (2015) and Vallance (2000) report that the bimodality can also be preserved in some sections of lahars.

The skewness of lahar GSD does not exhibit a trend (fig. 3.5a). However, the content of gravel and sand show an exchange between them, while there is little increase in finer particles (fig. 3.3).

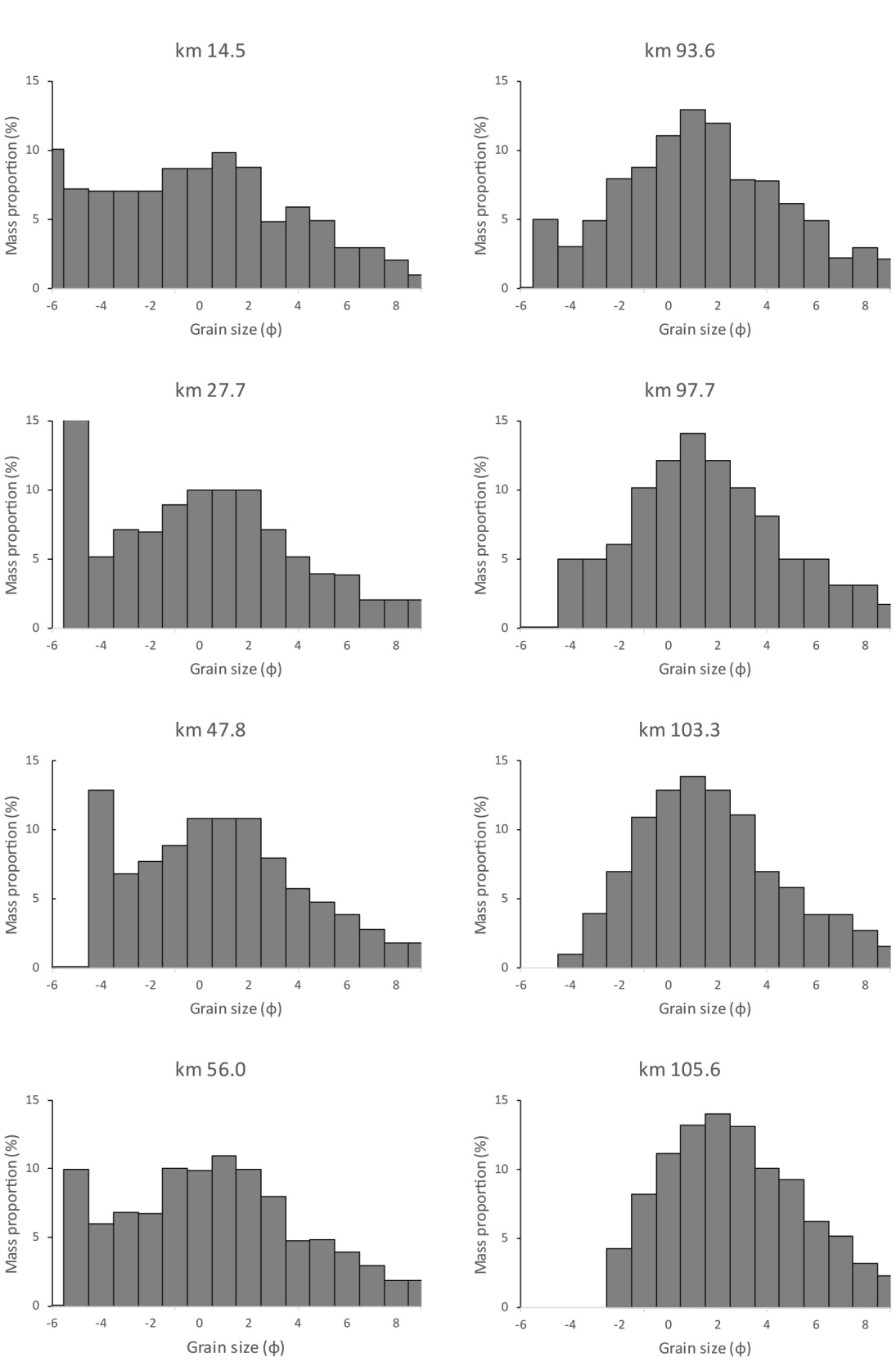

Figure 3.7: Grain size distribution histograms from the North Fork Lahar (Scott 1988). Data are from different locations indicated by the distance from the vent (in km) at the top of each plot.

3.6.3 Comparison

Geomorphologically, lahars and their deposits display considerable differences to VDADs due to different conditions and propagation processes generated mainly by the higher water content of lahars (Ui 1989; Smyth 1991; Iverson 1997; Scott et al. 2001; Siebert 2002). Saturated lahars involve strong turbulence and mixing of the incorporated sediment (Pierson and Scott 1985; Glicken 1991; Siebert 2002). This results in more homogeneous deposits where original stratigraphy is not preserved as recognised by Ui (1989) and Vallance (2000).

As the material becomes finer in VDADs, skewness becomes progressively lower and shifts from positive to negative, as coarse material is preserved in the mass to generate a bimodality. In lahars, histograms suggest a progressive preferential removal of the coarsest range of the GSD histogram, as described by Pierson and Scott (1985) and shown in fig. 3.6b and fig. 3.7, leading to an improvement in sorting (fig. 3.4a) (Pierson and Scott 1985), but not always generating an effect on skewness (fig. 3.5a) as the data presented by this study suggest. The observed patterns suggest that the process of debulking (Vallance 2000) is responsible for the fining and reduction of median grain size observed in lahars. The coarsest particles are progressively preferentially deposited (Pierson and Scott 1985) and the GSD becomes finer. The debulking of lahars is enabled because pore spaces are filled with water which acts as the transportation medium for the sediment (Smyth 1991).

Conversely, in VDAs, preferential fracturing of the finer particles means that a coarse mode is preserved even though the fine mode increases (fig. 3.6a). This leads to the skewness becoming progressively more negative (fig. 3.6b). The preferential comminution of particles coarser than sand (and preservation of sand-sized particles) (Davies et al. 1978), is evident by the lack of finer particles as the sand component increases (fig. 3.3). Therefore, in VDAs, fining is a result of progressive comminution.

GSD and bimodality as a factor for mobility might not be as important in lahars because water has a major role in lubricating the motion (Iverson 1997). Water is nearly incompressible compared to air and thus when it fills intergranular spaces it reduces the frequency and intensity of collisions and therefore energy dissipation (Glicken, 1996 and references therein). Therefore, saturated lahars with intergranular fluid pressure move

more efficiently than dry flows and are capable of much greater runouts (Iverson 1997; Denlinger and Iverson 2001). Due to water saturation, both liquid and solid interactions influence lahar behaviour, which fundamentally differentiates them from VDAs (Vallance and Iverson 2015).

3.6.4 Implications for the role of water

Some of the lahar deposits and VDADs compared by the present study originated from the same material (table 3.1); meaning that water content is likely to be the principal difference between them (Iverson 1997; Scott et al. 2001; Legros 2002; Griswold and Iverson 2007). These cases exhibit significant divergence in GSD. The findings support that the fining of lahars is the result of debulking of coarser particles enabled by water saturation of the propagating mass (Vallance and Iverson 2015). In the case of VDADs, fining is due to the comminution of the material, with progressive fragmentation of finer particles that require less energy (Davies et al. 1978). This process suggests frequent particle-particle interactions with no interstitial fluid.

The ability of VDAs to achieve runouts longer than expected by simple frictional models has led many authors to speculate that a fluid might be the agent reducing the dissipation of friction in the propagating mass (Kent 1966; Shreve 1968; Voight et al. 1983; Voight and Sousa 1994; reviewed in Legros 2002). As a fluidising medium, water is much more effective than air because of its properties making it much more incompressible (Legros 2002). Although it is suggested that VDAs are often not dry, they are likely only partially saturated (Legros 2002). However, in the case of the Mount St. Helens VDA Voight et al. (1983) argue that water had an important effect on propagation. The water would have been available from the ice-capping of the volcano, and the cone which was water-saturated prior to the event. There was also evidence of the water content in the deposit, in the form of lahars being generated hours after the deposition (Janda et al. 1981) and kettle holes from post-depositional melting of ice blocks (Voight et al. 1981). Crandell et al. (1984) considered that water was also important for the propagation of Mount Shasta VDAs. Examining the Rio Pita VDA, Cotopaxi, Smyth (1991) suggest that the volcano would have had an extensive snow cover and was affected by a wet weather system at the time of the event. They support that the mass was at least partly water-saturated. Also, VDAs such as at Shiveluch volcano (Belousov et al. 1999), Acajutla (Santa Ana volcano)

(Siebert et al. 2004), Pungarehu (Taranaki Volcano) (Roverato et al. 2015) and others are suggested to have included, or incorporated during propagation, significant amounts of water. Siebert (1984) supported that water is vital in weakening volcanic material and lubricating the flow of VDAs. Interstitial water can potentially locally reduce friction of a granular mass temporarily by partly supporting a fraction of the weight of the particles (Bagnold 1954; Legros 2002). The potential increase of pressure gradient in the fluid (even locally) could lead to support of solid loads and increase fluidity (Legros 2002). Voight et al. (1983, 1985) suggest that interstitial fluids and steam from heated water can at least locally contribute to buoyant forces and that enhanced mobility may be enhanced by the pressurized fluid-particle interactions.

However, in VDAs water is not present in quantities that enable it to become the transporting medium, as in lahars; or for complete fluidisation (Siebert 1984). As suggested by Smyth (1991) and by findings of the present study, water might have an impact on the mobility of VDA but is not the principal factor influencing propagation as is the case in lahars. In addition, present results showing the lack of debulking in VDAs suggest that water content is not sufficient to enable it and therefore that water does not become the transportation medium as it is in lahars. This confirms that particle-to-particle interactions as a leading role in the dynamics of VDAs.

3.7 Conclusions

This chapter carries out a quantitative assessment of the sedimentology of nine VDA and eight lahar deposits. The sedimentology is not only important for characterising the original mass, but the evolution of the sedimentology during propagation and emplacement can also provide evidence for the mechanisms and factors influencing propagation.

Descriptive statistics considered for the deposits are median grain size, sand, gravel and finer particle fractions, skewness and sorting. The decrease in median grain size of lahars is the result of debulking and progressive deposition of the coarsest particles. This is reflected in improved sorting due to the narrowing of the GSD can also be observed in the evolution of GSD histograms. Debulking is a process that is enabled because lahars are water-saturated and water is the transportation medium. In this case, particle-to-particle interactions are not as important for the evolution of the GSD as they are for VDAs.

In fact, data analysed here, suggest that particle-to-particle interactions during propagation in VDA are responsible for comminution due to fracturing, in agreement also with the findings of the authors of the considered studies. Results also suggest that preferential comminution occurs preferentially in finer particles as less energy is required. When particles reach sand-sized, further comminution stops and particles are preserved because they are often composed of single crystals (Davies et al. 1978). The combination of these processes leads to progressively more negative skewness and a bimodality developing in the GSD, with the finer mode composed of sand-sized particles as supported by geomorphic observations (Glicken 1996; Roverato et al. 2018). In addition, data show no evidence of debulking in VDAs confirming that the propagation mechanisms differ.

Although water content in VDAs might affect their propagation dynamics, present results on their GSD distribution characteristics confirm that they can be considered as dense granular masses where the effects of inertial interactions between solid fragments are more important than fluid effects. This demonstrates that particle-to-particle interactions are the main factor influencing the mobility of non-saturated mass wasting flows.

Chapter 4

The propagation and emplacement mechanisms of the Tenteniguada volcanic debris avalanche (Gran Canaria): Field evidence for brittle fault-accommodated spreading

Note, a version of this chapter examining the Tenteniguada volcanic debris avalanche and its propagation dynamics has been published in the Journal of Volcanic and Geothermal Research (Makris et al., 2023a). The published version is included in the supplementary material. Symeon Makris wrote the text, prepared all of the figures and developed the arguments therein. Symeon Makris, Matteo Roverato and Alejandro Lomoschitz carried out the fieldwork. All authors discussed the science and commented on the manuscript. The format of this chapter is not the same as the publication. Different sections have been integrated into different parts of this thesis. Furthermore, additional discussion relating to the topic of the thesis is included in this chapter that was not strictly relevant to the paper examining the specific deposit.

4.1 Introduction

This chapter examines the deposit of the Tenteniguada volcanic debris avalanche (Ten-VDA), located on the east of the island of Gran Canaria, Spain (fig. 4.1). This well-preserved and exposed deposit presents an opportunity to study internal structures and their distribution and sedimentology. The aim of this study is to evaluate the Ten-

VDA propagation and emplacement processes and the factors that controlled its material behaviour, structural evolution, stress accommodation and deformation history. The deposit is initially described by its structural and sedimentological features and specific outcrop properties. Their implications for the dynamics of the Ten-VDA are subsequently discussed, also in association to other volcanic debris avalanche deposits (VDADs) and theoretical and numerical models. The structural features of the Ten-VDAD and their evolution offer an insight into the dynamics of volcanic debris avalanches (VDAs) as they evolve from a slide of the initial edifice portion to a fluidised flow. Findings are relevant to VDAs composed of competent non-granular material, as well as other mass movements, such as rockslides, with the potential of further constraining their behaviour in conceptual models and contributing to the assessment of related hazards.

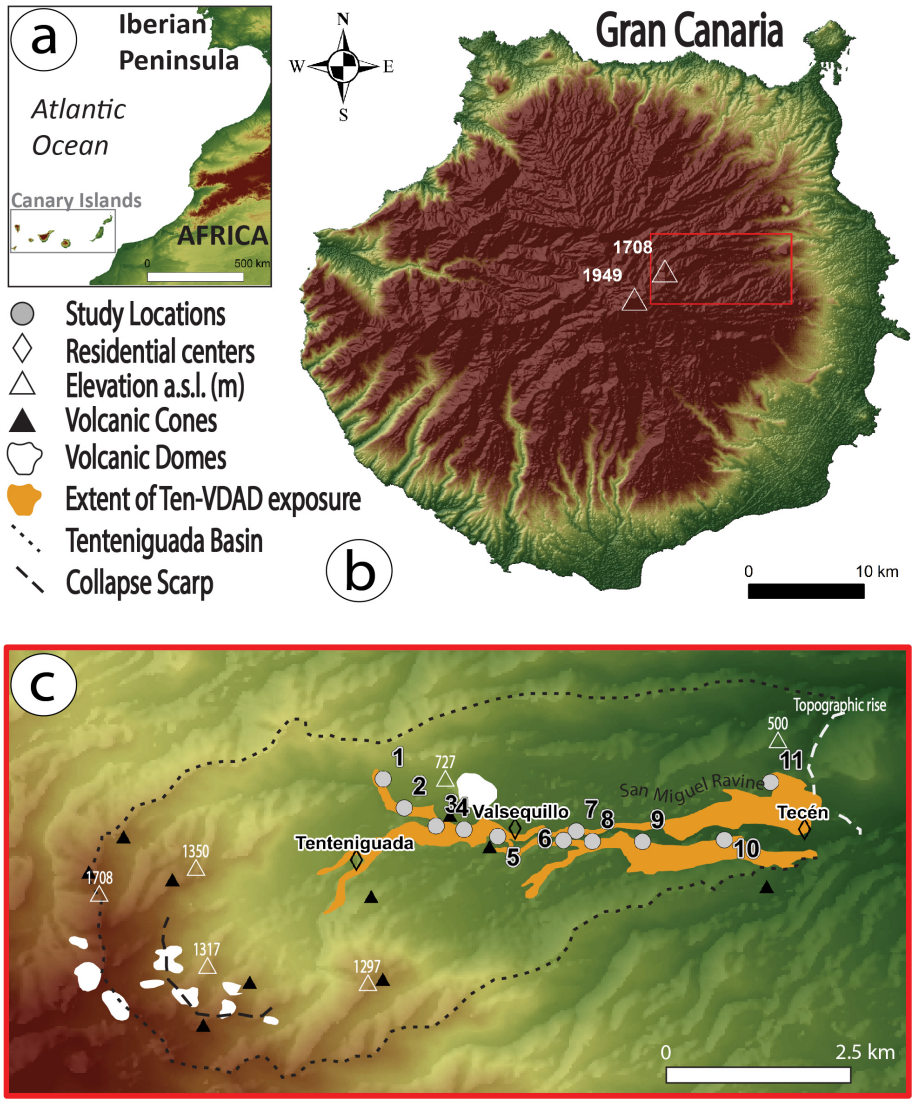

Figure 4.1: **A** Location of the Canary Islands. **B** The Island of Gran Canaria with the location of the Tenteniguada basin (red rectangle – also indicates the extent of c). **C** The Tenteniguada volcanic debris avalanche deposit exposed on the walls of the San Miguel Ravine in the Tenteniguada basin.

4.2 Geological and regional background

4.2.1 Geological background

All volcanic products on the island of Gran Canaria have been formed in the last 15 Ma (Lomoschitz et al., 2008). According to Funck and Schmincke (1998), this has taken place in three major magmatic cycles during the evolution of the Roque Nublo volcanic edifice, a classic stratovolcano formed in the collapsed proto-volcano Tejeda Caldera:

1. Rapid growth of a basaltic shield volcano in the Miocene was followed by the collapse of its centre to form the Tejeda Caldera. Subsequently, a 500 – 1000 m thick sequence of ignimbrites, lava flows and intrusive volcanics was formed in an eruptive phase. Finally, in the Miocene, the volcano experienced a volcanic activity hiatus of 3-4 Ma.

2. In the Pliocene, the Roque Nublo edifice >1000 m in height was constructed over the Miocene caldera. This period is represented in deposits of lava, pyroclastic flows, lahars, VDAs and intrusive phonolite domes.

3. Quaternary volcanism was limited to the northeast half of the island. This period is characterised by basanite lavas, pyroclastics and volcanic cones.

The Roque Nublo edifice was a classic stratovolcano consisted of alternating lava flows and pumiceous ignimbrites as well as lahars, conglomerates, and debris flow deposits (Mehl and Schmincke, 1999). Its cone at the centre of the island reached at least 2500 m tall ~3 Ma ago. However, the steep slopes made the structure unstable and at the time of the Ten-VDA gravitational collapses produced a horse-shoe amphitheatre open to the south and reduced the edifice height (Perez-Torrado et al., 1995). The most important collapses were in the south-southwest sector of the island (Lomoschitz et al., 2008) therefore some slopes might have been left more prone to collapse in the east, where the Ten-VDA occurred.

The Ten-VDAD overlies Mio-Pliocene rocks, and is overlain by Plio-Quaternary volcanic and sedimentary lithologies. Therefore, it is related to the second and third stages of the Roque Nublo development. Although its age is still not well constrained, Lomoschitz et al. (2008) place it between 276 ka and 1.97 Ma, in the Lower-Middle Pleistocene. From this phase, several VDAs have distributed material from the central highland towards the

coastline (Mehl and Schmincke, 1999). The well-preserved hummocky paleotopography displayed at the upper surface of the Ten-VDA deposit suggests an age close to that of the overlying basanite lava flows, i.e. ca. 276 ka. The lack of syn-eruptive pyroclastic deposits suggests that the triggering of the Ten-VDA was not related to a volcanic eruption according to the findings of Lomoschitz et al. (2008). Instead, Lomoschitz et al. (2008) suggest that it could have been triggered by a proximal earthquake unrelated to volcanic activity on Gran Canaria. The basanite lava flows that overly the deposit have contributed its preservation and protection from erosion.

4.2.2 Paleoclimate

The paleoclimate of the eastern Canary Islands during the Pleistocene has been assessed through the marine fauna in fossiliferous deposits by Meco et al. (2002, 2003). During the Miocene the climate was tropical, with low variability. However, ~3 Ma ago the climate became dominated by alternate humid and arid episodes. In the Quaternary, humid episodes enabled significant geomorphic disturbance in the area and have potentially had the effect of incising the paleoravine in which the avalanche propagated, conditioning the slope for the collapse of the Ten-VDA by raising the water table (Lomoschitz et al., 2008). One of these humid episodes (potentially ~420 ka ago) is suggested by Lomoschitz et al. (2008) to have contributed to the destabilisation of the mass, leading to the collapse of material that evolved to the Ten-VDA.

4.2.3 Edifice and deposit morphology

The Ten-VDAD is exposed along the San Miguel ravine, in the eastern part of the island of Gran Canaria (fig. 4.1). The VDA was, at least partially, channelized by a paleoravine at the same location and is exposed along the walls of the modern ravine by fluvial incision. Initially described by Balcells et al. (1990) as a Pliocene gravitational, non-volcanic landslide, it was later reported as a Quaternary VDA by Quintana and Lomoschitz (2005) and described in greater detail by Lomoschitz et al. (2008). The San Miguel Ravine has an area of 22.5 km^2 and a semi-circular head scarp crowned by phonolite domes (fig. 4.1) (Lomoschitz et al., 2008). The current head of the valley has a maximum elevation of 1708 m a.s.l.

The runout of the Ten-VDA was ~8.5 km, with an average width of 1.5 km and a deposit length of 7.1 km (Lomoschitz et al., 2008). The slope of the valley floor during the Ten-VDA was ~22º (Lomoschitz et al., 2008). Although the Ten-VDA was relatively small, with a deposit volume of 0.35 km^3, it still achieved an H/L ratio of ~0.16 (explained in Chapter 1, fig. 1.1). This is comparable to other VDAs and is significantly lower than the 0.5-0.6 predicted by simple frictional models (Davies, 1982; Ui, 1983; Legros, 2002). The thickness of the exposed outcrops of the deposit is variable between <5 m and >50 m, although the base of the deposit is not exposed, and therefore the true thickness could not be evaluated. The deposit terminates at a topographic rise (fig. 4.1c), which could have aided the termination of the propagation of the Ten-VDA (Lomoschitz et al., 2008).

4.3 Composition and internal structure of the Ten-VDAD

The exposed and accessible outcrops of the deposit, which were examined for this study, are illustrated in fig. 4.1 (and the table describing the outcrops in complementary material Appendix A). Field observations suggest that the deposit is dominantly composed of Pliocene phonolite–ignimbrite and basalt to tephrite lavas. These lithologies behave as the more competent, undisaggregated material in the Ten-VDAD. The basalt-tephrite is the most competent, often preserved as massive, homogenous VDA blocks (e.g. fig. 4.2). The phonolite-ignimbrite is less competent and more frequently suffers greater fragmentation generating a higher proportion of matrix (Lomoschitz et al., 2008). All the above-mentioned lithologies preserve the characteristic jigsaw-fractured pattern of VDA blocks (e.g. fig. 4.3a) (e.g. Siebert, 1984; Glicken, 1991). Jigsaw-fractured blocks and clasts exhibit a chaotic fracture network, where syn-propagation-generated fragments experience little relative displacement resulting in the lack of disaggregation of the fractured rock unit as illustrated in fig. 4.2c and 4.3a (e.g. Ui, 1983; Glicken, 1996; Bernard et al., 2021). Fragmented clasts remain coherent without dispersion of their components despite the fractured structure imposed on them (Pollet and Schneider, 2004). Therefore, a jigsaw-fit fabric of dense fracturing but no disaggregation and displacement of the component angular clasts is imposed on the material.

The deposit also contains a small proportion of hydromagmatic, and pyroclastic material (Lomoschitz et al., 2008). This material is weaker and generates cataclased disaggregated

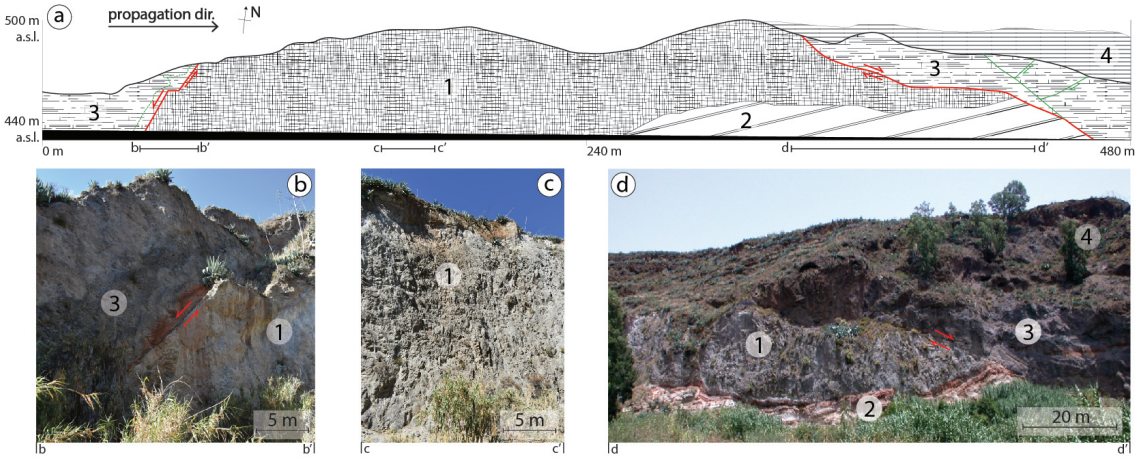

Figure 4.2: Location 7 represents a horst and graben structure with the largest exposed block of the deposit and normal faults on either side. **a** Schematic representation of the outcrop. **B** Proximal-facing normal fault and adjacent block to the west of the central block. **C** Central block with jigsaw-fractured undisaggregated fabric. **D** Distal-facing normal fault and adjacent block to the east of the central block. **Legend** 1. Jigsaw-fractured tephrite lava. 2. Ash and pumice phonolite deposit (1 and 2 are part of the same block, transported together). 3. Jigsaw-fractured tephrite lava (distinct lithology to 1). 4. Younger basanite lava flows over the Tenteniguada deposit.

blocks which do not preserve jigsaw fracturing. There is no evidence of hydrothermal alteration of the material prior to the Ten-VDA. Horizons with a distinctive red colour mark lithological boundaries within the body of the Ten-VDAD (fig. 4.4). These are baked margins likely generated by temperature increase of material underlying lava flows in the stratigraphy of the material composing the volcanic edifice.

Baked margins also consistently mark the top of the Ten-VDAD and its contact with the overlying basanite lava flow (fig. 4.5), which is exposed in the majority of the outcrops. These horizons are the result of a younger, overlying basanite lava flow increasing the temperature of the top of the deposit and generating the colour change of its upper boundary.

With the base of the deposit not exposed, substrate incorporation is only evident by a ripped-up block at location 6, which is the only one exhibited. The block is surrounded by the matrix-rich facies to which it has been incorporated when detached from the substrate (fig. 4.6a). The sedimentation of sand lenses near the top of the block (fig. 4.6a) and pumice-rich horizons at its base (fig. 4.6b) are likely to be related with water flow. Therefore, the material has been interpreted as a secondary deposit, incorporated from the path of the propagating avalanche. A set of normal faults displace the strata at the base of the block (fig. 4.6b).

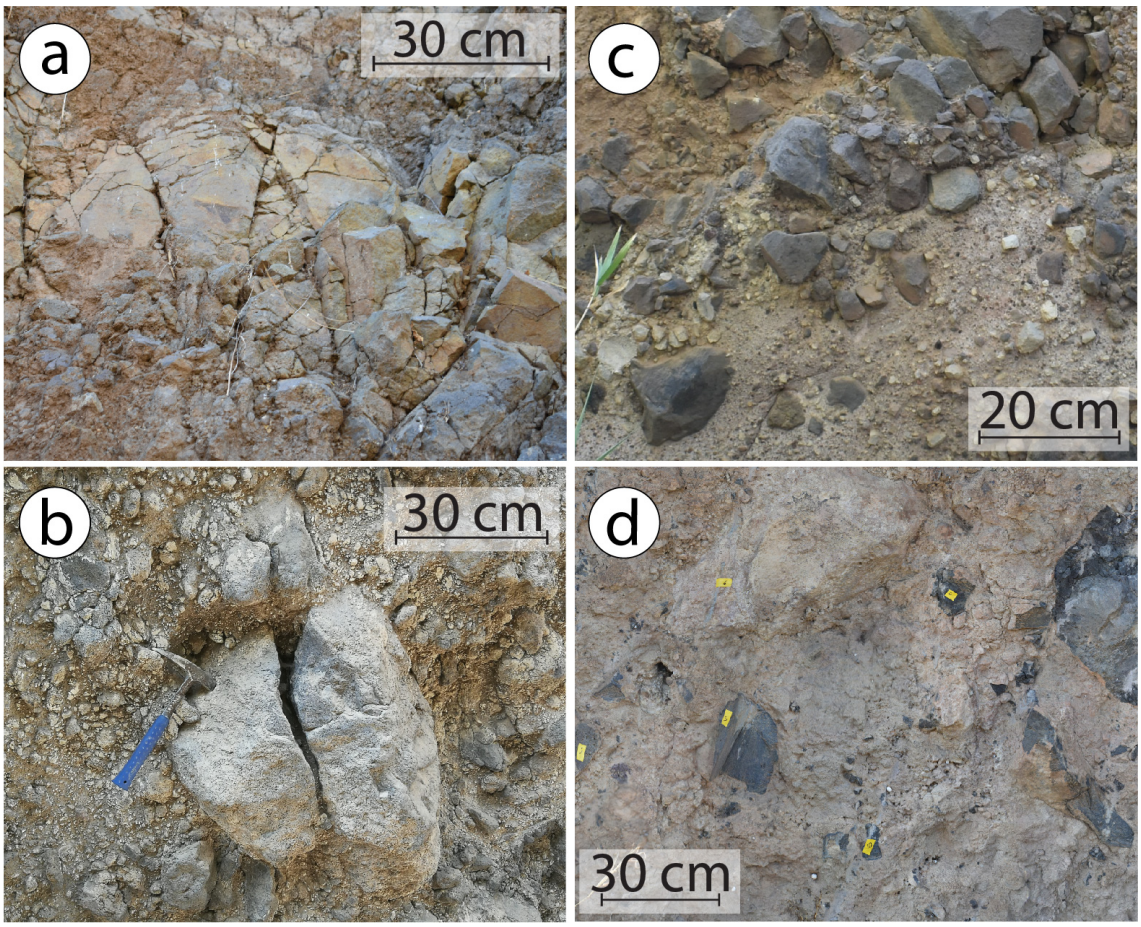

Figure 4.3: Progressive disaggregation of material from jigsaw-fractured clast (a) to interblock/intrablock matrix (d). The evolution is illustrated through clasts at different stages of disaggregation. **A** Jigsaw-fractured clast with component fragments preserving their original position. **B** Widening of the gap between clast components has provided space for the finer particles in the matrix to intrude. The outline of the original clast has been deformed. **C** Components of the original clast have diffused and the original outline of the clast has been eliminated. Incomplete mixing is evident by the concentration of clasts of identical lithology in a more heterolithic matrix. **D** A completely mixed, poorly sorted homogenous assemblage of clasts and matrix where clasts have been incorporated in and mixed with the matrix and no jigsaw fracturing is preserved.

4.3.1 Facies composition and distribution

The deposit can be subdivided into the characteristic VDA facies: the matrix-rich facies (after Roverato et al., 2011; matrix/mixed facies in previous VDA literature after Glicken, 1991) and the block facies (after Ui, 1989; Glicken, 1991). The term matrix is used in the sedimentological sense of finer grains surrounding larger particles (Mehl and Schmincke, 1999), which is scale-dependent rather than assigning a particular size (Vezzoli et al., 2017).

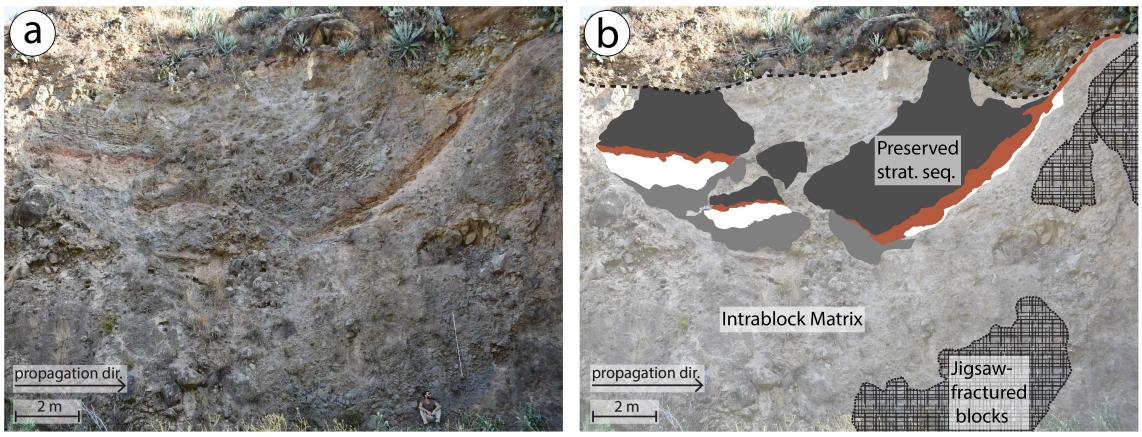

Figure 4.4: The outcrop in location 4 is composed of a block with components of variable disaggregation. It exhibits a component of preserved stratigraphy higher up in the outcrop, and jigsaw-fractured undisaggregated components lower down. The rest of the block is composed of an intrablock matrix. **A** Red horizons illustrate stratigraphic preservation (red shaded area in b). Person for scale. **B** Annotated image of the same outcrop. The dashed line marks the top of the deposit. The shaded areas represent distinct lithological units, illustrating the preserved stratigraphy.

Figure 4.5: The top of the Tenteniguada deposit between locations 8 and 9 is outlined by the white dashed line. Just below, the red baked horizon marks the top of the volcanic debris avalanche deposit and the contact with the overlying basanite lava flow deposit.

4.3.1.1 Block Facies

The Ten-VDAD is composed of a large proportion of blocks of the original volcanic edifice that are undisaggregated as exemplified in fig. 4.2, having suffered little fracturing, and in some cases preserving original stratigraphic sequence (fig. 4.4, 4.7). The term block is here used to refer to an unconsolidated, or poorly consolidated, portion of the source edifice transported and emplaced by the Ten-VDA, remaining unmixed with outside material (Glicken, 1991; Bernard et al., 2021). Fracturing refers to the fragmentation of

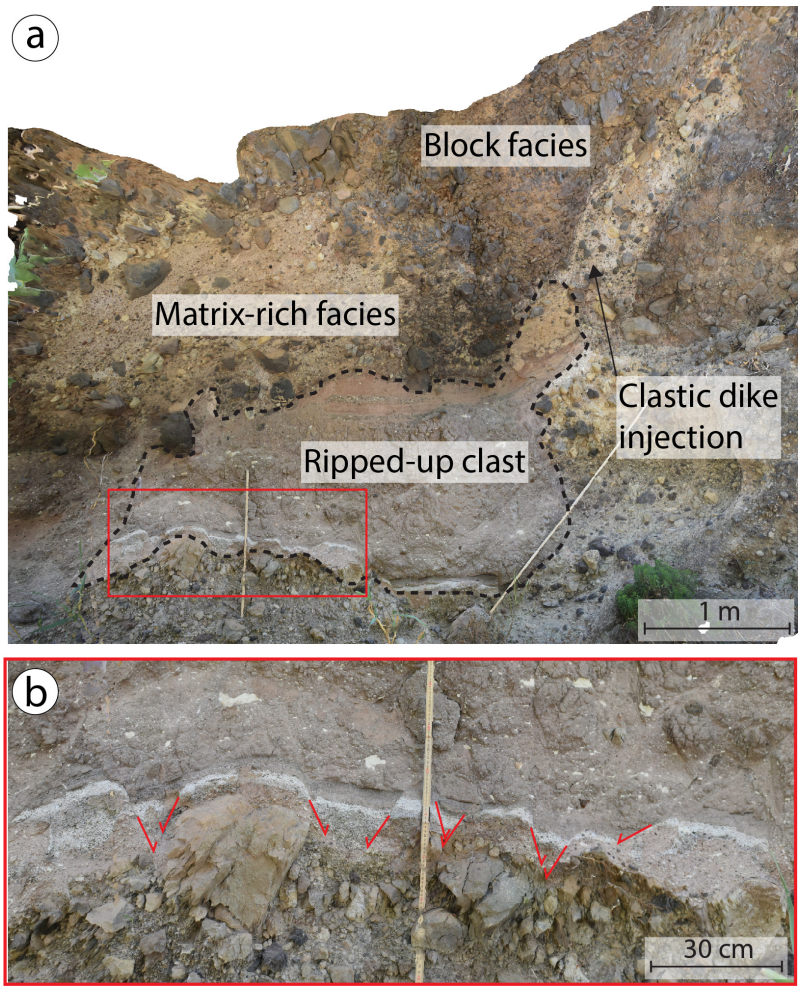

Figure 4.6: **A** At location 6 the deposit exhibits matrix-rich facies, block facies, and a block that has been incorporated from the substrate. The matrix has been injected as a clastic dike in the block facies. Red rectangle represents the extent of b. **B** At the base of the ripped-up block a series of normal faults have been generated, marked by the red lines.

a block resulting in a fabric of individual clasts composing it. Disaggregation implies the displacement of these components within a block, distorting the original placement, structure and outline (fig. 4.3). Blocks in the Ten-VDAD consist of relatively coherent blocks of phonolite, tephrite and to a lesser extent pyroclastic material (Lomoschitz et al., 2008). Conversely, fine material and matrix represent a very minor proportion of the deposit. Blocks reach tens of metres in exposure (fig. 4.2). The majority of blocks that preserve their original stratigraphy exhibit back-tilting compared to their original orientation as illustrated in fig. 4.4 and 4.7.

Blocks which preserve their original stratigraphy and texture that have not been jigsaw-fractured or disaggregated are exhibited at locations 2 (fig. 4.7), 4 (fig. 4.4), and 7 (fig. 4.2). Such blocks do not include any fine matrix. They are exclusively encountered higher up in the exposures, shallower in the deposit, and not close to the modern ravine floor. Moreover,

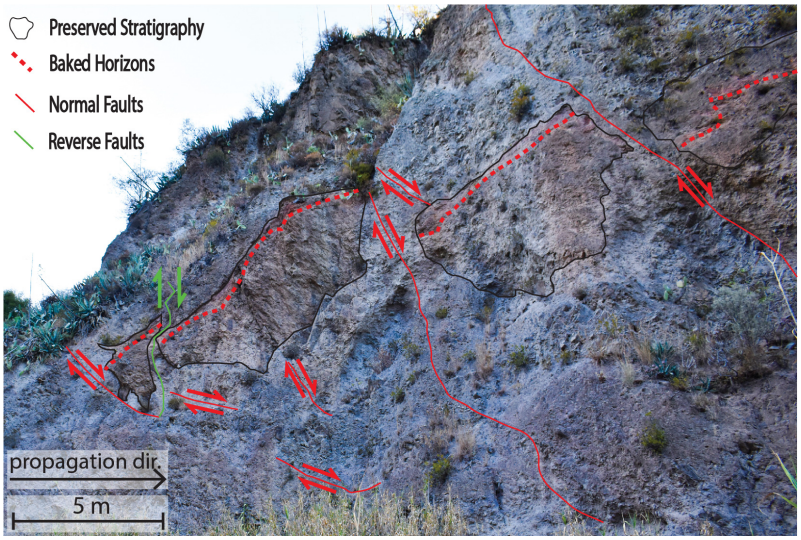

Figure 4.7: Part of the outcrop at location 2. Back-tilted blocks displaced to each other by normal faults have adopted a brittle shearband boudinage form. The blocks preserve their original stratigraphy (observable by the continuity of the red baked layers indicated by the red dashed line). More cataclased blocks of lava lithologies are exposed in the rest of the outcrop.

blocks with a jigsaw-fractured texture occur from the most proximal location 2 and up to location 8 (fig. 4.2c, 4.3a, 4.4). Such blocks exhibit a jigsaw-fit fabric composed of angular clasts. Nonetheless, clasts are not displaced relative to each other, and therefore the blocks remain fractured but undisaggregated (fig. 4.8a). The majority of such blocks correspond to basalt and tephrite lava flows which are massive and homogenous (Lomoschitz et al., 2008). The largest such block observed in the Ten-VDA, in location 7, is >300 m in width and >50 m high (fig. 4.2c). The block is composed of jigsaw-fractured tephrite lava, which has not been disaggregated and contains very little fine material and no matrix.

Other blocks are more severely fractured, cataclased and brecciated, nonetheless preserving their lithological distinctness and external boundaries unmixed (fig. 4.8b-d). Cataclasis refers to the gradual fracturing, comminution, disaggregation and production of matrix that generates in such blocks the diamicton fabric illustrated in fig. 4.8d. These cataclased blocks are most frequently exhibited in the distal areas of the deposit after location 7, but also lower in the exposures of the more proximal locations 2, 4, 5, 7 and 8. In these cases, a chaotic mixture of subangular to subrounded clasts is surrounded by a fine matrix of the same lithology, producing the diamicton texture (fig. 4.8c, d). This intrablock matrix (terminology after Roverato et al., 2015) exhibits greater mixing and poor sorting of more comminuted clasts composed of the same material represented in the blocks. In the Ten-VDAD the intrablock matrix is in most cases silty to sandy in grain size and its

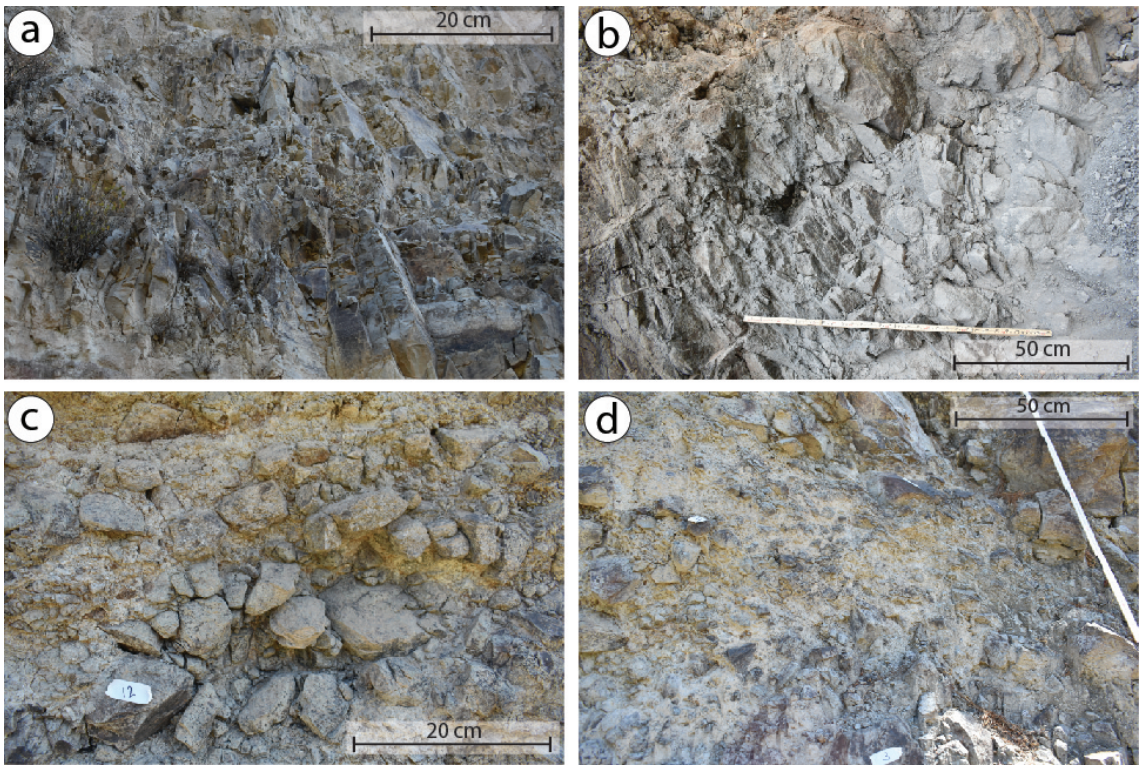

Figure 4.8: Stages of disaggregation from jigsaw-fractured block to monolithological diamicton illustrated through blocks at different stages of disaggregation. **A** Undisaggregated jigsaw-fractured block where the components are not displaced (location 2). **B** In this block angular clasts composing the jigsaw-fit fabric preserve their original order, however, small quantity of fine material has been generated between them (location 9). **C** The original structure of the component clasts has been eliminated and the block has the fabric of a monolithologic breccia (location 10). **D** The block here exhibits the texture of a matrix-enriched, disaggregated, matrix-supported monolithological diamicton (location 2).

proportion of the total volume is variable in different blocks according to the degree of cataclasis. The intrablock matrix is composed of one or more lithologies represented in the block. For example, the exposure at location 10 is composed of a monolithological disaggregated lava that has been fractured and evolved to a matrix-supported mixture of poorly sorted subangular clasts in an intrablock matrix of identical lithology (fig. 4.8c).

Diffuse contacts between blocks and the intrablock matrix, as well as blocks and the matrix-rich facies, have been observed, although not a common feature in the deposit (fig. 4.9). In such block boundaries, the particles composing the undisaggregated component of a block diffuse outwards mixing with the matrix surrounding them. In the periphery of the block, gaps are created between the particles which diffuse outwards. These gaps are intruded by outside material. These features illustrate local gradual mixing. Such contacts have only been observed in the lower sections of the exposures, closer to the valley floor. Except for the jigsaw fractures and signs of incomplete mixing in the matrix, there are no

other intrablock structures.

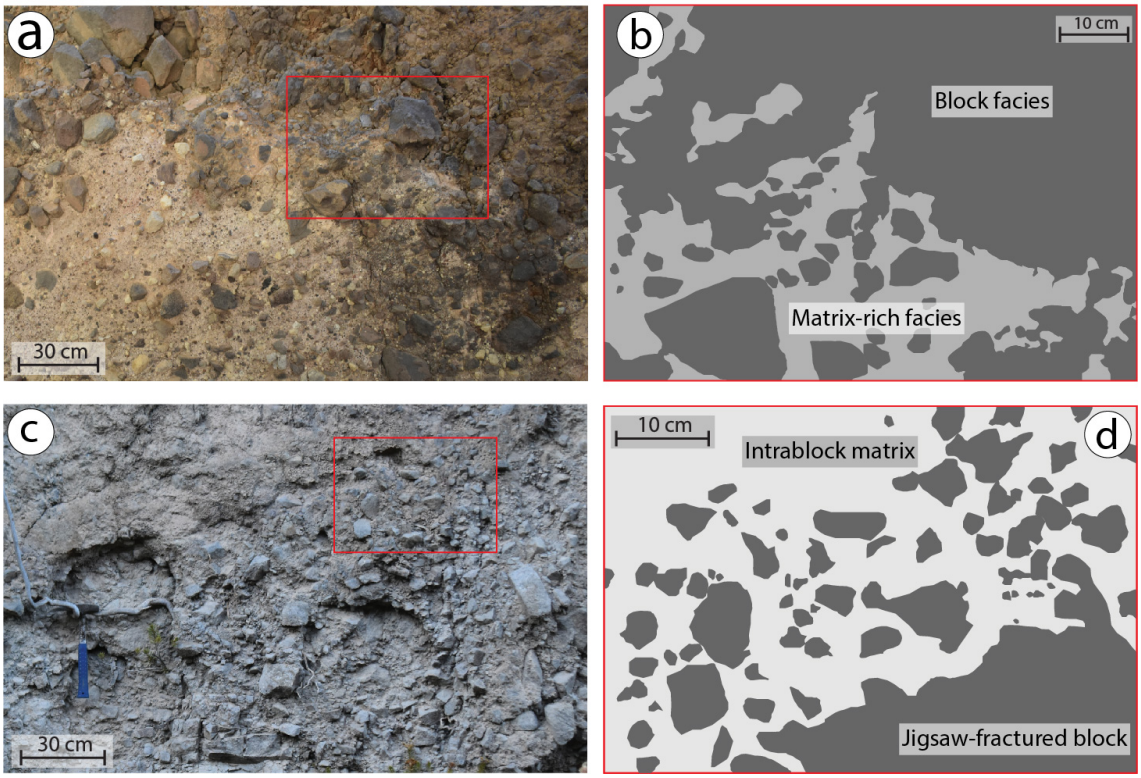

Figure 4.9: Diffuse contacts between the block facies and the matrix-rich facies (a, b) and between undisaggregated material and intrablock matrix within the matrix-rich facies (c, d). The red rectangles in a and c, represent the extent of b and d respectively. Material from the margins of undisaggregated blocks is exhibited diffusing and being incorporated into the matrix.

4.3.1.2 Matrix-rich Facies

The matrix-rich facies is exhibited from the more proximal locations 3, 5 and 6 to the most distal location 11 composed of a very poorly sorted, matrix-supported mixture of clasts and a fine interblock matrix (fig. 4.10). However, it only constitutes a small proportion of the deposit. Particles in the matrix-rich facies vary in size from micrometres, in the matrix, up to clasts >50 cm (e.g. fig. 4.10). Both components comprise lava flow lithologies as well as the hydromagmatic and pyroclastic fall layers of phonolitic composition that are originally less consolidated, with a granular texture. Such material in the initial collapsed edifice transition into the matrix-rich facies more easily (Lomoschitz et al., 2008). Clasts are angular to subrounded and are, on average, more rounded than the component clasts of jigsaw-fractured blocks. The term matrix-rich (Roverato et al., 2011) is used instead of mixed because the material is not always completely mixed (completely mixed material illustrated in fig. 4.3d, 4.10c) as defined by Glicken (1991). The facies forms a

heterolithological, poorly sorted mixture of clasts and matrix. Nonetheless, incomplete mixing is evident by the components of fractured blocks that have been deposited in the process of relative displacement and diffusing into the matrix as is illustrated by fig. 4.10a, b. At block boundaries, where cataclased blocks are being mixed with the matrix, their boundaries are incorporated into the matrix in diffuse margins (fig. 4.9a, b).

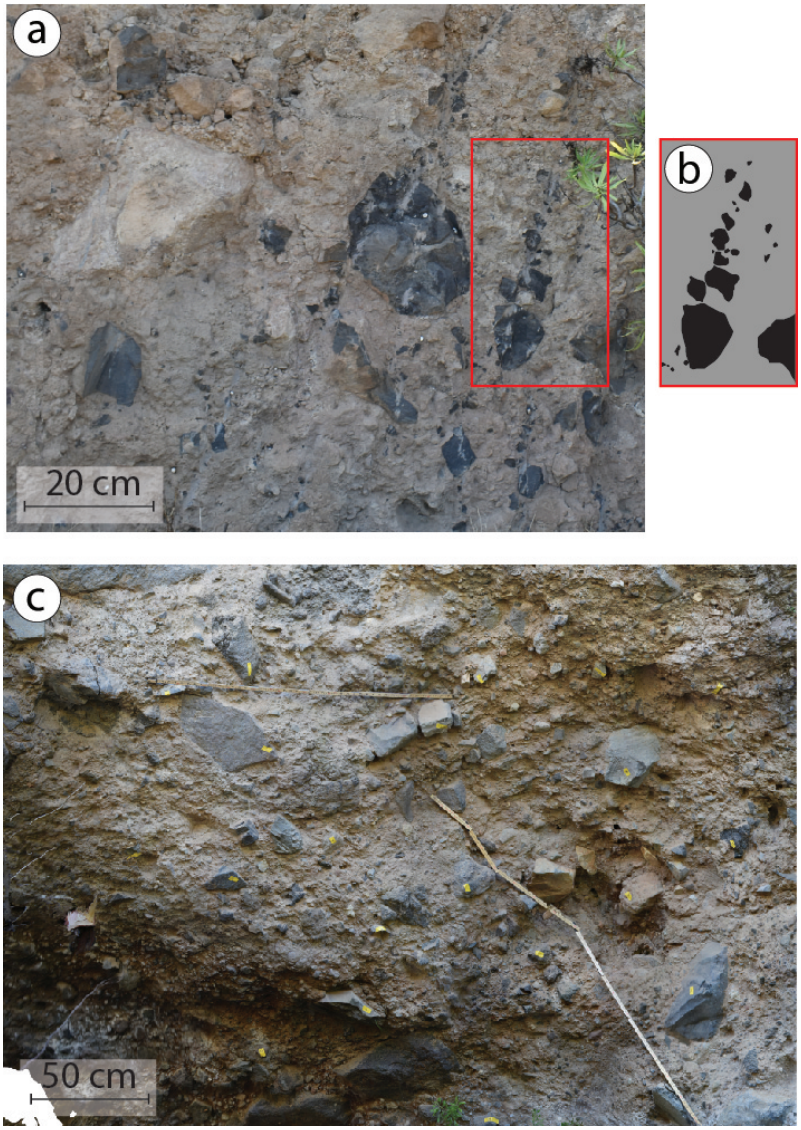

Figure 4.10: Matrix-rich facies. **A** The poorly sorted heterolithological matrix-rich facies exposure at location 11. The red rectangle represents the extent of b. **B** Incomplete gradual mixing is illustrated by clasts of identical origin preserved while diffusing into the matrix. **C** Mixed, poorly sorted mixture of clasts and matrix with no internal features in the matrix-rich facies in location 3.

4.3.2 Brittle features

Normal faults are exhibited at different scales in the deposit, and they are very common from the most proximal section of the deposit until location 8 (fig. 4.2, 4.11). The majority

of the faults are not continuous to the base of the deposit and change directions and merge lower. This is evidence that they are syn-propagational and not post-emplacement features. In location 7, illustrated in fig. 4.2, a large tephrite block (fig. 4.2c) is in contact with more fractured darker tephrite lava blocks on both sides (fig. 4.2b, d) of the exposure (Lomoschitz et al., 2008). The back-tilting generates a toreva block feature. The contact represents normal faults on either side of the block, one proximal-facing and one distal-facing (fig. 4.2a), constituting the large block as a horst feature, which potentially formed a hummock on the surface of the deposit.

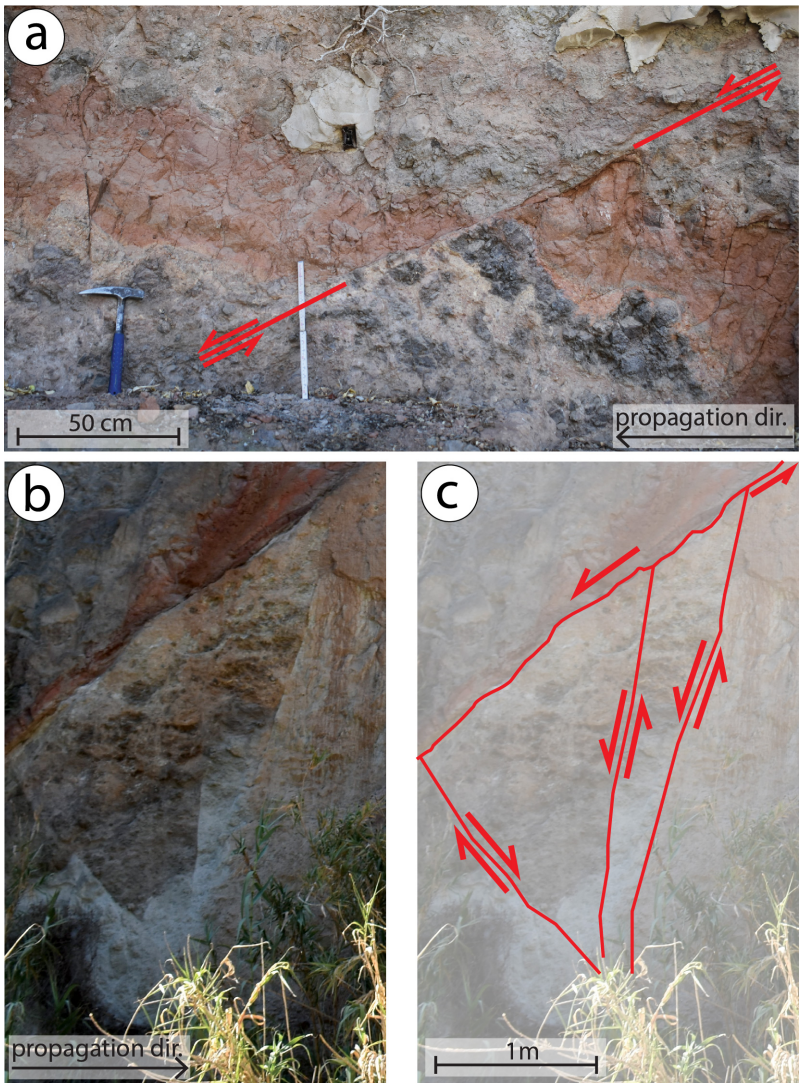

Figure 4.11: Small-scale normal faults. **A** Red baked horizon illustrates the normal fault at location 8. **B** Section from location 7. **C** Section from b with normal faults annotated.

At a smaller scale, normal faults are exhibited in the block facies displacing components of blocks (fig. 4.11) accommodated by normal faults. Additionally, blocks composed of portions of the original edifice of identical preserved stratigraphic sequence are exhibited displaced in relation to each other and tilted back towards the source of the Ten-VDA,

without exhibiting a discrete fault plane. Such blocks are exposed, for example, in locations 4 (fig. 4.4) and 2 (fig. 4.7). In location 2, the displacement between blocks has been accommodated in a brittle-ductile manner by surrounding intrablock matrix, giving the modules of the original block a brittle shearband (Goscombe et al., 2004) boudinage form (fig. 4.7). The deformation was accommodated by the intrablock matrix and blocks were displaced while not deformed. The resulting form is of asymmetric brittle shear/domino boudins displacing and back-tilting the components of the initial single block. This brittle behaviour is most abundant higher in the outcrops, although a few examples of brittle behaviour were encountered close to the modern ravine floor. These features are limited to the block facies.

4.3.3 Shearing and fluidal features

Shearing is illustrated by components of fractured clasts displaced in parallel, but opposite directions (fig. 4.12a). Sheared clasts are exhibited in the matrix-rich facies and highly disaggregated blocks in the block facies. However, they do not occur in the interior of blocks that are less disaggregated and preserve jigsaw fractures. Sheared material is exhibited lower in the exposures, and not higher on the ravine walls where stratigraphic preservation is more frequent.

However, shearing and fluidal behaviour is also observed at the boundaries between blocks. A shearband boudinage (Goscombe et al., 2004) feature is illustrated in fig. 4.12b between blocks. A flame injection of a clastic dike is exhibited in the normal fault between two blocks in location 7, suggesting shear between the blocks when the fault was active (fig. 4.12c-d, 4.2b). In location 6, illustrated in fig. 4.6, a clastic dyke injection of matrix-rich facies between blocks offers evidence of fluidal behaviour lower in the deposit. Other than these limited specific circumstances, in the interior of both the block and the matrix-rich facies, there is no evidence of mass shearing.

4.3.4 Longitudinal evolution

The deposit can be longitudinally separated into two distinct sections according to the internal structure and degree of disaggregation of the material: 1. Block facies with relatively low disaggregation, with blocks that preserve their jigsaw-fractured texture,

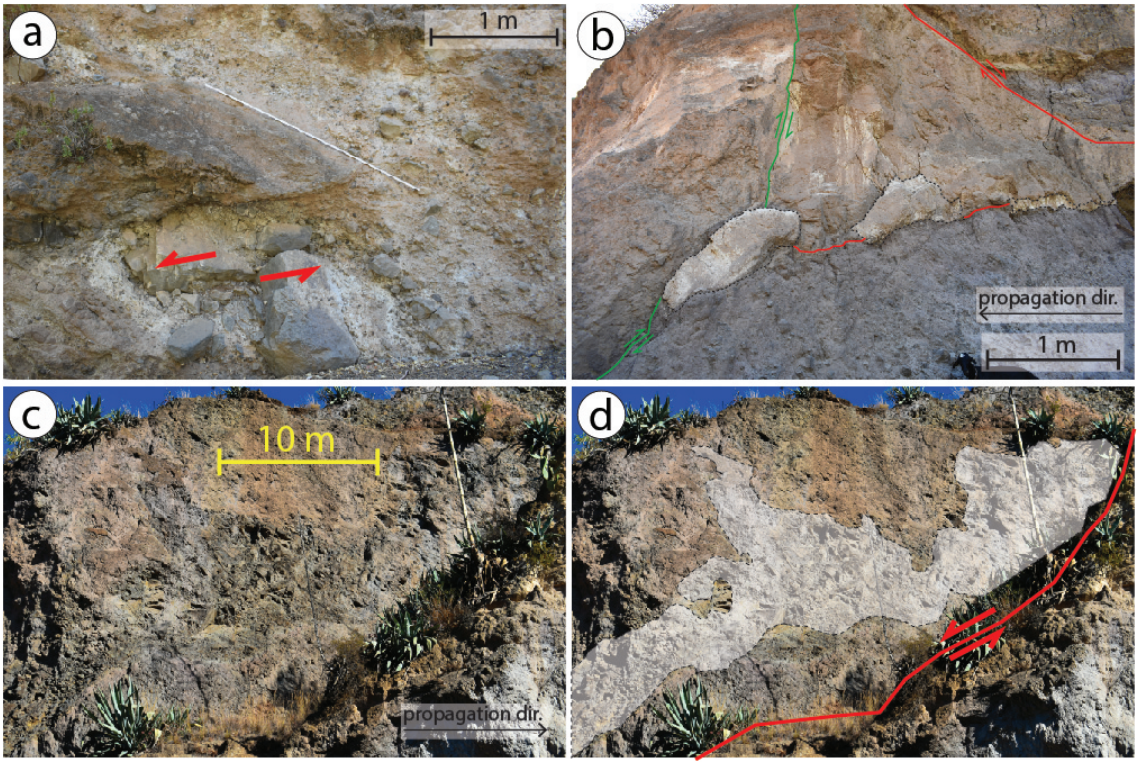

Figure 4.12: Shear features of the Ten-VDAD. **A** Sheared clasts at the base of the exposure at location 5. **B** The outcrop at location 11 illustrates brittle deformation between components of the block facies. Red lines represent normal fault displacement, whereas green lines represent reverse fault displacement. Brittle shearband boudinage has been generated, illustrated by the boudins formed, orientated in the propagation direction. **C** Normal fault at block boundary at location 7. C and D represent the same location. **D** Flame injection and normal fault illustrate the shear accommodated at this zone. The displacement between the blocks generates the normal fault at the east of the outcrop illustrated in fig. 4.2a and b

compose the majority of the volume of the proximal exposures, and up to location 8. 2. Block facies at the more distal locations 9 and 10 (as well as exposures between them), do not preserve a jigsaw-fractured texture, except in few cataclased blocks that remain fractured but undisaggregated within the intrablock matrix. Blocks are more disaggregated and cataclased with component clasts displaced in relation to each other. In these blocks, the proportion of intrablock matrix is greater. The degree of cataclasis and disaggregation generated the fabric of a monolithological diamicton (fig. 4.8c-d). Normal faults and brittle behaviour as well as shearing features are not observed in this distal section. Clasts in more disaggregated blocks are subangular to subrounded (e.g. fig. 4.8c-d); more rounded than the angular to subangular clasts in jigsaw-fractured blocks (e.g. fig. 4.8a-c). Nonetheless, the unmixed lithological distinctness of blocks is preserved.

4.4 Discussion

4.4.1 Brittle extensional behaviour

Extensional normal faults, horst formation and boudinage indicate the accommodation of extension during propagation. Normal fault alignment perpendicular to the propagation direction offers an indication of the extensional regime (Longchamp et al., 2016; Roberti et al., 2017). Such normal faults have been also observed in other VDADs (e.g. Siebe et al., 1992; Glicken, 1996; Siebert et al., 2006; Bernard et al., 2008; Roberti et al., 2017), with the Socompa VDAD being an illustrative example (Longchamp et al., 2016). Similar horst and graben structures are also reported in the Delcamp et al. (2017) study of the Momella VDAD. In the Ten-VDAD blocks of identical stratigraphy have been fractured and separated into smaller modules, subsequently displaced and back-tilted, as illustrated in fig. 4.4 and 4.7. Further evidence for the extension is offered by the lack of vertical stratigraphic repetition in all the faults, supporting the lack of extensive compressional environments as supported by Shea and van Wyk de Vries (2008). It is also probable that the lateral confinement of the avalanche by the ravine and frontal by the topographic rise at its toe generated compressional regimes and features in these areas. However, representative outcrops are not exposed. The small number of reverse faults, of limited extent (e.g. fig. 4.4, 4.7), potentially reflect momentum transfer in the material during propagation, as is later discussed. The abundance of brittle features observed in the majority of the deposit suggests large-scale brittle-type behaviour as the principal mode of propagation of the Ten-VDA (Shea and van Wyk de Vries, 2008; van Wyk de Vries and Delcamp, 2015). Shear was concentrated at the normal faults, as also suggested for the Momella VDAD by Delcamp et al. (2017). Focusing of shear stress at fault zones allowed the low degree of disaggregation and fragmentation at the interior of blocks. This results in the low amount of fine material and matrix generated, low disaggregation and a high degree of preservation, constituting a deposit that more closely resembles a non-volcanic blockslide deposit than a typical VDAD, as also observed in the case of the Jocotitlán VDAD by Dufresne et al. (2010b). The lack of fine, loosely consolidated, weak or hydrothermally altered material in the original destabilised portion of the edifice is likely to have contributed to this aspect of the character of the Ten-VDAD.

Blocks greater than 1 m in diameter are abundant in the Ten-VDAD, as exemplified in

fig. 4.2 and observed in other VDADs such as Augustine VDAD (Siebert et al., 1995) and the Parinacota VDAD (Clavero et al., 2002). Edifice blocks preserve their original stratigraphy and texture in locations 2 (fig. 4.7) and 4 (fig. 4.4). Furthermore, the abundance of undisaggregated jigsaw-fit clasts suggests high cohesion and low mixing (Ui et al., 2000). The preserved stratigraphy, jigsaw-fractured blocks, or even cataclased blocks with preserved outlines, suggest that large-scale turbulence and mixing can be excluded during the propagation of the Ten-VDA, as supported in other cases by Campbell et al., (1995), Reubi and Hernandez (2000), Voight et al., (2002) and Shea and van Wyk de Vries, (2008). Stratigraphic preservation indicates that the majority of the material experienced a frictional regime throughout the propagation (Manzella and Labiouse, 2013). In a collisional regime, where momentum transfer predominantly occurs through collisions (Iverson and Denlinger, 2001), the material would have experienced more disaggregation and mixing.

4.4.2 Local granular fluidal behaviour

Fluidal features such as clastic dikes (e.g. fig. 4.6, 4.12d) and sporadic diffuse contacts (e.g. fig. 4.9) between blocks and at the boundary between matrix-rich and block facies suggest a local granular fluid phase (van Wyk De Vries et al., 2001; Davies, 2015; van Wyk de Vries and Delcamp, 2015). Additionally, incomplete mixing offers evidence for agitated granular fluid behaviour in the matrix-rich facies (fig. 4.10a-b) as suggested by van Wyk De Vries et al. (2001) in their study of the Socompa VDA. The preservation of blocks with intact stratigraphy overlying more fragmented material is not unusual in VDA/rock avalanche deposits (e.g. Erismann and Abele, 2001; Schilirò et al., 2019). Shearing features (fig. 4.12) are also limited to block boundaries and lower outcrop sections.

Deeper in the Ten-VDAD, closer to the ravine floor, the convergence of normal faults, illustrated in fig. 4.7, is the reason for the higher disaggregation and poorer preservation of intact blocks. Convergence of the faults and the consequent higher shear stresses enable greater degrees of fracturing, thus leaving the mass more granular (as also predicted by the numerical model of Thompson et al. (2010) discussed in section 4.3). As a result, component clasts can move independently, become agitated and interact in collisions after the initial post-collapse decompression and dilation (fig. 4.13). This particle activity generates a granular temperature in these areas (Ogawa, 1978; Campbell, 1990; Iverson, 1997). The granular material interacts with the rough substrate to maintain a granular

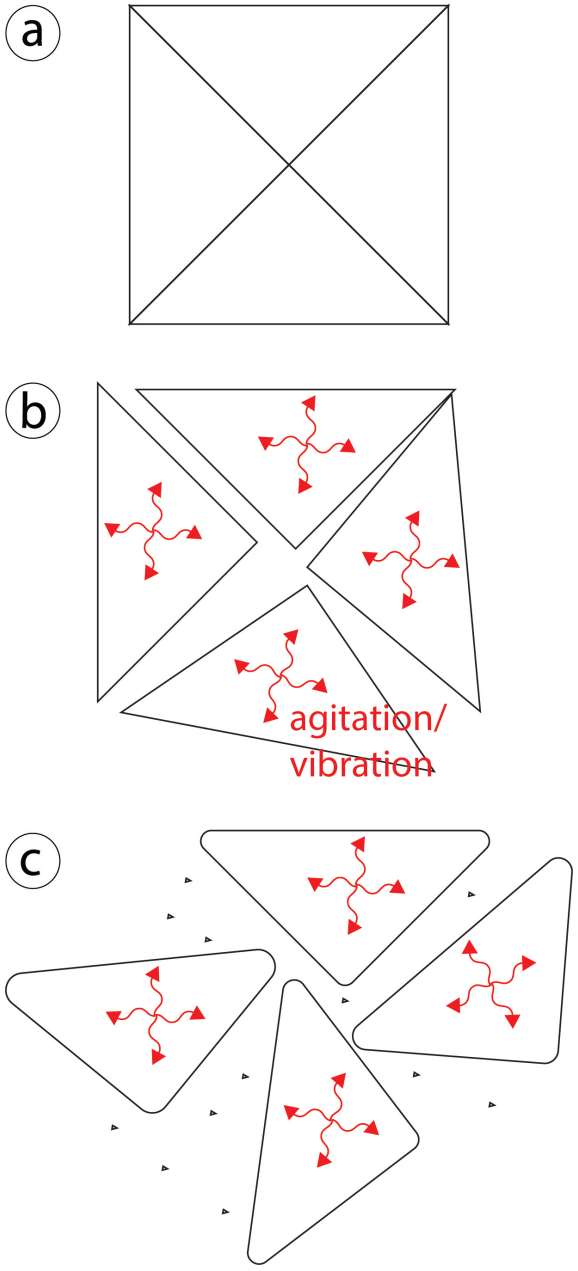

Figure 4.13: Gradual disaggregation of jigsaw-fractured clasts/blocks due to agitation and granular temperature. **A** Jigsaw fractured material initially preserves the location of component parts and remains undisaggregated. **B** Vibration due to agitation displaces the particles relative to each other. **C** The original structure is progressively eliminated. Clasts become more rounded due to abrasion in their interactions, which also adds material to the matrix. The matrix fills the space between them to give the material a diamicton fabric. Diffuse contacts form where disaggregating clasts/blocks add material to the intrablock/interblock matrix.

temperature (Cleary and Campbell, 1993; Iverson, 1997), which has even been suggested as capable of supporting the weight of the overriding material as a plug (e.g. Linares-Guerrero et al., 2007; Hu et al., 2021). Due to the granular temperature in the matrix as well as clasts in fractured block facies, the material behaves as an agitated granular fluidised mass (van Wyk De Vries et al., 2001; Thompson et al., 2009; Davies, 2015). The degree of agitation is low, if the flow remains laminar with low mixing, in accordance with the acoustic fluidisation theory as discussed by Collins and Melosh (2003). Although agitation was not great enough to generate turbulence, it did lead to relatively higher disaggregation of the material, and therefore, a reduction in preservation of stratigraphy and texture. This leads to the elimination of the jigsaw fabric by displacing component clasts (Campbell et al., 1995; Reubi and Hernandez, 2000; Clavero et al., 2002; Thompson et al., 2010), as illustrated in fig. 4.3. The agitation vibrates and microdisplaces the material, resulting in the fine matrix intruding fractures within a block or clast, widening them and dispersing block/clast components (fig. 4.3b). The material of the matrix-rich facies is initially injected in the block facies through the jigsaw fractures (fig. 4.3b). Then clasts are separated and incorporated into the matrix (fig. 4.3c-d) (Bernard et al., 2008; Roverato et al., 2015, 2018). As this occurs in blocks throughout the mass, this eventually leads to the mixing of lithologies observed in both the intrablock matrix (fig. 4.8) as well as the matrix-rich facies (fig. 4.3), and the gradual homogenisation of these domains, according to the process described by Roverato et al. (2015). Due to this process, the intrablock matrix is composed of the lithologies represented within a block. At the contacts, this diffusion process acts to add material from the outline of the block facies to the matrix-rich facies (fig. 4.9a-b) (Bernard et al., 2008). The observation of a tendency for clasts of similar lithology to occur in groups in the matrix-rich facies of the Ten-VDAD, also made by Lomoschitz et al. (2008), is evidence of such fluid-like behaviour and gradual homogenisation at an incomplete stage (fig. 4.10b).

The relatively higher degree of rounding (for example comparing the material in fig. 4.8a, b with the material in fig. 4.8c,d and 4.6a) of material in the matrix-rich facies and the intrablock matrix indicates abrasion during the viscous flow as suggested by Schneider and Fisher (1998). Fragmented particles are smoothed and rounded by frictional abrasion in the agitated mass in the process schematically illustrated in fig. 4.13(Schneider and Fisher, 1998; Perinotto et al., 2015; Paguican et al., 2021).

4.4.3 Shear accommodation, propagation and emplacement model

VDAs result from flank collapses, propagating as slides immediately after the initial collapse and usually progressively evolve into flows (Voight et al., 1983; Siebert, 1984; Glicken, 1991; Scott et al., 2001). Coarse fragmentation primarily occurs at the initial stages of edifice collapse due to decompression and dilation since the whole mass is in an extensional regime (Alidibirov and Dingwell, 1996; Longchamp et al., 2016) and the impact at the slope-break (Voight et al., 1983; Glicken, 1991, 1996; Bernard et al., 2008; Thompson et al., 2010). Subsequently, VDAs propagate further and progressive disaggregation continues (Roverato et al., 2015). Further fragmentation due to grain-to-grain collisions is thought to be minimal during propagation, and the generation of matrix is thought to be the result of disaggregation of already fractured material (e.g. Glicken, 1991; Palmer et al., 1991; Belousov et al., 1999; Bernard et al., 2008; Shea et al., 2008). Nonetheless, gradual abrasion of clasts in the more agitated regions can add small quantities of material to the matrix (Schneider and Fisher, 1998; Perinotto et al., 2015; Paguican et al., 2021). In the case of the Ten-VDA, the quantity of interblock matrix (fig. 4.14) and degree of gradual homogenisation are low.

Discrete element method numerical models by Thompson et al. (2010) have examined the propagation and emplacement of VDAs as granular avalanches where particles initially have a bond between them which can be broken when their strength is overcome by local stresses during propagation. Subsequent evolution of the mass, as well as shear accommodation, are dependent on the distribution of the degree of disaggregation. Due to their potential to consider the strength of the material, such models are suitable for evaluating VDAs composed of relatively competent material, as is the case for the Ten-VDA. The model reproduces features observed in the Ten-VDAD, such as the normal fault generation and convergence, and allows the evaluation of propagation processes and dynamics.

The jigsaw-fractured pattern extensively exhibited by the Ten-VDAD (e.g. fig. 4.2, 4.8a), has been suggested by Glicken (1996) to result from the expansion of a propagating mass at the initial collapse stage. Its preservation in the texture of the blocks in the interior of the proximal region of the Ten-VDAD suggests minimal agitation after the fracturing was generated by an impulsive force (Campbell et al., 1995; Schilirò et al., 2019). In agreement,

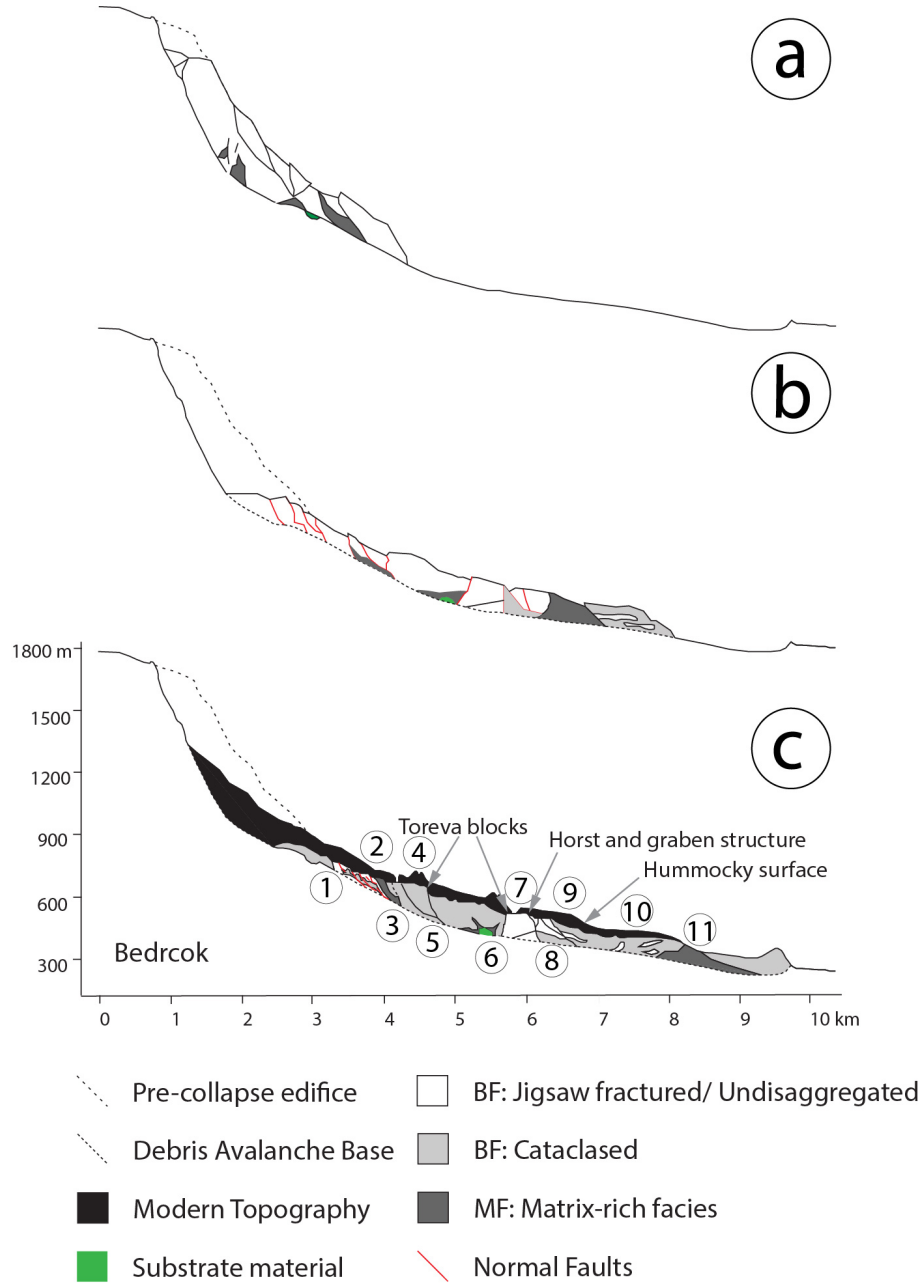

Figure 4.14: Schematic representation of the propagation and emplacement of the Tenteniguada debris avalanche. **A** The initial stage of the collapse and coarse fracturing of the material. **B** Propagation stage where fractures are activated as normal faults to accommodate the spreading of the mass. **C** The final deposit with the features that have been observed in the field. Circled numbers represent the study locations as illustrated on the map in fig. 4.1 and the table in the complementary material Appendix A.

the model of Thompson et al. (2010) suggests that the early stages of the collapse represent significant events for the fracturing and disaggregation of the mass. According to the model, during the initial collapse stress distribution is chaotic, however, the brittle failure initiating the fracturing of the mass, takes place even before the mass has evacuated the failure scarp. Analysis of the fractures of lava blocks in the Maronne Valley (Central Volcano, France) by Reubi and Hernandez (2000) also supports that fractures are primarily the result of shear stress at the initial stage of sliding. Fragmentation by rapid unloading is also supported by the pressure experimental findings of Alidibirov and Dingwell (1996). In the Ten-VDA this stage resulted in the coarse fracturing and large quantities of blocks observed in the deposit (e.g. fig. 4.14a). Nonetheless, the existence of matrix-rich facies in proximal exposures (location 3) indicates that it was already generated from this early collapse stage. Therefore, the degree of mixing and disaggregation is not exclusively related to the distance from the source as also suggested by Bernard et al. (2008). Instead, it is also a function of the chaotic local stress distribution according to the instantaneous arrangement of the self-weight of the mass.

The abundance of normal faults at proximal areas and the interior of the deposit suggests that subsequent propagation-induced shear stresses were accommodated in fault zones (fig. 4.14a). This regime allowed the spreading and back-tilting by rotational and sliding displacement of blocks, decreasing the avalanche thickness as exhibited, for example, at location 7 (fig. 4.2). The blocks displaced in this way generate toreva features as illustrated in fig. 4.14. In the Thompson et al. (2010) model, fractures generated during the initial collapse subsequently accommodate the spreading and resulting extension by activating as normal faults. The majority of the strain was accommodated in these shear zones and consequently, blocks were capable of preserving their internal stratigraphy (Thompson et al., 2010; Paguican, 2012). The model also predicts the observed large-scale toreva blocks in the medial area of the deposit (fig. 4.14) under the definition of a massive portion of intact material that slid and back-tilted without being significantly brecciated (also observed by van Wyk De Vries et al., 2001; Clavero et al., 2002; Shea and van Wyk de Vries, 2008). This is also observed in the proximal region of the Casana VDAD by Bustos et al. (2022). With progressive propagation, proximal and distal-facing normal faults generated the horst and graben complexes in the medial area of the Ten-VDAD, such as the one described in location 7 (fig. 4.2).

Closer to the ravine floor, and in locations more distal than location 8, poorer preservation (fig. 4.8c, d), more abundant intrablock matrix (fig. 4.13) and scarcity of brittle features suggest higher stress accommodation. In the Thompson et al. (2010) model, faults conjoin at the base of the deposit generating a blockier upper portion; and a base with more matrix-rich facies and fewer large blocks, which are instead more cataclased. This aspect of the model is in agreement with the Ten-VDAD observation of more frequent preservation of blocks shallower in the deposit. Much of the deformation, fracturing and disaggregation of the mass has been concentrated and magnified deeper in the deposit, as exemplified at locations 2 and 4 (fig. 4.4 and 4.7 respectively).

The incorporation of a block from the substrate and inclusion as a clastic dyke (fig. 4.6) occurred due to the shear of the substrate ploughing and detaching a section of the substrate (Dufresne et al., 2010a) and hosting it between two blocks. The built-up of pressure in the subsequent propagation forced part of the block into the fracture between the blocks generating the clastic dike. Gradual mixing enriched the surrounding matrix with substrate lithologies giving it a whiter colour (fig. 4.6a).

Regarding the disaggregation of the distal areas of the Ten-VDAD, distal portions of granular flows experience acceleration and propagate for longer than the more proximal locations due to momentum transfer from material at the back to the front (Heim, 1932; Van Gassen and Cruden, 1989; Okura et al., 2000; Legros, 2002; Manzella and Labiouse, 2013; Bartali et al., 2015; Fan et al., 2016). Therefore, they are exposed to greater stress and for a longer time duration. During the emplacement phase, the proximal deposit decelerates faster, while the front of the VDA is still accelerating (Thompson et al., 2010). The process of momentum transfer imposes compressive stresses on the material at the front of the propagating mass (Longchamp et al., 2016; Hu et al., 2020). In the Ten-VDA, the higher disaggregation of the distal portion of the deposit could be the result of such amplified stress accommodation.

The fact that distinct normal fault planes are more abundant higher in the deposit, as illustrated in location 2 (fig. 4.7), indicates the transition between the brittle behaviour to a relatively more liquefied/fluidised deeper in the Ten-VDA as suggested by Shea and van Wyk de Vries (2008). Nonetheless, the presence of a basal listric layer of major shear concentration could not be evaluated due to lack of exposure. Based on these observations,

it can be assumed that two shear accommodation regimes have been active during the propagation of the Ten-VDA:

1. In the more shallow domain of the deposit and in the proximal regions at the interior of the mass, the displacement was accommodated in normal faults between blocks, where shear was concentrated. Stress was not transmitted to the interior of blocks.

2. Deeper in the deposit, where faults conjoined and stresses were higher, and at more distal locations, a regime of a relatively agitated granular flow is evident. In these areas, stress and agitation are distributed throughout the mass, causing the generation of more mixed and rounded material. Nonetheless, the flow regime remains laminar. Particles adopted a behaviour between a rapid and quasistatic granular flow regime, rather than evolving into a pure rapid granular flow with a collisional regime (Campbell et al., 1995; Johnson et al., 2014).

Faults in the Thompson et al. (2010) model become progressively wider to facilitate the continuous spreading and extension, while the space is progressively filled by the increasing matrix-rich facies. The disaggregation allows the propagating mass to evolve into a fluidised granular flow. Deeper in the mass, in the model, the blocks are more likely to become disaggregated, and the material is stretched and thinned (Thompson et al., 2010). This is not observed in the Ten-VDAD, where matrix-rich facies is very scarce (fig. 4.14c), suggesting that the deposit was emplaced before evolving to this stage of the rockslide-to-granular flow progression (Voight et al., 1983; Glicken, 1991). A dense network of blocks makes up the majority of the Ten-VDAD, with the matrix-rich facies limited to only a few spaces between them (fig. 4.14c). The Ten-VDA did not fully evolve from a slide to a flow (Voight et al., 1983; Glicken, 1991), and that is the reason it more closely resembles a non-volcanic blockslide deposit (Dufresne et al., 2010b).

On the contrary, in DEM experiments where the particles have no bond between them, and therefore represent weaker, easily disaggregated granular material, the results are significantly different. Such were the experiments of Thompson et al. (2009) and Campbell et al. (1995), where a granular mass with no bond between the particles was released to propagate under gravity. In these experiments brittle deformation and preservation of unfractured blocks is significantly reduced. The mass spreads and evolves to a flow with agitated particles throughout the mass accommodating shear and imposing a fluid-like

behaviour. In this case, stretching and disaggregation are greater high in the deposit compared to closer to the base (Thompson et al. 2009). The comparison of the two models suggests that the strength of the material in the Ten-DAD (i.e. the abundance of competent lavas relative to weaker pyroclastic material) and the lack of weaker, loose and hydrothermally altered material has contributed to the brittle character of the propagation of the Ten-DAD and its low disaggregation. This comparison will be further discussed in Chapter 5. Both the types of experiments mentioned assume an inerodible propagation surface and thus neglect the potential impact of the substrate on the propagating mass, which is discussed in the following section.

For a VDA to evolve into a flow stresses need to overcome the strength of the propagating material in order to disaggregate the mass (Thompson et al., 2010). Once the majority of the mass can behave as a granular flow it is believed to assume the typical VDA flow behaviour (Voight et al., 1983; Glicken, 1996; Schneider and Fisher, 1998; Thompson et al., 2009). This has not been achieved by the Ten-VDA primarily because of the competent nature of the lava lithologies that compose the majority of the material. Other potential factors for the primarily brittle behaviour are: the low volume relative to other VDAs (Legros, 2002), the low slope of the path, and potential substrate interactions. Lomoschitz et al. (2008) suggest that the emplacement of the Ten-VDA might have also been aided by the topographic high where its toe has been deposited (fig. 4.14).

Nevertheless, considering that the Ten-VDA has achieved an H/L ratio of ~0.16 implies that it attained much greater horizontal runout distance compared to its initial fall height (fig. 4.15a). Given the runout and the low degree of disaggregation observed in the deposit two candidate processes can be proposed for the Ten-VDA propagation:

1. Normal faults and extensional features illustrate extensive spreading and lowering. Therefore, one explanation for the long runout of the Ten-VDA is the spreading of the mass. This implies that the material spread, lowering its centre of mass and pushing the front of the material further. This behaviour in granular material provides increased runout without increased mobility of the centre of mass (fig. 4.15) (Legros, 2002; Manzella and Labiouse, 2013). Therefore, no mechanism is required to explain reduced friction that would result in greater displacement of its centre of mass. In such a case, the runout is the result of normal fault-accommodated

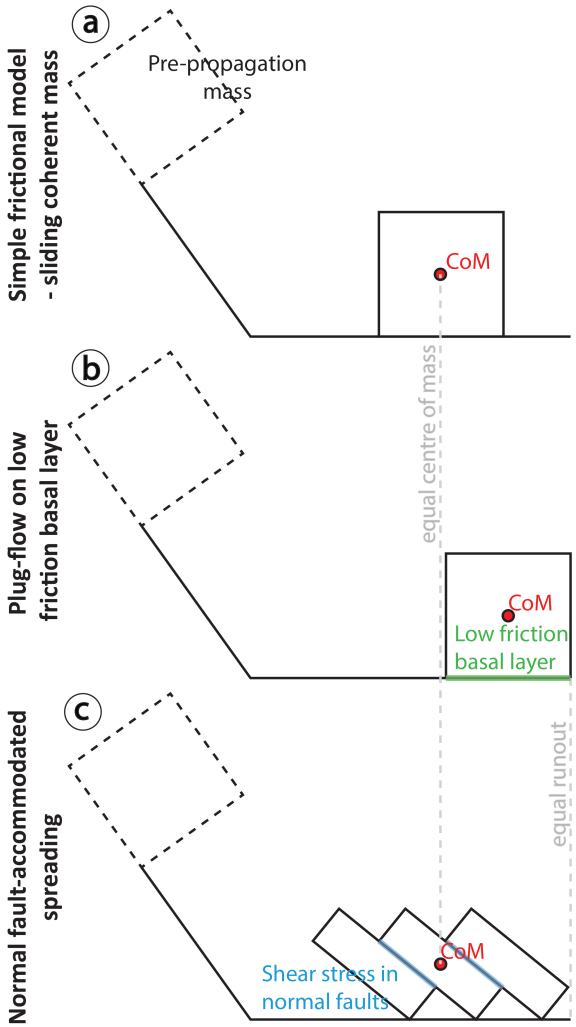

Figure 4.15: **A** Displacement of a mass after propagation, assuming a simple frictional model of a coherent sliding mass. **B** Plug-flow on a low friction basal layer: due to a reduction of friction the mass propagates further resulting in a longer runout and displacement of the centre of mass (CoM). **C** Normal fault-accommodated spreading: Spreading and extension of the mass results in a longer runout compared to a, while the displacement of the CoM remains unchanged. Back-tilting of blocks and activation of normal faults observed in the field is also consistent with this simple model.

spreading. Spreading has been proposed as a theory for the excessive runout of VDAs/RAs by Davies (1982) and Davies and McSaveney (1999). In fact, this process highlights the mechanical irrelevance of the H/L as a measure of mobility, since spreading generates a higher runout which is not necessarily reflected in the mobility of the centre of mass, and therefore energy dissipation (Davies, 1982; Legros, 2002; Dufresne et al., 2021a).

2. The lack of major shear accommodation in the body of the Ten-VDA could imply shear concentration in a basal listric layer. Shear concentration in a low frictional basal layer can result in reduced frictional losses and increased mobility (fig. 4.15b). In avalanches composed of weaker material, where disaggregation is more intense, a

basal shear layer is more likely to develop (Thompson et al., 2009). The convergence of faults and more fractured material at the base of the Ten-VDA might have allowed to evolve into a valley-confined plug flow if enough fractured/disaggregated material was generated at the base to allow local fluid granular behaviour (Paguican et al., 2021). In this case, the material at the interior of the flow would have travelled as a coherent plug over a basal and marginal low friction shear zone acting as a Bingham fluid (Voight et al., 1983; Takarada et al., 1999; Paguican et al., 2021). Takarada et al. (1999) suggest that this can be encouraged by greater proportions of weaker or hydrothermally altered lithologies since a significant amount of matrix is required to support the overlying material and initiate the plug flow phase (Paguican et al., 2021). However, large amounts of matrix are not observed in the Ten-VDAD (fig. 4.14). Consequently, deformation and shear have to be distributed through the avalanche body. Although the confinement by the paleoravine could encourage this process, the lack of weaker material that could be easily disaggregated is likely to have impeded the Ten-VDA from evolving into a plug flow on a low friction basal zone.

The lack of exposure of the base of the Ten-VDA does not permit a conclusive evaluation of the two hypotheses. However, the low degree of disaggregation and quantity of matrix in the exposed sections suggest that extensive basal shear accommodation is unlikely. It is, therefore, proposed that the mobility of the Ten-VDA was enabled by the normal fault-accommodated spreading of the mass by the extensional displacement of normal faults between blocks. This mechanism is also in agreement with the observations of undisaggregated blocks and brittle features since most of the shear of the displacement was accommodated in normal faults for the spreading of the mass, resulting in the lack of strain in the interior of blocks.

4.5 Conclusion

The facies distribution and structural analysis have led to the following model for the propagation and emplacement of the Ten-VDA:

1. The collapsed portion of the source edifice did not suffer a high degree of alteration and weakening that would precondition the mass for fracturing. Therefore, in the

initial collapse and slide phase, evolution of fractures, and coarse disaggregation of the mass were initiated but a major component of undisaggregated blocks was preserved (fig. 4.14a).

2. In the subsequent propagation, extension and spreading were accommodated in normal faulting activated in pre-existing fractures (fig. 4.14b). This led to shearing in the fault zones and back-tilting of blocks (fig. 4.7, 4.12).

3. Extension and lowering of the mass progressed, with disaggregation of blocks and matrix injected in fractures between blocks. In the matrix-rich facies, there was no turbulence or shearing and mixing was limited to gradual homogenisation generated by the agitation due to granular temperature (fig. 4.13). The VDA remained cohesive, as a dense network of blocks. Blocks were cataclased to various degrees but preserved their outline and distinct lithological composition. The cataclasis of the blocks generated a fine intrablock matrix, however, interblock mixing was limited to a small quantity of diffuse boundaries. Horst and graben structures developed as the extension proceeded (fig. 4.2, 4.14b).

4. Deeper in the deposit, the faults conjoin. There was a higher degree of shearing and agitation. Disaggregation and intrablock matrix generation were higher, eliminating jigsaw fracturing and imposing a diamicton fabric to the block facies. There was also a small amount of substrate incorporation.

5. The more distal part of the Ten-VDA exhibits higher disaggregation and gradual mixing due to agitation. This is the result of the higher stresses accommodated at the front for a longer duration due to the momentum transfer from the back and longer runout.

6. The poor disaggregation of the mass, large component of block facies and poor mixing between blocks suggest that the Ten-VDA did not fully evolve to a flow. A brittle type behaviour was dominant. The resultant deposit is comprised of a dense network of blocks.

The lack of exposure of the base of the landslide does not allow the assessment of the degree of shear accommodation at the base and the nature of the interaction with the substrate. Therefore, the excess mobility of the Ten-VDA could be attributed to two candidate processes: 1. The mobility could be the result of normal fault-accommodated

spreading and extension of the mass. In this case, the increased runout would be the result of the spreading of the material, while the centre of mass would not necessarily have achieved a high mobility (fig. 4.15c). 2. Alternatively, a low-friction basal layer might have accommodated the shear of the displacement, supporting the material above, which would have travelled as a plug-flow on a low-friction basal layer (fig. 4.15b) (*sensu* Takarada et al., 1999). The first process appears more likely due to the brittle behaviour of the material and lack of extensive quantities of matrix-rich facies. Although unlikely, the second process cannot be definitively rejected due to the lack of exposure of the deposit base.

The study presented in this chapter demonstrates the importance of detailed field observations to assess mechanisms affecting the mobility of VDA and puts in evidence how different processes are possible and should be taken into consideration when assessing the hazard related to these phenomena.

Chapter 5

Distributed stress fluidisation: Insights into the propagation mechanisms of the Abona volcanic debris avalanche (Tenerife) through a novel method for indurated deposit sedimentological analysis

Note, a version of this chapter examining the Tenteniguada volcanic debris avalanche and its propagation dynamics has been published in the Journal Frontiers in Earth Sciences - Volcanology (Makris et al., 2023b). The published version is included in the supplementary material. Symeon Makris wrote the text, prepared all of the figures and developed the arguments therein. Symeon Makris and Matteo Roverato carried out the fieldwork. All authors discussed the science and commented on the manuscript. The format of this chapter is not the same as the publication. Different sections have been integrated into different parts of this thesis. Furthermore, additional discussion relating to the topic of the thesis is included in this chapter that was not relevant to the paper examining the specific deposit.

5.1 Introduction

This chapter examines the Abona volcanic debris avalanche (Ab-VDA), located in the south of the island of Tenerife, Spain (fig. 5.1a). Although the deposit is indurated, field

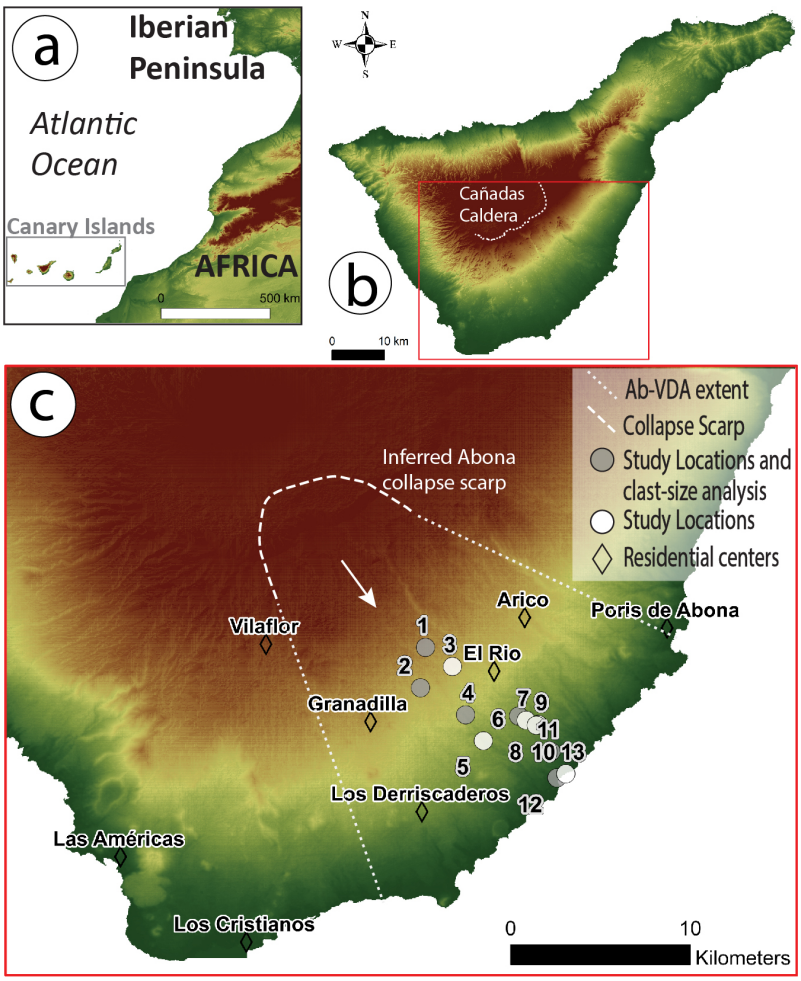

Figure 5.1: **A** Location of the Canary Islands. **B** The Island of Tenerife with the Cañadas caldera (dotted line); the red rectangle indicates the extent of c. **C** Extent of the Abona volcanic debris avalanche (Ab-VDA) as inferred by Dávila-Harris et al. (2011), with locations studied for this chapter and the locations where sampling for clast-size analysis was carried out.

observations combined with a novel clast-size analysis methodology allow its examination. The aim is to evaluate the dynamics through assessment of the propagation and emplacement processes that generated the deposit. Analysis of the findings and comparison to other deposits and models aims to ultimately evaluate potential propagation mechanisms that enable the long runouts of volcanic debris avalanches (VDAs). In order to interpret the deposits, our field investigations generated outcrop maps of the distribution of facies, textures, structures and internal sedimentology (Bernard et al., 2017). The deposit is initially described through its general structure, facies distribution and sedimentological features. The implications of these features for the dynamics of the Ab-VDA in association with other deposits and theoretical and numerical models are also discussed. Finally, this analysis permits the proposal of a new VDA model for the stress accommodation, propagation processes and the formation of the internal architecture and sedimentology

which is consistent with the observed structural features and kinematic implications (Shea and van Wyk de Vries, 2008). The findings offer information regarding VDAs which evolve into flows, as well as the factors which might enable such behaviour. The processes suggested offer constraints for conceptual models regarding VDA dynamics and stress distribution.

Clast-size analysis is a key element of sedimentological studies as it allows the study of the evolution of the deposit sedimentology and composition through the different phases of the propagation and the identification of possible mechanisms, including fragmentation (Dunning, 2004; Crosta et al., 2007; Dufresne and Dunning, 2017). The quantitative examination of clast-size distribution in the deposits can offer evidence regarding the distribution of stresses, as exemplified by the study of Dufresne and Dunning (2017), illustrating the sedimentological signature of zones of magnified shear stress. When a deposit is indurated or lithified, clast-size analysis is not possible using conventional sieving or laser diffraction (Merico et al., 2020). The consolidation of the material in ancient deposits is suggested by Tost et al. (2014) to have prohibited the study of VDA/ rock avalanche (RA) deposits (Merico et al., 2020). The novel methodology presented in this study allows the clast-size analysis of indurated/lithified deposits. Employment of the proposed methodology in other indurated deposits would extend sedimentological information on VDA deposits (VDADs) through the addition of more case studies.

5.2 Geological and regional background

5.2.1 Geological background

Tenerife is the second largest ocean-island volcano on Earth (after Mauna Loa, Hawaii). The island is composed of 90% by volume of a basaltic shield (Hürlimann et al., 1999). This is overlain by the Cañadas stratovolcano, post-shield volcanic complex. This composition reflects the dual, simultaneously active basalt and phonolite magmatic system. Basaltic volcanism began >12 Ma ago and is still active, with the most recent basaltic eruption in 1909 AD (Martí et al., 2010).

The Cañadas edifice is composed of basalt to phonolite lavas and pyroclastic deposits, generated by several eruptive events in the last 3.0-3.8 Ma (Hürlimann et al., 1999; Cas et

al., 2022). The evolution of the edifice was characterised by several constructive phases while destructive processes have also been important, with vertical and lateral collapses contributing to the geomorphic evolution of the island (Martí et al., 1997, 2010). Tenerife has hosted large landslides with volumes of 50–500 km^3 and travel distances of up to 100 km (TEIDE GROUP, 1997; Hürlimann et al., 2000; Masson et al., 2002). VDAs are the most common type of landslide mapped on the flanks of the Canary Islands (Lomoschitz et al., 2008). Large-volume VDAs are responsible for the formation of the major valleys on the flanks of Tenerife between the Upper Pliocene to Middle Pleistocene (Hürlimann et al., 1999; Martí et al., 2010; Dávila-Harris et al., 2011; Cas et al., 2022). The central volcanic complex has hosted major explosive eruptions from the phonolite magma system also generating the present-day Cañadas caldera (Martí et al., 2010). Today, the volcano structure includes the Teide and Pico Viejo stratovolcanoes, and the explosive caldera Cañadas complex (fig. 5.1b) of >1.8 Ma history with various collapse events (Dávila-Harris et al., 2011; Cas et al., 2022). The current phase corresponds to the constructive phase of the Teide/Pico Viejo complex inside the caldera.

5.2.2 Abona volcanic debris avalanche – edifice and deposit morphology

The Ab-VDAD was initially classified as a debris flow breccia (Bryan et al., 1998), although later identified as a VDAD by Dávila-Harris et al. (2011). It was generated 733 $\pm$3 ka ago by a lateral collapse of the Cañadas volcano during an ignimbrite-forming explosive eruption, as supported by petrological evidence and geochronology by Dávila-Harris et al. (2011). The fact that the trigger of the collapse is identified with relative confidence is not common, as most VDADs are difficult to assess with precise time constraints, and even then, triggering mechanisms might have left no evidence in the geological record. The Ab-VDA propagated and was deposited from the Cañadas volcano and towards the southeast, in the region of Abona for at least 21.6 km from the failure scarp thought to be its source (fig. 5.1). It covers 90 km^2, and extends further into the ocean (Dávila-Harris et al., 2011). The widespread exposure suggests that the deposit covered the entire region of Abona (Dávila-Harris et al., 2011). The Ab-VDA forms part of the Helecho Formation, which corresponds to the Lower Bandas del Sur Group (Dávila-Harris et al., 2023) and the Guajara Cycle (Cas et al., 2022).

5.3 Methodology

5.3.1 Structure and facies mapping

Due to the sedimentological heterogeneity in the Ab-VDAD, detailed facies mapping was necessary prior to sedimentological sampling. At different outcrops the structure, stratigraphy, lithology and other features were identified using the methodology described by Roverato et al. (2015) and Bernard et al. (2017). This allows for targeted sampling along the deposit in specific facies. Initially, the mapping allowed the generation of a structural overview (Bernard and van Wyk de Vries, 2017), identifying outcrops to be sampled for clast-size distribution differences as well as their potential longitudinal evolution along the deposit.

5.3.2 Clast-size sampling

In this study we have employed a novel combination of techniques and sampling strategies for clast-size analysis of the indurated Ab-VDAD. Size distributions were sampled exclusively for clasts (not matrix) in the matrix-rich facies (MF) at seven locations along the deposit (fig. 5.1c) to evaluate potential longitudinal evolution and variability of clast sizes and proportion of matrix. The method employed was based on manual photographic grid sampling analysis of clasts from scaled orthophotos generated parallel to the outcrop surface (e.g. Ibbeken et al., 1998; Blair and McPherson, 1999; Casagli et al., 2003; Attal and Lavé, 2006; Crosta et al., 2007; Zhang et al., 2015; Ferraro et al., 2018; Harvey et al., 2022).

A frequency-by-area approach methodology was proposed by Chayes (1956) for the mineral composition of cross sections and is based on an area-volume relationship supporting that the ratio of the area occupied by mineral A to the total measurement area is a consistent estimate of the volume percentage of mineral A in the sample (Chayes, 1956, p. 13; Glicken, 1996). This was adopted by Glicken (1996) exclusively for the sampling of the coarse component of VDA samples. The results of the described methodology are different in nature, but theoretically equivalent to the frequency-by-weight output of sieving analysis (Kellerhals and Bray, 1971). Image-based clast-size analysis methods are non-intrusive and provide a more efficient way to extract size distributions of non-cohesive material (Detert and Weitbrecht, 2020), and an alternative in cases where sieving is not an option

due to induration or lithification of the material. Additionally, while sieving methods produce grouped data, photographic analysis produces continuous data which allows more accurate statistical analysis (Buscombe, 2008).

The methodology proposed here utilises photogrammetry, using the commercially available software Agisoft Phtoscan, to combine data from multiple photographs in a single orthophoto sample. Measurements were made on samples at two scales: at the outcrop scale to ensure representation of the coarsest particles from the >1 m scale up to 5 mm, and smaller sample windows for finer particles up to 2 mm. Large-scale samples represent areas up to <32 m^2 and better represent larger clasts, without compromising the resolution of the sample. Conversely, in smaller-scale sample windows (up to ~10m^2), smaller particles are better represented due to the smaller area represented in every pixel. The resolution achieved by these smaller samples was <0.21 mm/pixel, allowing the sampling of particles up to >0.28 mm. Although the small sample windows had no upper size boundary, due to their small area, they were not suitable for representing larger clasts. Nonetheless, the area represented was up to ~10m^2 to ensure a sufficient sample size. The results from the two scales were combined to generate the clast-size distribution of the whole size range.

Glicken (1996), as well as other researchers (e.g. Crosta et al., 2007; Shugar and Clague, 2011), have used photographic methods to measure the area occupied by each and every particle over a threshold size in a single photograph to predict the area cover of a particular size range as a proxy for the volume percentage (instead of grid-counting), in accordance with the photo-sieving methodology proposed by Ibbeken and Schleyer (1986). Instead, in the methodology proposed here, the clast-size distribution is determined by grid-sampling individual clasts in an extensive orthophoto sample and calculating the area occupied by each size range. In the environment of the ImageJ software, the desired grid can be generated and geometric properties of clasts can be automatically calculated (Spychala et al., 2021) when their boundaries have been manually drawn (Berends and Eggenhuisen, 2018). Only the particles intersected by grid nodes were measured. The minimum Feret's diameter, defined as the smallest possible distance between two parallel tangents of an object, was used as the size measurement as it can be considered equivalent to the property by which particles are classified when sieved. Where a node was located over matrix, this was noted in the measurements to allow calculation of the percentage of matrix relative to

clasts following the methodology described by Blair (1987).

Although this methodology allows the clast-size analysis of the indurated deposit, it is restricted by the limitations of photographic analysis. Therefore, the full size range cannot be sampled because particles smaller than 2 mm could not be accurately and consistently measured. This was especially true of similar-colour particles in the matrix. Additionally, the sedimentological term matrix is an assemblage of smaller particles surrounding coarser particles (Bates and Jackson, 1984), and is therefore, scale-dependent rather than assigning a particular size (Vezzoli et al., 2017). Therefore, a lower boundary had to be established to maintain consistency when comparing matrix-proportion between the samples. For the purposes of this quantitative analysis matrix was considered to be composed of any particle of sand size or finer (<2 mm).

While the area of the large-scale sample orthophotos was generated to cover the largest possible area permitted by the outcrop exposure, and thus include the maximum heterogeneity, the clast sample size, for both the small- and large-scale samples, was chosen according to the guidelines of Bunte and Abt (2001) to ensure a <5% error around the mean with confidence of >95%. The calculation of the sample size requirement takes into consideration the median and sorting of the population generated by a pilot sample. One limitation of this methodology is that it does not allow lithological component analysis since lithologies cannot be reliably identified in small particles in the photographic samples. A full evaluation of the methodology, its uncertainties and limitations is included in the supplementary material (Appendix B).

5.4 Composition, structure and sedimentology of the Ab-VDA

The deposit is exposed across ~10 km from the first outcrop, 11.5 km from the current inferred scarp (location 1) to the coast (location 13) ~22 km from the inferred scarp (fig. 5.1c). The deposit does not outcrop more proximally than 11.5 km. The thickness of the deposit varies from 2-3 m in some locations up to a maximum thickness of 62 m (at location 4). The Ab-VDAD is predominantly composed of less competent scoria, clasts of ignimbrite lithologies and pumice fall material and substrate-incorporated pumice while it only contains a minor component of lava lithologies (Dávila-Harris et al., 2011). In marginal locations which represent the material deposited near the external boundaries

of the avalanche, the deposit thins and disappears on the slopes, illustrating that the avalanche was locally constrained and channelised by ravines in the paleotopography as illustrated in fig. 5.2. Therefore, at least in some sections, the flow was subdivided into different streams. Six exposed and accessible outcrops have been sampled and studied in terms of clast-size distribution. These locations are illustrated in fig. 5.1c, with further details in the supplementary material Appendix C.

Figure 5.2: Section of the outcrop at location 3. The red dashed line represents the boundaries of the deposit thinning against the slope of the paleotopography.

5.4.1 Facies composition and distribution

The deposit is a very poorly sorted, heterolithic breccia which exhibits characteristic VDA block and MF (Dávila-Harris et al., 2011). In this chapter the term edifice block facies (EBF) (equivalent to the block facies of Glicken, 1991) is used instead of block facies. The term was introduced by Bernard et al. (2021) and is here used because only blocks from the original collapsed edifice are observed and no blocks considered to have been incorporated from the propagation path substrate. Otherwise, the term is equivalent to the block facies used in the rest of the thesis. The EBF is composed of undisaggregated or poorly disaggregated portions of the original edifice, and the MF is composed of a heterolithic poorly sorted mixture of clasts and matrix. The facies distribution is chaotic and unsystematic, while outcrops exhibit both facies in proximity. The term matrix refers to finer grains surrounding larger particles (Mehl and Schmincke, 1999), which is scale-dependent rather than assigning a particular size (Vezzoli et al., 2017).

5.4.1.1 Edifice block facies (EBF)

The Ab-VDAD EBF is composed of unconsolidated, or poorly consolidated, portions of the original edifice (referred to as blocks) emplaced in the deposit unmixed with the surrounding material, retaining lithological distinctness (Bernard et al., 2021). Blocks are universally microfractured and to some degree disaggregated as clasts in their interior are displaced relative to each other. Disaggregation implies the displacement of these components, altering their original relative placement in the structure and fabric of the rock mass. Fracturing refers to the break-up of a block resulting in a fabric of individual component clasts. Lithologies composing blocks include the more competent hydrothermally altered and fresh lavas; the less competent and resistant scoria, ignimbrite and pumice fall lithologies clasts and substrate-incorporated material (Dávila-Harris et al., 2011). However, the proportion of the competent lavas compared to the less competent material is minor throughout the EBF. This is evident at location 2 where the main characteristics of EBF are illustrated in fig 5.3. The shape of blocks is distorted and elongated to lenticular shapes, as exemplified by the pumice and scoria units in fig 5.3c and d. Nonetheless, blocks retain lithological homogeneity and distinctness compared to surrounding material. Despite the fracturing and distortion, lithological units are preserved in the interior of blocks (fig 5.3). Sections of remnant stratigraphic sequence are preserved where these units maintain their original order as illustrated by the sequence of lithological units in fig 5.3c. These lithologies are interbedded and stretched to assume fluidal mixing forms (fig 5.3b, c). Each unit is composed of a poorly sorted diamicton of monolithological cataclased material. Cataclasis refers to the fracturing, comminution, disaggregation by the displacement of component parts and production of matrix that generates a granular diamicton fabric. Uninterrupted EBF domains extend for more than 100 m; however, undisaggregated portions of remnant stratigraphy are only observed in sections <12 m in length. The EBF with elongated remnant stratigraphic sequence and variable degrees of preservation forms pockets of less disaggregated material in a chaotic deposit where the degree of disaggregation is not systematically distributed. Such remnant stratigraphy is only preserved in pockets within the deposit at locations 5, 12 and 13, as exemplified in fig. 5.4c illustrating a pocket of EBF and preserved stratigraphy surrounded by MF. The area between undisaggregated blocks is filled by the intrablock matrix as illustrated in fig. 5.4.

Within the EBF, the intrablock matrix is composed of poorly sorted mixture of heterolithic

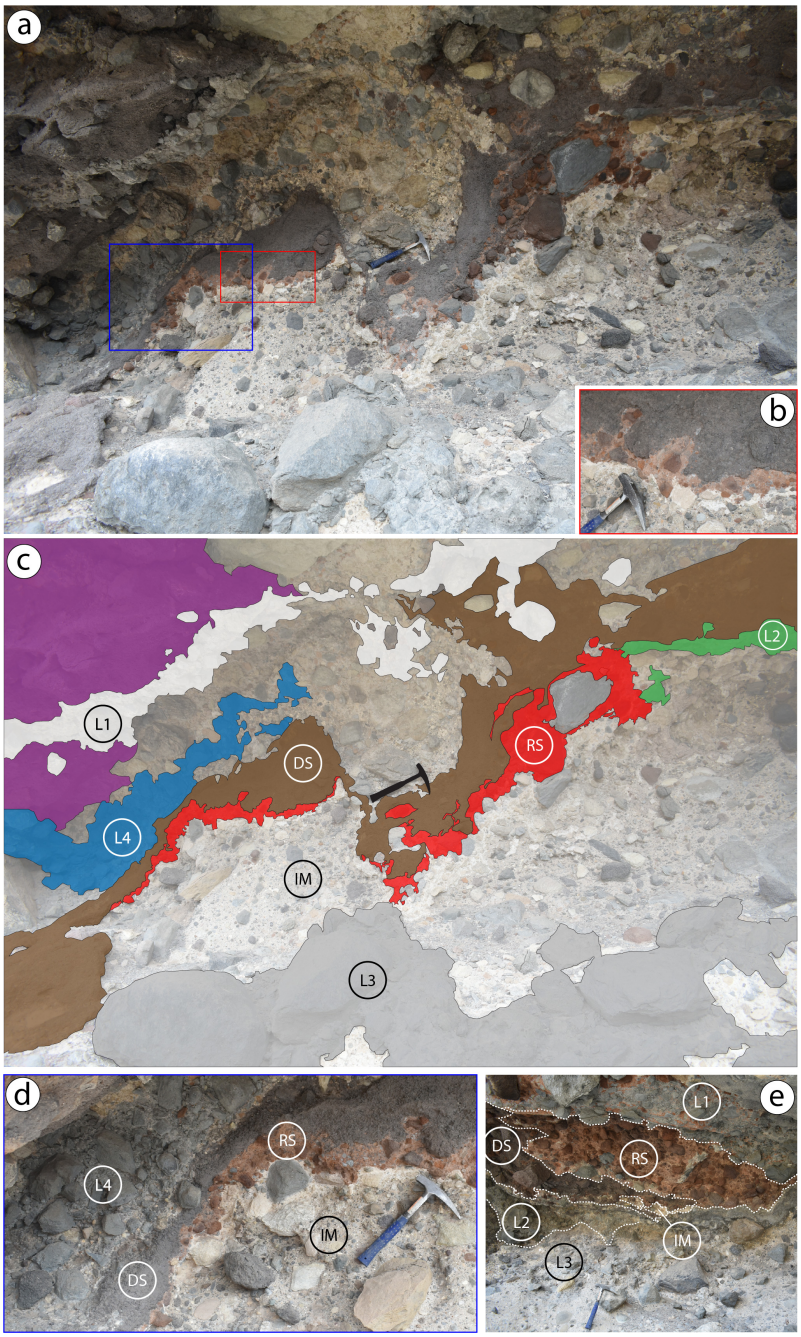

Figure 5.3: Several features from EBF of location 2: **A** Overview of a characteristic section from this location. Preservation of stretched lithological units as monolithological diamictons. The blue and red rectangles correspond to the extent of d and b respectively. **B** Fluidal form intrusion of one unit into another with no mixing. **C** The lithological units are here coloured to highlight their fluid-like behaviour, and preservation of stratigraphic sequence. IM: intrablock matrix; L1: lava unit 1; L2: Lava unit 2; L3: Lava unit 3; L4: Lava unit 4; DS: Dark scoria unit; RS: Red scoria unit. **D** Lava units and weaker scoria units exhibit different degrees of cataclasis even though they are found in adjacent positions. The lava unit at the left of the image is less comminuted with larger clasts compared to the dark scoria and red scoria units at the centre of the image. **E** The lithological units observed in c are here observed at a different area of the same location in a similar stratigraphic sequence.

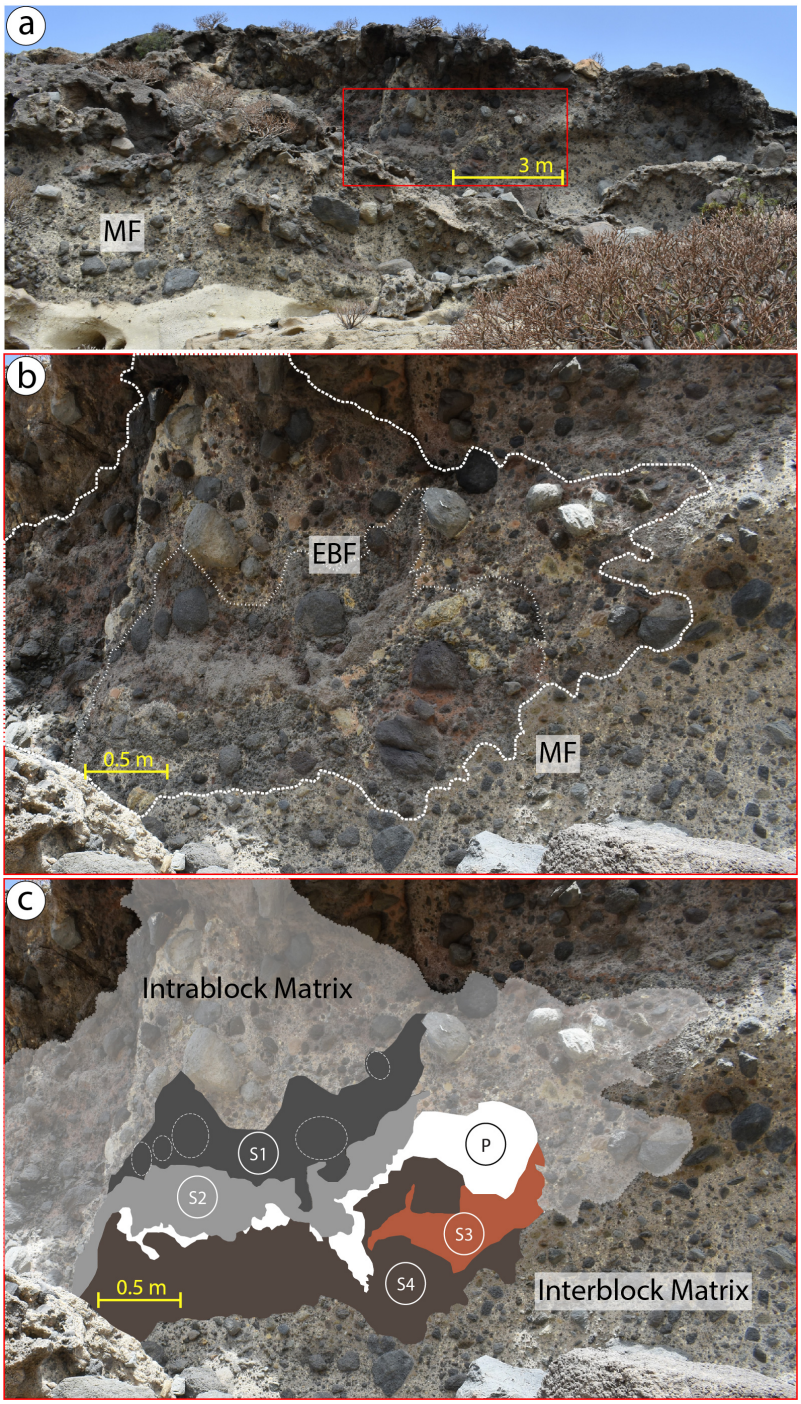

Figure 5.4: The internal structure of the Abona deposit at location 12. **A** The outcrop presents both the matrix-rich facies (MF) as well as the edifice block facies (EBF), and both interblock and intrablock matrix. The area of the red rectangle represents the extent of B and C. **B** The bold white dashed line encompasses the EBF which is surrounded by the MF. The contact between the two facies is diffusive. The finer white dashed line encompasses preserved stratigraphic sequence. The boundary between the matrix and the distinct lithological units is also diffusive. **C** Same extent as b. The section of preserved stratigraphy is composed of different lithological units of scoria: S1, S2, S3, S4; and pumice: P. Different units have been coloured to highlight their stratigraphic sequence and fluidal mixing. Dashed circles highlight rounded clasts.

clasts within a heterolithic matrix. A clast refers to any rock which would not break if passed through a sieve, or was immersed in water, after the definition by Glicken (1991).

The lithology of the clasts and matrix represents the lithologies present in the vicinity, within each block. This is evident locally around monolithologic blocks where the nearby matrix is enriched in that lithology. Pumice deposits make this particularly evident, as the nearby matrix has a visibly different composition enriched in the white pumice as illustrated in fig. 5.5. Here, the intrablock matrix adjacent to a pumice unit is visibly enriched by the diffusing pumice material (fig. 5.5).

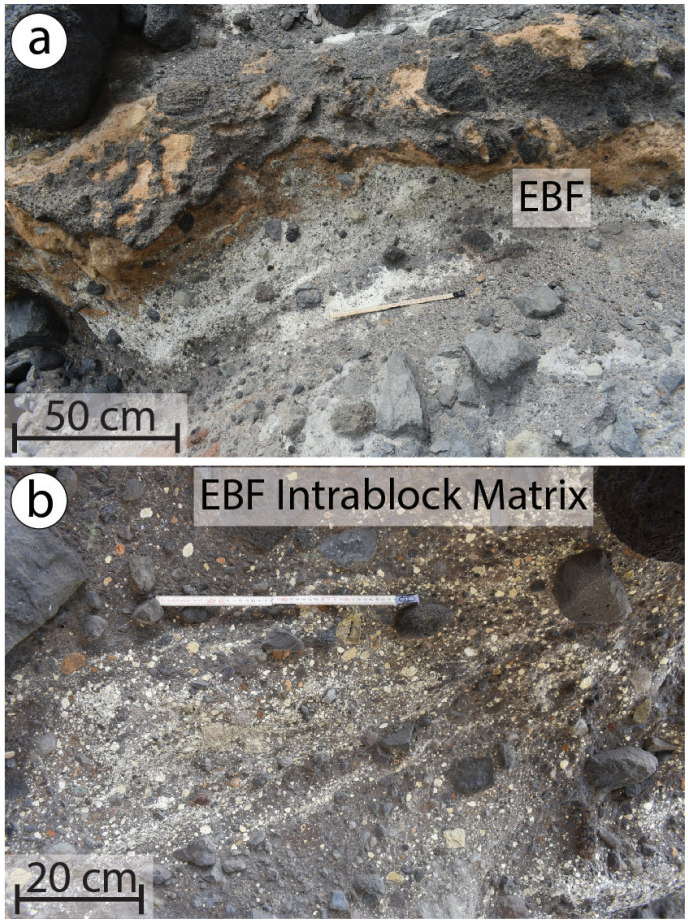

Figure 5.5: **A** Edifice block facies (EBF) from location 3 containing a unit of pumice. **B** The intrablock matrix proximal to this unit is enriched in pumice due to the progressive diffusion of material to the matrix.

The degree of mixing within the intrablock matrix exhibits some variability but is always lower than the interblock matrix, which is completely mixed and heterogeneous in the Ab-VDAD. The intrablock matrix (as well as the intrablock) exhibits no internal structures or features.

5.4.1.2 Matrix-rich facies (MF)

The MF is exposed in all the locations studied, from the most proximal to the most distal. Its abundance suggests it constitutes the dominant facies component of the deposit

although the proportion could not be quantified due to the interrupted exposure. The MF is similar to the equivalent facies reported in other VDADs (e.g. Glicken 1991; Bernard et al. 2021) and is notably uniform throughout the deposit. The MF consists of a well-mixed, heterolithic, very poorly sorted mixture of subangular-to-subrounded clasts and interblock matrix composed of material from the source edifice (fig. 5.4, 5.6a), pumice incorporated

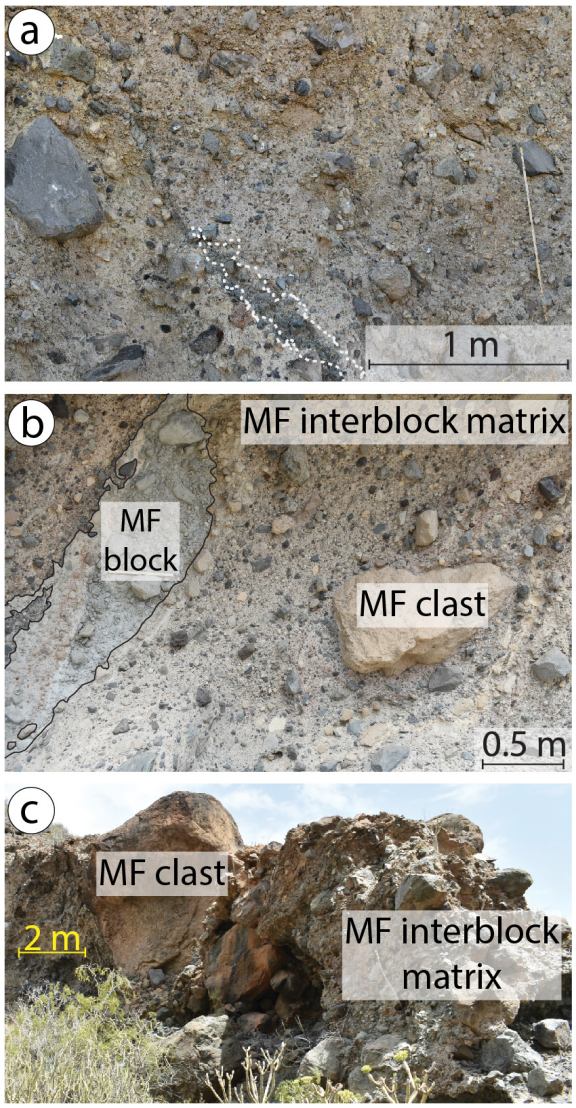

Figure 5.6: **A** Matrix-rich facies (MF) in location 2 including a lenticular block with its outline indicated by the dashed white line. This is an orthophoto generated using structure from motion photogrammetry. B and C illustrate features from location 4. **B** A portion of the MF composed of poorly sorted clasts, interblock matrix as well as a monolithological microfractured block. **C** The annotated MF clast is the largest encountered in the deposit and has a maximum diameter of 6m.

from the substrate during propagation (fig. 5.7), and a small amount of juvenile phonolite clasts. The juvenile clasts have chilled margins and were likely incorporated from a dome collapse (Dávila-Harris et al., 2011). Particles in the MF range from micrometres up to clasts of <6 m, as shown in fig. 5.6. Its composition represents the lithologies that also

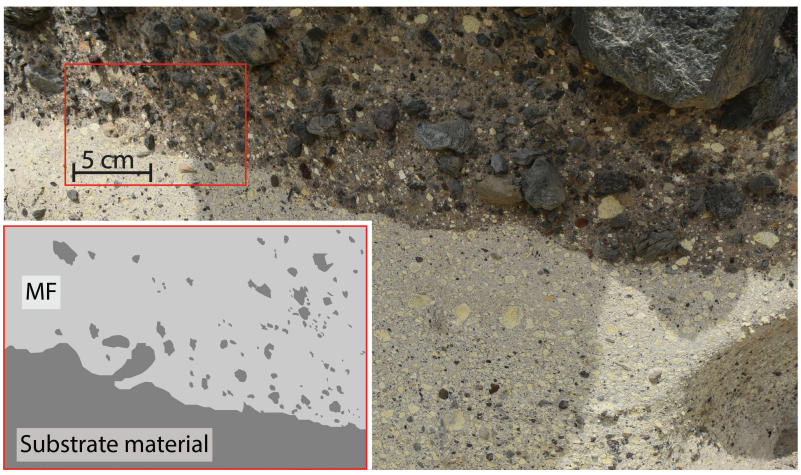

Figure 5.7: Basal contact between the deposit (Ab-VDAD) and the substrate at location 12. The red rectangle represents the extent of the insert at the bottom left of the figure. The insert highlights the incorporation and diffusion of substrate material (dark grey) into the matrix-rich facies (MF) (light grey) due to abrasion.

occur in the EBF. However, a greater degree of mixing and homogenisation produces a distinctive heterolithic matrix which differs from the cataclased but unmixed diamicton of the EBF, as well as the less heterolithic and less mixed intrablock matrix. The difference is illustrated by the comparison of fig. 5.4b with fig. 5.6a. The intrablock matrix of fig. 5.4 is much less poorly sorted, less polylithological and includes a greater proportion of clasts relative to matrix. The percentage of the matrix relative to clasts is highly variable. Although well mixed, the MF also contains a minor quantity of microfractured MF blocks with lenticular shapes (fig. 5.6a, b). These represent portions of the original edifice that although included in the MF have not been completely disaggregated. However, the MF lacks any stratification, grading or internal features.

5.4.2 Internal structure and sedimentology

5.4.2.1 Fracturing and cataclasis

At the metre and down to the finer than centimetre scale, the material in the EBF is universally fractured and cataclased. The cataclasis of the material generates lithological units composed of larger clasts in a finer matrix assuming the fabric of a diamicton while remaining unmixed and preserving their lithological distinctness as exhibited by different lithological units in fig. 5.8. Blocks suit the term of fragmental rock clasts used by Alloway et al. (2005) as fractured, deformed blocks in some cases preserving stratigraphic sequence (fig 5.3, 5.4). The products generated by the fracturing and comminution are the particles

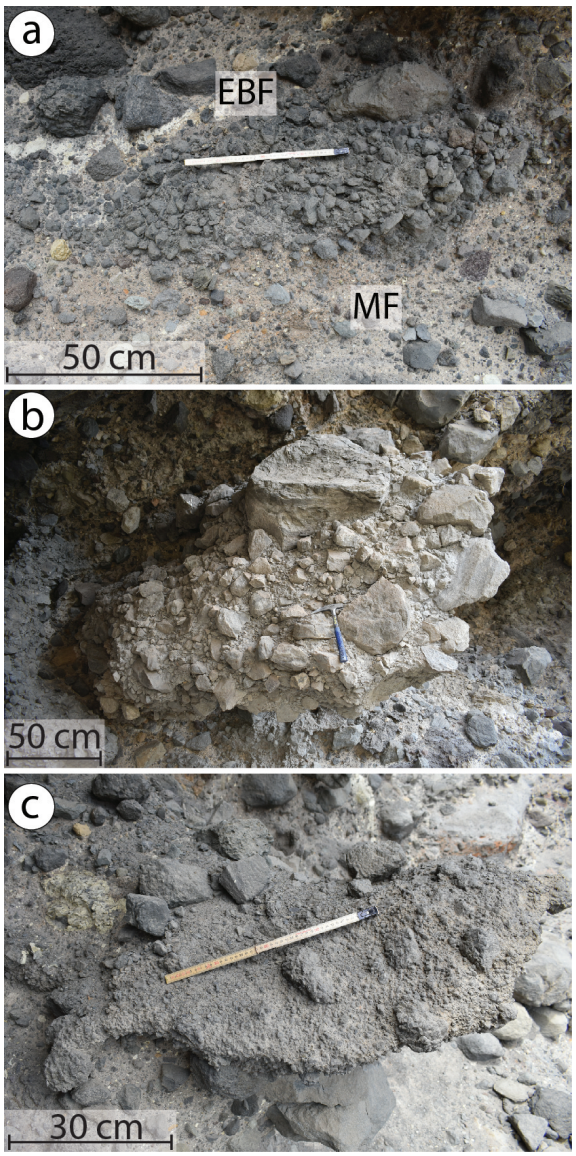

Figure 5.8: Monolithological diamictons. **A** Location 6. Cataclased diamicton in contact with the matrix-rich facies (MF), with diffusive boundaries and lenticular shape. **B** Location 5. Lava unit exposed in three dimensions due to the preferential erosion of the weaker lithologies around it. The cataclasis generated larger clasts and less matrix in comparison to the other lithologies. **C** Block of scoriaceous material at the most distal location 13.

constituting the intrablock matrix and the MF. Clasts range in roundness from subangular to subrounded and even rounded (e.g. fig. 5.4, roundness highlighted in fig. 5.4c). Other than the mentioned microfracturing, and the scarce shear displacement of some larger fractured clasts, no larger-scale brittle deformation, fracturing or faulting has been observed in the Ab-VDAD. In these clast components, displacement is caused by the shear stress parallel to the flow direction generated by differential rates of propagation. Such examples are illustrated in fig. 5.9a-b.

The degree of fracturing in blocks is not exclusively associated with the distance travelled

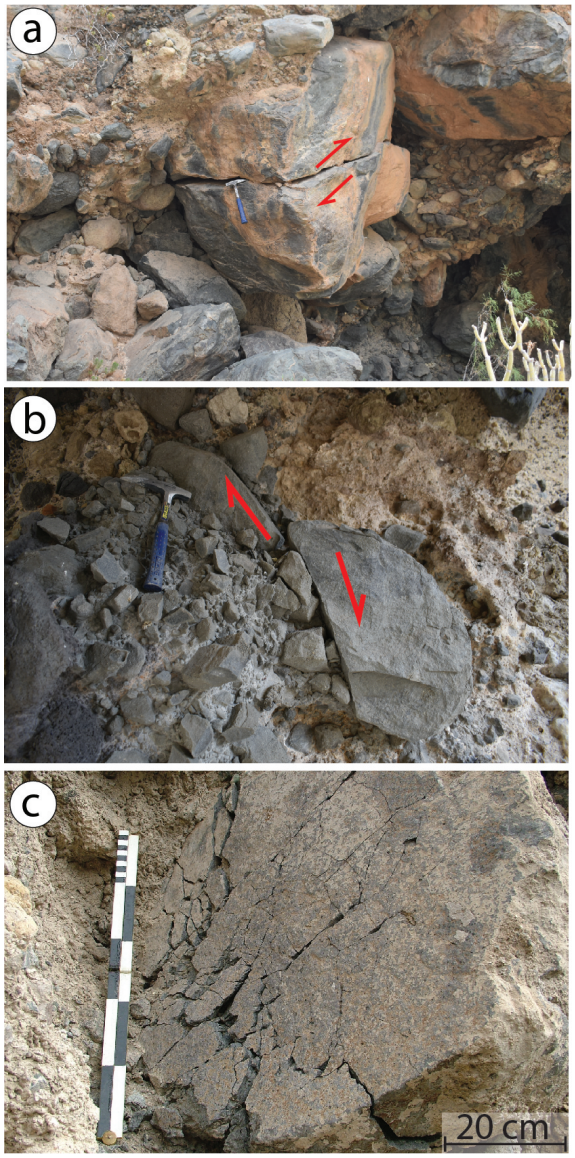

Figure 5.9: Brittle features of the Abona volcanic debris avalanche deposit. **A** Fractured clast with components displaced parallel to the propagation direction (location 4). **B** The relative displacement between clasts originating from the same particle illustrates the shear in the material (location 5). **C** Fractured block with components preserving their relative position in a jigsaw fabric. This was observed in location 4 but was a rare occurrence for the deposit.

by the Ab-VDA, as also suggested for other deposits (e.g. Reubi and Hernandez, 2000). The EBF exhibits a variable degree of cataclasis and disaggregation, especially between different lithological components, even at the same outcrop. Qualitative assessment of the Ab-VDAD suggests that less competent lithologies, such as scoria, exhibit more cataclasis than the more competent lavas, as also suggested by Dávila-Harris et al. (2011). The degree of cataclasis varies from pulverized dust to coarse breccias. The differential degree is most obvious where strata composed of competent lava lithologies are in proximity to strata of more cataclased scorias as demonstrated in fig 5.3b and d, where parts of the

same block, with different lithology exhibit dissimilar degrees of cataclasis and resultant clast sizes. Scoriaceous material, which is weak and porous, is the most strongly cataclased lithology producing a microfractured diamicton composed of clasts in a fine interblock matrix of sand-sized and finer particles, shown in fig. 5.8c. This style of cataclasis in weaker lithologies has been encountered throughout the Ab-DAD (fig 5.3, 4b). In contrast, the more competent lava lithologies, clasts produced are larger and the proportion of matrix is smaller (fig 5.3d, 5.8b).

5.4.2.2 Fluidal behaviour and features

At the larger outcrop scale, no brittle fracturing or faulting is exhibited. In the EBF, lithological units preserve their distinctness and outline despite assuming distorted thin, elongated, lenticular forms. Where lithologies are interbedded and stretched, they assume fluidal mixing forms where portions of one lithology intrude another unit (fig 5.3, 5.4), preserving their local homogeneity and giving the deposit a form similar to the mixing of viscous fluids as shown in fig 5.3c.

Lithological units within the EBF have diffuse boundaries where adjacent to the MF (fig. 5.10a), or intrablock matrix (fig. 5.10b). The material from the periphery of a specific unit appears to diffuse outwards from its boundary into the matrix, while gaps created between the diffusing particles are intruded by matrix material. This is illustrated in fig. 5.10a and b by the lighter-coloured matrix mixing with the darker undisaggregated block material at the boundaries.

Location 12, illustrated in fig. 5.4a serves as a good example of the internal structure of the Ab-VDAD. This outcrop is composed of MF, which surrounds fractured and partially disaggregated EBF blocks. The contacts between the two facies are diffuse with material from the EBF diffusing into the interblock matrix (fig. 5.4b). The blocks are composed of elongated lenticular monolithological units with preserved stratigraphic sequence and intrablock matrix (fig. 5.4c). The mixing of the stratigraphic units illustrates the fluidal behaviour (fig. 5.4c). Contacts between different units within the block and between the intrablock matrix are also diffusive. The intrablock matrix is composed of the lithologies within the block. Similarly, at location 5 (fig 5.3) monolithological units with fluidal features are preserved surrounded by a pumice-rich interblock matrix. Some contacts are

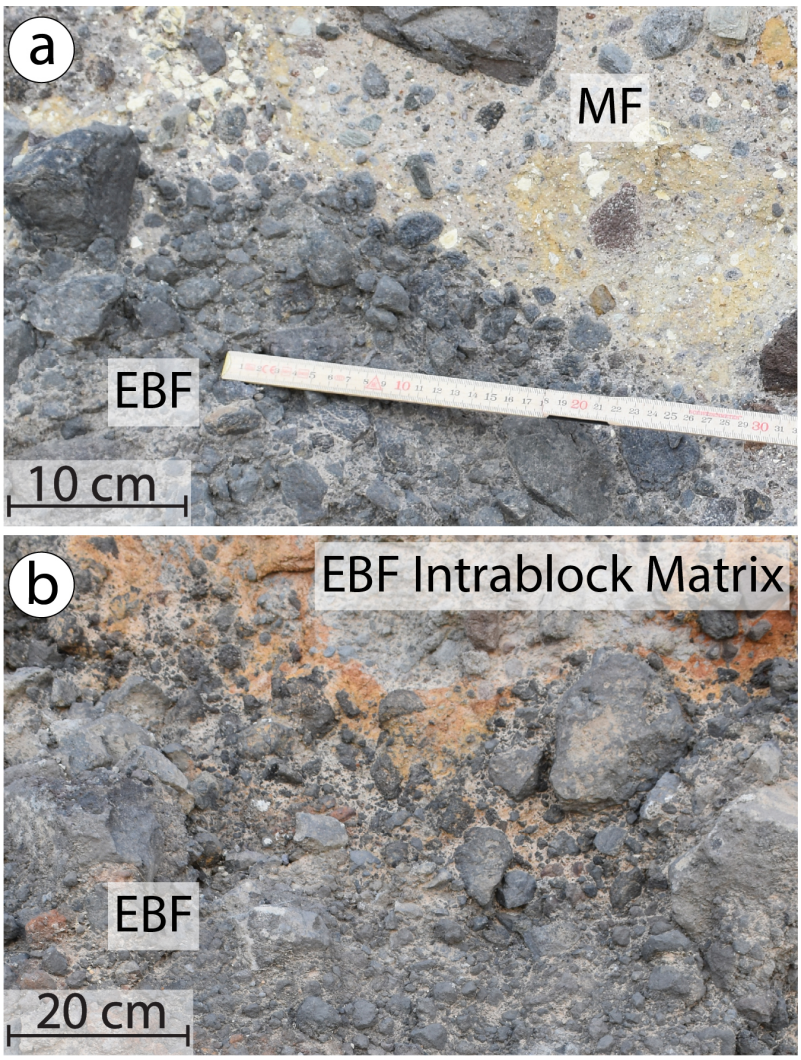

Figure 5.10: Diffusive contact **A** between the edifice block facies (EBF) and the matrix-rich facies (MF); and **B** between EBF preserved unmixed lithological unit and intrablock matrix. Both from location 11.

not diffusive, but instead, take the form of fluid-like injection of one unit into another, and in the intrablock matrix (fig 5.3b).

5.4.3 Clast-size analysis

Fig. 5.11 illustrates that clasts greater than -9.5ϕ are only encountered in locations more proximal than 13.05 km (loc. 2). However, other than this observation there is a lack of similarity or evolution with distance in the form of the histograms representing the clast-size distributions of fig. 5.11. The cumulative plots illustrated in fig. 5.12a also suggest a lack of systematic clast size variation. Fig. 5.12b illustrates the evolution of the different clast-size percentiles along the deposit. P10, P25 and P50 show very little variability. P90 and P75 exhibit a reduction until 17.8 km; however, this trend is subsequently not consistent. Median clast sizes vary between 19 mm and 61.5 mm (table 5.1). The clast-

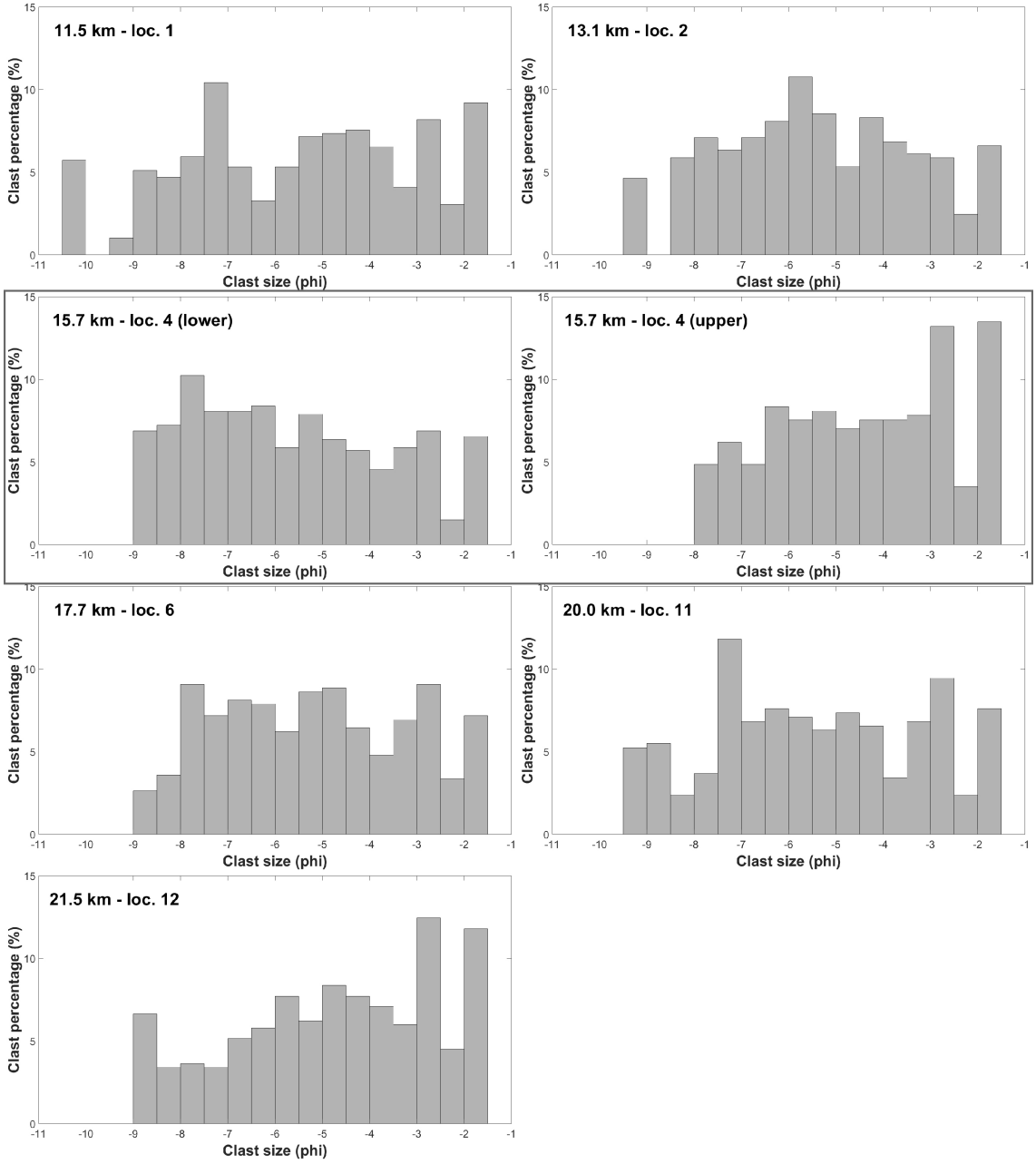

Figure 5.11: Clast-size distributions for clasts in the matrix-rich facies at different locations along the Abona volcanic debris avalanche deposit from proximal to distal.

size distributions illustrated in fig. 5.11 and fig. 5.12a, as well as the statistical percentile analysis presented in fig. 5.12b, illustrate no consistent systematic variation or longitudinal evolution correlated to the distance from the source along the 10 km that the deposit is exposed.

The analysis reveals a variable proportion of matrix between 36% and 65% at different locations of the MF (table 5.1). The proportion of matrix is also variable within the same outcrop as illustrated in table 5.1 by the two samples carried out for different positions within location 4 (15.67 km from source). This was the tallest outcrop (62 m), presenting

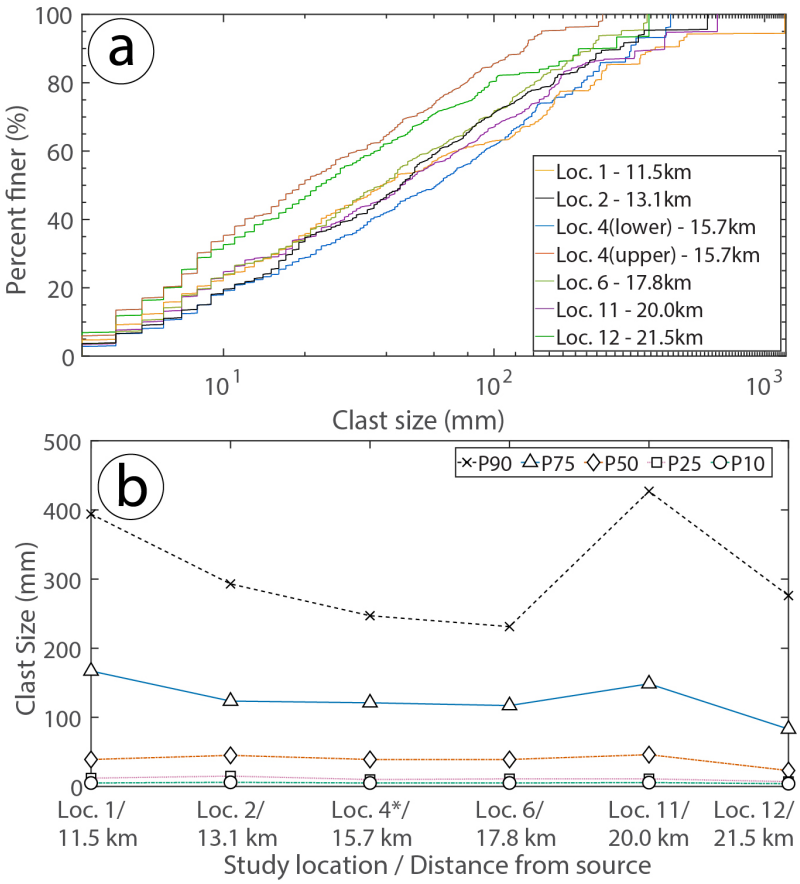

Figure 5.12: Clast size analysis results **A** Cumulative plots of the sampled clast populations from all the samples. The legend includes the distance of each location from the source. **B** Representation of the 90th, 75th, 50th (median), 35th and 10th percentiles at the different study locations along the deposit. (Note that the upper and lower sections of location 4 are considered together for b).

Table 5.1: Clast-size analysis at different locations along the Abon deposit. Location 4 is represented by 2 samples, one is from deeper closer to the base and one from shallower in the deposit, illustrated in supplementary material Appendix D.

Loc./ sample	Distance from source (km)	90th percentile (mm)	75 th percentile (mm)	50th percentile (mm)	25 th percentile (mm)	10th percentile (mm)	Matrix proportion (%)
1	11.5	394.0	167.0	39.0	12.0	5.0	52.4
2	13.0	293.0	123.5	45.0	15.0	6.0	59.1
4 upper	15.7	321.0	167.0	61.5	16.0	6.0	54.7
4 lower	15.7	129.8	62.8	19.0	8.0	4.0	35.6
6	17.7	231.2	117.0	39.0	11.0	5.0	52.6
11	20.0	427.0	148.5	46.0	11.0	5.6	64.9
12	21.5	276.1	83.0	23.0	7.0	4.0	50.8

high vertical variability in the MF. Sampling was carried out for the matrix at the upper and lower sections of the outcrop (Appendix D). Closer to the base the deposit contains a higher block component, being blockier, compared to the shallower part of the deposit. The lower sample contains a matrix proportion of 35.6%, while the lower contains 54.7% matrix. The difference is also reflected in a greater mean and median clast size in the lower section compared to the upper (table 5.1).

5.4.4 Substrate interactions

The substrate over which the Ab-VDA propagated is a pumice fall deposit (Moradas Fm. - 738 ±4 ka) in locations more proximal and up to location 10 (fig. 5.1). In the more distal locations, after location 10, the substrate is the pumice-rich ignimbrite of the Helecho Formation (Cobón Member - 733 ±3 ka) (Dávila-Harris et al., 2011). Between the Moradas formation and the deposit, a thin layer of soil is preserved. The soil represents the brief hiatus in eruptive activity that preceded the Ab-VDA (733 ±3 ka) (Dávila-Harris et al., 2011). Substrate deformation features observed in the deposit at different locations include bulldozing (where deformed but not incorporated) (fig. 5.13a), ploughing (where incorporated) (fig. 5.13b), flame injections (fig. 5.13c), faulting (fig. 5.13d) and sharp abrasive erosional contacts (fig. 5.7). Bulldozing is the pushing and compressing of substrate material into mounds due to the frictional shear of propagating VDA material. Ploughing, on the other hand, is the process whereby the pushed material is detached from the substrate and incorporated en masse (Dufresne et al., 2010a). Substrate incorporation is directly observed at locations that expose the basal contact of the Ab-VDA (e.g. fig. 5.7), as well as from the existence of pumice from the substrate higher up in the body of the deposit. At the basal contact portions of the substrate have been preserved in the process of being detached as illustrated in fig. 5.13b-d).

The perturbation of the substrate is highly variable and unsystematic throughout the deposit, even at the metre scale, and there is no systematic variation with distance from the source. Penetration of the substrate occurs by both blocks and matrix. The pumiceous soil layer between the pyroclastic deposits and the deposit is in places preserved (fig. 5.13e, f), while in others in the same outcrop missing or disturbed (fig. 5.13f).

5.5 Discussion

5.5.1 Internal morphology and sedimentology

5.5.1.1 Brittle fracturing

All the material in the Abona EBF is microfractured and cataclased, with monolithological units assuming the fabric of a diamicton, while highly mixed domains constitute the

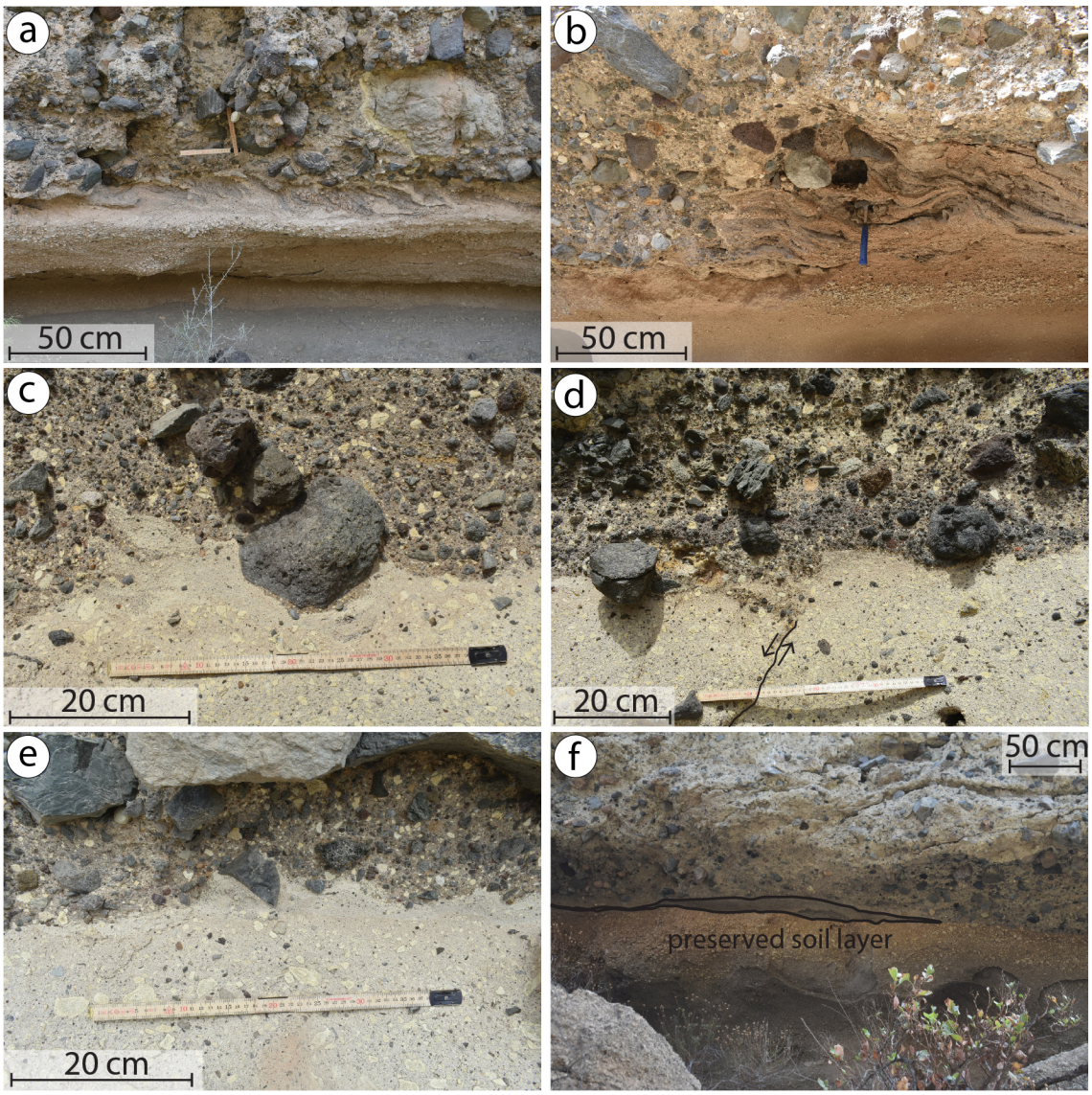

Figure 5.13: Interactions between the Abona deposit and the substrate. **A** Substrate bulldozing (location 10); **B** ploughing (location 7); **C** small-scale flame injection (location 12); **D** monolithological block in contact with the substrate, and faulting in the substrate due to the weight of the VDA (location 12); **E** the soil layer in the substrate is uneroded and almost unaffected by the passage of the VDA at this segment (location 12); **F** the soil layer is locally preserved while eroded in adjacent segments of the contact (location 3).

interblock and intrablock matrix. Undisaggregated material with original textures is almost non-existent in the deposit, despite unfractured and undisaggregated jigsaw blocks being a typical feature of other VDADs (Siebert, 1984; van Wyk De Vries et al., 2001; Chapter 4 of this thesis). Jigsaw-fractured clasts, like the one illustrated in fig. 5.9c, are few and restricted to specific locations within the deposit. In general, a VDA mass suffers rapid fragmentation and coarse disaggregation at the initial edifice collapse stage (Voight et al., 1983; Glicken, 1991; Longchamp et al., 2016). Nonetheless, in the Ab-VDA, the cataclasis exhibited throughout the deposit (except a minor number of large clasts) suggests syn-propagation progressive fragmentation (Dávila-Harris et al., 2011; Perinotto et al., 2015;

Roverato et al., 2015; Paguican et al., 2021) rather than an impulse of fragmentation due to the initial collapse. Syn-propagation fragmentation due to grain-to-grain contact is thought to be generally minimal in VDAs. However, depending on lithology and strength, fragmentation of intact rock can also occur through grain interactions. This has indeed been suggested by Dávila-Harris et al. (2011) for the Ab-VDAD and is supported by studies on other VDADs proposing fragmentation as a continuous process, such as Socompa VDA (Chile) (van Wyk De Vries et al., 2001), Parinacota (Chile) (Clavero et al., 2002), Taranaki (New Zealand) (Roverato et al., 2015) and the study of VDAs of La Réunion Island by Perinotto et al. (2015). Continuous progressive fragmentation and cataclasis have also been proposed by Davies et al. (1999) and McSaveney and Davies (2007) in their dynamic fragmentation proposed model, according to which particles store energy elastically, releasing it when fractured and contributing to the mobility of the mass. However, in their model Davies et al. (1999) suggested that fragmentation mainly occurs at the base. Nonetheless, in the Ab-VDA, signs of fragmentation, comminution and cataclasis are uniformly exhibited across the whole deposit.

Fragmented particles that do not experience further crushing, but are smoothed and rounded by frictional abrasion in the agitated mass to undergo further size reduction (Schneider and Fisher, 1998; Perinotto et al., 2015; Paguican et al., 2021). In the Ab-VDAD clasts composed of weaker lithologies are locally subrounded-rounded, as illustrated in the examples in fig. 5.4b, c. Rounded clasts are not a typical feature of VDA/RA deposits. In fact, in RA deposits, composed of more competent material, all clasts are angular due to brittle fractures. Less competent lithologies do rarely exhibit scratching or snubbing of corners in those cases (Hewitt et al., 2008). This feature potentially indicates the weakness of the material composing the Ab-VDAD.

In the Ab-VDAD, the rate of comminution of particles with distance is likely to be a function of lithology and rock strength, as also observed in other studies (e.g. van Wyk De Vries et al., 2001; Clavero et al., 2002; Roverato et al., 2015). This process is particularly relevant to volcanic flank collapses as it is potentially intensified by the lower competence and hydrothermal alteration of material prior to failure (Thompson et al., 2009; van Wyk de Vries and Delcamp, 2015). This property constitutes the material easier to comminute and pulverise as suggested by Roverato et al. (2015) for the case of the Pungarehu VDA (New Zealand). Scoriaceous material appears to be the least competent encountered in

the Ab-VDAD. Its cataclasis produces a diamicton composed of clasts in a fine interblock matrix, also described by Roverato et al. (2015). However, a similar cataclasis pattern is observed for all the lithologies in the Ab-VDAD to different degrees.

5.5.1.2 Fluidisation, spreading and stretching

At the outcrop scale, the most obvious feature of the deposit is the general stretching and thinning of lithological units in the EBF, which nonetheless preserve their lithological distinctness and stratigraphic sequence as illustrated in fig 5.3 and 5.4. The outline of the Ab-VDA blocks and their constituent lithological components becomes distorted by stretching as also described by Campbell et al. (1995) and Roberti et al. (2017), however, components maintain their relative position as they form bands in an arrangement of remnant stratigraphic sequence as described by Heim (1932), Shreve (1968), and Hewitt et al. (2008). Stretching and extension have been observed in other VDA/RA deposits (e.g. Siebert, 1984; Siebert et al., 1995; Schneider and Fisher, 1998; Clavero et al., 2002; Bernard et al., 2008; Shea et al., 2008; Roberti et al., 2017) after first described by Heim (1932) in the Elm RA (Switzerland). Stratigraphic sequence preservation has been observed for the Blackhawk RA (USA) (Shreve, 1968; Johnson, 1978) as well as VDADs (Ui and Glicken 1986; Ui 1989; Bernard et al. 2021) such as the Mount St. Helens (USA) (Glicken, 1991), and even for analogue (e.g. Hsü, 1975; Manzella and Labiouse, 2013) and numerical models (e.g. Campbell et al., 1995; Thompson et al., 2009).

Stretching of the EBF is interpreted to be a result of the laminar spreading of the mass during propagation. In a laminar flow regime, the spreading of granular material occurs parallel to the flow direction resulting in the stretching and thinning of units. Since particles are almost exclusively displaced parallel to the flow direction, lithological units preserve stratigraphic sequence. Sequence preservation suggests a spatially and temporally universal lack of large-scale turbulence and mixing in the Ab-VDA, as suggested by other studies (Campbell et al., 1995; Reubi and Hernandez, 2000; Voight et al., 2002; Shea and van Wyk de Vries, 2008; Magnarini et al., 2021). Turbulence leads to chaotic distributions of flow direction and velocity within a fluid. The laminar fluidal behaviour is suggested to be the result of mechanical fluidisation of the material (Davies, 1982), as is also supported by the fluidal mixing of lithological units exhibited in fig 5.3c and 5.4c. Also, the diffuse contacts suggest the fluid-like behaviour of clasts similar to agitated units

in a fluid and gradual displacement and mixing due to agitation in a fluidised granular flow (van Wyk De Vries et al., 2001). The absence of fluid-escape or other interstitial fluid-related structures, sorting or laminated layers suggests a negligible initial and incorporated fluid content. Such features would have likely been at least partially preserved given the lack of turbulence and preservation continuity of stratigraphic sequences even at the most distal locations. Nonetheless, models of dry granular flows also generate fluidal contacts (Campbell et al., 1995; Thompson et al., 2009) like those observed in the Ab-VDAD and other deposits (e.g. Davies, 2015; van Wyk de Vries and Delcamp, 2015). However, the occurrence of stretched blocks throughout the height of the deposit is dissimilar to their occurrence only deeper near the base in other deposits such as the Chimborazo VDAD (Ecuador) examined by Bernard et al. (2008). This observation suggests that stress, agitation and fluidisation of the mass were periodically distributed throughout the deposit and were not restricted to the base of the Ab-VDA.

5.5.2 Sedimentology and clast-size analysis

In VDAs/RAs, progressive fragmentation and comminution processes have been illustrated to produce a signal of gradual clast-size reduction with distance from the source (Bianchi Fasani, 2004; Crosta et al., 2007; Bustos et al., 2022) and gravel proportion decreasing as the proportion of sand-sized particles increases (Roverato et al., 2015; Chapter 3 of this thesis). Perinotto et al. (2015) also propose that the generation of finer material due to progressive comminution was responsible for the increased matrix with distance from the source that they observed. Therefore, an increase in the proportion of matrix compared to blocks with distance from the source would be expected in the Ab-VDAD. It would also be expected that the average clast size would be progressively reduced due to the gradual abrasion and fracturing of clasts in the agitated matrix (Schneider and Fisher, 1998; Perinotto et al., 2015; Paguican et al., 2021).

Nonetheless, in the Ab-VDAD the proportion of matrix is highly variable in different locations both in the interblock and intrablock matrix and there is no systematic longitudinal evolution in the proportion of matrix and size of clasts composing the MF (table 5.1). High variability has been observed within other VDA/RA deposits, but also between them (Hewitt et al., 2008). Likewise, the clast size percentiles in the MF of the Ab-VDAD do not exhibit a systematic longitudinal evolution (fig. 5.11 and table 5.1). Although a size

reduction in the first 17.8 km can be inferred from the P90 and P75 percentiles evolution (fig. 5.12b), no consistent systematic correlation to the distance travelled is observed in data for the whole of the 10 km along which the deposit is exposed. A number of reasons are potentially responsible for the ambiguity of this signal:

1. The addition of material from the EBF to the MF interferes with the progressive fining of the clasts in the MF, which are the subject of the sampling. This addition of material is also not uniform, occurring at variable rates in the deposit. Although progressive cataclasis is likely to contribute to the content of fines in the MF with distance travelled, the distribution of the fining likely depends on the distribution of the stresses agitating the mass encouraging mixing and adding material from the EBF to the MF.

2. Since parts of the same block, with a different lithology exhibit different degrees of cataclasis (fig 5.3d), the rate of comminution in blocks is not exclusively associated with the distance travelled. Instead, the degree of comminution is also a function of the lithology and the local stresses according to its location in the Ab-VDA. The lithological heterogeneity of the deposit results in an uneven distribution of comminution rate due to lithologies with different strength comminuting at different rates. Examining the Pungarehu (New Zealand) and Cubilche (Ecuador) VDADs, Roverato et al. (2015 and 2018 respectively) observed that weaker lithologies, such as scoria, are more rapidly comminuted. This is in agreement with the observation of higher degrees of cataclasis in scoria compared to lavas in the Ab-VDAD (fig 5.3d, 5.8). Scoriaceous material becomes cataclased to produce fine clasts in a fine intrablock matrix (fig. 5.8c). In contrast, lava lithologies produce coarser, more angular clasts and lower quantities of matrix (fig. 5.8b). This results in unsystematic interference in the relationship between comminution and the distance from the source.

3. Stress is not distributed uniformly in the deposit. This is the result of the uneven chaotic distribution of stress in ephemeral shear networks according to the instantaneous arrangement of the weight of the mass (as discussed in section 5.5.4). Therefore, this enforces an unsystematic distribution of stress, and consequently comminution rate.

5.5.3 Substrate implications

The nature of the substrate deformation and erosion caused by a mass movement can offer information regarding its propagation dynamics (Dufresne et al., 2010b). Substrate folding, faulting and detachment features similar to those exhibited by the Ab-VDAD have been studied in various VDA/RA deposits (e.g. Schneider and Fisher, 1998; Belousov et al., 1999; van Wyk De Vries et al., 2001; Clavero et al., 2004; Bernard et al., 2008; Hewitt et al., 2008; Shea and van Wyk de Vries, 2008; Dufresne et al., 2010a, b), allowing evaluation through comparison of the propagation dynamics they represent. The pumice and pumice-rich ignimbrite substrate were mechanically weak, deformable and easy to erode during the propagation of the Ab-VDA. Detachment of the substrate into flame injections, substrate inclusions and the absence of the thin soil layer, as for example in fig. 5.13, suggests an erosional base locally. Penetration of the substratum by both blocks and matrix, is also the case in the Chimborazo VDAD (Ecuador) (Bernard et al., 2008). The substrate is mostly eroded by basal abrasion and ploughing. Basal abrasion is the process in which particles at the base slide parallel to particles in the substrate and mobilising them resulting in sharp erosional contacts (Gauer and Issler, 2004) like the one illustrated in fig. 5.7, in contrast to ploughing where the flow intrudes the substrate and pushes material out (fig. 5.13a, b). Impact erosion (e.g. Bernard et al. 2008; Dufresne 2012) has potentially had a minor effect in the Ab-VDA, as illustrated by fig. 5.13c where the impact of a clast on the pumiceous topsoil layer is likely to have forced a flame injection.

Bulldozed, faulted, and ploughed substrate is evidence of local shear stresses between the Ab-VDA and the substrate. Below the Ab-VDAD this effect does not propagate deeper than 0.3-0.5 m (fig. 5.13a, b, d). This implies that due to the low coherence of the material, shear could not be effectively transmitted from the flow to the substrate. Compressional features, such as bulldozing and faulting, have been documented in other VDA/RA deposits with erodible substrate (e.g. Evans et al., 1994; Shea and van Wyk de Vries, 2008; Wang et al., 2019) as well as recreated in analogue experiments (Dufresne, 2012). The analogue experiments of Dufresne (2012) explore the relationship between a granular flow and different erodible substrate conditions using different granular materials to simulate diverse substrate properties. The findings support that low-friction material, like the pumice that constituted the substrate of the Ab-VDA, were readily mobilised and coupled with the granular mass. It is therefore likely that particles from the substrate under the

Ab-VDA were easily detached through abrasion due to low cohesion, as demonstrated in fig. 5.7, which illustrates the incorporation of individual clasts from the substrate to the propagating mass. Small-scale flame injections similar to what is illustrated in the Ab-VDAD (fig. 5.13c) were also formed in the experiments where low friction material was briefly sheared between the avalanche and the substrate forming small clastic dikes before being incorporated (Dufresne, 2012). Therefore, the small scale of these features in the deposit also suggests a limited-strength substrate. The lack of large injections and scarcity blocks of the substrate in the Ab-VDAD reflects the low cohesion of the material that cannot be incorporated in one intact piece (Bernard et al., 2008). Incorporated components were quickly disaggregated as described by Hewitt et al. (2008) unlike other VDA/RA deposits where substrate blocks are preserved unmixed, like for example the Tschirgant RA (Austria) (Dufresne et al. 2016b), the Nevado de Toluca VDAD (Mexico) (Caballero and Capra, 2011) and Cubilche VDAD (Ecuador) (Roverato et al., 2018).

The substrate was locally bulldozed and eroded while in other areas remained undisturbed (e.g. fig. 5.13f). This unsystematic erosional pattern suggests a spatially variable accommodation of shear stress at the Ab-VDA base. In locations where high shear stress was accommodated at the base during the propagation, shear stress was transferred to the substrate, eroding or deforming it. However, where shear was accommodated in the body, the substrate remains intact. The lack of shear concentration at the base inhibited the degree of substrate perturbation. The uneven distribution of substrate perturbation suggests that the Ab-VDA was not principally travelling as a plug with shear stress concentrated at the base, but as a fluidised granular mass where shear was distributed across the whole body of the flow.

The substrate resistance to motion influences the energetics of a granular flow, and therefore its mobility (Dufresne, 2012) since the majority of frictional resistance in granular flows is transmitted from the base to the rest of the material through force chains (Campbell, 2005). The presence of an erodible substrate distinctly changes the behaviour of granular avalanches (Dufresne, 2012). Numerical modelling by Mangeney et al. (2007) suggests that the presence of granular material at the surface of propagation of a granular flow can increase its mobility. With increasing thickness of the granular substrate, the dynamics of the propagating mass change from a decelerating avalanche to a travelling wave resulting in increased mobility (Mangeney et al., 2007, 2010). However, for the substrate to increase

the mobility of a granular flow, enough shear must be accommodated in the basal layer by lower basal friction (Dufresne et al., 2010a). Conversely, the analogue modelling of Shea and van Wyk de Vries (2008) finds a slowing of the mass and a decrease in spreading due to the energy expended in bulldozing the substrate. This is also supported by Dufresne (2012) who suggest that thick yielding substrates can consume momentum and inhibit mobility. In any case, such experiments support that substrate interaction can potentially have an impact on the mobility of granular flows thatis necessary to examine and incorporate in conceptual models and numerical modelling of these events (Mangeney et al., 2010). Nonetheless, the runout-enhancing substrate behaviour is not universally encountered and is therefore not a universal explanation for long runout of VDAs/RAs (Dufresne et al., 2010a). They are instead likely to add variation and complexities to the runout observations of different events, in a similar manner to topographic variability (Nicoletti and Sorriso-Valvo, 1991; Dufresne et al., 2010a).

5.5.4 Shear accommodation, propagation and emplacement model

VDAs result from flank collapses, propagating as slides immediately after the initial collapse and progressively evolving into granular flows (Voight et al., 1983; Siebert, 1984; Glicken, 1991; Scott et al., 2001). The behaviour of dry VDAs/RAs as dense granular flows with a partially collisional regime, where momentum transfer predominantly occurs through collisions, has been reinforced by several studies (e.g. Pierson and Costa, 1987; Iverson, 1997; Iverson and Denlinger, 2001; Dufresne and Davies, 2009; Roverato et al., 2015; Chapter 3 of this thesis). Therefore, discrete element method (DEM) modelling of individual interacting particles is suitable for investigating the dynamics of such granular flows, as supported by studies such as Cleary and Campbell (1993) and Crosta et al. (2001). The DEM simulations of Campbell et al. (1995) and Thompson et al. (2009) are of simplified granular flows with no bond between particles in the mass since their initiation. Particles are free to interact and are only affected by their collisions' momentum transfer, friction and potential energy transformed to kinetic. With these initial conditions, and no other external mechanisms, the collapsed masses evolve into granular flows. These simulations are successful in reproducing VDAD field observations of fluidal contacts (e.g. fig. 5.14), disperse boundaries and pockets of preserved stratigraphic sequence, like the ones observed in the Ab-VDAD. Characteristics of the simulated avalanches are also consistent with the laminar spreading and thinning of lithological units. Therefore,

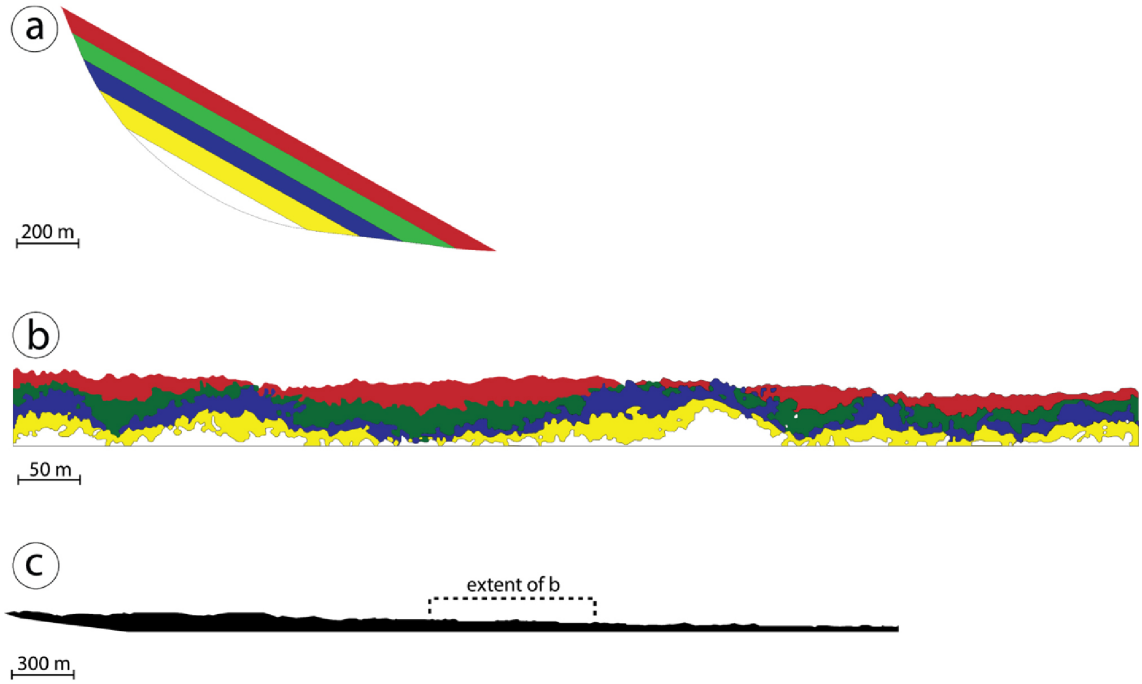

Figure 5.14: Interpretation of the DEM experimental results presented by Thompson et al. (2009), reproduced from figures published by the authors. **A** Particle arrangement before the propagation; **B** A portion of the final deposit exhibits unmixed spreading, elongation and fluidal mixing features in preserved stratigraphic sequence analogous to what has been observed in the field and is illustrated in figures 5.4 and 5.5. **C** Illustrates the location of b in the final deposit. Note the scale difference between a, b and c. Modified after Thompson et al. (2009).

these models are suitable for the evaluation of propagation dynamics and processes of VDAs, which are characterised by a disaggregated and fragmented mass comparable to a granular flow as in the Ab-VDA. For this reason, their results are discussed in comparison with field observations in proposing a propagation model for the Ab-VDA.

The initial collapse of the Ab-VDA is likely to have been critical for the coarse fragmentation and disaggregation of the original mass (fig. 5.15a, b) due to the existence of an extensional regime (Longchamp et al., 2016), rapid unloading of lithostatic pressure (Belousov et al., 2007), and impact stresses (Voight et al., 1983; Glicken, 1991, 1996; Bernard et al., 2008; Thompson et al., 2010). Areas that suffer the greatest strain and disaggregation at this stage are predisposed to evolve to the MF due to subsequent gradual homogenisation during propagation (fig. 5.15b) (Thompson et al., 2009; Roverato et al., 2015; Chapter 4 of this thesis). According to Campbell et al. (1995), the preservation of jigsaw-fractured blocks reflects local minimal agitation during propagation. The scarcity of jigsaw-fractured blocks in the Ab-VDAD supports that the disaggregation was not a process that occurred by the impulsive stress of the initial collapse, or during a violent termination of the

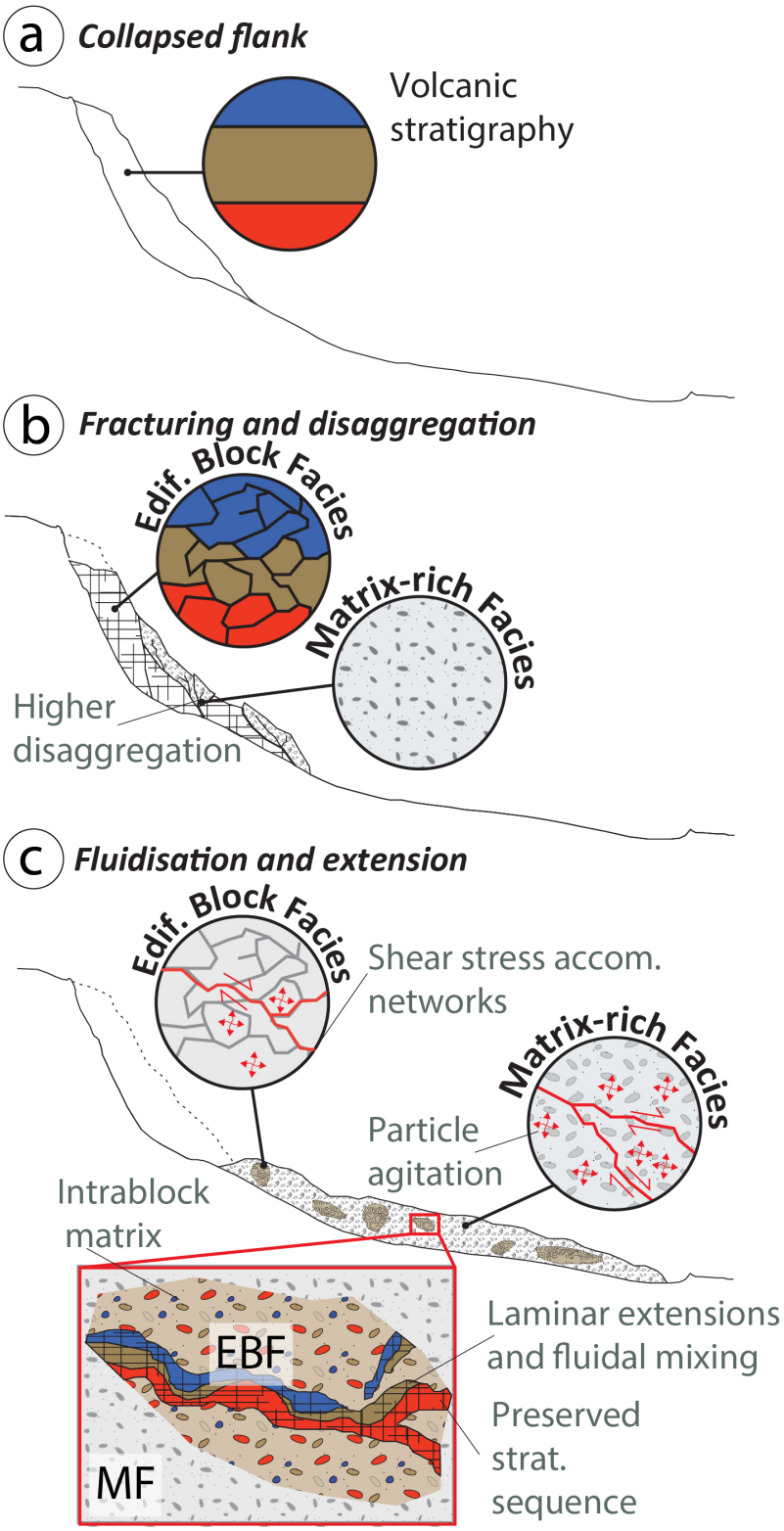

Figure 5.15: Schematic representation of the propagation and emplacement processes of the Abona volcanic debris avalanche. **A** Original stratigraphy prior to flank collapse. **B** Fracturing and disaggregation. The coarse fracturing leads to blocks with preserved stratigraphic sequences in the edifice block facies (EBF), whereas more intensely fractured areas evolve into the matrix-rich facies (MF). **C** Once the flank has disaggregated into a granular mass, ephemeral shear stress accommodation networks fluidise the material both in the MF and the EBF. Pockets of preserved stratigraphic sequence are preserved within the EBF where low degrees of stress and agitation have been accommodated (insert).

propagation. In lack of agitation except in specific impulses fractures would have been preserved in undisaggregared material (Campbell et al., 1995; Reubi and Hernandez, 2000; Clavero et al., 2002; Thompson et al., 2010). Instead, the diamicton texture of the Ab-VDA EBF suggests that the entirety of the mass periodically experienced strain and agitation during propagation (fig. 5.15c).

Further fragmentation and disaggregation transform the material into a granular mass where independent particles could engage in collisions (Ogawa, 1978; Campbell, 1990; Iverson, 1997; Roche et al., 2006). The elimination of particles greater than -9.5ϕ and reduction of the P90 and P75 percentile clast sizes in the first 17.6 km of the Ab-VDA (fig. 5.11 and 5.12) are likely to be a signal of the fracturing and comminution. Once the mass fractures, disaggregates and becomes granular a VDA can behave as a granular flow and assume fluidal behaviour at least locally (fig. 5.15c) (Voight et al., 1983; Glicken, 1996; Schneider and Fisher, 1998; Hewitt et al., 2008; Chapter 3 of this thesis). Fluidal contacts between lithological units (fig 5.3a, c, 5.4b, c) and diffuse boundaries (fig. 5.10) suggest that the material constituted a granular fluidised mass enabled by the agitation/vibration and collisions of independently interacting particles generating a granular temperature (Ogawa, 1978; Campbell, 1990; Iverson, 1997; Armanini et al., 2005; Roche et al., 2006). The process was likely enhanced in the Ab-VDA by the abundance of less competent lithologies like scoria and pumice, which require little energy to fracture and evolve into a granular material. Granular temperature measures the random vibration of particles and the agitation in the mass (Brilliantov and Pöschel, 2010). The concept of granular temperature is vital for understanding the behaviour of rapid granular flows as highlighted by Campbell (1990). As the agitation in a granular material increases and particle collisions are more frequent, relative to frictional contacts, the material dilates and behaves similarly to a fluid (Campbell, 1990; Brilliantov and Pöschel, 2010; Johnson et al., 2016). This behaviour is achieved by the transition from a quasistatic frictional regime, with predominantly persistent frictional contacts, to a rapid granular flow collisional regime (Drake, 1991; Campbell, 2005). In a collisional regime, particles are frequently engaged in collisions, to the extent that the mass approaches the behaviour of a molecular gas or fluid (Johnson et al., 2016). The transition to the fluidised behaviour, illustrated in fig. 5.15c, results in the reduction of effective friction due to the propagation achieved by particles when they are momentarily relieved of the static burden of the overlying weight after a collision, in the time they are not involved in frictional contacts (Melosh, 1979). The

mixing which resulted in the homogenous MF and the incompletely mixed intrablock matrix in Ab-VDA is not the result of turbulence, but rather gradual homogenisation due to the agitation and diffusion of granular particles (Perinotto et al., 2015; Roverato et al., 2015) as visualised in fig. 5.10, and explained in Chapter 4 of this thesis. Gradual homogenisation is the result of agitated particles vibrating and gradually displacing and chaotically mixing. Diffuse boundaries due to the agitation, vibration and displacement of the particles lead to the diffusion of units away from the boundary, and particles from the matrix filling the gaps. This behaviour is best demonstrated by the diffuse boundaries in fig. 5.10. The mixing eventually results in a homogenous unit such as the intrablock matrix illustrated in fig 5.3c, and from the interblock matrix in fig. 5.6a.

The lack of faults and brittle deformation in the deposit supports a fluidised Ab-VDA with no sections that sustained adequate coherence for brittle behaviour. Similarly, the universal microfracturing and fluidal features in the Ab-VDAD support that stresses were distributed throughout the mass (Pollet and Schneider, 2004; Friedmann et al., 2006; Dufresne et al., 2016a; Wang et al., 2019), and were not concentrated in long-lived shear zones either at the base or in the body of the flow (fig. 5.15). Nonetheless, the observation of preserved stratigraphic sequences and stretched continuous lithological units demonstrate that the emplacement remained laminar, without turbulence as also suggested in the DEM simulations of Thompson et al. (2010). The fluid-like behaviour combined with the laminar spreading produced the lenticular stretched shape and fluidal features in the EBF (e.g. fig 5.3). However, it is unlikely that VDAs are pure rapid granular flows with an exclusively collisional regime (Campbell et al., 1995; Johnson et al., 2016). It is more probable that particles in the Ab-VDA were engaged in frictional contacts for the majority of the propagation, thus adopting a behaviour between a rapid and quasistatic granular flow regime. Shear was accommodated in chaotically distributed, ephemeral energy chains, as distributed in fig. 5.15c, constituting temporary shear networks as described by Davies and McSaveney (2009), Thompson et al. (2009) and Dufresne et al. (2016a). Such shear zones are not necessarily continuously or constantly active during propagation. These energy chains form according to the instantaneous distribution of the self-weight of the material and are dissimilar to the uniform distribution in liquids or homogenous solids (De Blasio, 2011). Therefore, intergranular stresses are temporarily concentrated in these short-lived, interlinked assemblages aligned to the shear direction (Sammis et al., 1987; Anthony and Marone, 2005; Mair and Hazzard, 2007; Sammis and

King, 2007; Furbish et al., 2008). In such a deforming granular medium, grain bridges are continuously forming and breaking, producing highly heterogeneous deposits (Hooke and Iverson, 1995), as observed in the Ab-VDAD. Consequently, stress accommodation and granular behaviour were likely temporally and spatially variable in different sections of the Ab-VDA. Stress distribution heterogeneity within the propagating material is also suggested by Magnarini et al. (2021) through their study of the El Magnifico RA deposit (Atacama, Chile). This heterogeneity is also evident in the quantitative clast-size analysis, which reveals an unsystematic clast-size distribution variation with propagation distance. Moreover, the ephemeral and unsystematic distribution of the shear accommodation is evident from the spatially variable substrate perturbation, discussed in section 5.5.3. The ephemeral nature means that shear leaves no detectable trace in the sedimentological record as short-lived shear networks rearrange to different configurations through the deposit (Davies and McSaveney, 2009). Indeed, in the Ab-VDAD no zones of concentrated shear with distinct sedimentology are exhibited in the deposit, either at the base or within its body. Ephemeral shear accommodation in slip microsurfaces distributed throughout the mass and the base result in the cataclasis, disaggregation of the mass and the creation of the interblock and intrablock matrix. Internal shear accommodation (as opposed to basal) is more common in VDAs than it is in RAs (Dunning, 2004; Crosta et al., 2007; Davies and McSaveney, 2009). Roverato et al. (2015) suggest that the easier pulverisation of weak volcanic material, like scorias, is likely to encourage the formation of a fine matrix capable of accommodating shear. It is therefore likely that the source of the Ab-VDAD was a flank composed of weak material which was potentially already fractured or hydrothermally altered or weathered (Glicken, 1991; Palmer et al., 1991; Belousov et al., 1999; Bernard et al., 2008; Shea et al., 2008; Roverato et al., 2015). Therefore, the Ab-VDA has suffered more widespread disaggregation compared to VDAs/RAs composed of more competent material, such as the Tenteniguada VDAD (Chapter 4 of this thesis). In the Thompson et al. (2009) model the unsystematic distribution of stresses leads to pockets of material remaining less disaggregated, where less stress has been accommodated. Pockets of EBF preserved stratigraphic sequence in the Ab-VDAD, as illustrated in fig. 5.4, represent areas that happened not to experience high stresses during propagation. The properties exhibited by the Ab-VDAD offer field evidence to support these processes, which have so far only been proposed theoretically.

The DEM simulations, reproduce field observations despite the initial mass composed of

a homogenous granular material, and therefore due to the dynamic coevolution of the shear distribution and local stress conditions. The success of the models in recreating features observed in the field, from a mass composed of homogenous material supports that the domain emplacement hypothesis suggested by Clavero et al. (2002) for the Parinacota VDA (Chile) is not applicable in this case. The hypothesis proposes that the deposit morphology is a function of pre-failure structural and internal distribution material properties. However, their generation in the models from a purely gravity-driven collapse of a homogenous material, in combination with the field observations disputes this (Thompson et al., 2010).

The DEM simulations mentioned reproduce a process in which a purely gravity-driven homogenous avalanche can evolve into a flow due to increasing momentum and kinetic energy from its initial potential energy (Thompson et al., 2009). The sedimentological features of the AB-VDA are in agreement with the process of collective motion, distributed stresses and spreading in a laminar manner that the granular flow produces in Thomson et al. (2009). The findings support that the Ab-VDA was purely gravitational with no additional auxiliary friction-reducing mechanisms. The initial coherent sliding mass evolved into a flow with distributed shear stress generating in-situ fragmentation, as described in the VDADs examined by Reubi and Hernandez (2000). The syn-propagation fracturing and disaggregation of the mass were driven by the kinetic energy from the initial acceleration resulting in interparticle collisions as in the process described by Perinotto et al. (2015). Findings from the DEM studies suggest that the material in granular VDAs similar to Ab-VDA are completely shearing with no significant portion of the mass travelling as a plug and no shear concentration at the base of the flow (Campbell et al., 1995). This is illustrated by velocity profiles that confirm the vertically distributed shearing and dispute block/plug transport and basal shear layer theories (Campbell et al., 1995). Instead, these findings, add to the body of recent evidence that the shear is distributed randomly in ephemeral networks throughout the body as well as the base (Davies and McSaveney, 2009; Dufresne et al., 2016a) rather than being exclusively accommodated in a low friction basal layer (Campbell et al., 1995; Johnson et al., 2016).

5.5.5 Implications for volcanic debris avalanche long runout and mobility mechanisms

5.5.5.1 Propagation mechanisms

Paguican et al. (2021) propose three potential flow regime models for the runout dynamics of VDAs. (1) The plug flow model involves a coherent, poorly disaggregated mass transported over a highly deformed low friction shear layer at the base (Voight et al., 1983; Takarada et al., 1999). (2) In the transitional slide model spreading of the mass is accommodated in listric normal faults merging in a basal sliding plane (van Wyk De Vries et al., 2001; Paguican, 2012). The observations presented here suggest that the Ab-VDA is not compatible with the models of plug flow and translational slide due to the lack of a basal shear layer, and listric faults respectively. The presented findings add to the evidence that a low frictional basal layer is not the universal explanation for the mobility of long runout VDAs/RAs (Johnson et al., 2016). The third, (3) multiple shear zone model (Paguican et al., 2021) proposes the existence of zones of shear accommodation hosted by a matrix created by weaker lithologies within the body of an avalanche. These zones form a network around harder, difficult-to-fracture lithologies, effectively sheltering them from shear stress (Roverato et al., 2015). This is not observed in this deposit either, potentially due to the lack of a significant amount of competent material that would allow a significant EBF component. Therefore, a new alternative shear accommodation variation of the third model is here proposed for the Ab-VDA, where shear is distributed throughout the fractured granular mass, as also suggested by Campbell et al. (1995) for loose granular material. The proposed model is of a partially fluidised granular flow with distributed shear in temporary shear networks.

This model of propagation also offers an explanation for the volumetric effect of the mobility of long runout VDAs/RAs (Chapter 1). This is the observation of longer runouts and lower friction coefficient by more voluminous RAs/VDAs. According to the DEM simulations of Campbell et al. (1995), the apparent friction coefficient is an increasing function of shear rate. Shearing and fracturing of rock increase with the volume of material being added to the initial failure (Shreve, 1968). In the DEM simulations, different size avalanches travelled with the same average velocity; however, the thicker, larger avalanches experienced proportionally smaller shear rates and therefore frictional resis-

tance (Campbell et al., 1995; Johnson et al., 2016). With shear rate being the rate at which fluid laminae move past each other, a lower shear rate means lower energy dissipation, and consequently higher mobility.

Since the 1960s hypotheses and models have been proposed regarding the enhanced mobility of VDAs/RAs based on morphology, internal architecture, sedimentology, theoretical approaches, and numerical and analogue models as discussed in Chapter 2 (reviewed in Davies, 1982; Erismann and Abele, 2001; Hungr, 2002; Legros, 2002; Collins and Melosh, 2003; Friedmann et al., 2006; Manzella and Labiouse, 2008; Davies and McSaveney, 2012). Among those, for the Ab-VDA Dávila-Harris et al. (2011) suggest that the progressive fragmentation of the mass is most consistent with the acoustic fluidisation mechanism proposed by Melosh (1979), with shock waves propagating through the solid moving mass. According to Melosh (2015), vibrations create transient, high-frequency pressure fluctuations (or acoustic waves) in the propagating mass, that fluidise the homogenous debris through local variations in contact forces. These pressure fluctuations instantaneously relieve the overburden weight on individual clasts that become free to slip. This process creates an agitated laminar flow with low mixing between units and is capable of enhancing the mobility of granular flows (Collins and Melosh, 2003). The numerical modelling of Collins and Melosh (2003) suggests that under high-frequency pressure vibrations, a granular mass will develop into a fluid-like flow with uniform viscosity. The observations from the Ab-VDAD are in agreement with the velocity profiles reproduced by the DEM simulations of Campbell et al. (1995) and Johnson et al. (2014) and the processes and sedimentology generated are compatible with the acoustic fluidisation hypothesis (Johnson et al., 2016). Acoustic fluidisation could be the source of the distributed shear in an agitated mass with collisional contacts between particles generating a fluid-like behaviour in a flow that remains laminar. The simulations of Campbell et al. (1995) even reproduce the stratigraphic preservation, despite the bulk fluidisation of the flow, as also observed in the Ab-VDAD. This is the result of the uneven distribution of stress implied by the acoustic fluidisation mechanism (Melosh, 1979; Magnarini et al., 2021).

On the other hand, dynamic fragmentation is another process potentially active during the propagation of the Ab-VDA. Dynamic fragmentation is the effect generated by the fracturing of intact rock under rapid strain and confining pressure and can preserve the dilated state in a granular material as supported by studies such as Davies et al. (2010) and

Zhang and McSaveney (2017). Prior to fracturing, particles deform plastically under the shearing motion around them. When these forces exceed the local strength of a particle, it breaks and generates fractures. A proportion of the stored elastic energy is then released with the fractures radiating from the centre of mass of the clast. The elastic energy released during disintegration could contribute to the enhanced mobility of VDAs/RAs. This theory is disputed by Rait and Bowman (2016) with shear tests suggesting that kinetic energy produced in this manner is quickly dissipated in the matrix with no long-lasting impact. Nonetheless, Paguican et al. (2021) suggest that elastic energy in combination with acoustic fluidisation waves might be responsible for fracturing and dilatancy of a granular mass. Whether elastic energy or acoustic waves enhanced the mobility of the material cannot be confirmed by the findings of this study, but both these theories are consistent with the field observations of the Ab-VDA. Both mechanisms do not require the presence of exotic processes, which confirms the ability of VDA to show high mobility by internally generated mechanisms.

5.5.5.2 Explosive eruptions and long runouts

Although the majority of VDAs occur on active volcanoes (Siebert, 1984; Voight, 2000), they are not necessarily triggered by volcanic activity, and can also be initiated by seismic activity or slope destabilisation due to precipitation or weakening of slopes composed of volcanic material (Belousov et al., 1999; Capra et al., 2002; Lomoschitz et al., 2008; Roverato et al., 2021). Phreatic explosive eruptions are often inferred as the trigger of slope failures in volcanic environments, even though precise timing is not constrained with certainty, and explosions may instead be triggered by the failure relieving confining pressure from the magmatic/hydrothermal system (Siebert, 2002). The Ab-VDA occurred during an explosive eruption as suggested by the petrological evidence and geochronology presented by Davila-Harris et al. (2011). The fact that the association to the collapse is identified with relative confidence is not common, as most VDADs are difficult to assess with precise time constraints, and even then, volcanic activity and triggering mechanisms might have left little or no evidence in the geological record. Independent of the series of events, it has been suggested that explosive eruption accompanying VDAs have the potential of increasing their mobility (e.g. Sousa and Voight, 1991; Clement et al., 1993). Glicken (1996) propose that the coeval explosion from the eruption of the Mount St. Helens volcano during the 1980 VDA possibly enhanced the mobility of its MF due to promoting

dilation and grain flow and therefore reducing intergranular friction. However, VDAs that are undoubtedly not related to eruptions or even active hydrothermal systems also display enhanced mobility (Siebert, 2002), suggesting that even if the explosion can enhance mobility, other processes must be responsible for the long runouts. This is an important observation regarding the discussion on the factors for the long runout of VDAs/RAs. The presence of poorly consolidated fragmental pyroclastic and hydrothermally altered materials composing volcanic flanks might be a more important factor affecting the processes enabling enhanced mobility (Belousov, 1995; Siebert, 2002; Vezzoli et al., 2017).

5.6 Comparison between the Abona and Tenteniguada debris avalanches

The Tenteniguada volcanic debris avalanche (Ten-VDA) (Chapter 4) and the Ab-VDA have produced very different deposits owing to the difference in the material that constituted each. The Ten-VDA was principally composed of competent lava lithologies resulting in low disaggregation, preservation of original structures and shear localisation in block boundaries. In contrast, the Ab-VDA was composed of weak pyroclastic products which quickly disaggregated into a granular mass with particles free to interact and become agitated periodically (section 5.5.4). Analogously, numerical simulations have been able to recreate a range of realistic structural features and distributions observed in the field by simulating the propagation of avalanches composed of uniform homogenous material (Thompson et al., 2009, 2010). However, the propagation dynamics and deposits generated in these models are distinct under different material properties.

For example, in the Thompson et al. (2009) model, which represents an avalanche as an unbonded granular mass, the weak material generates fluidal contacts and mixing, laminar spreading and preserved stratigraphic sequence (fig. 5.14). The model suggests the evolution of the mass from a collapse to an organised, laminar flow (Thompson et al., 2009) with distributed stress dynamics comparable to the Ab-VDA (fig.5.16).

In contrast, the Thompson et al. (2010) model implements an initial bond between the particles that can be broken during propagation if its strength is surpassed, to simulate strength in the material. In these simulations, there is shear concentration in early-formed

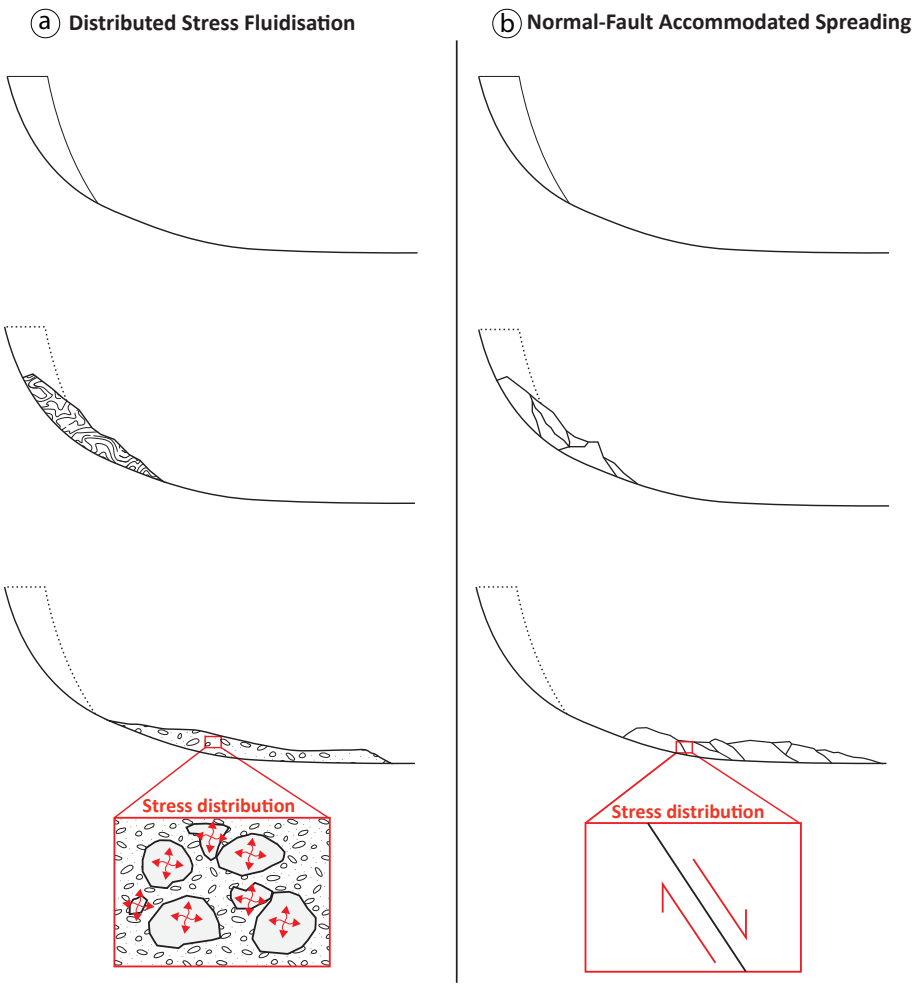

Figure 5.16: Conceptual models for the propagation dynamics of the volcanic debris avalanches examined by this thesis. The topography and morphology of the deposits is schematic, it does not realistically reflect the features of the deposits but merely aims to highlight their differences as end members. **A** Distributed Stress fluidisation - Abona volcanic debris avalanche. Particles in the granular mass are free to become agitated and accommodate stress. **B** Normal-fault accommodated spreading - Tenteniguada volcanic debris avalanche. Stress is accommodated as shear in block boundary fractures created by the early fragmentation of the mass.

fractures (as discussed in Chapter 4) which shields undisaggregated and undistorted blocks from stress and agitation resulting in their preservation. This behaviour is consistent with what is observed in the Ten-VDA, under fault-accommodated spreading (fig. 5.16b). Various authors have supported that the initial coarse disaggregation that breaks up the mass into blocks might be more important for the fracturing of the mass with only minor subsequent fragmentation during transport (Ui, 1983; Voight et al., 1983; Belousov et al., 1999; Reubi and Hernandez, 2000), and this is likely to have been the case for the Ten-VDA where the initial fragmentation appears to have generated the coarse breakup of the mass with no substantial further fragmentation. Subsequent stress accommodation is limited to the areas that developed into matrix, interblock and intrablock and block boundaries with

large proportions of the mass not accommodating stress and strain during transport and preserved as blocks with original structure.

The success of these uniform material models in recreating deposit features (Thompson et al., 2010) combined with the comparison of the material and resultant deposits of the Ab-VDA and the Ten-VDA suggests that the spatial variation in material properties may not be as important in determining propagation dynamics. Instead, material properties of the original mass such as rock strength, presence of hydrothermal alteration weakening and other lithology-dependent properties might play a more important role. If VDA movement begins as a slide and progressively evolves into a flow during propagation (e.g. Voight et al., 1983; Glicken, 1991), the strength and structure of the material involved must play a vital role in the rate of the advancement of this process. This is in contrast to the suggestion of Clavero et al. (2002) proposing that pre-failure structure and distribution of discontinuities in a mass define the morphology and internal structure of a deposit.

The lithological, and resultant material property, differences between the Ab-VDA and the Ten-VDA deposits are likely to be responsible for their distinct characteristics and the propagation dynamics they hold evidence for. The VDAs have propagated with different rheology and produced different deposits. Their material properties constitute them end-members with the Ten-VDA propagating under normal-fault accommodated spreading and the Ab-VDA generating distributed stress fluidisation. This divergence highlights the importance of lithological properties in VDA dynamics and its importance for the structural evolution of the mass.

5.7 Conclusion

The distribution of facies and structures and sedimentological analysis, in comparison with conceptual and numerical models and other VDA/RA deposits, have led to the following conceptual model for the propagation dynamics of the Ab-VDA:

1. The source mass was composed mainly of pyroclastic material and a small proportion of lavas (fig. 5.15a). Due to the high cataclasis of the material it is assumed possible that the material could have been hydrothermally altered or weathered, weakened and preconditioned for fracturing. The destabilisation and collapse of the mass

occurred during an explosive eruption.

2. The initial slide phase led to a coarse disaggregation of the mass and generated fractures, splitting the mass into blocks that preserved their internal sedimentary sequence. Areas that sustained more strain were more intensely fractured and later disaggregated and evolved into the MF through gradual homogenisation (fig. 5.15b).

3. Once the mass moved out of the failure scarp it evolved into a flow and experienced laminar spreading. This is likely because the front of the flow was travelling faster than the proximal part, leading to the extension and elongation of the mass, including embedded blocks. This was enabled by the high degree of microfracturing of the material constituting the mass granular, with particles capable of moving independently and engaging in collisions (fig. 5.15c). Collisional/vibrational contacts between particles in the mass gradually led to the microfractured diamicton texture of the block facies through both disaggregation of existing fractures and comminution due to grain interactions. The agitation gave the mass a granular temperature causing it to behave as a fluidised granular mass. This led to the fluidal features and diffuse contacts observed in the deposit. Mixing within the blocks was minimal, caused by gradual homogenisation. This behaviour was enabled due to the weakness of the material and the resultant disaggregation that allowed spatially distributed shear instead of concentrated shear at the base or in shear zones.

4. The shear stress of this movement was distributed unsystematically in ephemeral networks throughout the body and the base of the mass. The spatially and temporally variable nature of the shear accommodation is also reflected in the inconsistent influence of the flow on the substrate. Areas where shear was high exhibit bulldozing and substrate incorporation while in areas of low shear the substrate remains unaffected. The low coherence of the substrate is evident by the disaggregation of incorporated material and the shallow deformation beneath the flow that did not allow shear to be transmitted deep underneath the Ab-VDA.

5. The unsystematic distribution of stresses and therefore mixing and comminution in the mass is responsible for the lack of a longitudinal evolution in the clast size and the proportion of matrix illustrated in the deposit through the quantitative clast-size and matrix-content analysis of the MF.

6. The result of these processes is the emplacement of a microfractured deposit with pockets of EBF and preserved stratigraphy surrounded by the MF (fig. 5.15c).

The present findings add to the evidence that challenges the view that all long runout VDAs/RAs propagate as a plug on a low frictional basal layer accommodating the shear of the propagating mass (Campbell et al., 1995; Johnson et al., 2016). They add to the body of recent evidence that the shear is distributed randomly in ephemeral networks throughout the avalanche as well as the base (Davies and McSaveney, 2009; Dufresne et al., 2016a). The observations are also compatible with both the theories of acoustic fluidisation and dynamic fragmentation that could have been active during the propagation of the mass.

This study highlights the importance of field studies for understanding VDA propagation dynamics. The novel methodology for the sedimentological examination of indurated deposits presented here provides a new tool to study deposits that were not considered before, increasing the capacity for collecting field evidence and to further understand VDA/RAs and the hazard they pose.

Chapter 6

Bidispersity as a factor for the long runout of large mass flows: scale effects in granular avalanche experiments

6.1 Introduction

Propagating volcanic debris/rock avalanches (subsequently VDA/RAs) are believed to behave as dense granular flows where grain interactions are the most important energy dissipation process (Voight et al., 1983; Campbell, 1990; Schneider and Fisher, 1998; Davies and McSaveney, 1999; Reubi and Hernandez, 2000; Chapter 3 of this thesis). Recent work supports that VDA/RAs behave as ideal granular avalanches where fluid effects are negligible (e.g. Legros, 2002; Chapter 3 of this thesis). The flow is characterised by a distributed shear motion where individual particles interact with each other and the flow boundaries (Pierson and Costa, 1987; Iverson, 1997; Dufresne and Davies, 2009). Flow dynamics are controlled by particle interactions (collisions and longer-lasting frictional contacts), their internal and basal friction coefficients, and interactions with flow boundaries and path geometry (Denlinger and Iverson, 2001; Roche et al., 2021). The energy exchange, referred to as the granular effect, is driven by particle interactions, resulting in momentum transfer and dissipation (Hu et al., 2020). The magnitude of the energy exchange is measured as the granular temperature (Campbell, 1990; Iverson, 1997; Sanvitale and Bowman, 2016). The granular effect is a function of the particles' friction, shape, density, size, hardness and roughness (Bartali et al., 2015) and the processes controlling their interactions. Therefore, grain-size distribution properties can potentially affect propagation dynamics. The energy dissipated through the granular effect and the mechanisms involved are crucial

for understanding the propagation dynamics and energetics of granular flows (Hu et al., 2020).

Natural granular flows including VDA/RAs, as well as block-and-ash pyroclastic flows, debris flows and turbidity currents; along with granular flows in industrial processes (such as solid conveying), contain a wide range of particle sizes (Phillips et al., 2006; Hungr et al., 2013; Yang et al., 2015) . VDA/RA deposits are composed of angular/subangular clasts spanning a size range from fine particles smaller than 1 μm up to tens of metres (e.g. Voight, 1978; McSaveney and Davies, 2002; Roche et al., 2006). Even in cases where the source material is homogeneous in terms of particle size, heterogeneity can arise from fragmentation and comminution during propagation (McSaveney and Davies, 2002; Crosta et al., 2007; Davies and McSaveney, 2012; De Blasio and Crosta, 2014; Dufresne and Dunning, 2017) due to heterogeneous fracturing of the original rock mass (Knapp and Krautblatter, 2020). Furthermore, VDA/RA deposits are characterised by bidisperse to polydisperse grain-size distributions (e.g. Scott et al., 1995; Glicken, 1996; Vallance, 2000; Pollet and Schneider, 2004; Vallance and Iverson, 2015; Bernard et al., 2017). Bidispersity implies the existence of two dominant particle sizes or size ranges in the grain-size distribution. Bidispersity is exhibited in volcanic debris avalanche deposits, at least locally (Ui and Glicken, 1986; Siebert et al., 1989; Glicken, 1996; Siebert, 2002; Bernard and van Wyk de Vries, 2017); while in the case of rock avalanche deposits, bidispersity develops especially in zones of concentrated shear stresses (Dufresne and Dunning, 2017). This is supported by analogue experiments suggesting that bidisperse distributions are generated with increased shear stresses or confining pressures (Iverson et al., 1996; Caballero et al., 2014). Since in idealised granular flows grain interactions are the principal process responsible for energy dissipation, grain-size distribution properties potentially play an important role in VDA/RA dynamics. Accordingly, recent studies have supported that a bidisperse grain-size distribution is capable of providing a more energy-efficient shear accommodation arrangement reducing frictional losses at the base of VDA/RAs. Studies including Linares-Guerrero et al. (2007), Yang et al. (2015), and more recently Bartali et al. (2020), Hu et al. (2021) and Duan et al. (2022) propose bidispersity as a contributing factor to the long runouts observed in VDA/RAs.

Many scaled analogue models have reproduced certain VDA/RA features, dynamics and behaviours (Davies and McSaveney, 1999; Denlinger and Iverson, 2001; Iverson et al., 2004;

Yang et al., 2011; Dufresne, 2012). The scarcity, inaccessibility and complexity of deposits encourage analogue and numerical modelling studies. However, the theoretical description and mathematical measurement and modelling of granular avalanche dynamics is a challenging task from the geophysics and granular physics perspective (Delannay et al., 2017), as well as the geomorphological and sedimentological. This extends to lab experiments where there are complicated scaling issues. Nonetheless, laboratory experiments can provide important information on the propagation processes of granular avalanches despite idealised experimental conditions (Davies and McSaveney, 1999; Manzella and Labiouse, 2008, 2009, 2013; Shea and van Wyk de Vries, 2008; Dufresne, 2012; Longchamp et al., 2016). In recent years, column collapse and granular avalanche experiments (e.g. Phillips et al., 2006; Goujon et al., 2007; Moro et al., 2010; Degaetano et al., 2013; Yang et al., 2015; Hu et al., 2020; Li et al., 2021), as well as numerical models (e.g. Linares-Guerrero et al., 2007; Cabrera and Estrada, 2021; Hu et al., 2021), have been employed to study the behaviour of granular mixtures composed of more than one particle sizes. Analogue experiments such as those of Goujon et al. (2007), Yang et al. (2015), Bartali et al. (2020), Hu et al. (2020) and Duan et al. (2022) evaluate the behaviour of granular avalanches (i.e. not column collapse) composed of combinations of two size species of particles (binary and bidisperse) at various proportions. Yang et al. (2015) and Félix and Thomas (2004) also consider the effect of the addition of a third size species to examine polydispersity. Such studies have observed that the addition of a small proportion of finer particles to a granular mixture generates enhanced runouts under particular conditions (e.g. Roche et al., 2006; Moro et al., 2010; Yang et al., 2015; Duan et al., 2022). Although empirical relationships between single parameters under bidispersity have been established, limited attention has been given to the particle interaction mechanisms affecting energy dissipation and mobility (Li et al., 2021). Even less consideration has been taken regarding the applicability of the relevant granular effects to natural, large-scale geophysical flows, which has not been directly addressed so far.

The current study evaluates the impact of bidisperse grain-size distributions on the propagation processes and energy dissipation in small-scale analogue granular flow experiments. This is achieved by combining different binary particle size mixtures. The combined effect with volume, inclination, and size ratio between particles is also evaluated. Moreover, the impact of a slope-break between the inclined plane and the horizontal emplacement surface is considered. The propagation of the centre of mass and frontal

velocity are also examined in order to evaluate the mechanisms responsible for the runout and dynamics of granular avalanches. By examining the dynamics of the modelled avalanches this study aims to constrain the processes under which bidispersity enhances granular avalanche mobility. Subsequently, the potential of these processes as a factor for the enhanced mobility of VDA/RAs and other natural geophysical flows is evaluated.

6.2 Bidispersity and mobility - Background

Lab-scale analogue experiments suggest that granular avalanches containing more than one particle size (i.e. bidisperse or polydisperse) diverge in their macroscale properties from avalanches with monodisperse grain-size distributions (e.g. Reubi et al., 2005; Phillips et al., 2006; Roche et al., 2006; Goujon et al., 2007; Yang et al., 2015). One of the main differences is the effect of the addition of a second size species on their runout. It is commonly observed that the addition of a small fraction of fine particles to a mass composed of coarser generates a lubrication effect resulting in increased velocity and runout of the centre of mass and the front of avalanches (e.g. Phillips et al., 2006; Roche et al., 2006; Degaetano et al., 2013; Yang et al., 2015). The proportion of fine particles to the total mass is denoted as ψ. Analogue experiments suggest that maximum frontal runout is achieved at a critical ψ value (ψ_{CRf}) (e.g. Phillips et al., 2006; Moro et al., 2010; Kokelaar et al., 2014; Bartali et al., 2020; Hu et al., 2020). The ψ_{CRf} has been suggested under the bidisperse experimental conditions of Phillips et al. (2006), Roche et al. (2006), and Hu et al. (2020) to be equal to ψ_{CRf}=0.30. In the experiments of Moro et al. (2010), ψ_{CRf} was equal to 0.25; for Degaetano et al. (2013) ψ_{CRf}=0.50, and Duan et al. (2022) ψ_{CRf}=0.05. The ψ_{CRf} was found to be variable according to the granular size composition and other experimental conditions, such as slope inclination of the flow path (Goujon et al., 2007; Yang et al., 2015). It should be noted that the value of ψ_{CRf} enabling maximum frontal runout is not always equal to the ψ value which enables maximum displacement of the centre of mass (ψ_{CRCoM}). A list of the abbreviations used in this chapter is provided at the end of the chapter (section 6.7).

The investigation of the mechanisms facilitating the increased runout effect by Phillips et al. (2006) reveals that in small-scale avalanches fine particles migrate rapidly to the base. Once at the base, fine particles reduce the frictional areas between the coarse particles and

the substrate by occupying the area between them and acting as 'ball-bearings' (Roche et al., 2006; Linares-Guerrero et al., 2007). They simultaneously act as 'rollers' to encourage rolling as opposed to frictional sliding (Phillips et al., 2006; Hu et al., 2021). Rolling reduces the friction coefficient at the base of the flow as it is less expensive in terms of energy dissipation, and increases the efficiency of kinetic energy transfer (Phillips et al., 2006; Hu et al., 2020, 2021). This process finds support in numerical modelling of granular avalanches composed of binary size distributions, from which findings suggests that rotational motion is enhanced at the base of bidisperse granular avalanches (Linares-Guerrero et al., 2007; Hu et al., 2021). In effect, a basal layer of fine particles lubricates the contact between the granular body and the propagation surface (Lai et al., 2017), inhibiting frictional energy losses. Since energy dissipation in granular avalanches occurs through the transformation of the total potential energy to thermal, acoustic and inelastic deformation energy, as well as mechanical work and kinetic energy (Nicoletti and Sorriso-Valvo, 1991), a process that reduces frictional losses makes more energy available for kinetic according to the law of conservation of energy (Fan et al., 2016; Knapp and Krautblatter, 2020). Bidisperse granular avalanche and column collapse analogue experiment findings and numerical modelling have therefore offered support for bidispersity as more energy-efficient at accommodating shear stress (e.g. Phillips et al., 2006; Linares-Guerrero et al., 2007; Yang et al., 2015; Hu et al., 2021).

However, this idealised behaviour has to be linked to the scale and processes of natural events. One hypothesis connecting bidispersity and the mobility of VDA/RAs has been supported by the studies of Linares-Guerrero et al. (2007), Yang et al. (2015), Lai et al. (2017), Hu et al. (2021) and Duan et al. (2022) and suggests that fine particles migrate and lubricate the base, in a process identical to the described lab experiments. Fine particles enable rolling instead of sliding, locally accommodating shear stress with the rest of the mass carried, sliding on the basal layer, without experiencing agitation or shear stress (Hu et al., 2021). An alternative hypothesis involves the sedimentology of shear zones observed in the field. Bidispersity is observed in VDA/RAs, especially in shear zones of magnified shear stresses (Glicken, 1996; Dufresne and Dunning, 2017). The concentrated accommodation of shear principally in shear zones with the efficient bidisperse arrangement can potentially be a contributing mechanism for long runouts. Shear zones are found primarily in the basal domains, but also within the body of VDA/RAs (van Wyk De Vries et al., 2001; Hewitt, 2002; Weidinger et al., 2014; Roverato et al., 2015; Dufresne

and Dunning, 2017). They are suggested to focus shear and act as corridors of shear accommodation around more coherent domains that are sheltered from shear stress (Crosta et al., 2007; Roverato et al., 2015; Paguican et al., 2021). Areas protected from shear maintain a quasistatic behaviour with low particle interactions and energy dissipation. Li et al. (2021 - pp 1793) propose that the bidisperse arrangement of shear zones potentially efficiently accommodates shear limiting frictional losses within them. This shear concentration limits overall frictional losses in the system potentially contributing to long runout and low apparent friction angles. However, further evaluation of both suggested hypotheses is required to understand their potential and the mechanisms by which bidispersity could enhance mobility in granular avalanches in laboratory experiments and natural granular flows.

6.3 Methodology

This study employs small-scale analogue granular avalanches to investigate the effect of bidispersity of the grain-size distribution on their propagation and emplacement. Different binary granular mixtures are considered by changing the factor ψ. Furthermore, the combined effect of bidispersity with other parameters, namely the total material volume, slope inclination and size difference between coarse and fine particles are examined.

6.3.1 Experimental setup and measuring systems

The setup is comprised of a 1.5 m long inclined plane and a 2.0 m horizontal depositional surface (fig. 6.1a). The material is laterally confined throughout the propagation by transparent plastic walls, limiting its width to 0.3 m but allowing observation of the avalanche and the deposit. The smoothness of the walls and the fact that the ratio between the mean particle diameter (of even the largest size species) and the flow width is <1/20 ensure that there is no boundary effect (Valentino et al., 2008; Jiang and Zhao, 2015; Ahmadipur et al., 2019; Schilirò et al., 2019). Even though confined avalanches do not exhibit the flow and depositional morphologies of unconfined, the purpose was the detailed examination of the effect of individual parameters and processes and not the recreation of deposit geometry. The confinement did not permit lateral spreading, however, it is assumed that there is no significant effect on the flow dynamics in the flow direction (Thompson et al., 2009 - pp246). The inclination of the inclined plane was varied

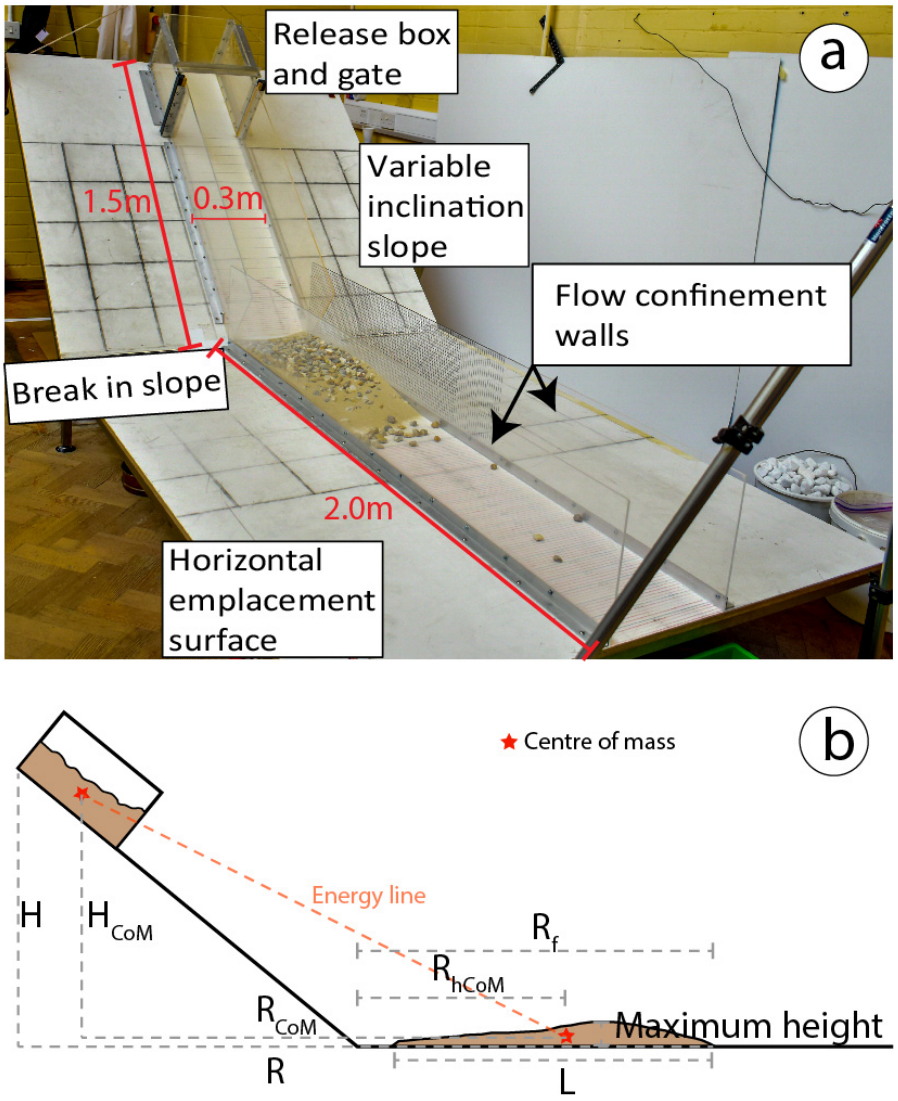

Figure 6.1: **A** Experimental setup. **B** Measurements and descriptors of the deposit and propagation. H: fall height from the highest point of the material in the box to the horizontal plane; H_{CoM}: fall height of the centre of mass (CoM). R: avalanche front runout from the release position; R_{CoM}: centre of mass runout from the release position. R_f: avalanche front runout on the horizontal plane; R_{hCoM}: centre of mass runout on the horizontal plane. The energy line links the position of the centre of mass before release and in the final deposit (adapted from Manzella and Labiouse, 2009).

between 35°, 40° and 45° as required. The geometry of the slope-break between the incline and horizontal surfaces is dictated by this inclination.

Prior to release, the material was held in a release box with a sluice gate removable by sliding upwards. The rapid removal of the gate initiates the flow of the material on the inclined plane under gravity. After propagating down the incline, the material interacts with the slope-break and subsequently propagates on the horizontal surface. The final deposit is formed when all material is immobilised. In this study, propagation is defined as the flow of the material after the release in the incline and horizontal planes. The final deceleration and deposition of the material is defined as the emplacement stage.

Measurements of the geometry of the material prior to release were made manually and photographs were taken so that the location of the pre-release centre of mass could be calculated. Manual measurements were taken for the frontal runout (R_f), the length of the deposit (L) and the maximum height of the final deposit (fig. 6.1). R_f is defined as the distance travelled by the most distal position on the horizontal plane from the slope-break, where particles are still in contact with the main body of the deposit. However, for confirmation and higher accuracy measurements, an oblique photogrammetry survey was conducted, as in the experiments of Li et al. (2021). Photographs of the final deposit were processed in the commercially available software *Agisoft Metashape* generating a 3D model for each. For each deposit, at least 90 pictures were taken with a DSLR camera at a resolution of 4000x6000 pixels to build the rendering (fig. 6.2a). The generated models achieve high accuracy (0.25mm x 0.25mm/pixel) (fig. 6.2b). A digital elevation model (fig. 6.2c) allowed calculating the average deposit thickness, the location of the centre of mass of the deposit, the length of the deposit L, and the frontal runout R_f.

Two high-definition cameras recorded the avalanches, one frontal and one lateral as illustrated in fig. 6.3. The lateral camera view (25 fps, HDV 1440 x 1080) was used to observe the interaction of the avalanche with the slope-break and allow observation of the thickness of the avalanche at different times. The frontal velocity (Vf) was obtained through the analysis of 50 fps (FHD 1920 x 1088) videos recorded for each experiment. The location of the front of the flow at each frame was manually located, and the displacement between frame intervals was calculated. A moving average is used in the presented time series, with a period of three frames to smooth out short-term fluctuations and highlight

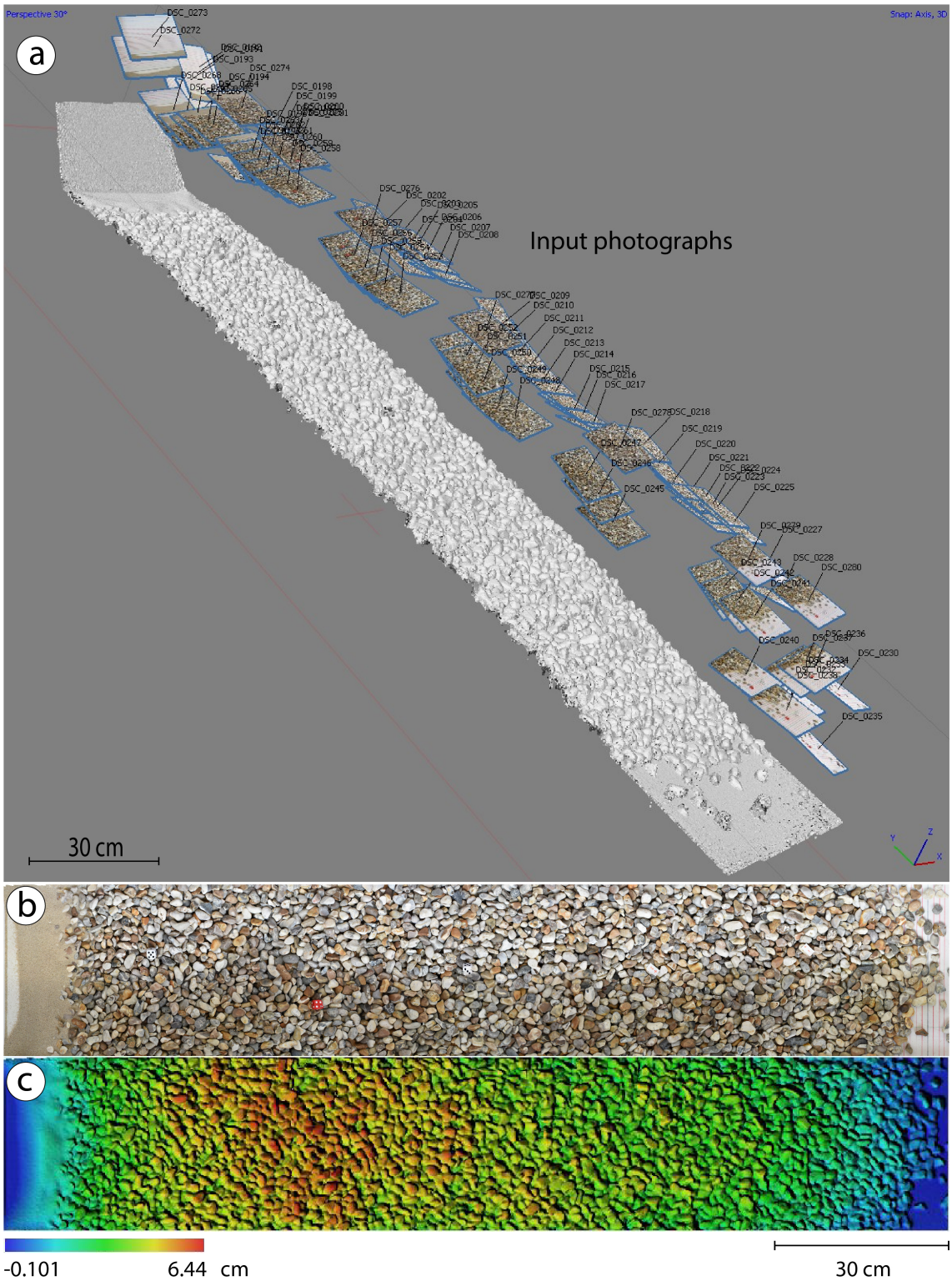

Figure 6.2: **A**Structure for motion photogrammetry. a Photographs used to produce a rendering of the deposit. **B** 3-D model represented in an orthophoto. **C** Digital elevation model of the final deposit.

Figure 6.3: Camera setup during the experiments. **A** Frontal camera placement. **B** Frontal camera frame view. **C** Lateral camera placement. **D** Lateral camera frame view.

longer-lasting trends. Only one of the runs is illustrated in fig. 6.8 and 6.11, for clarity of illustration. The repeatability of the experiments was ensured by confirming each of the minimum of three runs.

H/R (also H/L in the literature) is the ratio between the fall height from the highest point of the material in the box to the horizontal plane (H) and the horizontal runout of the front of the avalanche from the front of the material pre-release (R) (fig. 6.1). This ratio is used as a measure of avalanche mobility in landslide literature (initially by Heim, 1932). Although it is often calculated as the distance between the furthest location of the scarp and the toe of the deposit, in this study it is also calculated for the height fallen (H_{CoM}) and horizontal displacement (R_{CoM}) of the centre of mass, as H_{CoM}/R_{CoM} (also referred to as the gradient of the energy line in literature) (Legros, 2002). H_{CoM}/R_{CoM} is not usually used in field studies because it is very difficult to determine in natural

deposits (Bowman et al., 2012). However, the displacement of the centre of mass is a better measure when considering the energy dissipation of granular flows, as it excludes the effect of spreading of the mass on R (Davies, 1982). Following studies such as Goujon et al. (2007), Yang et al. (2015) and Hu et al., (2020) the proportion of material was assigned by weight (rather than volume). Therefore, also due to the differences in mass configuration (i.e., pore spaces between the coarse particles are sometimes void and sometimes filled by the finer particles), the volume of the material was not identical in all experiments (fig. 6.4). Normalised runout (R_n) is used to illustrate and compare findings. The R_n is represented by the equations R_n=R_f/h* and the normalised propagation of the centre of mass by R_{nCoM}=R_{CoM}/h*, where the Rf and the RCoM are normalised by the cubic root of the volume of the material (h* = $V^{1/3}$). Davies and McSaveney (1999) suggest that such normalised quantities can be compared to real events. Total spreading (S_n) is measured as the normalised L of the final deposit, S_n=L/h* (Manzella and Labiouse, 2013). The normalised distance between Rf and the propagation of the centre of mass on the horizontal plane (R_{hCoM}) was also used ((S_f=R_f-R_{hCoM})/ h*) as a measure of the spreading at the front of the deposit (S_f) which is not affected by material left behind during the emplacement stage or pile on the slope.

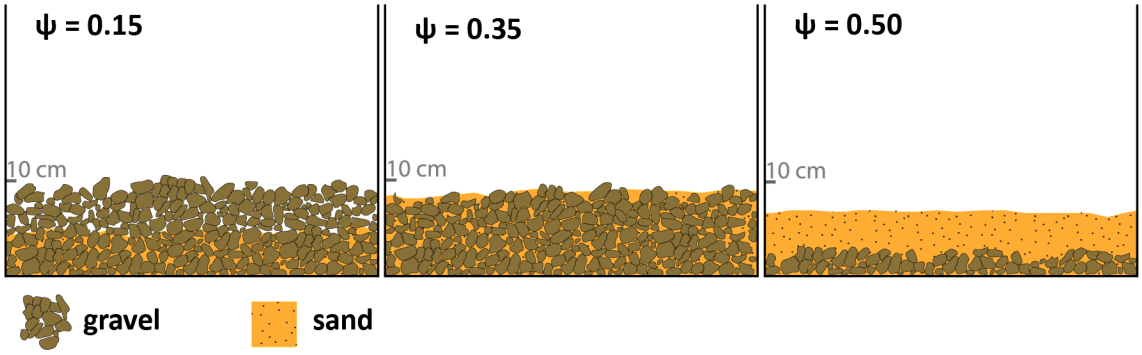

Figure 6.4: Schematic representation of the pre-release arrangement of material in the release box. Note the difference in volume at different size combinations (although weight is equal), as well as the pore spaces between coarse particles at low fractions of fine particles (ψ).

6.3.2 Scaling

Scaling is critical in designing experiments and correlating the findings of small-scale granular avalanches to geophysical mass flows (Iverson et al., 2004; Iverson, 2015). The similarity between analogue models and real events must be addressed by introducing some geometric and dynamic dimensionless parameters to satisfy the continuum hypoth-

Table 6.1: Properties of the material used in the granular avalanche experiments.

	GRAVEL 9.5-16mm	GRAVEL 16-22.4mm	SAND 0.355-0.50mm	SAND 0.5-1mm
Basal friction angle	25.2°	22.3°	30.3°	29.8°
Critical angle of repose	32.2°	29.1°	27.4°	29.3°

esis (Iverson, 1997, 2015; Shea and van Wyk de Vries, 2008; Manzella and Labiouse, 2013). Geometric parameters refer to the size and morphology of the particles and the system of the avalanche. Dynamic parameters refer to the ratio between forces within the body of the avalanche, which are later discussed. The presented experiments follow the scaling considerations of the mentioned previous studies.

Firstly, particle size is large enough to reduce the impact of electrostatic effects to negligible levels (Drake, 1991; Davies and McSaveney, 1999; Iverson and Denlinger, 2001; Manzella and Labiouse, 2009). Additionally, it is assumed there is a similarity to large-scale avalanches regarding the geometric shape, air and grain densities and drag coefficient between grains and air (Davies and McSaveney, 1999). Moreover, Drake (1991) suggests that the avalanche depth needs to be at least ten times larger than the mean particle diameter, which is also fulfilled. If these conditions are met, it is believed that the findings can contribute to the understanding of natural geophysical granular avalanches (Manzella and Labiouse, 2013). These are the scaling guidelines most consistently followed by granular avalanche experiments and the present study. Geometric and dynamic scaling parameters and their scaling effects are further addressed in Section 6.5.7, also regarding their implications for the current experiments and specific studies from the literature.

6.3.3 Material and experimental conditions

The material used in this study consists of four different granular sizes composed of subrounded gravels and subangular corundum sand (fig. 6.5). In granular avalanche experiments angular-subangular natural rock material has been used in most cases in an attempt to maintain a close approximation to the modelled phenomena (Davies and McSaveney, 1999; Shea and van Wyk de Vries, 2008; Cagnoli and Romano, 2010; Li et al., 2021). The properties of the material used in the current experiments are illustrated in table 6.1. Basal friction angles were measured by tilting plane tests (Pudasaini and Hutter, 2007; Mancarella and Hungr, 2010; Jiang and Towhata, 2013). This involves placing a sample of the material on the variable inclination plane and steadily increasing the inclination until

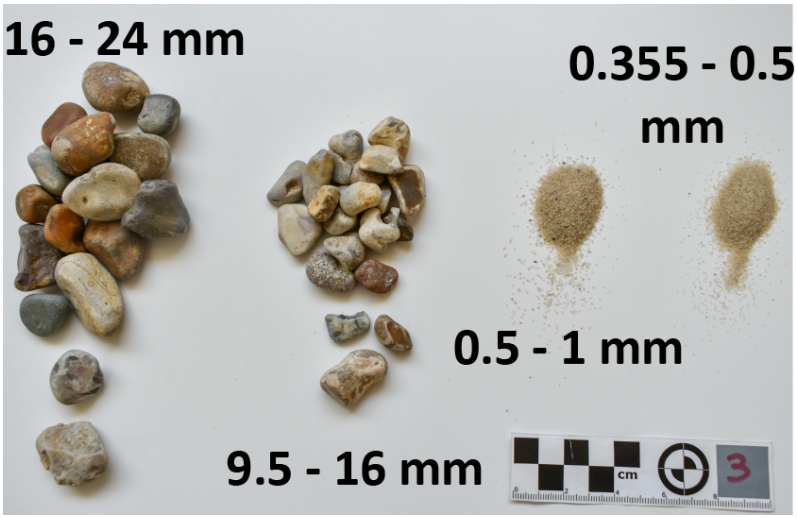

Figure 6.5: The material used in different proportions in the granular avalanches. These are four different granular sizes composed of subrounded gravels and subangular corundum sand.

motion is initiated. The inclination angle was then measured. The critical angle of repose was measured by gently releasing a pile of material from a 5 litre bucket onto a horizontal surface into a conical pile and measuring the steepest slope angle in a digital elevation model from a photogrammetric rendering of the pile. In all experiments, the angle of the inclined plane was greater than the basal and internal angle of the material.

For the bidisperse experiments, a proportion (by mass) of finer granular material was added to the granular mass composed of coarser particles. For each set of experiments, this proportion ψ of fine material mass was varied between ψ=0 (all coarse) and ψ=1 (all fine). Prior to the initiation of the avalanche, coarse and finer particles were placed in the release box so that the fine particles filled the pore spaces between the largest particles from the bottom up (figure 4). In cases where low quantities of fine material was used, void pore spaces remained at the top of the material (fig. 6.4). Conversely, when the volume of the fine material was greater than the pore space between the coarse, excess fines were positioned above the coarse material.

For each ratio of fine material, other factors were changed in order to additionally examine the effect of bidispersity combined with different parameters (volume, inclination and different grain sizes). The experiments are divided into five series according to the conditions and parameters under examination. All the experimental conditions are illustrated in table 6.2. Each experiment was repeated a minimum of three times to generate data to be averaged and to ensure their reproducibility.

Table 6.2: The five experimental series examining different parameters.

Experiment series	GRAVEL 9.5-16mm	GRAVEL 16-22.4mm	SAND 0.355-0.50mm	SAND 0.5-1mm	Mass (kg)	Inclination (°)
A		-	-		20	40
B		-	-		40	40
C		-	-		20	35
D		-	-		20	45
E	-			-	20	40

6.4 Results

6.4.1 Morphology

Under all the conditions of bidisperse granular avalanches, the following common morphological features are observed. At low ψ values (ψ<0.5-0.15 depending on experimental conditions) the addition of fines causes the final deposits to initially became longer (normalised length=L/h*) and lower in height (normalised average height=average height/h*) compared to avalanches composed solely of coarse particles (e.g. fig. 6.6). They also achieve greater runouts (fig. 6.7: 0.00 – 0.15). At a critical value of ψ_{CRf}, maximum Rf is achieved (fig. 6.7: 0.15). However, further increase of ψ, progressively results in a decreased Rf (fig. 6.7> 0.15). With progressively higher ψ (ψ>~0.8) a stage is reached where L is smaller and deposit thickness is higher than the monodisperse flow composed entirely of coarse particles. At low ψ values, coarse particles travel with the fine forming

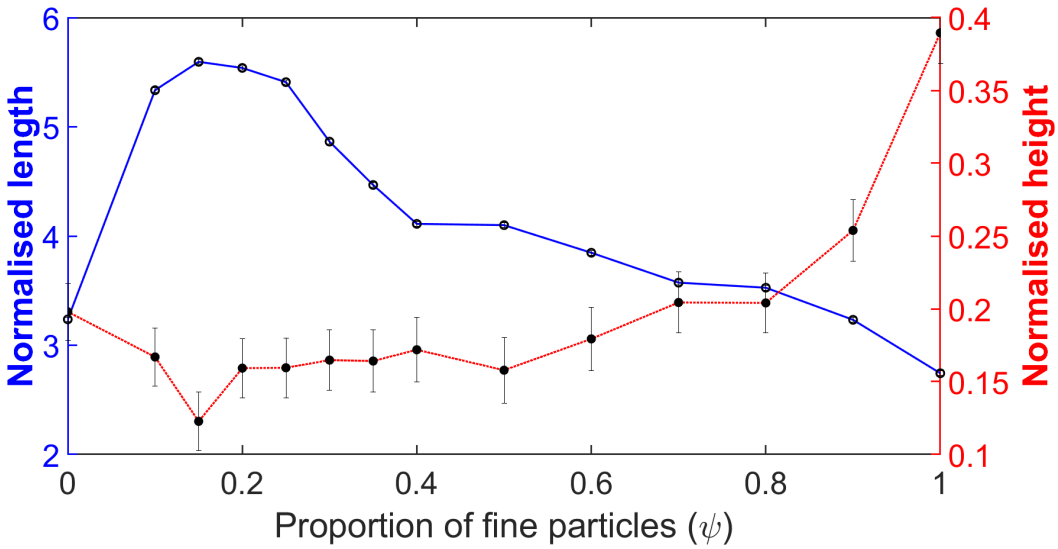

Figure 6.6: Normalised length and height of the experimental avalanches of series A.

a continuous cover over the deposit surface (fig. 6.7: 0.00 – 0.30). At higher ψ they are emplaced at the rear of the deposit near the slope-break (fig. 6.7: 0.50-0.70). An

exception arises when coarse particles that separate from the avalanche early and travel independently, deposited in front of it.

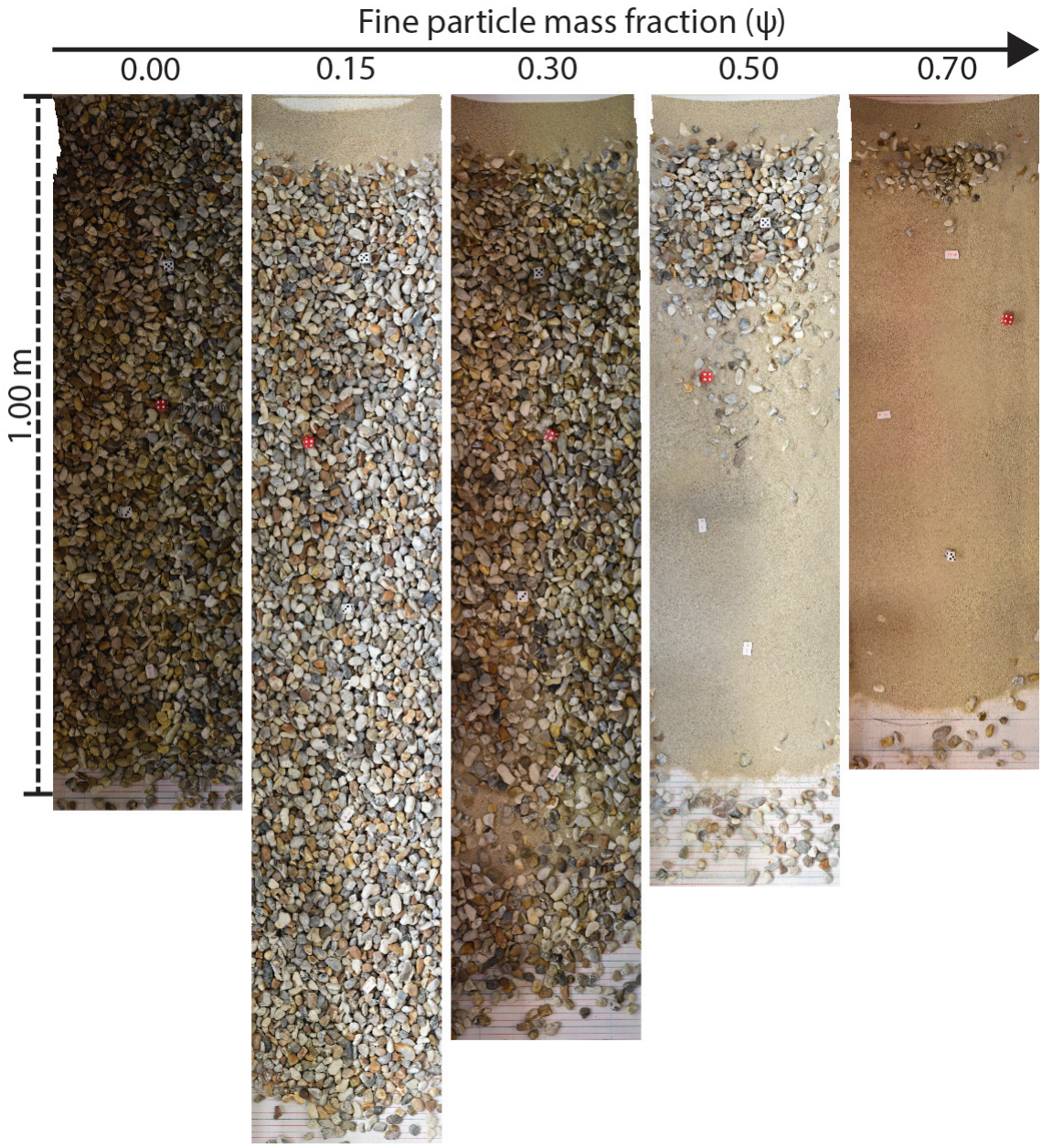

Figure 6.7: Orthophotos of the deposits of experimental avalanches in series A illustrating their runout and morphology. The flow direction is downwards.

6.4.2 Frontal velocities

According to Rait and Bowman (2016), in rock avalanches, the main phases are: the acceleration under gravity phase, and the phase of deceleration of the avalanche after its impact with the near-horizontal valley floor. For the purposes of the analysis of propagation dynamics and energy dissipation, these phases are here considered separately,

and the second phase is further subdivided to address the effect of the slope-break. The Vf of the avalanches is therefore divided temporally into three parts from the release of the material through propagation and up to their emplacement. These phases are exhibited, with variation according to the experimental conditions, in all the experiments (fig. 6.8):

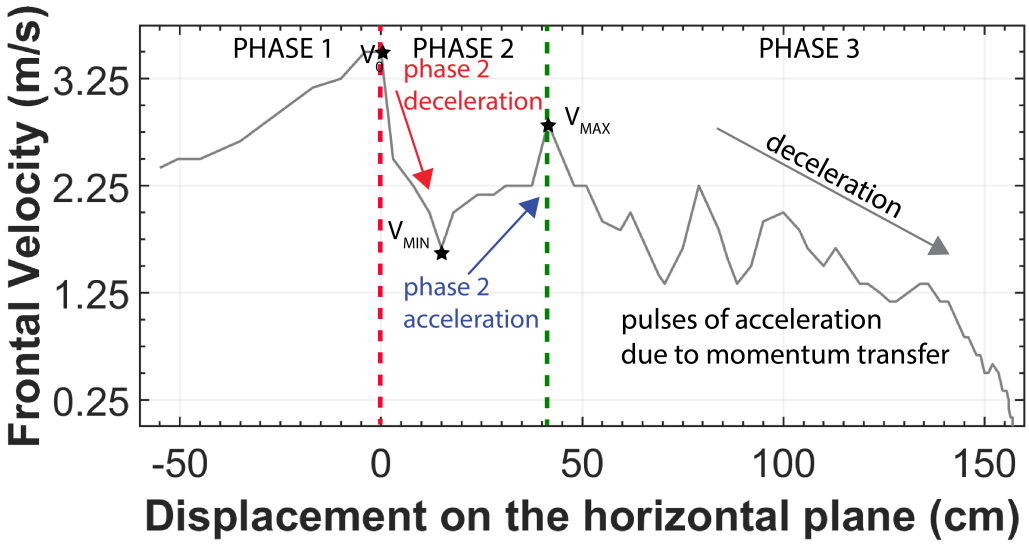

Figure 6.8: The frontal velocity of the fine particle content of ψ=0.15 avalanche of experimental series B with the velocity phases annotated. V_0: frontal velocity at the slope-break; V_{MIN}: lowest frontal velocity of phase 2; V_{MAX}: velocity the front accelerates to at the end of phase 2

.

PHASE 1 – ACCELERATION ON THE INCLINED SLOPE: This is the stage of acceleration following the release of the material. This phase ends when the material at the front of the avalanche interacts with the slope-break to begin their transition to the horizontal plane.

PHASE 2 – INTERACTION WITH THE SLOPE-BREAK: This phase begins when the avalanche front first interacts with the geometric irregularity of the slope-break and suffers a deceleration. This deceleration is followed by a rapid acceleration as the material behind the front (greater in mass) transfers momentum to the front. This can be observed the video frames of the avalanches illustrated in fig. 6.9. The degree and duration of both the deceleration and acceleration of this phase are a function of a number of variables like the angle of the slope-break, the size of the granular material and ψ. Once the acceleration reaches peak velocity (V_{MAX}) in phase 2, and starts decelerating again, phase 2 ends. This is when the material at the front stops receiving energy directly from the momentum of material interacting with the slope-break. The peak velocity V_{MAX} in phase 2 is not

reached again by the flow.

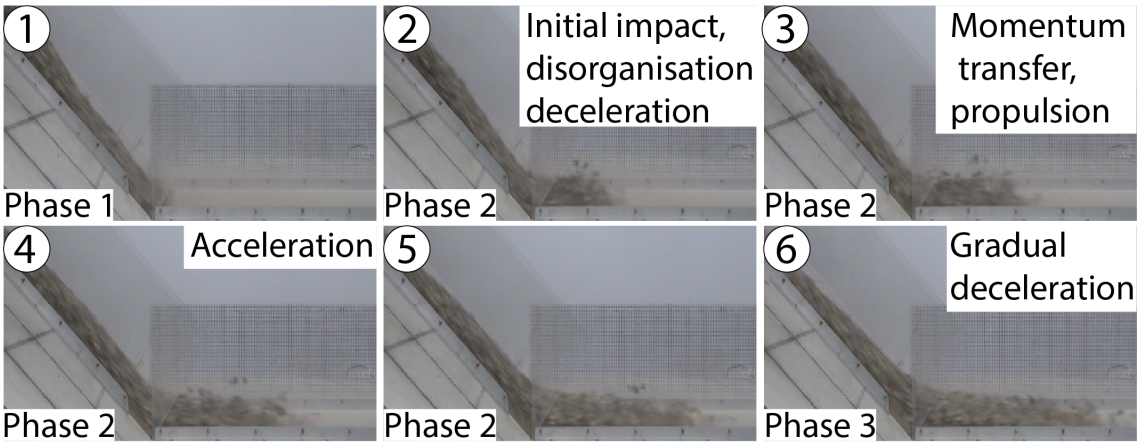

Figure 6.9: Frames from the interaction of the front of the avalanche (ψ=0.15, series B) with the slope-break.

Phase 2 deceleration is calculated here as the rate of velocity change between the interaction of the front with the slope-break (V_0) and the recording of the minimum velocity of phase 2 (V_{MIN}), as in the equation:

$$\text{Phase 2 percentage deceleration} = \frac{V_0 - V_{MIN}}{V_{MIN}} \tag{6.1}$$

where V_0 is the frontal velocity at the slope-break, and V_{MIN} is the lowest frontal velocity of phase 2 (fig. 6.8). Phase 2 acceleration is calculated as the rate of velocity change between the lowest velocity of phase 2 and the velocity the front accelerates to at the end of phase 2 (V_{MAX}):

$$\text{Phase 2 percentage acceleration} = \frac{V_{MAX} - V_{MIN}}{V_{MIN}} \tag{6.2}$$

where V_{MAX} is the velocity the front accelerates to at the end of phase 2 (fig. 6.8).

PHASE 3 – DECELERATION AND EMPLACEMENT: After the interaction with the slope-break stops disturbing the front of the flow, a deceleration phase eventually leads to the emplacement of the material. This phase is characterised by pulses of deceleration of the frontal material and subsequent acceleration (fig. 6.8). The Vf is lower for each subsequent pulse. The amplitude of these waves appears to be a function of the volume of the granular mass as later discussed. Phase 3 ends when the material comes to a halt after losing momentum and energy and each particle settles in its position in the final deposit.

Phase 3 deceleration is calculated here as the average rate of velocity change between the initiation of phase 3 and the final deposition (fig. 6.8) using the following equation:

$$\text{Phase 3 average deceleration} = \frac{V_{MAX}}{\text{Time duration of phase 3}} \tag{6.3}$$

6.4.3 Fine particle content (ψ)

Experiment series A (table 6.1) has the primary aim of examining the impact of ψ on the runout and the mobility of the centre of mass of the granular avalanches. It is also the reference case for the rest of the experiments. Fig. 6.10a illustrates that changes in ψ result in variation of both the R_n and R_{nCoM} propagation metrics. The initial addition of fines for ψ=0.10 leads to an increase of R_n and R_{nCoM}. The maximum Rn exhibited at ψ_{CRf}=0.15 represents an increase of 87% from the all-coarse avalanche. In the case of the centre of mass, at ψ_{CRcom}=0.10 the equivalent increase is ~100%. There is, therefore, a divergence in ψ value for the maximum R_n in comparison to the maximum R_{nCoM}. Further increases in ψ, past ψ_{CRf} and ψ_{CRcom}, result in reduced R_n and R_{nCoM} (fig. 6.10a). Greatest R_n

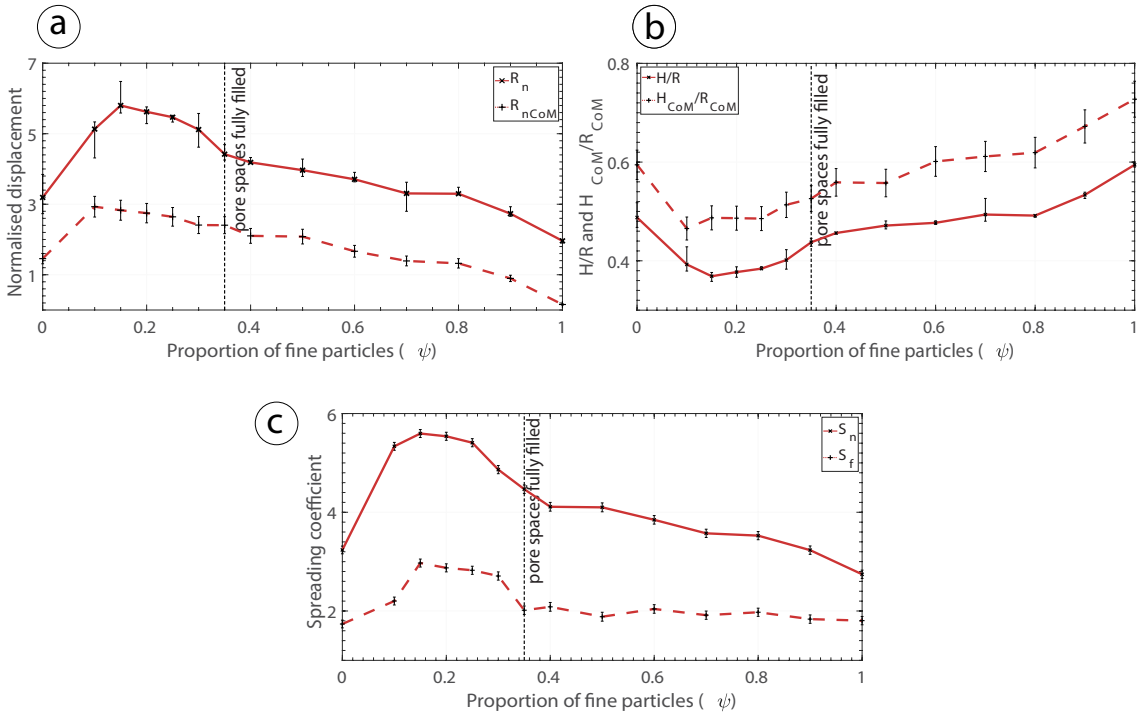

Figure 6.10: Results from experimental series A. **A** Frontal runout (R_n) and propagation of the centre of mass (R_n) at different proportions of fines (ψ). **B** H/R and H_{CoM}/R_{CoM} at different proportions of fines ψ. **C** Total spreading (S_n) and frontal spreading (S_f) at different proportions of fines ψ.

and R_{nCoM} variability is observed at ψ between 0.10 and 0.35. However, R_n and R_{nCoM} remain above the all-coarse avalanche up to ψ=0.80. The sensitivity of R_n and R_{nCoM} to ψ decreases after all the pore spaces between the coarse particles are filled by fines at ψ=0.35 (fig. 6.10a). These observations are confirmed by fig. 6.10b. The H/R and H_{CoM}/R_{CoM} measure propagation including the location of the mass before their release and confirm that the relationships are not an effect of the initial position of the centre of mass. fig. 6.10c illustrates that spreading Sn and Sf are greater at ψ=0.15, despite the ψ divergence between ψ_{CRf} and ψ_{CRcom}. The value of ψ appears to greatly affect the degree of spreading when there are pore spaces between the coarse particles (ψ<0.35). Once the pore spaces are completely filled up with fine particles, ψ variation has less impact on spreading (fig. 6.10c). Particularly the S_f remains almost constant after pore spaces are filled.

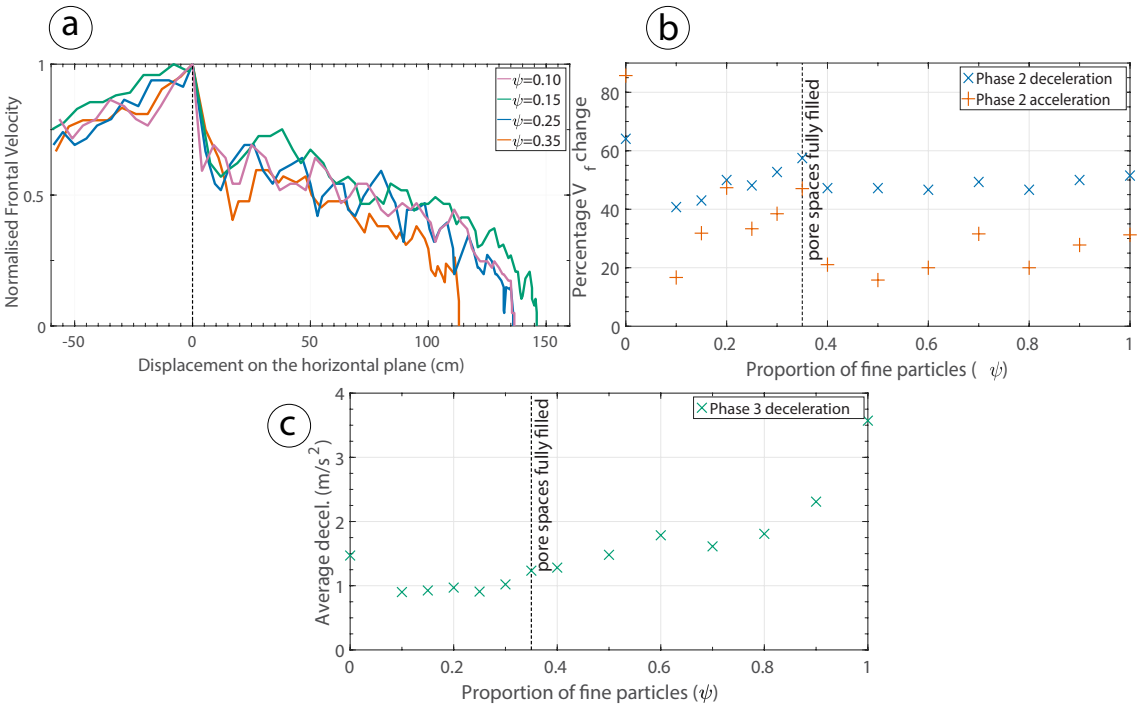

Figure 6.11: Velocity results from experimental series A. **A** Velocity normalised by the maximum velocity achieved for 4 avalanches. Dashed horizontal line represents the location of the slope-break. **B** Velocity change during the acceleration and deceleration of phase 2. **C** Phase 3 average deceleration.

Vf observations suggest that ψ affects phase 2 (interaction with the slope-break) and phase 3 (deceleration and emplacement). There does not appear to be a systematic impact on phase 1 (acceleration on inclined slope, fig. 6.11a). In phase 2, the deceleration after the slope-break is consistently increased with increasing ψ (fig. 6.11b). Phase 2 acceleration increases with ψ between 0.10 and 0.35. In this range increases in ψ result in lower

acceleration (fig. 6.11b). The average deceleration of the material in phase 3 (fig. 6.11c) is not significantly reduced at low ψ between 0.10 and 0.35 (pore spaces not fully filled). At higher ψ, the average deceleration increases throughout the range of ψ values.

6.4.4 Volume

Experiment series B (table 6.1) examines the combined effect of bidispersity and volume. Bidispersity has the impact observed in series A also at the higher volume, increasing mobility (runout and centre of mass displacement) at low ψ and progressively diminishing (fig. 6.12a). However, fig. 6.12a illustrates that with higher volume, R_n values are greater. Nonetheless, R_{nCoM} is not increased. This trend is confirmed by fig. 6.12b, illustrating H/R and H_{CoM}/R_{CoM}. Fig. 6.12c suggests that spreading is greater for the higher volume avalanches.

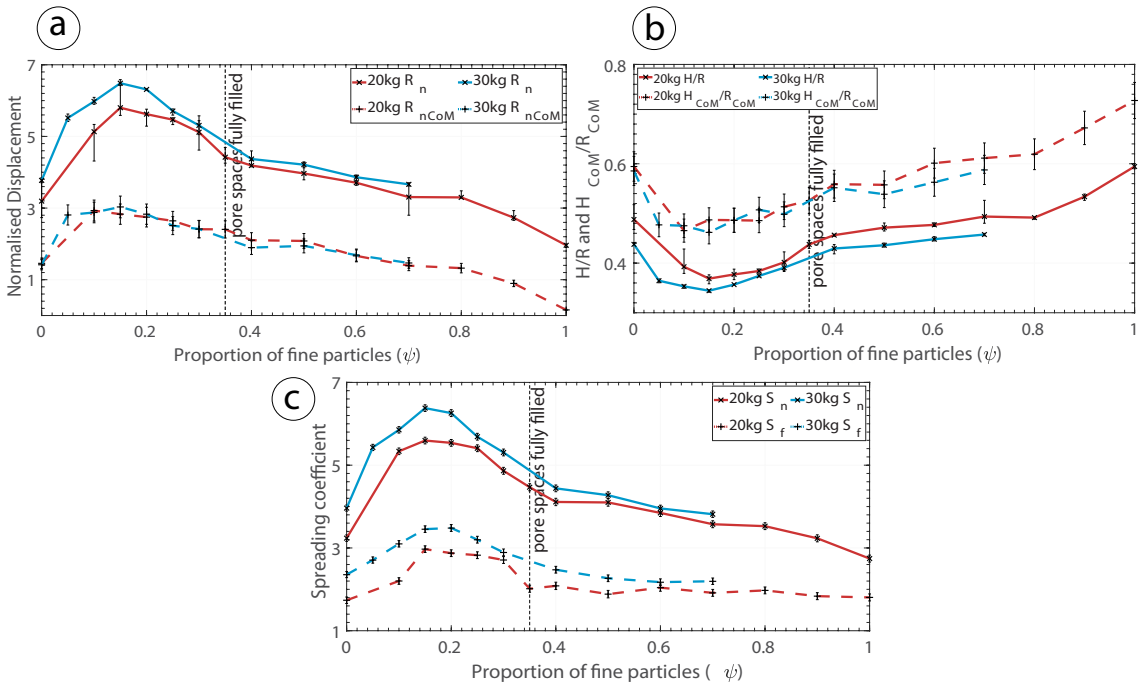

Figure 6.12: Results from experimental series B. **A** Frontal runout (R_n) and propagation of the centre of mass (R_n) at different proportions of fines (ψ). **B** H/R and H_{CoM}/R_{CoM} at different proportions of fines ψ. **C** Total spreading (S_n) and frontal spreading (S_f) at different proportions of fines ψ.

Volume does not systematically affect Vf in phase 1 in comparison to series A. In phase 2, at the slope-break series B avalanches (lower volume) experienced similar deceleration on impact with the slope-break series A. However, the acceleration of phase 2 achieves higher velocities and lasts longer in higher volume avalanches (fig. 6.13).

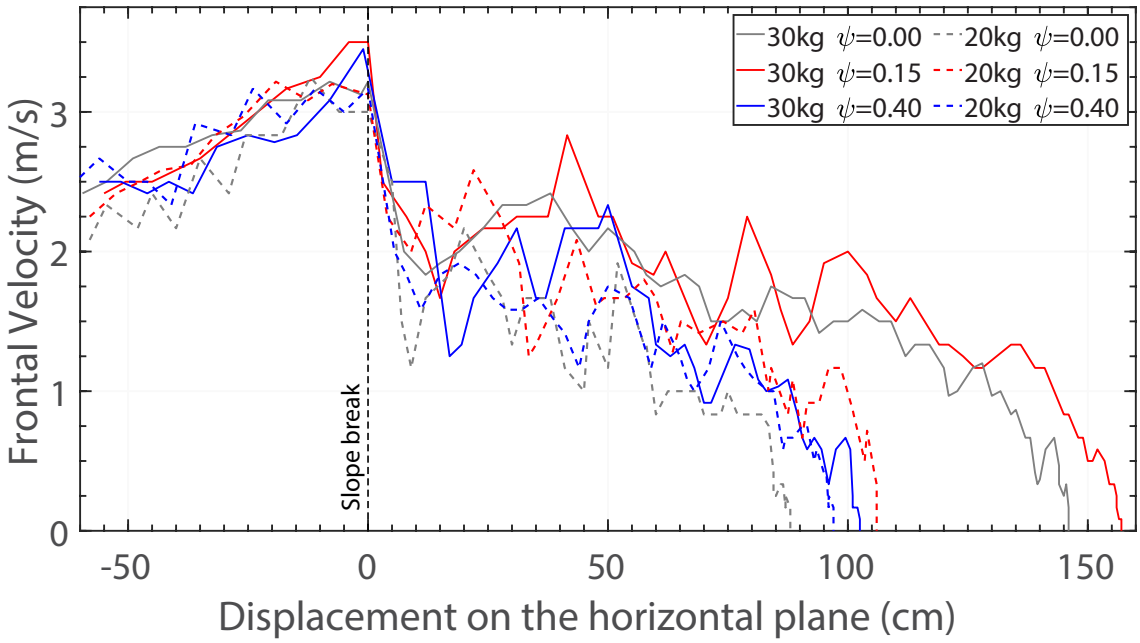

Figure 6.13: Frontal velocity comparison between the avalanches of series A (20kg) and B (30kg).

In phase 3, pulses of acceleration and deceleration show a higher Vf amplitude in the higher volume avalanches. The V_{MAX} achieved in these pulses are greater at greater volumes. They are then decelerated and accelerated again to high velocities throughout phase 3 compared to the less voluminous series A (fig. 6.13).

6.4.5 Slope inclination

For experiment series C and D (table 6.1) the slope inclination was 35° and 45° respectively, also altering the angle of the slope-break. In a simplified conceptual model, VDA/RAs can be separated into two phases: (1) An acceleration phase initiated directly after the detachment/release of the material from the source, and (2) a decelerating runout phase terminating with emplacement (Rait and Bowman, 2016). In some cases, there is a transition in the geometry of the path between the two phases when the material descends a slope and is deposited on a flat surface at the base of it, on a valley floor. The impact of this transition is examined here, represented by the slope-break formed between the inclined plane and the horizontal depositional surface (fig. 6.1). By changing the inclination of the slope on which the material was released the H, horizontal runout distance on the slope and height of the centre of mass prior to release are altered. For this reason, we use their H/R and H_{CoM}/R_{CoM} for comparison for series C and D (instead of R_n and R_{CoM}). fig. 6.14a presents findings that suggest that between 35° and 45°, increased slope

inclination generates less mobile avalanches, both in terms of their centre of mass as well as frontal runout. Although the maximum mobility of the centre of mass is achieved for all inclinations at ψ_{CRcom}=0.10, in the case of the maximum R, a divergence is observed. The maximum is at ψ_{CRf}=0.15 for 40° and 45°, whereas it is at ψ_{CRf}=0.10 for 35°. Spreading also diverges as illustrated in fig. 6.14b. The effect of bidispersity on the degree of spreading is more intense at low ψ, before all pore spaces are filled. The 35° experiments achieve the lowest spreading, which is progressively increased at higher inclinations.

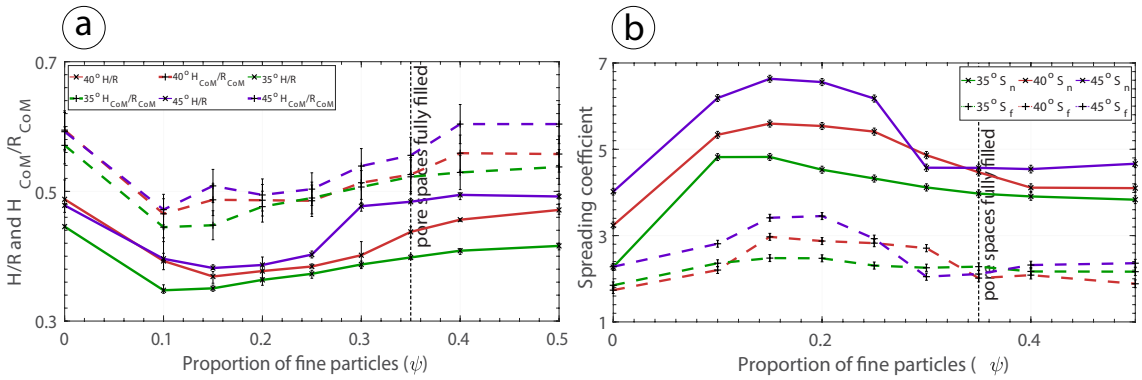

Figure 6.14: Results from experimental series C and D. **A** H/R and H_{CoM}/R_{CoM} at different proportions of fines ψ. **B** Total spreading (S_n) and frontal spreading (S_f) at different proportions of fines ψ.

6.4.6 Size-ratio between particle species (Δ)

In experimental series E (table 6.1) the granular mixtures were composed of finer fine particles and coarser coarse particles, thus increasing the size ratio (Δ) between the two species (Δ= coarse particles mean diameter/ fine particles mean diameter). Previous experimental series have a size ratio Δ=~17, whereas series E had a size ratio Δ=~45. Fig. 6.15a illustrates that increased Δ results in greater R_n and R_{nCoM} at low ψ. Fig. 6.15b, which also considers the difference in the centre of mass prior to release due to the difference in their sizes, confirms that at low ψ=0.05 and ψ=0.10 the granular mixture with greater Δ is more mobile in terms of Rn and R_{nCoM}. At ψ values greater than ψ>0.10, series E avalanches with greater Δ are less mobile. The peak in Rn and R_{nCoM} for experiment series E comes at ψ_{CRf}= ψ_{CRcom}=0.05, compared to ψ_{CRcom} =0.10 and ψ_{CRf}=0.15 for series A. In series E, spreading is greater for all ψ values when only the front of the deposit is considered (S_f) (fig. 6.15c). When the whole length of the deposit is considered (S_n), the spreading of flows from series A and E is very similar after the pore spaces between the coarse particles are filled by fine particles.

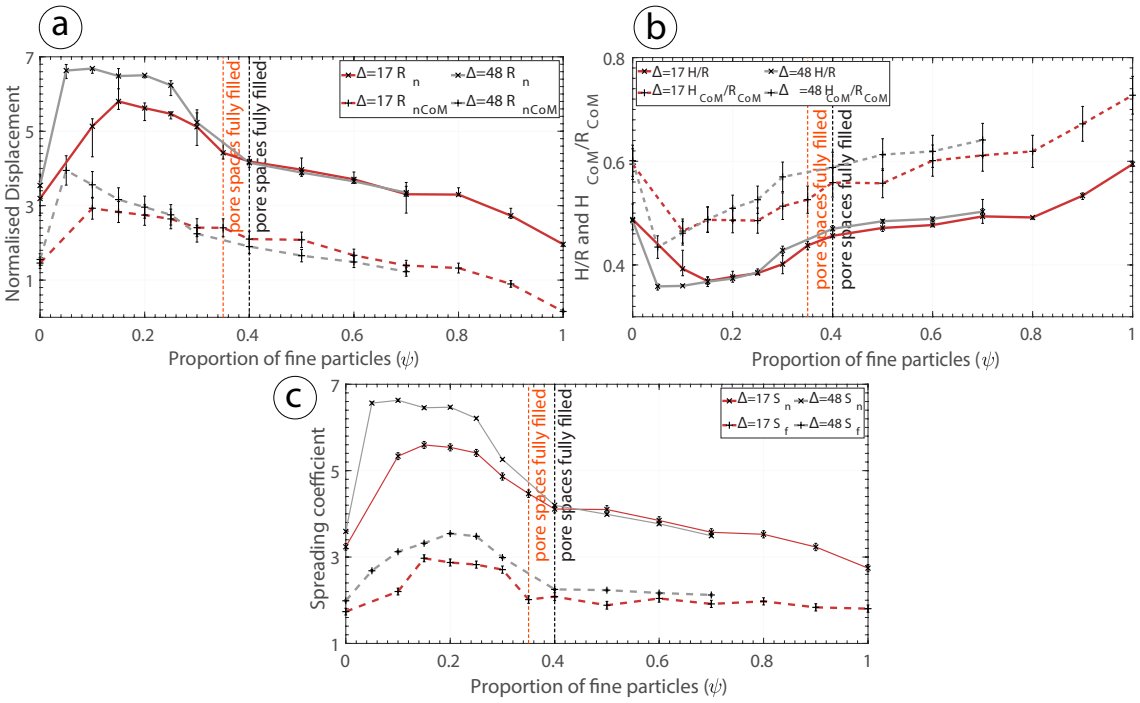

Figure 6.15: Results from experimental series E. **A** Frontal runout (R_n) and propagation of the centre of mass (R_n) at different proportions of fines (ψ). **B** H/R and H_{CoM}/R_{CoM} at different proportions of fines ψ. **C** Total spreading (S_n) and frontal spreading (S_f) at different proportions of fines ψ.

6.5 Discussion

6.5.1 Deposit morphology observations

VDA/RAs on flat valley floors generate horizontal runouts much greater than the initial fall height (McSaveney et al., 2000; Hungr, 2002; Legros, 2002). This feature was recreated in the presented experiments with H/R values as low as 0.35. Although long-runout avalanches are difficult to recreate at the lab scale (Friedmann et al., 2006; Manzella and Labiouse, 2013), R_n values >6.5 have been achieved with bidisperse mixtures, compared to R_n=3.2-3.3 that is the maximum achieved by most monodisperse end member avalanches. These values are in line with values exhibited by some natural VDA/RAs like the Elm (Switzerland)(R_n=5.1) and Frank (Canada) (R_n=5.6) RAs. However, the appropriateness of such comparisons is discussed in section 6.5.7.

Segregation of the size species is observed in the deposit in the vertical and longitudinal direction of the deposit for different values of ψ (fig. 6.7). This observation confirms that the effective composition of the flow is variable in time at different flow locations in the experimental conditions, while grading of the material and migration of fines to the

base take place. When ψ increases, coarse particles are unable to travel independently, in agreement with what is observed by Phillips et al. (2006), as they are trapped in the mass of fine particles generating a sand-trap absorbing their kinetic energy (Bartali et al., 2020). Thus, coarse particles are observed deposited on top of the fine particles close to the break of slope (fig. 6.7).

6.5.2 Frontal velocities during propagation

6.5.2.1 Phase 1

Phase 1 represents the propagation of the material under gravity. Vf is greater at greater slope inclinations because friction is reduced, and rolling is encouraged, as discussed in section 6.5.5. Changes in ψ, volume and Δ do not have a systematic impact on Vf in this phase.

6.5.2.2 Phase 2

Velocity measurement and video observations from this study support that the interaction of the avalanche with the slope-break causes loss of momentum (also observed by Crosta et al. 2017) and disorganisation in the particle position in the mass (fig. 6.9) (also observed by Manzella and Labiouse 2009). The deceleration on initial contact with the horizontal plane is the result of increased friction due to the higher overburden stress at the change of direction of movement (Manzella and Labiouse, 2009; Yang et al., 2011). The deceleration is followed by acceleration as momentum is transferred by the rear of the flowing avalanche to the front, which decelerates earlier. As the material at the front decelerates and transitions to a compressive regime, material still on the slope interacts with them before they decelerate, pushing them forward, transferring energy and momentum (Longchamp et al., 2016; Hu et al., 2020). This process was also observed in the monodisperse experiments of Manzella and Labiouse (2009), and described by Heim (1932), Van Gassen and Cruden (1989), Okura et al. (2000), Legros (2002), Bartali et al. (2015) and Fan et al. (2016).

6.5.2.3 Phase 3

Pulses of acceleration and deceleration of the front observed during propagation on the horizontal depositional surface (e.g. fig. 6.8, 6.11a, 6.13) have also been described by Van

Gassen and Cruden (1989) and Bartali et al. (2015). Bartali et al. (2015) describe them as density waves travelling through the propagating mass generating stick-slip motion. Van Gassen and Cruden (1989) suggest that as the leading material decelerates due to friction, the approaching material from further back has not yet experienced equal retardation. It is therefore approaching at higher velocities than the material ahead. This leads to an interaction of momentum transfer between the particles at the avalanche front and the following material (Hu et al., 2021). The leading particles are propelled forward while the following material is decelerated to lower velocities or deposition. This process is referred to as energy transmission through impact by Van Gassen and Cruden (1989) and has also been reported through close videos examination of the experiments of Manzella and Labiouse (2009 - monodisperse) and Yang et al. (2011 – bidisperse/polydisperse). This can be observed by careful examination of the videos of the experiments presented in this chapter. The cyclic recurrence of this process continues throughout the propagation and is evident through Vf oscillation pulses (fig. 6.8). Each subsequent pulse achieves lower velocities as the energy in the system decreases until the momentum and energy are depleted and the material is emplaced (Van Gassen and Cruden, 1989). By using energy equations to describe the momentum transfer occurring in these processes, Van Gassen and Cruden (1989) produced a model that suggests that a granular mass changing and interacting in the manner described above results in significantly longer runouts (>1.5 times longer) than predicted by simple sliding block models with no momentum transfer. The transfer of momentum from the rear to the front causes the mass to spread and the front of the flow to travel farther (Legros, 2002; Manzella and Labiouse, 2009). The importance of spreading is addressed throughout the discussion.

6.5.3 Fine particle content (ψ)

The findings are in agreement with previous studies reporting increased runout in granular avalanches composed of bidisperse mixtures compared to monodisperse (e.g. Phillips et al. 2006; Roche et al. 2006; Moro et al. 2010; Degaetano et al. 2013; Yang et al. 2015; Bartali et al. 2020). Maximum runouts are recorded at different proportions of ψ in different experiments as a function of parameters such as Δ and slope inclination. In experiment series A, R_n increases between ψ values of 0.0 and 0.15 (where maximum R_n occurs), and R_{nCoM} increases until ψ=0.10. The effect of ψ on mobility is consistent with previous bimodal granular avalanche and column collapse experiments (e.g. Phillips et

al., 2006; Roche et al., 2006; Moro et al., 2010; Degaetano et al., 2013; Yang et al., 2015). It is observed that at low ψ fine particles segregate and position themselves at the bottom of the avalanche through kinetic sieving even if they are not initially positioned there, as also observed by Phillips et al. (2006). Observations confirm the propositions of Goujon et al. (2007) that segregation is a very fast process in bidisperse mixtures at the scale of these experiments. Once at the base, the fine particles reduce frictional contact areas, acting as ball-bearers (e.g. Roche et al., 2006; Linares-Guerrero et al., 2007), and encourage rolling as opposed to frictional sliding (Phillips et al., 2006). This process reduces the friction coefficient at the base of the flow and inhibits frictional energy losses (Phillips et al., 2006; Hu et al., 2020, 2021). Consequently, the R_n and R_{nCoM} are increased. In series A, this process is most efficient at ψ=0.10 where maximum R_{nCoM} occurs (fig. 6.10a). This is because when considering the energetics, the propagation of the centre of mass has to be considered, which does not take into account the spreading of the mass. At lower ψ values (<0.10), there are not enough fine particles to optimally lubricate all frictional contact surfaces at the base of the flow because not all coarse particles are supported by fines (fig. 6.16a) (Moro et al., 2010). The numerical modelling of Linares-Guerrero et al. (2007) suggests that the most efficient arrangement is one with a single grain size thickness layer continuous sheet of fines at the base of an avalanche. In such a case, the basal contacts are lubricated; but no particles are present within the avalanche body (fig. 6.16b) (Moro et al., 2010).

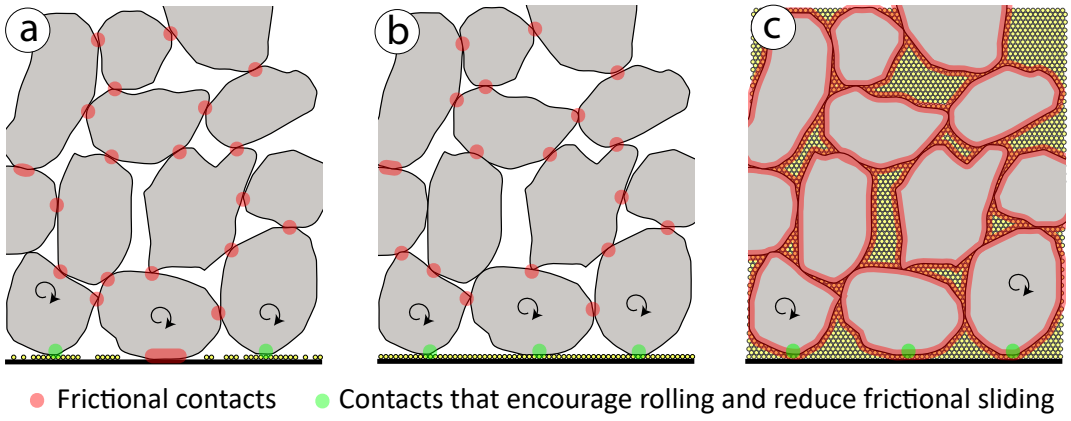

Figure 6.16: Types of contacts between the fine (yellow) and the coarse (gray) particles at different mixture proportions.

As ψ increases (>0.10), fines cover the base and start filling pore spaces between the coarse particles within the avalanche. Interparticle frictional contact surfaces increase as the pore

spaces between the coarse particles are filled (fig. 6.16c). This progressively inhibits R_n and R_{nCoM} further with subsequent ψ increases as illustrated by fig. 6.10a, supporting the trend reported in other studies (Phillips et al., 2006; Moro et al., 2010; Yang et al., 2011; Bartali et al., 2020; Hu et al., 2020, 2021). The increased frictional losses in the interparticle contacts begin to offset the energy conserved at the base, as it becomes a major energy sink (Moro et al., 2010; Hu et al., 2020). However, it is important to note that even after all the pore spaces between coarse particles are filled (0.35>ψ<0.80 for series A), bidispersity enables mobilities greater than the monodisperse avalanches with all-coarse or all-fine particles (fig. 6.10a). Therefore the frictional energy loss conserved at the base is not offset by friction in the body of the avalanche. This non-monotonic relationship between R_n and R_{nCoM} and ψ is reported in similar bidisperse experiments (e.g. Phillips et al., 2006; Goujon et al., 2007; Moro et al., 2010; Yang et al., 2015).

The ψ_{CRf} has been suggested by various experimental studies to be between 0.25 and 0.50 (table 6.3) (Roche et al., 2006; Moro et al., 2010; Degaetano et al., 2013; Yang et al., 2015; Hu et al., 2020). Phillips et al. (2006), Roche et al. (2006), and Hu et al. (2020) found ψ_{CRf} to be equal to ψ_{CRf}=0.30. In the experiments of Moro et al. (2010), ψ_{CRf} was equal to 0.25; for Degaetano et al. (2013) ψ_{CRf}=0.50, and Duan et al. (2022) ψ_{CRf}=0.05.In the current experiments, it is ψ_{CRf}=0.15 in the majority of cases; however, it changes to ψ_{CRf}=0.10 for the 35° slope inclination (exp. series C) and ψ_{CRf}=0.05 for the experiments with greater Δ (exp. series E). Therefore, the findings suggest that ψ_{CRf} is not constant under all conditions but is a function of the geometry of the flow path and Δ, according to the parameters here examined.

Table 6.3: Comparison of experimental conditions in relevant studies

	Particle diameters (mm)	Volumne (mm cubed)	Mass (kg)	ψ_{CRf}	Δ	System-to-grain size ratio□	N^{Sa}
Goujon et al. (2007)	0.132, 0.225, 0.275, 0.325	*	0.176	variable	2.5	**	***
Moro et al. (2010)	0.15, 0.20, 1.00	*	10	0.25	6.7	**	***
Yang et al. (2015)	0.1-0.3, 0.42-2.00, 4.75-9.503	$1.15x10^6$	3	variable	35.6	$3.3x10^4$	***
Bartali et al. (2020)	3.0, 1.5, 0.375	*	4	<0.07	4.0-21.3	**	***
Hu et al. (2020)	1.0-4.0, 4.0-8.0, 8.0-12.0, 12.0-16.0	*	10	0.3	5.6	**	***
Li et al. (2021)	0.175, 1.5	$2.00x10^7$-$8.00x10^7$	*	*	8.6	$4.8x10^7$-$1.9x10^8$	$1.0x10^{-3}$-$1.0x10^{-1}$
Duan (2022)	<0.075, 0.075-0.5	$1.80x10^6$	*	0.05	7.7	$4.4x10^8$-$3.0x10^9$	***
This study	0.355-0.500, 0.5-1.0, 9.5-16.0, 16.0-22.4	$1.33x10^7$-$20.00x10^7$	20-30	0.05-0.15	17.0-44.9	$5.0x10^4$ - $6.9x10^4$	$1.5x10^{-2}$-$1.7x10^{-1}$

** not reported, ** could not be calculated - volume not reported, *** not calculated - required data was not available, □ at ψ=0.5, ◊ for experimental series A*

The ψ affects the propagation of the centre of mass by basal lubrication. However, the

spreading of the mass is affected in a process that appears to be independent as they do not follow the same trend (fig. 6.10, 6.12, 6.14, 6.15). Greater runout does not necessarily imply greater propagation of the centre of mass. Therefore, ψ_{CRf} does not always coincide with ψ_{CRcom}. The difference between R and R_{CoM} has been long identified by Hsü (1975). Investigating R_{CoM} reflects the energy dissipation of the flow and is therefore more appropriate for investigating the energetics of granular flows (Legros, 2002). In fact, H/R is mechanically irrelevant as a measure of mobility, since spreading can produce higher runouts irrespective of the centre of mass, and therefore kinetic energy dissipation (Davies, 1982; Legros, 2002; Dufresne et al., 2021a). Thus, as initially suggested by Hsü (1975), the interpretation of the H/R (or Fahrböschung) as the friction angle is incorrect when considering the energetics of avalanches, and should instead be measured as the inclination of the line connecting the centre of gravity of the material pre-release and post-deposition ($H_{CoM/RCoM}$ or energy line gradient) (fig. 6.1). In turn, H_{CoM}/R_{CoM} is not capable of considering the contribution of spreading to the runout (Davies, 1982; Davies and McSaveney, 1999). Therefore, a comparison of the two metrics, along with quantification of spreading, is needed to assess the impact and variability of spreading. Assessment of the spreading is important as it contributes to the runout. In terms of hazard assessment this is vital in affecting the potential areas affected by mass flows.

Vf observations suggest that ψ affects the interaction of the avalanche with the slope-break (phase 2) and the subsequent propagation on the horizontal plane (phase 3). This is in agreement with the findings of the granular flow experiments of Fan et al. (2016) suggesting that material with different grain-size distributions produce different Vf during propagation. The findings of the current study suggest that small ψ values drastically lower phase 2 deceleration and the average deceleration rate of phase 3 compared to monodisperse endmembers (fig. 6.11b, c). Fan et al. (2016) observed more pronounced decelerations in phase 2 in lower grain sizes. In accordance, the deceleration of the fine particles in phase 2 of the current experiments leads to accumulation of material at the toe of the slope. This is the result of the greater size ratio between particles and the slope-break discontinuity (Manzella and Labiouse, 2013). Furthermore, momentum transfer from the rear was not efficient at high ψ values as the accumulated fines acted as a sand-trap, absorbing the kinetic energy of coarser particles (Fan et al., 2016; Bartali et al., 2020). Nonetheless, the lower deceleration rate observed in phase 3 at ψ<0.7 (fig. 6.11c) supports that the addition of fine particles imposes a more efficient flow arrangement. The reduced

fricitonal energy dissipation they enable at the base makes more energy available as kinetic and reduces the deceleration of the material, generating longer runouts.

6.5.4 Volume

Examination of the H/R of natural events suggests that more voluminous VDA/RAs produce longer runouts (Shea and van Wyk de Vries, 2008). In the current experiments increased total volume (exp. series B) results in increased Rn (fig. 6.12a). However, in agreement with the monodisperse granular avalanche experiments in Manzella and Labiouse (2009), the increased R_f does not correspond to increased R_{CoM}. An examination of the spreading of the flows at different volumes in fig. 6.12c suggests that the greater Rn at higher volumes results from greater spreading instead increased mobility of R_{CoM}. This results in a more spread, longer deposit even though the propagation of the centre of mass is similar (fig. 6.12). Spreading contributes the additional Rn, as also reported by Li et al. (2021) and Yang et al. (2011). Davies (1982) and Davies and McSaveney (1999) support that the long runouts of VDA/RAs is the result of spreading rather than the mobility of the centre of mass exceeding what is predicted by simple frictional models. However, it has to be highlighted that both the mobility of the centre of mass and the spreading of the mass contribute to the overall runouts to a different extent under different conditions in the current experiments. In fact, VDA/RA events have been suggested to have lower H_{CoM}/R_{CoM}, as well as H/R, to what is predicted by simple frictional models (Legros, 2002). While spreading contributes mass flow propagation it is not the only factor responsible for the high mobility of these phenomena.

The change in volume does not affect Vf during the propagation on the inclined plane and the deceleration part of phase 2, as also observed by Manzella and Labiouse (2009). The divergence in Vf occurs with the initiation of momentum transfer from the rear to the front, in the acceleration stage of phase 2. At this stage, greater volumes generate greater momentum transfer resulting in greater acceleration for a longer time as also reported by Manzella and Labiouse (2008). The greater Vf amplitude in phase 3 is due to greater pulses of momentum transfer between the avalanche front and the material behind it. This is the result of the greater potential energy with higher volume, which is also more concentrated as a thicker flow with a lower proportion of the material in contact with the substrate. With greater volumes, and thus particle numbers, collisional opportunities also

increase in constrained flows (Okura et al., 2000; Yang et al., 2011). Numerical modelling by Okura et al. (2000) supports that increased frequency of collisions could be a factor for longer runouts due to enhanced momentum transfer. This is proposed as the reason for the higher amplitude of the acceleration-deceleration pulses observed by Yang et al. (2011). These pulses propel the material at the front, in phases 2 and 3, enhanced spreading, and consequently R_n.

6.5.5 Slope inclination

Within the range of inclinations in these experiments (35° – 45°), higher inclinations lead to greater spreading (fig. 6.14b), but lower H_{CoM}/R_{CoM} and H/R (fig. 6.14a). This is primarily due to the interaction of the avalanches with the slope-break. The impact of path irregularities on granular avalanche propagation has been previously highlighted by researchers such as Heim (1932), Pudasaini et al. (2005) and Manzella et al. (2013).

At higher inclinations, the S_f is greater at low ψ (ψ=0.1 – 0.3) (fig. 6.14c). The energy conserved due to the lubrication of the base by the fines is transferred as momentum to the front of the flow resulting in increased spreading. However, there is also loss of momentum between the particles and the propagation surface, and energy is lost outside the avalanche system. The slope-break causes an increase in shear and loss of momentum at the time of the impact and interaction (Crosta et al., 2017). The effect of a geometric irregularity in the path of an avalanche on its mobility is a function of the size ratio between the irregularity itself and the size of particles in the granular mass (Heim, 1932; Friedmann et al., 2006; Manzella et al., 2013). Increased slope angles generate a greater irregularity in the path resulting in greater energy dissipation (Manzella et al., 2013). The collision with the slope-break causes disorganisation in the particle arrangement and momentum transfer, shifting the avalanche towards a more collisional regime (Manzella and Labiouse, 2013), as observed in close examination of the lateral videos of the experiments here described. However, the transfer of momentum decelerates the material at the back limiting the overall kinetic energy acting in the propagation direction. Therefore, the mobility of the centre of mass is reduced at higher inclinations with a steeper slope-break. This leads to higher H/R and H_{CoM}/R_{CoM} for greater inclinations (fig. 6.14a). The increase in spreading is offset by the lower R_{CoM}, and consequently runouts are lower. At lower inclinations, there is less disorganisation of the mass, fewer collisions and less energy

exchange. As earlier discussed, fig. 6.14b illustrates the contribution of spreading to runout is a function of the slope and the geometry of the path combined with the effect of bidispersity. At lower angles (less extreme path discontinuity), the flow regime is less collisional, and less momentum is transferred between the particles to cause the spreading. Consequently, spreading is less, and its contribution to the overall runout is less important, compared to the lubricating effect of bidispersity.

6.5.6 Size ratio between particles (Δ)

In experimental series E, where two granular materials with greater Δ are used, fines are more effective at lubricating the avalanche at lower ψ. At ψ_{CRf} avalanches with higher Δ achieve greater R_n (fig. 6.15a). However, at greater ψ values (ψ>0.25) the R_{nCoM} is lower in the experiments with higher Δ. This is the result of the smaller fine particles losing more energy at the slope-break, suffering greater deceleration in phase 2 due to the greater size ratio between the grains and the slope-break (Fan et al., 2016). Fine particles in sufficient quantities (ψ>0.25) can absorb the momentum of coarser particles making the kinetic energy transfer in phase 2 less efficient. It is likely that finer particles in mixtures with greater Δ are more efficient at limiting energy dissipation by reducing frictional surfaces at the base or more effectively encouraging rolling. However, in higher quantities, they inhibit mobility by acting as a sand-trap. Previous studies have proposed that the mobility-enhancing effect of bidispersity is intensified with increased Δ (Roche et al., 2006; Bartali et al., 2020; Hu et al., 2020). In the bidisperse experiments of Goujon et al. (2007) avalanches with higher Δ resulted in more spread deposits with lower thickness compared to equivalent single-size end-members. In the bidisperse experiments of Hu et al. (2020) greatest R and deposit lengths are exhibited by experiments with greater Δ. The value of ψ_{CR} is different in avalanches with different Δ in the current experiments. Duan et al. (2022) propose the existence of a correlation between the size of the particles in the avalanche and ψ_{CR}. However, a more systematic study is required to determine this relationship and the effect of Δ, as the results from the different studies are not consistent.

6.5.7 Scaling, granular flow regimes and kinetic sieving

Assessment of experimental scaling is essential in designing and evaluating the findings of granular avalanche experiments regarding their geomorphological and mechanical

relevance to the dynamics of VDA/RAs (Iverson, 2015). Other than geometric scaling parameters, mentioned in the methodology, dynamic scaling parameters refer to the ratio between forces within the body of a granular avalanche and describe the evolving dynamics of the system (Iverson, 2015). Dynamic scaling parameters are crucial to ensure the similarity in conditions between experiments and real events. However, this scaling aspect of experimental design is very frequently overlooked (Iverson, 2015). Nonetheless, since the perfect correspondence between physical experiments and real events is not possible, some distorted scale effects are inevitably introduced (Heller, 2011). The potential scale-dependence of the simulated conditions must be assessed and is thus discussed in the subsequent sections.

6.5.7.1 Scaling of analogue experiments

At the scale of these experiments, rolling motion at the base of the avalanche generates agitation and collisions between particles, leading to a collisional regime, as also described by Hu et al. (2021). The flow regime was initially qualitatively assessed in the current experiments through observation and the videos. The collisional and frictional regimes, introduced by Drake (1990, 1991), describe a difference in the behaviour of propagating granular avalanches. In a frictional regime, the majority of the propagation particles are engaged in persistent frictional contacts, which are responsible for the majority of momentum transfer. An avalanche under this regime is characterised by the majority of the material propagating as a coherent plug over a basal agitated zone. Plug behaviour implies material in a coherent state, lacking agitation and propagating experiencing insignificant shear stresses. In contrast, in the collisional regime, the majority of momentum transfer is due to frequent particle collisions in an agitated mass with a high granular temperature. Different regimes and resultant granular behaviour (i.e. particle interaction frequency, duration etc.) alter the energy dissipated by avalanches and their mobility (Cagnoli and Piersanti, 2015).

The Savage number (N_{Sa}) is the ratio between particle collision stress and the load on the bed due to the weight of particles and can be approximated as (Iverson, 1997; Iverson et al., 2004):

$$N_{Sa} \approx \frac{u^2 \delta^2}{gT^3} \tag{6.4}$$

where u is the maximum speed (ms^{-1}), δ is the typical grain diameter (m), g is the

gravitational acceleration (ms^{-2}) and T is the avalanche thickness. The typical grain diameter is characterised as the mean particle diameter D_{43} (Gu et al., 2016; Breard et al., 2020), calculated as the volume average mean diameter:

$$D_{43} = n_q d_q \tag{6.5}$$

where n_q is the mass fraction of a particle class q with diameter d_q. The N_{Sa} is a non-dimensional characterisation of the flow regime, differentiating between the frictional and collisional regime by quantifying the relative importance of inertial stresses over the total stresses in steady, gravity-driven flows with free upper surfaces (Savage, 1984; Hsu et al., 2014). When the N_{Sa} is larger than 0.1, the regime is collisional with significant collisional stresses (Iverson and Vallance, 2001; Hsu et al., 2014; Iverson, 2015). Greater N_{Sa} values imply increasing particle collisions. Conversely, when N_{Sa} is smaller than 0.1, the regime is frictional and friction-dominated (Savage and Hutter, 1989; Iverson and Vallance, 2001). The N_{Sa} quantifies this ratio independent of the scale of the avalanche (Iverson, 1997).

Two important factors for the N_{Sa} are the typical grain diameter δ and avalanche thickness T (equation 6.4). The flume tests of Cagnoli and Romano (2012) and Cagnoli and Piersanti (2015) suggest that changes in the mobility of small-scale granular avalanches triggered by grain size and volume changes are, in fact, due to the resultant variation of granular agitation and the N_{Sa}. The agitation and nature of particle interactions is a principal factor for energy dissipation and should be considered when interpreting such avalanches (Li et al., 2021). Indeed, avalanches in this study with different ψ (table 6.4) have variable δ and T, according to the proportion of each particle size species. For experimental series A, the N_{Sa} was calculated for their propagation on the horizontal plane after the slope-break. For the majority of the experiments, the N_{Sa} is above 0.1 (fig. 6.17a), confirming that the material propagated under a collisional regime which is not representative of VDA/RAs (table 6.4). For experimental series A, only experiments with ψ>0.80 result in N_{Sa} values in the frictional regime (fig. 6.17a).

The T component of the N_{Sa} equation is directly correlated to the number of particles in an avalanche (assuming equal δ). The system-to-grain size ratio proposed by Cabrera and Estrada (2021) is essentially a proxy for the number of particles in a granular system. The system-to-grain size ratio is here defined as the ratio of the volume occupied in the

Table 6.4: Experimental series A – Savage number, system-to-grain size ratio and information required for their calculation.

ψ	Characteristic diameter (δ)	Volume	Flow thickness (T)	System-to-grain size ratio	Savage number
0.00	1.3E-02	1.7E-02	6.0E-02	1.1E+04	7.7E-01
0.10	1.2E-02	1.6E-02	5.7E-02	1.4E+04	7.4E-01
0.15	1.1E-02	1.5E-02	5.4E-02	1.6E+04	7.8E-01
0.20	1.0E-02	1.5E-02	5.5E-02	1.9E+04	6.6E-01
0.25	9.8E-03	1.5E-02	5.1E-02	2.2E+04	7.4E-01
0.30	9.2E-03	1.4E-02	5.5E-02	2.6E+04	5.2E-01
0.35	8.6E-03	1.3E-02	5.1E-02	2.9E+04	5.7E-01
0.40	8.0E-03	1.2E-02	4.8E-02	3.2E+04	5.8E-01
0.50	6.8E-03	1.1E-02	4.5E-02	5.0E+04	5.1E-01
0.60	5.6E-03	1.2E-02	5.1E-02	1.0E+05	2.4E-01
0.70	4.4E-03	1.4E-02	5.1E-02	2.4E+05	1.5E-01
0.80	3.2E-03	1.4E-02	6.3E-02	6.4E+05	4.1E-02
0.90	2.0E-03	1.3E-02	6.5E-02	2.5E+06	1.5E-02
1.00	7.5E-04	1.3E-02	3.0E-02	4.5E+07	2.1E-02

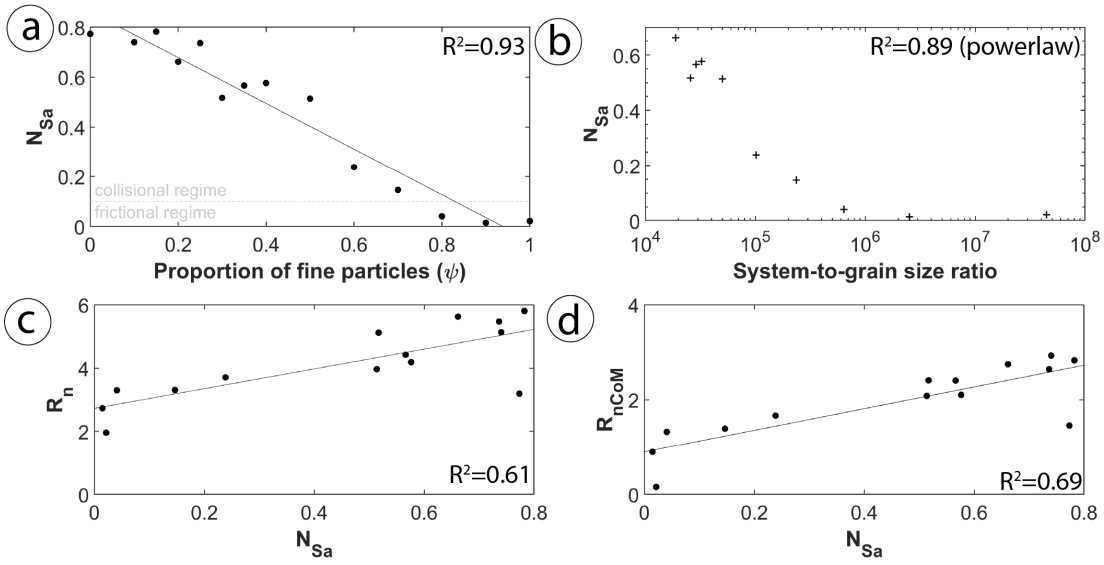

Figure 6.17: Scaling evaluation of experimental series **A** N_{Sa} as a function of ψ. **B** N_{Sa} as a function of the system-to-grain size ratio. **C** R_n as a function of N_{Sa}. ΔR_{nCoM} as a function of N_{Sa}.

mass by a single particle of mean diameter when assuming spherical particles arranged in simple cubic packing to the total volume of material:

$$\text{system} - \text{to} - \text{grain size ratio} = \frac{V}{4\sqrt{2}\left(\frac{\delta}{2}\right)^3} \tag{6.6}$$

The system-to-grain size ratio of the presented experiments is similar to the experiments previously mentioned (table 6.3). Li et al. (2021) support that larger grain sizes/smaller volumes (i.e., smaller system-to-grain size ratio) increase collisions, the granular temperature and the N_{Sa}. The findings of this study also support a negative correlation between the system-to-grain size ratio and the N_{Sa} in experimental series A (fig. 6.17b).

Li et al. (2021) find that increasing the volume and decreasing δ have the same effect since they both affect the system-to-grain size ratio. The findings of Cabrera and Estrada (2021) support that with sufficiently large system-to-grain-size ratios (expected in natural avalanches) the mobility and shear strength of granular column collapses is independent of grain-size distribution variations. As granular systems become larger, grain size effects weaken (Cabrera and Estrada, 2021). Consequently, small system behaviour can be biased by small system-to-grain size ratios and flow height, resulting in high N_{Sa} values and energy exchange dominated by collisions. Such conditions are unrepresentative of natural processes (Cabrera and Estrada, 2021; Li et al., 2021). With small numbers of particles, agitation is greater per unit of flow mass since agitation is able to propagate up from the base and agitate a higher proportion of the avalanche (Cagnoli and Romano, 2010, 2012). Li et al. (2021) observe that a reduction of δ or increase in volume leads to localisation and magnification of shear stress at the base of the avalanche, leaving the overriding material to travel as a plug with no agitation. This is also observed in numerical simulations of granular avalanches (e.g. Walton, 1993; Silbert et al., 2001). The N_{Sa} of the plug is zero, resulting in extremely low overall N_{Sa} values for such avalanches (Li et al., 2021).

Small system-to-grain size ratios can lead to behaviours unrepresentative of large-scale events due to the small number of particles involved in the experimental systems (grain size effect), rather than the grain-size composition and distribution (Cabrera and Estrada, 2019, 2021; Li et al., 2021). The increase in the R_n and R_{CoM} observed in avalanches from this study exhibit a correlation with the N_{Sa} (fig. 6.17c, d). The correlation suggests that the difference might be correlated to the alteration of the N_{Sa} and the collisional regime, instead of ψ being the exclusive factor.

Therefore, to achieve geomorphological and mechanical relevance experiments of VDA/RAs require scales which are large enough (number of particles/avalanche thickness) to permit a frictional regime behaviour (Iverson, 2015). High N_{Sa} values and the observation of collisional behaviour is very frequent in the reporting of lab-scale granular avalanche experiments. Li et al. (2021) calculate and report that N_{Sa} values of their experiments reflect a frictional regime for the majority of their experimental conditions. However, in the experiments of Cagnoli and Romano (2012), N_{Sa} is reported to have been larger than the threshold of 0.1. Lai et al. (2017), Bartali et al. (2020) and Duan et al. (2022) report their qualitative observation of collisional behaviour without further examining or

commenting on the implications of this behaviour to the comparison with natural events.

The estimated N_{Sa} values of natural VDA/RAs are typically much lower than 0.1 (data collected and presented in Appendix Table table 6.2 of Li et al. 2021). The granular temperature in VDA/RAs is much lower than hypothesised in the past. A uniform collisional regime does not occur in natural events and thus values of shear stresses are affected by the experimental scale, producing processes dissimilar to small-scale avalanches (Iverson et al, 2004). When N_{Sa} is high, grain collision stresses have a higher importance in the flow of the avalanche (Savage and Hutter, 1989). As highlighted by Duan et al. (2022), in a collisional regime the energy-transferring collisions and the expansion of the mass are enhanced. Therefore, the current experiments, as well as a large part of lab-scale granular avalanche experiments, occur in the collisional regime with shear stresses being principally generated by particle collisions rather than frictional contacts. As explained above, VDA/RAs are unlikely to adopt a collisional regime. Therefore, the flow regime, dynamics and shear stresses observed are scale-dependent.

6.5.7.2 Granular avalanche propagation processes comparison at different scales

As observed in the current experiments, in small free-surface avalanches composed of binary mixtures the finer particles percolate to the bottom through the coarse particles to generate size segregation. Increased mobility requires fine particles at the base of the flow, between coarse particles and the substrate. The segregation process is essential to permit bidispersity to enhance mobility. Dispersive pressure has been proposed as a mechanism potentially enabling size segregation in natural granular avalanches (Bagnold, 1954; Cruden and Hungr, 1986). However, this would require a density difference between different sizes which is not consistent with natural material (Legros, 2002). In the current experiments, the process that generates the segregation is kinetic sieving. This is the process where the granular mass dilates during the agitated motion with voids opening between the coarse particles for the finer ones to percolate through to the base due to gravity (Savage and Lun, 1988). Hu et al. (2021) propose that this process takes place throughout the body of a granular avalanche, leading to inverse grading with smaller particles located nearer to the base. They argue that similarly to bidisperse mixtures in lab experiments, kinetic sieving allows fine particles to migrate to the base and lubricate VDA/RAs. This is based on the idea, that was prevalent in the past, where VDA/RAs were

envisaged as rapid granular flows with their dynamics dominated by chaotic and energetic particle collisions (e.g. De Blasio, 2011). Accordingly, some researchers have suggested that VDA/RAs are efficient at sorting particles by size due to kinetic sieving (e.g. Savage and Lun 1988). This would lead to inverse grading observed across deposits (Middleton, 1976; Cruden and Hungr, 1986; Hungr and Evans, 2004; Dufresne, 2009). Although some studies do report grading at the deposit scale (e.g. Hewitt, 1998; Crosta et al., 2007), others observe the lack of it (e.g. Shreve, 1966; McSaveney, 1978; Schilirò et al., 2019). More recent work supports that grading is a bias introduced by the presence of a coarse carapace at the top of RA deposits and does not persist lower in their body (Dunning, 2006; Dunning and Armitage, 2011; Dufresne and Dunning, 2017). In contrast to the experiments, in natural VDA/RAs, the entirety of a granular mass is not as well-mixed or homogeneous. Grading is not generally observed in deposits and it is no longer believed that flows are dominated by chaotic particle collisions and high granular temperatures (e.g. Dunning, 2006; dufresne et al., 2016a; Paguican et al., 2021; Chapter 3, 4 and 5 of this thesis).

Schilirò et al. (2019) propose the existence of dimensional limits for kinetic sieving. They propose a threshold in flow velocity and particle number/flow thickness over which agitation at the base and body of the flow are not attainable. Above the critical thickness value and below a critical velocity a flow develops an agitated basal layer with the areas above travelling as a plug (frictional regime). Agitation throughout the material is essential for kinetic sieving, and in the lack of it, segregation is not possible. The hypothesis of bidispersity increasing mobility by acting to increase rotation and decreasing frictional areas at the base necessitates inverse grading. However, the low threshold velocity and high particle numbers required to allow the agitation and segregation are unrealistic and very far from the values for the velocities and the thickness at the scale of natural VDA/RAs as explained by Schilirò et al (2019). Therefore, sedimentological observations are in agreement with the lack of grading observed and offer support for the existence of the dimensional limit for agitation and kinetic sieving. This is an important observation in light of the presented experiments. Bidispersity is observed in the grain-size distribution of VDA/RAs, however, kinetic sieving is not capable of imposing segregation, which as the experiments suggest is vital for enhancing mobility. Additionally, an agitated basal layer composed of the fine particles would not be capable of supporting a rocky slab plug at the scale of VDA/RAs for realistic values of the coefficient of restitution and propagation angles of real events according to the force balance calculations of De

Blasio and Elverhøi (2008). This bidispersity mechanism can therefore be excluded as a friction-reducing mechanism at the scale of VDA/RAs.

Nonetheless, basal agitation and grading have been reported by authors in other granular flows including debris flows (Iverson, 2005; Conway et al., 2010), lahars (Major and Voight, 1986; Scott, 1988; Vallance, 2000; Saucedo et al., 2008), wet snow avalanches (Bartelt and McArdell, 2009), rockslides (Bertran, 2003) and pyroclastic flows (Calder et al., 2000; Iverson and Vallance, 2001). It is more likely that the enhanced mobility due to bidispersity is more applicable to these other specific types of geophysical events such as smaller-scale landslides and block-and-ash pyroclastic flows rather than VDA/RAs (Phillips et al., 2006; Schilirò et al., 2019).

6.5.7.3 Implications for volcanic debris/rock avalanches

Small-scale experiments are not capable of reproducing some of the processes enabled at the scale of natural geophysical flows (Iverson et al., 2004). Naturally, laboratory experiments cannot simulate fragmentation processes due to the low energies in the system as an example (Bowman et al., 2012; De Blasio and Crosta, 2014). Nonetheless, the numerical modelling of Rait and Bowman (2016) supports that kinetic energy contributed to the flow through dynamic fragmentation is likely to be quickly dissipated and unlikely to be solely responsible for the enhanced mobility exhibited by geophysical flows. Likewise, the seismicity of the event cannot be simulated (Davies and McSaveney, 1999). Even so, if fluid effects are negligible, major features of VDA/RAs can still be reproduced by analogue experiments with appropriate scaling since their dynamics are principally controlled by the internal and basal friction coefficients and the interaction of the avalanche with its path (Davies and McSaveney, 1999; Iverson and Denlinger, 2001; Iverson et al., 2004; Yang et al., 2011; Dufresne, 2012). However, scepticism regarding the effectiveness of small-scale experiments centres around their being too brief, idealised and restricted by initial conditions and artificial boundaries to represent the vast complexities of natural geophysical processes (e.g. Baker, 1996). Iverson (2015) caution that the geomorphological relevance of small-scale granular flow experiments carried out in the past decades (e.g. Iverson et al., 2004; Pudasaini and Hutter, 2007; Mangeney et al., 2010) should be critically evaluated, in terms of scaling and interpretation of the experimental processes in comparison to natural processes, before being extended to direct comparison with natural phenomena. Direct

comparison can lead to long-established misperceptions in landslide science (Iverson, 2015).

To highlight the distorted scale effects, the '*Scheidegger*' plot (H/R plotted against volume) of all the experimental avalanches is compared to a VDA/RA inventory (fig. 6.18) (Hürlimann and Ledesma, 2003; van Wyk de Vries and Delcamp, 2015). The relationship between the H/R and volume can be reasonably described by a power law (Scheidegger, 1973). Regression illustrates a relationship; albeit with wide dispersion increasing the degree of uncertainty ($0.36 < R^2 < 0.63$, Shea and van Wyk de Vries 2008). Data dispersion, partially mitigated by the log scale, constitutes the comparison of such trends inherently problematic. Nonetheless, the findings from the current experiments plotted in the same area in fig. 6.18 suggest that the avalanches do not follow the same relationship. They produce H/R values equivalent to some events, but with considerably smaller volumes, suggesting that the processes involved are scale-dependent and non-equivalent.

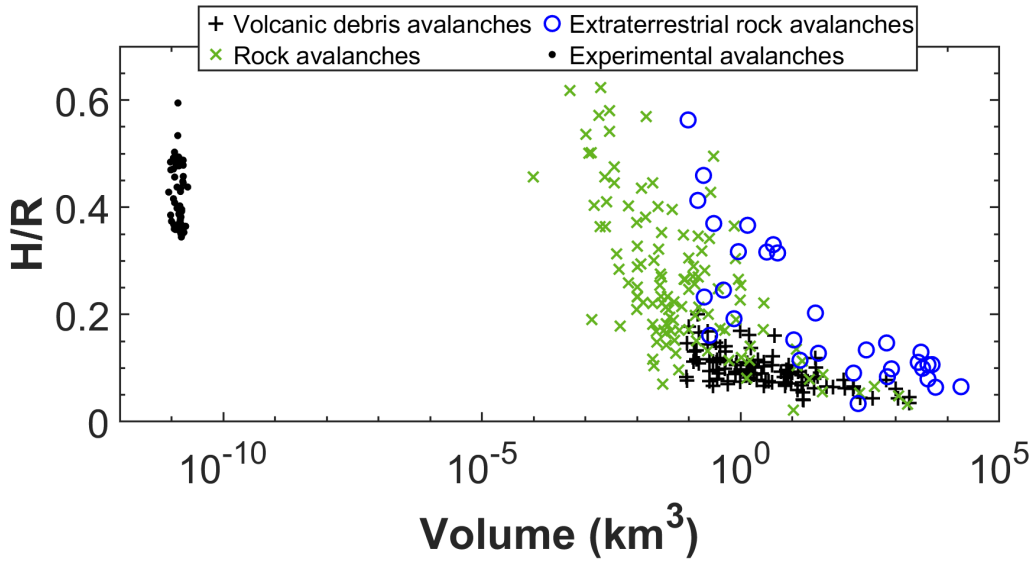

Figure 6.18: Apparent coefficient of friction (H/R) versus volume for volcanic debris avalanches, rock avalanches and extraterrestrial rock avalanches (modified from van Wyk de Vries and Delcamp (2015) and Hürlimann and Ledesma (2003) in comparison to the experimental avalanches of the current study.

The findings of this study suggest that the presence of collisional regime and kinetic sieving in the experiments are fundamental to create the necessary conditions for the hypothesis that bidispersity can lead to higher runout by facilitating the creation of an agitated basal layer of fine material supporting an overriding plug of inertial material. However, the collisional regime and the kinetic sieving are not observed in VDA/RAs

since deposits are not graded (see section 5.4 as an example) making this hypothesis not plausible for real events. This highlights that analogue experiments have the potential to contribute to the understanding of natural granular avalanches for example allowing the identification of processes that are scale dependent. However, caution and a rigorous approach are crucial in their design and the interpretation of their results (Iverson, 2015). Geomorphological and mechanical relevance should not be assumed on the basis of superficial or morphometric similarity, as it does not necessarily imply similarity in processes as exemplified here (Iverson, 2015). Dynamic scaling analysis must become a standard procedure in designing and interpreting analogue granular avalanche experiments to ensure the effectiveness of the experiments in examining the desired processes and dynamics.

The hypothesis of a basal low friction zone, with a bidisperse grain-size distribution supporting the weight of a plug above it, is also disputed by the observation of shear zones throughout the body of VDA/RA deposits at various depths (e.g. Roverato et al., 2015; Dufresne et al., 2016a; Dufresne and Dunning, 2017; Wang et al., 2019; Hughes et al., 2020; Chapter 4 of this thesis). The shear zones confirm that shear is not exclusively accommodated at the base (Dufresne and Dunning, 2017). Such shear zones are also characterised by bidisperse distributions according to the observations of Dufresne and Dunning (2017). Therefore, their bidisperse grain-size distribution could potentially constitute a more efficient network for the accommodation of shear stress. According to the multislide plug flow model (Roverato et al., 2015; Paguican et al., 2021), shear zones with bidisperse grain sizes can efficiently accommodate shear within the body of the avalanche. Indeed, frictionites have been reported within shear zones in the body of the deposit at Köfels rockslide supporting that they represent areas of shear concentration (Dufresne and Dunning, 2017). Therefore, it is plausible that at the scale of VDA/RAs with large volumes, the multi-slide plug flow could potentially accommodate multiple levels of plugs supported above shear zones. In this case, agitation and a segregation mechanism are not required as bidispersity can be generated in situ. These shear zones are similar to the distributed stress fluidisation model presented in Chapter 5 - section 5.5.4, however they are more stable and continuously active during the propagation. Both these models are compatible with the shear zone observations. Experimental findings suggest that bidisperse distributions are generated with increased shear or confining pressures (Iverson et al., 1996; Caballero et al., 2014) either by fine particles generated through shearing or the preservation of larger survivor clasts through the preferential

comminution of smaller particles around them (Dufresne and Dunning, 2017; Chapter 3 of this thesis). Shear zones potentially focus shear stresses and act as corridors that localise shear accommodation around more coherent domains that are less exposed to shear and thus lacking agitation dissipate less energy in particle interactions (Crosta et al., 2007; Roverato et al., 2015; Li et al., 2021; Paguican et al., 2021). Therefore, only a small proportion of the propagating mass is engaged in high energy dissipation motion (Li et al., 2021). The analogue experiments of Li et al. (2021) and numerical simulations of Lai et al. (2017) support the assumption that the material above such areas of shear localisation can be transported as a plug accommodating lower shear. If the bidisperse grain-size distribution can inhibit frictional energy losses, more energy would be available for kinetic energy and the propagation of the mass, effectively reducing the apparent friction angle. Most importantly, this theory is consistent with the geomorphic and sedimentological features of deposits. The network of shear zones required for the multislide plug flow model is also a feature observed in the field (Roverato et al., 2015; Paguican et al., 2021). The suggested bidispersity of the shear zones is identified in the field (Dufresne and Dunning, 2017); while areas of preserved stratigraphy between the shear zones are a diagnostic feature of VDA/RA deposits (Shreve, 1968; Siebert, 1984; Glicken, 1996; Voight et al., 2002; Dufresne et al., 2021b; Chapter 4 of this thesis). However, the experiments presented here only examine the reduction of frictional losses and enhanced mobility under specific conditions. The multiple plug flow hypothesis aided by bidisperse grain-size distribution requires a more detailed and systematic evaluation.

6.6 Conclusions

Analogue granular flow experiments were carried out in a scaled setup to investigate the effects of bidispersity on granular avalanche propagation processes and dynamics. Analysis of the findings leads to the following conclusions:

- Bidispersity has the potential to affect energy dissipation in granular avalanches and increase their runout, at the scale and under the considered experimental conditions. It was found that low ψ values between ψ=0.05 and ψ=0.15 (depending on experimental conditions) are most efficient at enhancing mobility. Mobility refers to the frontal runout and the propagation of the centre of mass. At higher ψ values, up to ψ=0.80, the mobility is still greater than ψ=0.00. The mobility is more sensitive

to ψ when not all pore spaces in the mass are filled by fine particles.

- The effect of bidispersity is altered according to the inclination of the slope before the horizontal depositional surface. However, it is not affected by the volume of the material. Spreading is also affected by the inclination of the slope before the horizontal depositional surface and the angle of the slope-break. Increases in runout with increased volumes are the result of enhanced spreading. Runout is affected by both the displacement of the centre of mass as well as the spreading of the mass.

- A slope-break generates disorganisation of the mass, loss of momentum, and increase of collisions that transfer momentum from the back of the avalanche to the front. Greater slope angles generate a more effective slope-break that causes more disorganisation and therefore encourages momentum transfer and spreading in the mass.

- At low ψ, increased Δ is more effective at increasing mobility, resulting in longer runouts. However, the finer particles lose more energy at the slope-break due to the greater size ratio between them and the path irregularity. When present at higher quantities their earlier deposition acts as a sand-trap for the coarser particles and reduces runout.

- The increase in mobility due to bidispersity is the effect of fines at the base of the flow, between coarse particles and the propagation surface, limiting frictional surfaces and encouraging rolling. Due to the observation of this process in small-scale experiments, several studies have proposed this as a mechanism for the enhanced mobility of VDA/RAs. Examination of the runout-enhancing mechanisms in this study suggests that this process requires size segregation by kinetic sieving. The occurrence of this process in small-scale experiments is scale-dependent and does not occur at the scale of natural VDA/RAs. This is evident by the lack of grading in their deposits. Therefore, bidispersity is unlikely to enhance the mobility of VDA/RAs by providing a more efficient shearing arrangement at their base. This effect is caused by scale-dependent processes due to the collisional regime of small-scale avalanches in the lab, which is different from the largely frictional regime of VDA/RAs.

- This study highlights that dynamic scaling analysis must become a standard procedure in designing and interpreting analogue granular avalanche experiments to ensure the effectiveness of the experiments in examining the desired processes and

dynamics in studies with the aim of constraining the mechanisms behind the long runout of VDA/RAs and assess the hazard they pose.

6.7 List of abbreviations

Abbreviation	Definition
R	horizontal runout of the front of the avalanche from the front of the material pre-release
R_{hCoM}	propagation of the centre of mass on the horizontal plane
R_{CoM}	horizontal propagation distance of the centre of mass
R_f	frontal runout on the horizontal plane
R_n	normalised frontal runout on the horizontal plane
R_{nCoM}	normalised propagation of the centre of mass on the horizontal plane
ψ	proportion of fine particles
ψ_{CRf}	critical proportion of fine particles for maximum frontal runout
ψ_{CRcom}	critical proportion of fines for maximum propagation of the centre of mass
Vf	frontal velocity
H	maximum fall height
H_{CoM}	vertical difference between the location of the centre of mass in the box and in the final deposit
V	volume
h*	$= V^{1/3}$
S_n	total spreading
S_f	frontal spreading
L	deposit length
Δ	size ratio between coarse and fine particles
V_0	frontal velocity at the slope-break
V_{MIN}	minimum frontal velocity in phase 2
V_{MAX}	maximum frontal velocity in phase 2
N_{Sa}	Savage number

Abbreviation	Definition
δ	typical grain diameter (m)
g	gravitational acceleration (ms^{-2})
T	avalanche thickness

Chapter 7

Conclusion

Volcanic debris avalanches (VDAs) are large mass movements entraining large volumes of material and attaining long runouts. The hazard they pose to communities proximal to volcanoes requires a better understanding of their propagation processes. Theoretical and numerical models are currently unable to account for their runout while being consistent with field observations of the deposits of all events. The mechanisms enabling long runouts remain controversial and unresolved, demanding an evaluation of theoretical models in comparison to real events and their deposits. This thesis examines the factors that enable VDA long runouts, linking field observations with the findings of experimental and numerical studies and theories to provide a more robust understanding of their dynamics. The main methods and results of the thesis are summarised in fig. 7.1a.

More specifically, the first objective towards this aim, addressed in Chapter 3, was to assess the role of water as a factor for long runouts. A sedimentological comparison of VDAs and lahars, using data compiled from previous studies published in the literature or provided by the authors of the original studies, evaluates water as a potential fluidising medium. A systematic comparison was carried out using statistical descriptor metrics for the two mass flow types. The differences in the original material involved in each, and their evolution during propagation, are explored. Previous studies have carried out statistical analysis to characterise individual deposits, and the sedimentological differences between the two mass flows have been addressed. However, this is the first systematic comparison study including multiple events with the aim of assessing the potential role of water in the propagation dynamics of VDAs, by evaluating the propagation mechanisms of both VDAs and lahars.

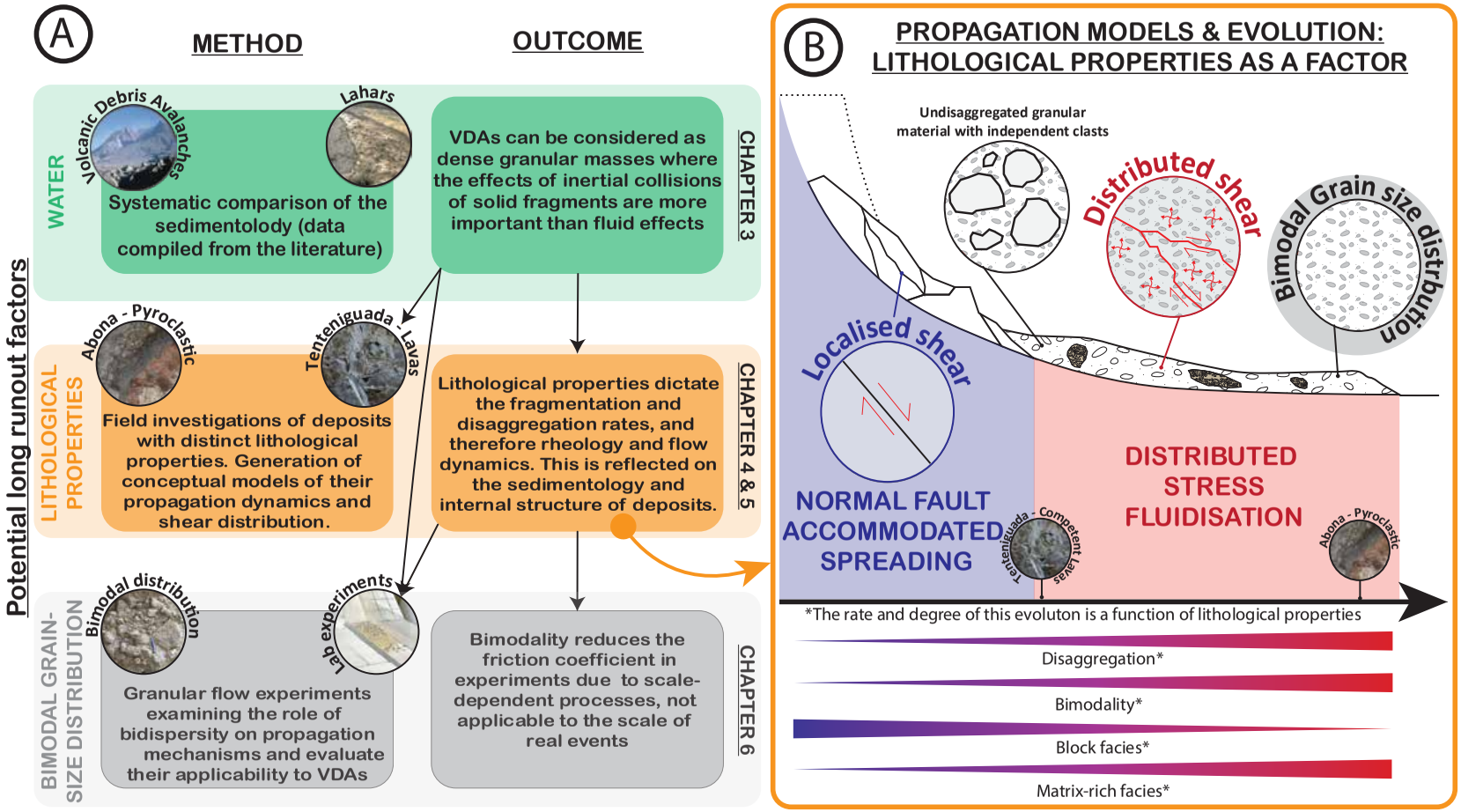

Figure 7.1: **A**. Potential runout-enhancing mechanisms examined, methods and outcomes of this thesis. The sequence and connections between chapters are illustrated. **B**. Propagation mechanisms and stress accommodation in coherent material such as undisaggregated lavas as opposed to disaggregated granular material. The rate and degree to which this disaggregation occurs are a function of lithological properties as highlighted by the comparison between the Abona and Tenteniguada VDAs. Abona, composed of less competent pyroclastic material disaggregated and evolved into a granular flow with distributed shear. Tenteniguada, composed of competent lavas, preserved a large proportion of blocks resulting in localised shear.

Subsequently, the influence of lithological properties on the propagation mechanism and stress distribution in VDAs is explored. The method of examining the internal structure and sedimentology of VDA/RA deposits to obtain information regarding their propagation dynamics and stress accommodation is an established technique and a valuable tool which has been applied to individual deposits and has contributed to the understanding of these events. However, Chapters 4 and 5 examine lithological properties as a factor for VDA dynamics of two specific deposits with distinct lithologies, providing evidence which allows the generation of conceptual models for their propagation (fig. 7.1b). Their comparison has provided new evidence for lithological properties as a factor for the propagation dynamics and stress distribution in mass flows. The Abona VDA deposit (VDAD) offers field evidence for distributed stress fluidisation, while a new mode of propagation and stress accommodation is described for the fault-accommodated spreading of the Tenteniguada VDA. The induration of the deposits has hindered the study of VDA/rock avalanche (RA) sedimentology in the past. A photogrammetry sampling analysis technique is proposed in Chapter 5, which allows the examination of such indurated deposits.

Finally, bidispersity is evaluated as a factor for long runouts through granular flow experiments, and their scaling is evaluated. Through these experiments, the potential of analogue lab experiments as a method for the study of VDAs is also examined in Chapter 6. Lab-scale granular flow experiments are often used for the examination of VDA/RA dynamics. However, the scaling of the forces (dynamic scaling) involved in these events is often overlooked and not addressed in the design or interpretation of these experiments. The dynamic scaling requirements for analogue granular avalanche experiments are evaluated here. The criteria for the dynamic scaling are outlined here so that it is possible to assess experimental granular flow conditions in comparison to geophysical processes in the field.

The findings are summarised below, corresponding to the outlined objectives :

1. The systematic comparison presented here allows the evaluation of water as a factor in mass flow propagation. The findings support that a decrease in the median grain size of lahars is the result of debulking and progressive deposition of the coarsest particles enabled by the role of water as a transporting medium. In contrast,

particle to particle interactions are the principal momentum exchange mechanism in VDAs. During such particle interactions, fracturing favours the comminution of finer particles due to a lower energy requirement. This drives an evolution towards a bidisperse grain-size distribution. This bidispersity is linked to, and further evaluated as a potential mobility-enhancing property in Chapter 6. The findings suggest that VDAs can be considered dense granular masses where the effects of inertial interactions of solid fragments are more important than fluid effects. Even though it is well established that VDAs are clearly differentiated in their dynamics from saturated flows, the potential role of small quantities of water evaluated here is important for subsequent work and to better understand the dynamics of these flows. The evaluation of the fluidising medium suggests that such a mechanism is not likely to be an important factor in VDA propagation. Therefore, in the subsequent chapters, VDAs are considered as idealised granular flows where grain interactions are the principal process responsible for energy dissipation, with negligible fluid effects (fig. 7.1).

2. The study of two VDADs with different lithological characteristics examines VDA dynamics, kinematics and stress distribution and how they reflect in VDADs. The field studies presented in Chapters 4 and 5 allowed the evaluation of the lithological properties of the material involved in VDAs as a factor for their dynamics and propagation processes. The Tenteniguada VDAD is principally composed of competent lava lithologies. Disaggregation is low, with widespread preservation of the original structure, although displaced by brittle deformation. The Tenteniguada VDAD has provided evidence for a new mode of propagation for undisaggregated mass flows composed of competent material. This process is described in Chapter 4 and referred to as brittle fault-accommodated spreading. In contrast, the majority of Abona is composed of weak pyroclastic products. It exhibits high disaggregation and fracturing, constituting the mass granular and enabling fluidised spreading with distributed shear. Both propagation mechanisms are illustrated and summarised in fig. 7.1 b. The study of the Abona VDAD provides field evidence for mass flow propagation under distributed stress in ephemeral, rearranging shear networks, which had previously only been proposed theoretically. The material properties of the two VDAs constitute them end-members that highlight the importance of lithological properties in VDA dynamics. They propagated with distinct rheology

and dynamics and produced different deposits, owing to material properties. The conceptual models of their propagation suggest that VDA mobility does not require auxiliary friction-reducing mechanisms. It is suggested that purely gravity-driven avalanches can evolve into flows due to increasing momentum and kinetic energy from their initial potential energy. However, other mechanisms can also enable long runouts, as exemplified by the runout of the Tenteniguada VDA, which achieved a long runout without evolving into a flow. These findings demonstrate the potential of field studies for providing evidence for mass flow kinematics and stress accommodation through the examination of the sedimentology and internal structure of their deposits. The findings support that lithological properties are a factor for VDA dynamics and propagation processes which is reflected in their internal structure and sedimentology.

3. A methodology is proposed in Chapter 5 for the clast-size analysis of VDADs and other indurated deposits. This methodology proposes a novel combination of existing techniques and sample strategies. By utilising structure-from-motion photogrammetry at the outcrop scale, the coarsest particles with diameters on the scale of >1 m are included in the sample. Photogrammetry merges information from multiple photographs generating large-area samples at a high resolution. Grain-size analysis on samples of this scale is a novel proposal addressing the under-representation of the coarse component of the grain-size distribution in VDA/RA deposit sedimentological analysis, a known weakness of conventional sieving methodologies. Previous photographic techniques utilise single photographs, which cannot include large areas while preserving a high-resolution representation of all particles. To cover the finer component of the grain-size distribution, smaller sample windows were sampled at a greater resolution in the proposed methodology, allowing better representation of up to sub-millimetre particles. To achieve statistical validity despite the heterogeneity of VDADs, smaller sample windows are carried out in multiple locations in the same outcrop where necessary. Combining these two scales is also a novel component of the methodology proposed here. Although photographic grain-size analysis is indeed an established technique, it has previously been applied at specific scales separately, e.g. at the thin section scale or at the fluvial gravel deposit scale. Additionally, statistical error and uncertainty margin calculation are included in this technique. This tool has allowed the study of the Abona VDA, which would

not have been possible with conventional sieving methodologies, and therefore, offers the potential of broadening the number of events that can be studied. This could increase the capacity for collecting field evidence and to further understand VDA/RAs and the hazards these complex and hazardous phenomena pose.

4. In Chapter 6, a series of analogue granular avalanche experiments explore the potential of bimodality as a factor for the long runout of VDA/RAs. The bidispersity observed in VDAD/RA deposits has been proposed as a potential factor for the long runout of these mass flows and supported with small-scale analogue experiments in previous studies. The process responsible for the long runouts in lab experiments is described as the percolation of fine particles to the base of the avalanche, through kinetic sieving, where they reduce frictional contact areas between the avalanche and the substrate, while also encouraging rolling (over frictional sliding) which is a more energy efficient mode of propagation. This is a process that has been described in previous work. Nonetheless, the flow regime and dynamics required to enable these processes (i.e. kinetic sieving, agitated flow regime) and their applicability in the scale of VDA/RAs are here specifically addressed. The findings suggest that the processes generating increased runout in small-scale avalanches are scale-dependent and not representative of VDA/RAs granular behaviour and propagation dynamics. Therefore, bidispersity is unlikely to enhance the mobility of VDA/RAs employing the same mechanisms of basal lubrication that are enabled at the lab scale.

5. The examination of Chapter 6 proposes geometric and dynamic scaling requirements for designing and interpreting analogue granular avalanche experiments to ensure the effectiveness of the experiments in examining the desired processes and dynamics. Although vital for the effectiveness of analogue experiments, dynamic scaling is often overlooked in experimental studies. In fact, it was not directly assessed in many of the studies proposing bimodality as a runout-enhancing factor. The scaling assessment guidelines given here represent an important contribution to studies of analogue granular flows as they provide an assessment framework for the scaling of analogue experiments relative to field dynamics and processes and will constitute a reference for future granular flow studies examining mass flow dynamics.

In summary, this work provides constraints for the development of theoretical, numerical and analogue models through the description of VDA dynamics as they are reflected in

their internal structure and sedimentology and from analogue granular flow experiments. The findings provide valuable observations for future theoretical and numerical models to be evaluated against and calibrated with. In conclusion, this thesis brings several important contributions to the field. It reviews and compares data from the literature, field and laboratory studies, it critically analyses limitations and constraints of currently used methods to study VDAs and RAs and develops innovative methods and frameworks for the analysis of field and laboratory data that address and overcome those limitations. This allows the acquisition of new and reliable data that could set the ground for a renewed and in-depth understanding of these complex hazardous phenomena.

Chapter 8

Outlook for future work

Understanding the dynamics of volcanic debris avalanches (VDAs) is fundamental for the assessment of the hazard they pose to communities close to volcanoes. The same applies to rock avalanches (RAs) in tectonically active mountainous regions. This work of this thesis illustrates the effectiveness of coupling field examinations and physical experiments in understanding such dynamics and highlights the importance of numerical modelling in the future advancement of our understanding of the physical processes involved and hazard assessment capabilities. Based on the findings of this thesis dry granular avalanche dynamics have to be studied with consideration for the particular properties of VDAs such as their large volume, material heterogeneity internally, but also between different events, and the properties of the material such as the weakness of pyroclastic products and hydrothermally altered material within a collapsed flank. Deposit interpretations regarding the dynamics, kinematics and stress distribution during propagation need to guide, constrain, and validate numerical and analogue modelling and the development of conceptual models and theories for the dynamics of VDAs/RAs.

Numerical simulations are a potent tool for understanding the mechanisms and dynamics of VDA/RAs as well as assessing the hazard in areas at risk. Different models such as discrete element method modelling, or continuum mechanics models can be most appropriate depending on the application and process under study. However, none of the models currently encompass the vast complexity of VDAs from their initiation to their deposition, and only a few events have been modelled in detail with numerical methods (Procter et al., 2021; Roverato and Dufresne, 2021). The majority of numerical modelling attempts currently focus on understanding individual processes such as granular avalanche particle

interactions models (e.g. Okura et al., 2000; Linares-Guerrero et al., 2007; Cabrera and Estrada, 2021; Hu et al., 2021), granular mass movement dynamics (e.g. Thompson et al., 2009, 2010; Rait and Bowman, 2016; Lai et al., 2017) or avalanche-substrate interactions (e.g. Crosta et al., 2009, 2017). Exploring individual processes and the factors affecting them is a crucial prerequirement for the simulation of complex VDA/RA events. However, the aim is to increase the overall complexity of numerical models by parameterising and incorporating individual physical properties (Procter et al., 2021). The process examination presented in this thesis contributes towards more comprehensive models in the future, able to incorporate more aspects of VDADs for more holistic simulations.

Analogue experimental studies are also valuable for studying specific mechanisms and calibrating numerical models of physical processes. For example, the granular temperature attained by granular avalanches under different conditions, such as pressure from an overlying mass, would be instrumental in understanding the behaviour of granular masses at the scale of real events. However, as the findings of this research suggest, the evaluation of experimental planning in terms of geometric and dynamic scaling is essential for the correct interpretation of experimental findings in terms of their relation and applicability to large-scale events.

Analogue and numerical models need to be informed, constrained and validated by field observations and their interpretation, such as the vertical and longitudinal distribution of sedimentological and structural features, and the dynamics that they imply. Therefore, it is necessary that more events are studied to generate well-constrained lithological and propagation properties. The methodology here proposed for the examination of indurated deposits could be applied to more case studies in order to examine their distinct dynamics, evaluate the factors that dictated them and improve the understanding of VDA/RA propagation. This methodology would be even more effective if it is further developed to include smaller particle sizes and cover the entire size distribution. With the current limitations, the methodology cannot consider the clay content or processes that involve particles smaller than sand. An addition of samples from thin sections (e.g. Bernard and van Wyk de Vries 2017) or polished slabs (e.g. Ferraro et al., 2018) could allow the analysis of smaller particles. However, the challenge, in this case, would be the statistical validity of these samples as they would represent very small areas of deposits which is very heterogeneous. Nonetheless, strategic sampling and a large sample number might

reduce the uncertainties to acceptable levels.

A systematic comparison of the properties and the deposits of VDAs and RAs might also allow new insight into material properties as a factor for the dynamics of large avalanches. This is highlighted in the current thesis by the comparison of the lithologies involved in the Tenteniguada and Abona VDAs and the divergence in their dynamics and distribution of stress accommodation. Thus, differences in initial conditions and material properties such as the amount of unconsolidated material, percentage of finer material, steepness of volcanic terrain, water content and the presence of hydrothermally altered minerals in volcanic environments have all been identified as potential factors contributing to a potential divergence in mobility (Ui, 1983; Hayashi and Self, 1992; Hürlimann et al., 1999; Robinson et al., 2015). These factors should be systematically compared to assess their weight as a factor for the behaviour of VDA/RAs. The Campo di Giove RA (Italy) (Di Luzio et al., 2004; Fasani et al., 2011), for example, presents a valuable case study opportunity which has not been taken yet. The RA is a Quaternary catastrophic rock slope failure related to the intense uplift of the central Apennines (Di Luzio et al., 2004; Fasani et al., 2011) emplacing an L-shaped deposit due to channelisation (Di Luzio et al., 2004). Its evaluation would allow the assessment of the material and the behaviour of the avalanche, as well as a better assessment of the hazard to communities in tectonically active mountainous regions, such as the Himalayas today. Geotechnical characterisation (e.g. del Potro and Hürlimann, 2008) of material in different deposits evaluated in association with their runout and dynamics might also be beneficial in examining the impact of material properties, but also as a potential quantitative input in propagation models.

Ultimately, being able to add to the hazard assessment of potential volcanic sector collapses with models with more constraints regarding the propagation mechanisms and runout of VDAs would be an important contribution. Although the complexity of these events makes the modelling of entire events challenging, providing accurate hazard assessment scenarios is essential (Procter et al., 2021). For example, the potential for VDAs from the flanks of Taranaki volcano (New Zealand) has been considered as it is a stratovolcano with a history of VDAs (Zernack et al., 2012; Cronin et al., 2021; Mead et al., 2022). Being able to assess the hazard of future events as accurately as possible would contribute in mitigating potential economic and life losses in the region. A flank instability has been identified also on the flanks of Pacaya volcano (Guatemala) (Gonzalez-Santana and Wauthier, 2021).

Assessing the hazard from a potential sector collapse VDA could be more accurate if the properties of the material were quantified, enabling the propagation mechanisms they would initiate to be part of a propagation model and simulation. Similarly, in tectonically active mountainous regions, such as the Himalayas better constrained models of RA propagation would allow more effective hazard assessment. Targeted studies with structure, material properties and potential propagation mechanisms and stress accommodation taken into consideration to assess the potential runout and hazard is currently not attainable, but further study of VDA/RAs with different approaches could allow that in the future.

References

Abele, G., 1974. Bergstürze in den Alpen: ihre Verbreitung, Morphologie und Folgeerscheinunge. Wissenschaftliche Vereinshefte.

Ahmadipur, A., Qiu, T., Sheikh, B., 2019. Investigation of basal friction effects on impact force from a granular sliding mass to a rigid obstruction. Landslides 1089–1105. https://doi.org/10.1007/s10346-019-01156-0

Alidibirov, M., Dingwell, D.B., 1996. Magma fragmentation by rapid decompression. Nature 380, 146–148.

Alloway, B., Mc Comb, P., Neall, V., Vucetich, C., Gibb, J., Sherburn, S., Stirling, M., 2005. Stratigraphy, age, and correlation of voluminous debris-avalanche events from an ancestral Egmont Volcano: Implications for coastal plain construction and regional hazard assessment. J. R. Soc. New Zeal. 35, 229–267. https://doi.org/10.1080/03014223.2005.9517782

Anthony, J.L., Marone, C., 2005. Influence of particle characteristics on granular friction. J. Geophys. Res. Solid Earth 110.

Armanini, A., Capart, H., Fraccarollo, L., Larcher, M., 2005. Rheological stratification in experimental free-surface flows of granular-liquid mixtures. J. Fluid Mech. 532, 269–319. https://doi.org/10.1017/S0022112005004283

Attal, M., Lavé, J., 2006. Changes of bedload characteristics along the Marsyandi River (central Nepal): Implications for understanding hillslope sediment supply, sediment load evolution along fluvial networks, and denudation in active orogenic belts. Spec. Pap. Geol. Soc. Am. 398, 143–171. https://doi.org/10.1130/2006.2398(09)

Bagnold, R.A., 1954. Experiments on a gravity-free dispersion of large solid spheres in a Newtonian fluid under shear. Proc. R. Soc. London. Ser. A. Math. Phys. Sci. 225, 49–63. https://doi.org/10.1098/rspa.1954.0186

Bagnold, R.A., 1954. Experiments on a gravity-free dispersion of large solid spheres in a Newtonian fluid under shear. Proc. R. Soc. London. Ser. A. Math. Phys. Sci. 225, 49–63. https://doi.org/10.1098/rspa.1954.0186

Baker, V.R., 1996. Hypotheses and geomorphological reasoning, in: Rhoads, B.L., Thorn, C.E. (Eds.), The Scientific Nature of Geomorphology. Wiley, New York, pp. 57–85.

Balcells, R., Barrera, J., Gómez, J., 1990. Mapa Geológico de España a escala 1: 25,000 Gran Canaria, Maps 1109 II (Telde) and 1109 III (San Bartolomé de Tirajana).

Banks, N.G., Hoblitt, R.P., 1981. Summary of temperature studies on1980 deposits, in: Lipman, P.W., D.R., M. (Eds.), The 1980eruptions of Mount St. Helens. USGS, Washington, DC, pp. 295–314.

Banton, J., Villard, P., Jongmans, D., Scavia, C., 2009. Two-dimensional discrete element models of debris avalanches: Parameterization and the reproducibility of experimental results. J. Geophys. Res. Earth Surf. 114, 1–15. https://doi.org/10.1029/2008JF001161

Bartali, R., Rodríguez Liñán, G.M., Torres-Cisneros, L.A., Pérez-Ángel, G., Nahmad-Molinari, Y., 2020. Runout transition and clustering instability observed in binary-mixture avalanche deposits. Granul. Matter 22. https://doi.org/10.1007/s10035-019-0989-0

Bartali, R., Sarocchi, D., Nahmad-Molinari, Y., 2015. Stick-slip motion and high speed ejecta in granular avalanches detected through a multi-sensors flume. Eng. Geol. 195, 248–257. https://doi.org/10.1016/j.enggeo.2015.06.019

Bartelt, P., McArdell, B.W., 2009. Instruments and methods granulometric investigations of snow avalanches. J. Glaciol. 55, 829–833. https://doi.org/10.3189/002214309790152384

Bates, R.L., Jackson, J.A., 1984. Dictionary of geological terms. Anchor Books.

Beddingfield, C.B., Beyer, R.A., Singer, K.N., McKinnon, W.B., Runyon, K., Grundy, W., Stern, S.A., Bray, V., Dhingra, R., Moore, J.M., Ennico, K., Olkin, C.B., Schenk, P., Spencer, J.R., Weaver, H.A., Young, L.A., 2020. Landslides on Charon. Icarus 335, 1–8. https://doi.org/10.1016/j.icarus.2019.07.017

Belousov, A., Belousova, M., Voight, B., 1999. Multiple edifice failures, debris avalanches and associated eruptions in the Holocene history of Shiveluch volcano, Kamchatka, Russia. Bull. Volcanol. 61, 324–342. https://doi.org/10.1007/s004450050300

Belousov, A., Voight, B., Belousova, M., 2007. Directed blasts and blast-generated pyroclastic density currents: a comparison of the Bezymianny 1956, Mount St Helens 1980, and Soufrière Hills, Montserrat 1997 eruptions and deposits. Bull. Volcanol. 69, 701–740.

Belousov, A., 1995. The Shiveluch volcanic eruption of 12 November 1964—explosive eruption provoked by failure of the edifice. J. Volcanol. Geotherm. Res. 66, 357–365.

Berends, S.H., Eggenhuisen, J.T., Pohl, F., 2018. Grain size analysis by thin section images of Permian deep-marine sediments from the Fort Brown Formation, Karoo Basin, South Africa. Universiteit Utrecht.

Bernard, B., Takarada, S., Andrade, S.D., Dufresne, A., 2021. Terminology and Strategy to Describe Large Volcanic Landslides and Debris Avalanches, in: Roverato, M., Dufresne, A., Procter, J. (Eds.), Volcanic Debris Avalanches: From Collapse to Hazard. Springer book series advances in volcanology, pp. 51–73.

Bernard, B., van Wyk de Vries, B., Barba, D., Leyrit, H., Robin, C., Alcaraz, S., Samaniego, P., 2008. The Chimborazo sector collapse and debris avalanche: Deposit characteristics as evidence of emplacement mechanisms. J. Volcanol. Geotherm. Res. 176, 36–43. https://doi.org/10.1016/j.jvolgeores.2008.03.012

Bernard, B., van Wyk de Vries, B., Barba, D., Leyrit, H., Robin, C., Alcaraz, S., Samaniego, P., 2008. The Chimborazo sector collapse and debris avalanche: Deposit characteristics as evidence of emplacement mechanisms. J. Volcanol. Geotherm. Res. 176, 36–43. https://doi.org/10.1016/j.jvolgeores.2008.03.012

Bernard, B., Van Wyk de Vries, B., Leyrit, H., 2009. Distinguishing volcanic debris avalanche deposits from their reworked products: The perrier sequence (French Massif Central). Bull. Volcanol. 71, 1041–1056. https://doi.org/10.1007/s00445-009-0285-7

Bernard, K., Thouret, J.C., van Wyk de Vries, B., 2017. Emplacement and transformations of volcanic debris avalanches-A case study at El Misti volcano, Peru. J. Volcanol. Geotherm. Res. 340, 68–91. https://doi.org/10.1016/j.jvolgeores.2017.04.009

Bernard, K., van Wyk de Vries, B., 2017. Volcanic avalanche fault zone with pseudotachylite and gouge in French Massif Central. J. Volcanol. Geotherm. Res. 347, 112–135. https://doi.org/10.1016/j.jvolgeores.2017.09.006

Bertran, P., 2003. The rock-avalanche of February 1995 at Claix (French Alps). Geomorphology 54, 339–346. https://doi.org/10.1016/S0169-555X(03)00041-2

Bianchi Fasani, G., 2004. Grandi frane in roccia: Fenomenologia ed evidenze di terreno. Univ. Studi di Roma "'La Sapienza"', Rome.

Blair, T.C., 1987. Sedimentary processes, vertical stratification sequences, and geomorphology of the Roaring River alluvial fan, Rocky Mountain National Park, Colorado. J. Sediment. Petrol. 57, 1–18. https://doi.org/10.1306/212F8A8A-2B24-11D7-8648000102C1865D

Blair, T.C., McPherson, J.G., 1999. Grain-size and textural classification of coarse sedimentary particles. J. Sediment. Res. 69, 6–19. https://doi.org/10.2110/jsr.69.6

Bowman, E.T., Take, W.A., Rait, K.L., Hann, C., 2012. Physical models of rock avalanche spreading behaviour with dynamic fragmentation. Can. Geotech. J. 49, 460–476. https://doi.org/10.1139/T2012-007

Breard, E.C., Dufek, J., Fullard, L. and Carrara, A., 2020. The basal friction coefficient of granular flows with and without excess pore pressure: Implications for pyroclastic density currents, water-rich debris flows, and rock and submarine avalanches. Journal of Geophysical Research: Solid Earth, 125(12), p.e2020JB020203.

Brilliantov, N. V, Pöschel, T., 2010. Kinetic theory of granular gases. Oxford University Press on Demand, Oxford, UK.

Bryan, S.E., Martí, J., Cas, R.A.F., 1998. Stratigraphy of the Bandas del Sur Formation: an extracaldera record of Quaternary phonolitic explosive eruptions from the Las Cañadas edifice, Tenerife (Canary Islands). Geol. Mag. 135, 605–636.

Bunte, K., Abt, S.R., 2001. Sampling Surface and Subsurface Particle-Size Distributions in Wadable Gravel- and Cobble-Bed Streams for Analyses in Sediment Transport, Hydraulics, and Streambed Monitoring. US Dep. Agric. For. Serv. Rocky Mt. Res. Station. 450.

Buscombe, D., 2008. Estimation of grain-size distributions and associated parameters from digital images of sediment. Sediment. Geol. 210, 1–10. https://doi.org/10.1016/j.sedgeo.2008.06.007

Bustos, E., Capra, L., M, A., Norini, G., 2022. Volcanic debris avalanche transport and emplacement at Chimpa volcano (Central Puna, Argentina): Insights from morphology, grain-size and clast surficial textures. J. Volcanol. Geotherm. Res. https://doi.org/10.1016/j.jvolgeores.2022.107671

Caballero, L., Capra, L., 2011. Textural analysis of particles from El Zaguán debris avalanche deposit, Nevado de Toluca volcano, Mexico: Evidence of flow behavior during emplacement. J. Volcanol. Geotherm. Res. 200, 75–82. https://doi.org/10.1016/j.jvolgeores.2010.12.003

Caballero, L., Sarocchi, D., Soto, E., Borselli, L., 2014. Rheological changes induced by clastfragmentation in debrisflows. J. Geophys. Res. Earth Surf. 119, 1800–1817. https://doi.org/10.1002/2013JF002871.Received

Cabrera, M., Estrada, N., 2019. Granular column collapse: Analysis of grain-size effects. Phys. Rev. E 99, 1–7. https://doi.org/10.1103/PhysRevE.99.012905

Cabrera, M., Estrada, N., 2021. Is the Grain Size Distribution a Key Parameter for Explaining the Long Runout of Granular Avalanches? J. Geophys. Res. Solid Earth 126, 1–9. https://doi.org/10.1029/2021JB022589

Cagnoli, B., Romano, G.P., 2010. Effect of grain size on mobility of dry granular flows of angular rock fragments: An experimental determination. J. Volcanol. Geotherm. Res. 193, 18–24. https://doi.org/10.1016/j.jvolgeores.2010.03.003

Cagnoli, B., Romano, G.P., 2012. Effects of flow volume and grain size on mobility of dry granular flows of angular rock fragments: A functional relationship of scaling parameters. J. Geophys. Res. Solid Earth 117, 1–13. https://doi.org/10.1029/2011JB008926

Cagnoli, B., Piersanti, A., 2015. Grain size and flow volume effects on granular flow mobility in numerical simulations: 3-D discrete element modeling of flows of angular rock fragments. J. Geophys. Res. Solid Earth 3782–3803. https://doi.org/10.1002/2015JB012608.Received

Calder, E.S., Sparks, R.S.J., Gardeweg, M.C., 2000. Erosion, transport and segregation of pumice and lithic clasts in pyroclastic flows inferred from ignimbrite at Lascar Volcano, Chile. J. Volcanol. Geotherm. Res. 104, 201–235. https://doi.org/10.1016/S0377-

0273(00)00207-9

Campbell, C.S., 1989. Self-Lubrication for Long Runout Landslides. J. Geol. 97, 653–665.

Campbell, C.S., 1990. Rapid granular flows. Annu. Rev. Fluid Mech. 22, 57–90.

Campbell, C.S., 2005. Stress-controlled elastic granular shear flows. J. Fluid Mech. 539, 273–297.

Campbell, C.S., Cleary, P.W., Hopkins, M., 1995. Large-scale landslide simulations: global deformation, velocities and basal friction. J. Geophys. Res. 100, 8267–8283. https://doi.org/10.1029/94JB00937

Capra, L., Macías, J.L., Scott, K.M., Abrams, M., Garduño-Monroy, V.H., 2002. Debris avalanches and debris flows transformed from collapses in the Trans-Mexican Volcanic Belt, Mexico - Behavior, and implications for hazard assessment. J. Volcanol. Geotherm. Res. 113, 81–110. https://doi.org/10.1016/S0377-0273(01)00252-9

Capra, L., Norini, G., Groppelli, G., Macías, J.L., Arce, J.L., 2008. Volcanic hazard zonation of the Nevado de Toluca volcano, México. J. Volcanol. Geotherm. Res. 176, 469–484. https://doi.org/10.1016/j.jvolgeores.2008.04.016

Cas, R.A.F., Wolff, J.A., Martí, J., Olin, P.H., Edgar, C.J., Pittari, A., Simmons, J.M., 2022. Tenerife, a complex end member of basaltic oceanic island volcanoes, with explosive polygenetic phonolitic calderas, and phonolitic-basaltic stratovolcanoes. Earth-Science Rev. 230, 103990. https://doi.org/10.1016/j.earscirev.2022.103990

Casagli, N., Ermini, L., Rosati, G., 2003. Determining grain size distribution of the material composing landslide dams in the Northern Apennines: Sampling and processing methods. Eng. Geol. 69, 83–97. https://doi.org/10.1016/S0013-7952(02)00249-1

Chayes, F., 1956. Petrographic modal analysis. John Wiley, New York.

Church, M., McLean, D., Wolcott, J., 1987. River bed gravels: sampling and analysis, in: Thornr, C., Bathurst, J., Hey, R. (Eds.), Gravel Bed Rivers. John Wiley, pp. 43–87.

Clague, J.J., Stead, D., 2013. Landslides: Types, Mechanisms and Modeling, Journal of Chemical Information and Modeling. https://doi.org/10.1017/CBO9781107415324.004

Clavero, J., Polanco, E., Godoy, E., Matthews, S., Sparks, R.S.J., 2004. Substrata influence in the transport and emplacement mechanism of the Ollagüe debris avalanche (northern Chile). Acta Vulcanol. J. Natl. Volcan. Gr. Italy pp.59-76.

Clavero, J., Sparks, R., Huppert, H., Dade, W., 2002. Geological constraints on the emplacement mechanism of the Parinacota debris avalanche, Northern Chile. Bull. Volcanol. 64, 40–54. https://doi.org/10.1007/s00445-001-0183-0

Cleary, P.W., Campbell, C.S., 1993. Self-lubrication for long runout landslides: Examination by computer simulation. J. Geophys. Res. Solid Earth 98, 21911–21924.

Clement, B.M., Connor, C.B., Graper, G., 1993. Paleomagnetic estimate of the emplacement temperature of the long-runout Nevado de Colima volcanic debris avalanche deposit, Mexico. Earth Planet. Sci. Lett. 120, 499–510.

Collins, G.S., Melosh, H.J., 2003. Acoustic fluidization and the extraordinary mobility of sturzstroms. J. Geophys. Res. Solid Earth 108, 1–14. https://doi.org/10.1029/2003jb002465

Conway, S.J., Decaulne, A., Balme, M.R., Murray, J.B., Towner, M.C., 2010. A new approach to estimating hazard posed by debris flows in the Westfjords of Iceland. Geomorphology 114, 556–572. https://doi.org/10.1016/j.geomorph.2009.08.015

Corominas, J., 1996. The angle of reach as a mobility index for small and large landslides.

Crandell, D.R., 1971. Postglacial lahars from Mount Rainier Volcano, Washington. U. S. Geol. Surv. Prof. Pap. 667, 80.

Crandell, D.R., 1989. Gigantic Debris Avalanche of Pleistocene Age From Ancestral Mount Shasta Volcano , California , and Debris-avalanche Hazard Donation. U.S. Geol. Surv. Bull. 1861.

Crandell, D.R., Miller, C.D., Glicken, H.X., Christiansen, R.L., Newhall, C.G., 1984. Catastrophic debris avalanche from ancestral Mount Shasta volcano, California. Geology 12, 143–146. https://doi.org/10.1130/0091-7613(1984)12<143:CDAFAM>2.0.CO;2

Cronin, S.J., Zernack, A. V., Ukstins, I.A., Turner, M.B., Torres-Orozco, R., Stewart, R.B., Smith, I.E.M., Procter, J.N., Price, R., Platz, T., Petterson, M., Neall, V.E., McDonald, G.S., Lerner, G.A., Damaschcke, M., Bebbington, M.S., 2021. The geological history and hazards of a long-lived stratovolcano, Mt. Taranaki, New Zealand. New Zeal. J. Geol. Geophys. 64, 456–478. https://doi.org/10.1080/00288306.2021.1895231

Crosta, G.B., Calvetti, F., Imposimato, S., Roddeman, D., Frattini, P., Agliardi, F., 2001. Granular flows and numerical modelling of landslides. Rep. DAMOCLES Proj. 16–36.

Crosta, G.B., De Blasio, F.V., De Caro, M., Volpi, G., Imposimato, S., Roddeman, D., 2017. Modes of propagation and deposition of granular flows onto an erodible substrate: experimental, analytical, and numerical study. Landslides. https://doi.org/10.1007/s10346-016-0697-3

Crosta, G.B., Frattini, P., Fusi, N., 2007. Fragmentation in the Val Pola rock avalanche, Italian Alps. J. Geophys. Res. Earth Surf. 112, 1–23. https://doi.org/10.1029/2005JF000455

Crosta, G.B., Imposimato, S., Roddeman, D., 2009. Numerical modelling of entrainment/deposition in rock and debris-avalanches. Eng. Geol. 109, 135–145. https://doi.org/10.1016/j.enggeo.2008.10.004

Cruden, D., Hungr, O., 1986. The debris of the Frank Slide and theories of rockslide–avalanche mobility. Can. J. Earth Sci. 23, 425–432. https://doi.org/10.1139/e86-044

Cruden, D.M., Varnes, D.J., 1996. Landslide types and processes. In Turner, AK and Schuster, RL (eds.), Landslides-Investigation and Mitigation. Washington DC, National Academy Press, Transportation Research Board Special Report 247, pp. 36-75.

Cuomo, S., 2020. Modelling of flowslides and debris avalanches in natural and engineered slopes: a review. Geoenvironmental Disasters 7, 1–25. https://doi.org/10.1186/s40677-019-0133-9

Davies, D.K., Quearry, M.W., Bonis, S.B., 1978. Glowing avalanches from the 1974 eruption of the volcano Fuego, Guatemala. Bull. Geol. Soc. Am. 89, 369–384. https://doi.org/10.1130/0016-7606(1978)89<369:GAFTEO>2.0.CO;2

Davies, T., 1982. Spreading of rock avalanche debris by mechanical fluidization. Rock Mech. 24, 9–24.

Davies, T., 2015. Hazards and Disasters Series: Landslide Hazards, Risks, and Disasters. Academic Press. https://doi.org/10.1016/B978-0-12-394846-5.01001-8

Davies, T., McSaveney, M., 1999. Runout of dry granular avalanches. Can. Geotech. J. https://doi.org/10.1139/t98-108

Davies, T., McSaveney, M., 2009. The role of rock fragmentation in the motion of large landslides. Eng. Geol. 109, 67–79. https://doi.org/10.1016/j.enggeo.2008.11.004

Davies, T., McSaveney, M., 2002. Dynamic simulation of the motion of fragmenting rock avalanches. Can. Geotech. J. 39, 789–798. https://doi.org/10.1139/t02-035

Davies, T., McSaveney, M., 2012. Mobility of long-runout rock avalanches. Landslides–

types, Mech. Model. Ed. by JJ Clague D. Stead. 50–58.

Davies, T., McSaveney, M., Kelfoun, K., 2010. Runout of the Socompa volcanic debris avalanche, Chile: A mechanical explanation for low basal shear resistance. Bull. Volcanol. 72, 933–944. https://doi.org/10.1007/s00445-010-0372-9

Davies, T., McSaveney, M.J., Hodgson, K.A., 1999. A fragmentation-spreading model for long-runout rock avalanches. Can. Geotech. J. https://doi.org/10.1139/t99-067

Dávila-Harris, P., Branney, M.J., Storey, M., 2011. Large eruption-triggered ocean-island landslide at Tenerife: Onshore record and long-term effects on hazardous pyroclastic dispersal. Geology 39, 951–954. https://doi.org/10.1130/G31994.1

De Blasio, F.V., 2011. Introduction to the Physics of Landslides, Introduction to the Physics of Landslides. https://doi.org/10.1007/978-94-007-1122-8

De Blasio, F.V., Crosta, G.B., 2014. Simple physical model for the fragmentation of rock avalanches. Acta Mech. 225, 243–252. https://doi.org/10.1007/s00707-013-0942-y

De Blasio, F.V., Elverhøi, A., 2008. A model for frictional melt production beneath large rock avalanches. J. Geophys. Res. Earth Surf. 113, 1–13. https://doi.org/10.1029/2007JF000867

Degaetano, M., Lacaze, L., Phillips, J.C., 2013. The influence of localised size reorganisation on short-duration bidispersed granular flows. Eur. Phys. J. E 36. https://doi.org/10.1140/epje/i2013-13036-9

del Potro, R., Hürlimann, M., 2008. Geotechnical classification and characterisation of materials for stability analyses of large volcanic slopes. Eng. Geol. 98, 1–17. https://doi.org/10.1016/j.enggeo.2007.11.007

Delannay, R., Valance, A., Mangeney, A., Roche, O., Richard, P., 2017. Granular and particle-laden flows: From laboratory experiments to field observations. J. Phys. D. Appl. Phys. 50. https://doi.org/10.1088/1361-6463/50/5/053001

Delcamp, A., Kervyn, M., Benbakkar, M., Kwelwa, S., Peter, D., 2017. Large volcanic landslide and debris avalanche deposit at Meru, Tanzania. Landslides 14, 833–847. https://doi.org/10.1007/s10346-016-0757-8

Denlinger, R.P., Iverson, R., 2001. Flow of variably fluidized granular masses across three-dimensional terrain: 2. Numerical predictions and experimental tests. J. Geophys. Res. Solid Earth 106, 537–552. https://doi.org/10.1029/2000JB900329

Detert, M., Weitbrecht, V., 2020. Determining image-based grain size distribution with suboptimal conditioned photos, in: Uijttewaal, W., Franca, M.J., Valero, D., Chavarrias, V., Ylla Arbos, C., Shielen, R., Crosato, A. (Eds.), River Flow 2020. CRC Press, Lodon, pp. 1045–1052.

Di Luzio, E., Bianchi-Fasani, G., Esposito, C., Saroli, M., Cavinato, G.P., Scarascia-Mugnozza, G., 2004. Massive rock-slope failure in the Central Apennines (Italy): The case of the Campo di Giove rock avalanche. Bull. Eng. Geol. Environ. 63, 1–12. https://doi.org/10.1007/s10064-003-0212-7

Di Traglia, F., Bartolini, S., Artesi, E., Nolesini, T., Ciampalini, A., Lagomarsino, D., Martí, J., Casagli, N., 2018. Susceptibility of intrusion-related landslides at volcanic islands: the Stromboli case study. Landslides 15, 21–29. https://doi.org/10.1007/s10346-017-0866-z

Drake, T.G., 1990. Structural features in granular flows. J. Geophys. Res. Solid Earth 95, 8681–8696.

Drake, T.G., 1991. Granular flow physical experiments and their implications for microstructural theories. J. Fluid Mech. https://doi.org/10.1017/S0022112091001994

Duan, Z., Wu, Y. Bin, Peng, J.B., Xue, S.Z., 2022. Characteristics of sand avalanche motion

and deposition influenced by proportion of fine particles. Acta Geotech. 0123456789. https://doi.org/10.1007/s11440-022-01653-y

Duan, Z., Wu, Y. Bin, Tang, H., Ma, J.Q., Zhu, X.H., 2020. An analysis of factors affecting flowslide deposit morphology using Taguchi method. Adv. Civ. Eng. 2020. https://doi.org/10.1155/2020/8844722

Dufresne, A., 2009. Influence of runout path material on rock and debris avalanche mobility: field evidence and analogue modelling . Sci. York 268.

Dufresne, A., 2012. Granular flow experiments on the interaction with stationary runout path materials and comparison to rock avalanche events. Earth Surf. Process. Landforms 37, 1527–1541. https://doi.org/10.1002/esp.3296

Dufresne, A., Bösmeier, A., Prager, C., 2016a. Sedimentology of rock avalanche deposits – Case study and review. Earth-Science Rev. 163, 234–259. https://doi.org/10.1016/j.earscirev.2016.10.002

Dufresne, A., Davies, T., 2009. Longitudinal ridges in mass movement deposits. Geomorphology 105, 171–181. https://doi.org/10.1016/j.geomorph.2008.09.009

Dufresne, A., Davies, T., McSaveney, M.J., 2010a. Influence of runout-path material on emplacement of the Round Top rock avalanche, New Zealand. Earth Surf. Process. Landforms 35, 190–201. https://doi.org/10.1002/esp.1900

Dufresne, A., Dunning, S., 2017. Process dependence of grain size distributions in rock avalanche deposits. Landslides 14, 1555–1563. https://doi.org/10.1007/s10346-017-0806-y

Dufresne, A., Geertsema, M., Shugar, D.H., Koppes, M., Higman, B., Haeussler, P.J., Stark, C., Venditti, J.G., Bonno, D., Larsen, C., Gulick, S.P.S., McCall, N., Walton, M., Loso, M.G., Willis, M.J., 2017. Sedimentology and geomorphology of a large tsunamigenic landslide, Taan Fiord, Alaska. Sediment. Geol. 364, 302–318. https://doi.org/10.1016/j.sedgeo.2017.10.004

Dufresne, A., Prager, C., Bösmeier, A., 2016b. Insights into rock avalanche emplacement processes from detailed morpho-lithological studies of the Tschirgant deposit (Tyrol, Austria). Earth Surf. Process. Landforms 41, 587–602. https://doi.org/10.1002/esp.3847

Dufresne, A., Salinas, S., Siebe, C., 2010b. Substrate deformation associated with the Jocotitlán edifice collapse and debris avalanche deposit, Central México. J. Volcanol. Geotherm. Res. 197, 133–148. https://doi.org/10.1016/j.jvolgeores.2010.02.019

Dufresne, A., Siebert, L., Bernard, B., 2021a. Distribution and geometric parameters of volcanic debris avalanche deposits, in: Volcanic Debris Avalanches. Springer, pp. 75–90.

Dufresne, A., Zernack, A., Bernard, K., Thouret, J.-C., Roverato, M., 2021b. Sedimentology of Volcanic Debris Avalanche Deposits, in: Roverato, M., Dufresne, A., Procter, J. (Eds.), Volcanic Debris Avalanches: From Collapse to Hazard. Springer book series advances in volcanology, Cham, pp. 175–210. https://doi.org/10.1007/978-3-030-57411-6_8

Dunning, S., 2004. Rock Avalanches in High Mountains. PhD Thesis. University of Luton.

Dunning, S., 2006. The grain-size distribution of rock avalanche deposits in valley-confined settings. Ital. J. Eng. Geol. Environ. 1, 117–121. https://doi.org/10.4408/IJEGE.2006-01.S-15

Dunning, S., Armitage, P.J., 2011. The Grain-Size Distribution of Rock-Avalanche Deposits: Implications for Natural Dam Stability, in: Natural and Artificial Rockslide Dams. Springer, Berlin, Heidenberg, pp. 479–498. https://doi.org/10.1007/978-3-642-04764-0

Eaton, B.C., Moore, R.D., MacKenzie, L.G., 2019. Percentile-based grain size distribution analysis tools (GSDtools)--estimating confidence limits and hypothesis tests for comparing

two samples. Earth Surf. Dyn. 7, 789–806.

Einav, I., 2007. Breakage mechanics-Part II: Modelling granular materials. J. Mech. Phys. Solids 55, 1298–1320. https://doi.org/10.1016/j.jmps.2006.11.004

Erismann, T.H., 1979. Mechanisms of large landslides. Rock Mech. Felsmechanik Mécanique des Roches. https://doi.org/10.1007/BF01241087

Erismann, T.H., Abele, G., 2001. Dynamics of Rockslides and Rockfalls, Journal of Chemical Information and Modeling. Springer Science & Business Media. https://doi.org/10.1017/CBO9781107415324.004

Evans, S., Hungr, O., Enegren, E.G., 1994. The Avalanche Lake rock avalanche, Mackenzie mountains, northwest territories, Canada: description, dating, and dynamics. Can. Geotech. J. 31, 749–768.

Fan, X., Tian, S., Zhang, Y., 2016. Mass-front velocity of dry granular flows influenced by the angle of the slope to the runout plane and particle size gradation. J. Mt. Sci. 13, 234–245.

Fasani, G.B., Di Luzio, E., Esposito, C., Martino, S., Scarascia-Mugnozza, G., 2011. Numerical modelling of Plio-Quaternary slope evolution based on geological constraints: A case study from the Caramanico valley (Central Apennines, Italy). Geol. Soc. Spec. Publ. 351, 201–214. https://doi.org/10.1144/SP351.11

Félix, G., Thomas, N., 2004. Relation between dry granular flow regimes and morphology of deposits: Formation of levées in pyroclastic deposits. Earth Planet. Sci. Lett. 221, 197–213. https://doi.org/10.1016/S0012-821X(04)00111-6

Ferraro, F., Grieco, D.S., Agosta, F., Prosser, G., 2018. Space-time evolution of cataclasis in carbonate fault zones. J. Struct. Geol. 110, 45–64. https://doi.org/10.1016/j.jsg.2018.02.007

Fisher, R. V., Schmincke, H.-U., Fisher, R. V., Schmincke, H.-U., 1984. Lahars, in: Pyroclastic Rocks. Springer Berlin Heidelberg, pp. 297–311. https://doi.org/10.1007/978-3-642-74864-6_11

Folk, R.L., 1968. Petrologie of sedimentary rocks. Hemphll Publ. Company, Austin 170. https://doi.org/10.1017/CBO9781107415324.004

Francis, P.W., Gardeweg, M., Ramirez, C.F., Rothery, D.A., 1985. Catastrophic debris avalanche deposit of Socompa volcano, northern Chile. Geology 13, 600–603. https://doi.org/10.1130/0091-7613(1985)13<600:CDADOS>2.0.CO;2

Francis, P.W., Self, S., 1987. Collapsing Volcanoes. Sci. Am. 256, 90–99.

Francis, P.W., Wells, G.L., 1988. Landsat Thematic Mapper observations of debris avalanche deposits in the Central Andes. Bull. Volcanol. 50, 258–278. https://doi.org/10.1007/BF01047488

Friedmann, S.J., Taberlet, N., Losert, W., 2006. Rock-avalanche dynamics: Insights from granular physics experiments. Int. J. Earth Sci. 95, 911–919. https://doi.org/10.1007/s00531-006-0067-9

Funck, T., Schmincke, H.-U., 1998. Growth and destruction of Gran Canaria deduced from seismic reflection and bathymetric data. J. Geophys. Res. Solid Earth 103, 15393–15407.

Furbish, D.J., Schmeekle, M.W., Roering, J.J., 2008. Thermal and grain bridge effects in experimental, sloping granular flow in a channel. Earth Surf. Process. Landforms 33, 2108–2117.

Gauer, P., Issler, D., 2004. Possible erosion mechanisms in snow avalanches. Ann. Glaciol. 38, 384–392. https://doi.org/10.3189/172756404781815068

Glicken, H., 1991. Sedimentary architecture of large volcanic-debris avalanches, in: Sedi-

mentation in Volcanic Settings. pp. 99–106. https://doi.org/10.2110/pec.91.45.0099

Glicken, H., 1996. Rockslide-debris avalanche of May 18, 1980, Mount St. Helens volcano, Washington. USGS Open File Report 96-677. Bull. Surv.

Godoy, B., Rodríguez, I., Pizarro, M., Rivera, G., 2017. Geomorphology, lithofacies, and block characteristics to determine the origin, and mobility, of a debris avalanche deposit at Apacheta-Aguilucho Volcanic Complex (AAVC), northern Chile. J. Volcanol. Geotherm. Res. 347, 136–148. https://doi.org/10.1016/j.jvolgeores.2017.09.008

Goguel, J., 1978. Scale-dependent rockslide mechanisms, with emphasis on the role of pore fluid vaporization, in: Voight, B. (Ed.), Rockslides and Avalanches, 1. Natural Phenomena. Elsevier Scientific Publishing Company, pp. 693–705. https://doi.org/10.1016/B978-0-444-41507-3.50028-3

Gonzalez-Santana, J., Wauthier, C., 2021. Unraveling long-term volcano flank instability at Pacaya Volcano, Guatemala, using satellite geodesy. J. Volcanol. Geotherm. Res. 410, 107147. https://doi.org/10.1016/j.jvolgeores.2020.107147

Gorshkov, G.S., Dubik, Y.M., 1970. Gigantic directed blast at Shiveluch volcano (Kamchatka). Bull. Volcanol. 34, 261–288. https://doi.org/10.1007/BF02597790

Goscombe, B.D., Passchier, C.W., Hand, M., 2004. Boudinage classification: End-member boudin types and modified boudin structures. J. Struct. Geol. 26, 739–763. https://doi.org/10.1016/j.jsg.2003.08.015

Goujon, C., Dalloz-Dubrujeaud, B., Thomas, N., 2007. Bidisperse granular avalanches on inclined planes: A rich variety of behaviors. Eur. Phys. J. E 23, 199–215. https://doi.org/10.1140/epje/i2006-10175-0

Graham, D.J., Rollet, A.-J., Piégay, H., Rice, S.P., 2010. Maximizing the accuracy of image-based surface sediment sampling techniques. Water Resour. Res. 46.

Griswold, J.P., Iverson, R., 2007. Mobility Statistics and Automated Hazard Mapping for Debris Flows and Rock Avalanches Scientific Investigations Report 2007 – 5276. USGS Sci. Investig. Rep. 2007–5276, 62.

Gu, Y., Ozel, A. and Sundaresan, S., 2016. Rheology of granular materials with size distributions across dense-flow regimes. Powder technology, 295, pp.322-329.

Guerit, L., Barrier, L., Liu, Y., Narteau, C., Lajeunesse, E., Gayer, E., Métivier, F., 2018. Uniform grain-size distribution in the active layer of a shallow, gravel-bedded, braided river (the Urumqi River, China) and implications for paleo-hydrology. Earth Surf. Dyn. 6, 1011–1021.

Harvey, E.L., Hales, T.C., Hobley, D.E.J., Liu, J., Fan, X., 2022. Measuring the grain-size distributions of mass movement deposits, Earth Surface Processes and Landforms. https://doi.org/10.1002/esp.5337

Hayashi, J.N., Self, S., 1992. A comparison of pyroclastic flow and landslide mobility. J. Geophys. Res. 97, 9063–9071.

Heim, A., 1882. Der Bergsturz von Elm. Zeitschrift der Dtsch. Geol. Gesellschaft 74–115.

Heim, A., 1932. Bergsturz und menschenleben. Fretz & Wasmuth 77.

Heinrich, P., Boudon, G., Komorowski, J.C., Sparks, R.S.J., Herd, R., Voight, B., 2001. Numerical simulation of the December 1997 debris avalanche in Montserrat, Lesser Antilles. Geophys. Res. Lett. 28, 2529–2532.

Heller, V., 2011. Scale effects in physical hydraulic engineering models. J. ofHydraulic Res. 49, 293–306. https://doi.org/10.1080/00221686.2011.578914

Hewitt, K., 1998. Catastrophic landslides and their effects on the Upper In-

dus streams, Karakoram Himalaya, northern Pakistan. Geomorphology 26, 47–80. https://doi.org/10.1016/S0169-555X(98)00051-8

Hewitt, K., 2002. Styles of rock avalanche depositional complexes conditioned by very rugged terrain, Karakoram Himalaya, Pakistan. Geol. Soc. Am. Rev. Eng. Geol. XV, 345–377.

Hewitt, K., Clague, J.J., Orwin, J.F., 2008. Legacies of catastrophic rock slope failures in mountain landscapes. Earth-Science Rev. 87, 1–38. https://doi.org/10.1016/j.earscirev.2007.10.002

Hooke, R.L., Iverson, R., 1995. Grain-size distribution in deforming subglacial tills: role of grain fracture. Geology 23, 57–60. https://doi.org/10.1130/0091-7613(1995)023<0057:GSDIDS>2.3.CO;2

Hörz, F., Cintala, M.J., See, T.H., Cardenas, F., Thompson, T.D., 1984. Grain size evolution and fractionation trends in an experimental regolith. J. Geophys. Res. 89, C183. https://doi.org/10.1029/jb089is01p0c183

Hsü, K.J., 1975. Catastrophic debris streams (sturzstroms) generated by rockfalls. Bull. Geol. Soc. Am. https://doi.org/10.1130/0016-7606(1975)86<129:CDSSGB>2.0.CO;2

Hsu, L., Dietrich, W.E., Sklar, L.S., 2014. Mean and fluctuating basal forces generated by granular flows: Laboratory observations in a large vertically rotating drum. J. Geophys. Res. Earth Surf. 119, 1283–1309. https://doi.org/10.1002/2013JF003078

Hu, Y. xiang, Li, H. bo, Lu, G. da, Fan, G., Zhou, J. wen, 2021. Influence of size gradation on particle separation and the motion behaviors of debris avalanches. Landslides. https://doi.org/10.1007/s10346-020-01596-z

Hu, Y. xiang, Li, H. bo, Qi, S. chao, Fan, G., Zhou, J. wen, 2020. Granular Effects on Depositional Processes of Debris Avalanches. KSCE J. Civ. Eng. 24, 1116–1127. https://doi.org/10.1007/s12205-020-1555-3

Hughes, A., Kendrick, J.E., Salas, G., Wallace, P.A., Legros, F., Di Toro, G., Lavallée, Y., 2020. Shear localisation, strain partitioning and frictional melting in a debris avalanche generated by volcanic flank collapse. J. Struct. Geol. 140. https://doi.org/10.1016/j.jsg.2020.104132

Hungr, O., 2002. Rock Avalanche Occurrence, Process and Modelling, in: Evans, S., Scarascia-Mugnozza, G., Strom, A., Hermanns, R. (Eds.), Landslides from Massive Rock Slope Failure. Springer, Dordrecht, pp. 285–304.

Hungr, O., Evans, S., 2004. Entrainment of debris in rock avalanches: An analysis of a long run-out mechanism. Bull. Geol. Soc. Am. 116, 1240–1252. https://doi.org/10.1130/B25362.1

Hungr, O., Leroueil, S., Picarelli, L., 2013. The Varnes classification of landslide types, an update. Landslides 11, 167–194. https://doi.org/10.1007/s10346-013-0436-y

Hürlimann, M., Garcia-Piera, J.O., Ledesma, A., 2000. Causes and mobility of large volcanic landslides: Application to Tenerife, Canary Islands. J. Volcanol. Geotherm. Res. 103, 132–134. https://doi.org/10.1016/S0377-0273(00)00219-5

Hürlimann, M., Ledesma, A., 2003. Giant Mass Movements in Volcanic Islands: the Case of Tenerife, in: Occurence and Mechanisms of Flow-like Landslides in Natural Slopes and Earthfills. Sorrento, pp. 105–115.

Hürlimann, M., Ledesma, A., Martí, J., 1999. Conditions favouring catastrophic landslides on Tenerife (Canary Islands). Terra Nov. 11, 106–111. https://doi.org/10.1046/j.1365-3121.1999.00233.x

Ibbeken, H., Schleyer, R., 1986. Photo-sieving: A method for grain-size analysis of coarse-grained, unconsolidated bedding surfaces. Earth Surf. Process. Landforms 11, 59–77. https://doi.org/10.1002/esp.3290110108

Ibbeken, H., Warnke, D.A., Diepenbroek, M., 1998. Granulometric study of the Hanaupah Fan, Death Valley, California. Earth Surf. Process. Landforms 23, 481–492. https://doi.org/10.1002/(SICI)1096-9837(199806)23:6<481::AID-ESP906>3.0.CO;2-T

Inman, D., 1952. Measures for Describing the Size Distribution of Sediments. SEPM J. Sediment. Res. https://doi.org/10.1306/d42694db-2b26-11d7-8648000102c1865d

Iverson, R., 1997. The physics of debris flows. Rev. Geophys. 35, 245–296. https://doi.org/10.1029/97RG00426

Iverson, R., 2005. Debris-flow mechanics, in: Jacob, M., Hungr, O. (Eds.), Debris-Flow Hazards and Related Phenomena. Springer-Praxis, Berlin, pp. 105–134.

Iverson, R., 2015. Scaling and design of landslide and debris-flow experiments. Geomorphology 244, 9–20. https://doi.org/10.1016/j.geomorph.2015.02.033

Iverson, R., Denlinger, R.P., 2001. Flow of variably fluidized granular masses across three-dimensional terrain: 1. Coulomb mixture theory. J. Geophys. Res. Solid Earth. https://doi.org/10.1029/2000JB900329

Iverson, R., Hooyer, T.S., Hooke, R.L., 1996. A laboratory study of sediment deformation: Stress heterogeneity and grain-size evolution. Ann. Glaciol. 22, 167–175. https://doi.org/10.1017/s0260305500015378

Iverson, R., Logan, M., Denlinger, R.P., 2004. Granular avalanches across irregular three-dimensional terrain: 2. Experimental tests. J. Geophys. Res. Earth Surf. 109, 1–16. https://doi.org/10.1029/2003jf000084

Iverson, R., Reid, M., Logan, M., LaHusen, R.G., Godt, J.W., Griswold, J.P., 2011. Positive feedback and momentum growth during debris-flow entrainment of wet bed sediment. Nat. Geosci. 4, 116–121. https://doi.org/10.1038/ngeo1040

Iverson, R.M., Vallance, J.W., 2001. New views of granular mass flows. Geology 29, 115–118. https://doi.org/10.1130/0091-7613(2001)029<0115:NVOGMF>2.0.CO;2

Janda, R.J., Scott, K.M., Nolan, M., Martinson, H., 1981. Lahar movement, effects, and deposits, in: Lipman, P.W., D.R., M. (Eds.), The 1980 Eruption of Mount St. Helens, Washington. U.S. Geol. Surv., Prof. Pap., pp. 461–478.

Jiang, Y.J., Towhata, I., 2013. Experimental study of dry granular flow and impact behavior against a rigid retaining wall. Rock Mech. Rock Eng. 46, 713–729. https://doi.org/10.1007/s00603-012-0293-3

Jiang, Y.J., Zhao, Y., 2015. Experimental investigation of dry granular flow impact via both normal and tangential force measurements. Geotech. Lett. 5, 33–38. https://doi.org/10.1680/geolett.15.00003

Johnson, B.C., 1978. Blackhawk landslide, California, U.S.A., in: Voight, B. (Ed.), Rockslides and Avalanches, 1. Natural Phenomena. pp. 481–504. https://doi.org/10.1016/B978-0-444-41507-3.50022-2

Johnson, B.C., Campbell, C.S., Melosh, J.H., 2016. The reduction of friction in long runout landslides as an emergent phenomenon. J. Geophys. Res. Earth Surf. 300–316. https://doi.org/10.1002/2013JF002871

Johnson, M.R., 1994. Thin section grain size analysis revisited. Sedimentology 41, 985–999. https://doi.org/10.1111/j.1365-3091.1994.tb01436.x

Katayama, N., 1974. Old records of natural phenomena concerning the Shimabara catas-

trophe. Sci. Rept. Shimabara Volcano Obs. Fac. Sci. Kyushu Univ 9, 1–45.

Kelfoun, K., 2011. Suitability of simple rheological laws for the numerical simulation of dense pyroclastic flows and long-runout volcanic avalanches. J. Geophys. Res. Solid Earth 116, 1–14. https://doi.org/10.1029/2010JB007622

Kelfoun, K., Druitt, T.H., 2005. Numerical modeling of the emplacement of Socompa rock avalanche, Chile. J. Geophys. Res. Solid Earth. https://doi.org/10.1029/2005JB003758

Kellerhals, R., Bray, D.I., 1971. Sampling procedures for coarse fluvial sediments. J. Hydraul. Div. 97, 1165–1180.

Kent, P.E., 1966. The Transport Mechanism in Catastrophic Rock Falls. J. Geol. 74, 79–83.

Knapp, S., Krautblatter, M., 2020. Conceptual Framework of Energy Dissipation During Disintegration in Rock Avalanches. Front. Earth Sci. 8, 1–9. https://doi.org/10.3389/feart.2020.00263

Kokelaar, B.P., Graham, R.L., Gray, J.M.N.T., Vallance, J.W., 2014. Fine-grained linings of leveed channels facilitate runout of granular flows. Earth Planet. Sci. Lett. 385, 172–180. https://doi.org/10.1016/j.epsl.2013.10.043

Lade, P. V., Yamamuro, J.A., Bopp, P.A., 1996. Significance of particle crushing in granular materials. J. Geotech. Eng. 122, 309–316. https://doi.org/10.1061/(ASCE)0733-9410(1996)122

Lai, Z., Vallejo, L.E., Zhou, W., Ma, G., Espitia, J.M., Caicedo, B., Chang, X., 2017. Collapse of Granular Columns With Fractal Particle Size Distribution: Implications for Understanding the Role of Small Particles in Granular Flows. Geophys. Res. Lett. 44, 12,181-12,189. https://doi.org/10.1002/2017GL075689

Lavigne, F., Thouret, J.C., 2002. Sediment transportation and deposition by rain-triggered lahars at Merapi Volcano, Central Java, Indonesia. Geomorphology 49, 45–69. https://doi.org/10.1016/S0169-555X(02)00160-5

Le Friant, A., Boudon, G., Deplus, C., Villemant, B., 2003. Large-scale flank collapse events during the activity of Montagne Pelée, Martinique, Lesser Antilles. J. Geophys. Res. Solid Earth 108, 1–15. https://doi.org/10.1029/2001jb001624

Legros, F., 2002. The mobility of long-runout landslides. Eng. Geol. 63, 301–331. https://doi.org/10.1016/S0013-7952(01)00090-4

Leyrit, H., 2000. Flank collapse and debris avalanche deposits. Volcaniclastic Rocks, from Magmas to Sediments. Ed. by H. Leyrit C. Montenat 111–129.

Li, K., Wang, Y., Lin, Q., Cheng, Q., Wu, Y., 2021. Experiments on granular flow behavior and deposit characteristics: implications for rock avalanche kinematics. https://doi.org/10.1007/s10346-020-01607-z

Linares-Guerrero, E., Goujon, C., Zenit, R., 2007. Increased mobility of bidisperse granular avalanches. J. Fluid Mech. 593, 475–504. https://doi.org/10.1017/S0022112007008932

Lomoschitz, A., Hervás, J., Yepes, J., Meco, J., 2008. Characterisation of a Pleistocene debris-avalanche deposit in the Tenteniguada Basin, Gran Canaria Island, Spain. Landslides 5, 227–234. https://doi.org/10.1007/s10346-008-0115-6

Longchamp, C., Abellan, A., Jaboyedoff, M., Manzella, I., 2016. 3-D models and structural analysis of rock avalanches: The study of the deformation process to better understand the propagation mechanism. Earth Surf. Dyn. 4, 743–755. https://doi.org/10.5194/esurf-4-743-2016

Magnarini, G., Mitchell, T.M., Goren, L., Grindrod, P.M., Browning, J., 2021. Implications of longitudinal ridges for the mechanics of ice-free long runout landslides. Earth Planet.

Sci. Lett. 574, 117177. https://doi.org/10.1016/j.epsl.2021.117177

Magnarini, G., Mitchell, T.M., Grindrod, P.M., Goren, L., Schmitt, H.H., 2019. Longitudinal ridges imparted by high-speed granular flow mechanisms in martian landslides. Nat. Commun. 10, 1–7. https://doi.org/10.1038/s41467-019-12734-0

Mair, K., Hazzard, J.F., 2007. Nature of stress accommodation in sheared granular material: Insights from 3D numerical modeling. Earth Planet. Sci. Lett. 259, 469–485.

Major, J.J., Voight, B., 1986. Sedimentology and clast orientations of the 18 May 1980 southwest- flank lahars, Mount St. Helens, Washington. J. Sediment. Petrol. 56, 691–705. https://doi.org/10.1306/212F8A1C-2B24-11D7-8648000102C1865D

Makris, S., Manzella, I., Cole, P., Roverato, M., 2020. Grain size distribution and sedimentology in volcanic mass-wasting flows: implications for propagation and mobility. Int. J. Earth Sci. https://doi.org/10.1007/s00531-020-01907-8

Makris, S., Roverato, M., Lomoschitz, A., Cole, P., and Manzella, I., 2023a. The propagation and emplacement mechanisms of the Tenteniguada volcanic debris avalanche (Gran Canaria): Field evidence for brittle fault-accommodated spreading. J. Volcanol. Geotherm. Res. 435C, 107773. doi:10.1016/j.jvolgeores.2023.107773

Makris, S., Roverato, M., Dávila-harris, P., Cole, P., Manzella, I., 2023b. Distributed stress fluidisation: Insights into the propagation mechanisms of the Abona volcanic debris avalanche (Tenerife) through a novel method for indurated deposit sedimentological analysis. Front. Earth Sci. 11, 1–22. https://doi.org/10.3389/feart.2023.1177507

Mancarella, D., Hungr, O., 2010. Analysis of run-up of granular avalanches against steep, adverse slopes and protective barriers. Can. Geotech. J. 47, 827–841. https://doi.org/10.1139/T09-143

Mangeney, A., Roche, O., Hungr, O., Mangold, N., Faccanoni, G., Lucas, A., 2010. Erosion and mobility in granular collapse over sloping beds. J. Geophys. Res. Earth Surf. 115 (F3), 1–21. https://doi.org/10.1029/2009JF001462

Mangeney, A., Tsimring, L.S., Volfson, D., Aranson, I.S., Bouchut, F., 2007. Avalanche mobility induced by the presence of an erodible bed and associated entrainment. Geophys. Res. Lett. 34, 1–5. https://doi.org/10.1029/2007GL031348

Manzella, I., 2008. Dry rock avalanche propagation: unconstrained flow experiments with granular materials and blocks at small scale. École Polytechnique Fédérale de Lausanne.

Manzella, I., Einstein, H.H., Grasselli, G., 2013. DEM and FEM/DEM modelling of granular flows to investigate large debris avalanche propagation, in: Landslide Science and Practice: Spatial Analysis and Modelling. pp. 247–253. https://doi.org/10.1007/978-3-642-31310-3-33

Manzella, I., Labiouse, V., 2008. Qualitative analysis of rock avalanches propagation by means of physical modelling of non-constrained gravel flows. Rock Mech. Rock Eng. 41, 133–151. https://doi.org/10.1007/s00603-007-0134-y

Manzella, I., Labiouse, V., 2009. Flow experiments with gravel and blocks at small scale to investigate parameters and mechanisms involved in rock avalanches. Eng. Geol. 109, 146–158. https://doi.org/10.1016/j.enggeo.2008.11.006

Manzella, I., Labiouse, V., 2010. Physical modelling to better understand rock avalanches 1259–1265. https://doi.org/10.1201/b10554-209

Manzella, I., Labiouse, V., 2013. Empirical and analytical analyses of laboratory granular flows to investigate rock avalanche propagation. Landslides 10, 23–36. https://doi.org/10.1007/s10346-011-0313-5

Manzella, I., Penna, I., Kelfoun, K., Jaboyedoff, M., 2016. High-mobility of unconstrained rock avalanches: Numerical simulations of a laboratory experiment and an Argentinian event. Landslides Eng. Slopes. Exp. Theory Pract. 1959.

Martí, J., Hürlimann, M., Ablay, G.J., Gudmundsson, A., 1997. Vertical and lateral collapses on Tenerife (Canary Islands) and other volcanic ocean islands: Comment. Geology 26, 861–862. https://doi.org/10.1130/0091-7613(1998)026<0861:VALCOT>2.3.CO;2

Martí, J., Soriano, C., Galindo, I., Cas, R.A.F., 2010. Resolving problems with the origin of Las Cañadas caldera (tenerife, Canary Islands): Los Roques de García Formation-part of a major debris avalanche or an in situ, stratified, edifice-building succession? Spec. Pap. Geol. Soc. Am. 464, 113–132. https://doi.org/10.1130/2010.2464(06)

Masson, D.G., Watts, A.B., Gee, M.J.R., Urgeles, R., Mitchell, N.C., Le Bas, T.P., Canals, M., 2002. Slope failures on the flanks of the western Canary Islands. Earth-Science Rev. 57, 1–35.

Mcguire, W.J., 1996. Volcano instability: A review of contemporary themes, in: Mcguire, W.J., Jones, A.P., Neuberg, J. (Eds.), Geological Society Special Publication. Geological Society Special Publication, pp. 1–23. https://doi.org/10.1144/GSL.SP.1996.110.01.01

McSaveney, M., Davies, T., 2007. Rockslides and their motion, in: Progress in Landslide Science. Springer, pp. 113–133.

McSaveney, M.J., 1978. Sherman glacier rock avalanche, alaska, U.S.A., Developments in Geotechnical Engineering. Elsevier Scientific Publishing Company. https://doi.org/10.1016/B978-0-444-41507-3.50014-3

McSaveney, M.J., Davies, T., 2002. Rapid rock-mass flow with dynamic fragmentation: inferences from the morphology and internal structure of rockslides and rock avalanches, in: Evans, S., Scarascia Mugnozza, G., Strom, A., Hermanns, R. (Eds.), Landslides from Massive Rock Slope Failure. Springer, Dordrecht, pp. 285–304.

McSaveney, M.J., Davies, T., Hodgson, K.A., 2000. A contrast in deposit style and process between large and small rock avalanches, in: Proceedings of the 8th International Symposium on Landslides, Cardiff, UK. pp. 26–30.

Mead, S., Procter, J., Bebbington, M., Rodriguez-Gomez, C., 2022. Probabilistic Volcanic Hazard Assessment for National Park Infrastructure Proximal to Taranaki Volcano (New Zealand). Front. Earth Sci. 10, 1–17. https://doi.org/10.3389/feart.2022.832531

Meco, J., Guillou, H., Carracedo, J.-C., Lomoschitz, A., Ramos, A.-J.G., Rodriguez-Y\ánez, J.-J., 2002. The maximum warmings of the Pleistocene world climate recorded in the Canary Islands. Palaeogeogr. Palaeoclimatol. Palaeoecol. 185, 197–210.

Meco, J., Guillou, H., Carracedo, J.-C., Lomoschitz, A., Ramos, A.-J.G., Rodriguez-Y\ánez, J.-J., 2002. The maximum warmings of the Pleistocene world climate recorded in the Canary Islands. Palaeogeogr. Palaeoclimatol. Palaeoecol. 185, 197–210.

Mehl, K.W., Schmincke, H.U., 1999. Structure and emplacement of the Pliocene Roque Nublo debris avalanche deposit, Gran Canaria, Spain. J. Volcanol. Geotherm. Res. 94, 105–134. https://doi.org/10.1016/S0377-0273(99)00100-6

Melosh, H.J., 1979. Acoustic fluidization: a new geologic process? J. Geophys. Res. 84, 7513–7520. https://doi.org/10.1029/JB084iB13p07513

Melosh, H.J., 2015. Acoustic fluidization: what it is, and is not. Bridg. Gap III Impact Cratering Nature, Exp. Model. 1861, 1004.

Merico, A., Iezzi, G., Pace, B., Ferranti, L., Cremona, M., Scafa, M., Cavallo, A., Colella, A., Nazzari, M., Scarlato, P., 2020. Grain size and grain size distribution of a lithified fault core in carbonates rocks using multi-scale image analysis: The example of

the San Benedetto-Gioia dei Marsi fault (Central Italy). J. Struct. Geol. 134, 104017. https://doi.org/10.1016/j.jsg.2020.104017

Middleton, G. V, 1976. Subaqueous sediment transport and deposition by sediment gravity flows. Mar. sediment Transp. Environ. Manag. 197–218.

Moro, F., Faug, T., Bellot, H., Ousset, F., 2010. Large mobility of dry snow avalanches: Insights from small-scale laboratory tests on granular avalanches of bidisperse materials. Cold Reg. Sci. Technol. 62, 55–66. https://doi.org/10.1016/j.coldregions.2010.02.011

Nicoletti, P.G., Sorriso-Valvo, M., 1991. Geomorphic controls of the shape and mobility of rock avalanches. Geol. Soc. Am. Bull. 103, 1365–1373. https://doi.org/10.1130/0016-7606(1991)103<1365:GCOTSA>2.3.CO;2

Ogawa, S., 1978. Multitemperature theory of granular materials, in: Proc. of the US-Japan Seminar on Continuum Mechanical and Statistical Approaches in the Mechanics of Granular Materials, 1978. pp. 208–217.

Okura, Y., Kitahara, H., Sammori, T., Kawanami, A., 2000. Effects of rockfall volume on runout distance. Eng. Geol. 58, 109–124. https://doi.org/10.1016/S0013-7952(00)00049-1

Paguican, E. M. R., (2012). The structure, morphology, and surface texture of debris avalanchedeposits: field and remote sensing mapping and analogue modelling. Dissertation, Clermont-Ferrand: Université Blaise Pascal

Paguican, E.M., Roverato, M., Yoshida, H., 2021. Volcanic Debris Avalanche Transport and Emplacement Mechanisms, in: Roverato, M., Dufresne, A., Procter, J. (Eds.), Volcanic Debris Avalanches: From Collapse to Hazard. Springer book series advances in volcanology, pp. 143–173. https://doi.org/10.1007/978-3-030-57411-6_7

Palmer, B., Alloway, B., Vincent, N., 1991. Volcanic-Debris-Avalanche Deposits in New Zealand—Lithofacies Organization in Unconfined, Wet-Avalanche Flows. Sediment. Volcan. Settings 89–98. https://doi.org/10.2110/pec.91.45.0089

Perez-Torrado, F.J., Carracedo, J.C., Mangas, J., 1995. Geochronology and stratigraphy of the Roque Nublo Cycle, Gran Canaria, Canary Islands. J. - Geol. Soc. 152, 807–818. https://doi.org/10.1144/gsjgs.152.5.0807

Perinotto, H., Schneider, J.L., Bachèlery, P., Le Bourdonnec, F.X., Famin, V., Michon, L., 2015. The extreme mobility of debris avalanches: A new model of transport mechanism. J. Geophys. Res. Solid Earth. https://doi.org/10.1002/2015JB011994

Phillips, J.C., Hogg, A.J., Kerswell, R.R., Thomas, N.H., 2006. Enhanced mobility of granular mixtures of fine and coarse particles. Earth Planet. Sci. Lett. 246, 466–480. https://doi.org/10.1016/j.epsl.2006.04.007

Pierson, T.C., Costa, J.E., 1987. A rheologic classification of subaerial sediment-water flows. GSA Rev. Eng. Geol. 7, 1–12. https://doi.org/10.1130/REG7-p1

Pierson, T.C., Scott, K.M., 1985. Downstream Dilution of a Lahar: Transition From Debris Flow to Hyperconcentrated Streamflow. Water Resour. Res. 21, 1511–1524. https://doi.org/10.1029/WR021i010p01511

Pollet, N., Schneider, J.L.M., 2004. Dynamic disintegration processes accompanying transport of the Holocene Flims sturzstrom (Swiss Alps). Earth Planet. Sci. Lett. 221, 433–448. https://doi.org/10.1016/S0012-821X(04)00071-8

Procter, J.N., Zernack, A. V, Cronin, S.J., 2021. Computer simulation of a volcanic debris avalanche from Mt. Taranaki, New Zealand, in: Roverato, M., Dufresne, A., Procter, J. (Eds.), Volcanic Debris Avalanches: From Collapse to Hazard. Springer, pp. 281–310.

Pudasaini, S.P., Hutter, K., 2007. Avalanche dynamics: dynamics of rapid flows of dense

granular avalanches. Springer Science & Business Media.

Pudasaini, S.P., Wang, Y., Hutter, K., 2005. Rapid motions of free-surface avalanches down curved and twisted channels and their numerical simulation. Philos. Trans. R. Soc. A Math. Phys. Eng. Sci. 363, 1551–1571. https://doi.org/10.1098/rsta.2005.1595

Purinton, B., Bookhagen, B., 2019. Introducing PebbleCounts: a grain-sizing tool for photo surveys of dynamic gravel-bed rivers. Earth Surf. Dyn. 7, 859–877.

Quintana, A., Lomoschitz, A., 2005. Characterisation of a debris avalanche deposit based on its geomorphic and internal features. Tenteniguada Basin, Gran Canaria (Spain). Abstr. 6th Int. Conf. Geomorphol. Zaragoza, Spain 313.

Rait, K.L., Bowman, E.T., 2016. Influences of strain rate and shear rate on the propagation of large scale rock avalanches. Landslides Eng. Slopes. Exp. Theory Pract. 3, 1707–1714. https://doi.org/10.1201/b21520-212

Reubi, O., Hernandez, J., 2000. Volcanic debris avalanche deposits of the upper Maronne valley (Cantal Volcano, France): Evidence for contrasted formation and transport mechanisms. J. Volcanol. Geotherm. Res. 102, 271–286. https://doi.org/10.1016/S0377-0273(00)00191-8

Reubi, O., Ross, P.S., White, J.D.L., 2005. Debris avalanche deposits associated with large igneous province volcanism: An example from the Mawson Formation, central Allan Hills, Antarctica. Bull. Geol. Soc. Am. 117, 1615–1628. https://doi.org/10.1130/B25766.1

Roberti, G., Friele, P., van Wyk de Vries, B., Ward, B., Clague, J.J., Perotti, L., Giardino, M., 2017. Rheological evolution of the mount meager 2010 debris avalanche, southwestern british columbia. Geosphere 13, 1–22. https://doi.org/10.1130/GES01389.1

Robinson, T.R., Davies, T., Reznichenko, N. V., De Pascale, G.P., 2015. The extremely long-runout Komansu rock avalanche in the Trans Alai range, Pamir Mountains, southern Kyrgyzstan. Landslides. https://doi.org/10.1007/s10346-014-0492-y

Roche, O., Gilbertson, M.A., Phillips, J.C., Sparks, R.S.J., 2006. The influence of particle size on the flow of initially fluidised powders. Powder Technol. 166, 167–174. https://doi.org/10.1016/j.powtec.2006.05.010

Roche, O., Van Den Wildenberg, S., Valance, A., Delannay, R., Mangeney, A., Corna, L., Latchimy, T., 2021. Experimental assessment of the effective friction at the base of granular chute flows on a smooth incline. Phys. Rev. E 103, 1–18. https://doi.org/10.1103/PhysRevE.103.042905

Roverato, M., Capra, L., 2013. Características microtexturales como del transporte y emplazamiento de dos depósitos de avalancha de escombros del Volcán de Colima (México). Rev. Mex. ciencias geológicas 30, 512–525.

Roverato, M., Capra, L., Sulpizio, R., Norini, G., 2011. Stratigraphic reconstruction of two debris avalanche deposits at Colima Volcano (Mexico): Insights into pre-failure conditions and climate influence. J. Volcanol. Geotherm. Res. 207, 33–46. https://doi.org/10.1016/j.jvolgeores.2011.07.003

Roverato, M., Cronin, S., Procter, J., Capra, L., 2015. Textural features as indicators of debris avalanche transport and emplacement, Taranaki volcano. Bull. Geol. Soc. Am. 127, 3–18. https://doi.org/10.1130/B30946.1

Roverato, M., Di Traglia, F., Procter, J., Paguican, E.M., Dufresne, A., 2021. Factors contributing to volcano lateral collapse, in: Roverato, M., Dufresne, A., Procter, J. (Eds.), Volcanic Debris Avalanches: From Collapse to Hazard. Springer book series advances in volcanology, pp. 91–119.

Roverato, M., Dufresne, A., 2021. Volcanic debris avalanches: introduction and book

structure, in: Roverato, M., Dufresne, A., Procter, J. (Eds.), Volcanic Debris Avalanches: From Collapse to Hazard. Springerbook series advances in volcanology, pp. 1–10.

Roverato, M., Larrea, P., Casado, I., Mulas, M., Béjar, G., Bowman, L., 2018. Characterization of the Cubilche debris avalanche deposit, a controversial case from the northern Andes, Ecuador. J. Volcanol. Geotherm. Res. https://doi.org/10.1016/j.jvolgeores.2018.07.006

Sammis, C., King, G., Biegel, R., 1987. The kinematics of gouge deformation. Pure Appl. Geophys. PAGEOPH 125, 777–812. https://doi.org/10.1007/BF00878033

Sammis, C., King, G.C.P., 2007. Mechanical origin of power law scaling in fault zone rock. Geophys. Res. Lett. 34.

Sanvitale, N., Bowman, E.T., 2016. Using PIV to measure granular temperature in saturated unsteady polydisperse granular flows. Granul. Matter 18, 1–12. https://doi.org/10.1007/s10035-016-0620-6

Saucedo, R., Macías, J.L., Sarocchi, D., Bursik, M., Rupp, B., 2008. The rain-triggered Atenquique volcaniclastic debris flow of October 16, 1955 at Nevado de Colima Volcano, Mexico. J. Volcanol. Geotherm. Res. 173, 69–83. https://doi.org/10.1016/j.jvolgeores.2007.12.045

Savage, S.B., 1984. The mechanics of rapid granular flows. Adv. Appl. Mech. 24, 289–366.

Savage, S.B., Hutter, K., 1989. The motion of a finite mass of granular material down a rough incline. J. Fluid Mech. 199, 177–215.

Savage, S.B., Lun, C.K.K., 1988. Particle size segregation in inclined chute flow of dry cohesionless granular solids. J. Fluid Mech. 189, 311–335. https://doi.org/10.1017/S002211208800103X

Scheidegger, A.E., 1973. On the prediction of the reach and velocity of catastrophic landslides. Rock Mech. Felsmechanik Mécanique des Roches 5, 231–236. https://doi.org/10.1007/BF01301796

Schilirò, L., Esposito, C., De Blasio, F.V., Scarascia Mugnozza, G., 2019. Sediment texture in rock avalanche deposits: insights from field and experimental observations. Landslides 16, 1629–1643. https://doi.org/10.1007/s10346-019-01210-x

Schneider, J.L., Fisher, R. V., 1998. Transport and emplacement mechanisms of large volcanic debris avalanches: evidence from the northwest sector of Cantal Volcano (France). J. Volcanol. Geotherm. Res. 83, 141–165. https://doi.org/10.1016/S0377-0273(98)00016-X

Schuster, R.L., Crandell, D.R., 1984. Catastrophic debris avalanches from volcanoes. Fourth Int Symp Landslides Proc Toronto 1, 567–572.

Scott, K., Macias, J.L., Naranjo, J.A., Rodriguez, S., McGeehin, J.P., 2001. Catastrophic debris flows transformed from landslides in volcanic terrains: Mobility, hazard assessment, and mitigation strategies, US Geological Survey Professional Paper.

Scott, K., Vallance, J.W., Pringle, P.T., 1995. Sedimentology, behavior, and hazards of debris flows at Mount Rainier, Washington. U. S. Geol. Surv. Prof. Pap. 1547, 1–66. https://doi.org/10.1016/j.radonc.2016.01.020

Scott, K., 1988. Origins, behavior, and sedimentology of lahars and lahar-runout flows in the Toutle-Cowlitz River system. U. S. Geol. Surv. Prof. Pap. 74. https://doi.org/-

Sharpe, C.F.S., 1938. Landslides and related phenomena: a study of mass movement of soil and rock. Columbia Uni. Press. New York 136pp.

Shea, T., van Wyk de Vries, B., 2008. Structural analysis and analogue modeling of the kinematics and dynamics of rockslide avalanches. Geosphere 4, 657–686. https://doi.org/10.1130/GES00131.1

Sheridan, M.F., Stinton, A.J., Patra, A., Pitman, E.B., Bauer, A., Nichita, C., 2003. Evaluating

Titan2D mass-flow model using the 1963 Little Tahoma Peak avalanches, Mount Rainier, Washington. J. Volcanol. Geotherm. Res. 139, 89–102.

Shreve, R.L., 1966. Sherman landslide, Alaska. Science (80). 154, 1639–1643.

Shreve, R.L., 1968. The Blackhawk Landslide. Geol. Soc. Am. Spec. Pap. 108.

Shugar, D.H., Clague, J.J., 2011. The sedimentology and geomorphology of rock avalanche deposits on glaciers. Sedimentology 58, 1762–1783. https://doi.org/10.1111/j.1365-3091.2011.01238.x

Siebe, C., Komorowski, J.-C., Sheridan, M.F., 1992. Morphology and emplacement of an unusual debris-avalanche deposit at Jocotitlán volcano, Central Mexico. Bull. Volcanol. 54, 573–589. https://doi.org/10.1007/BF00569941

Siebert, L., 1984. Large volcanic debris avalanches: Characteristics of source areas, deposits, and associated eruptions. J. Volcanol. Geotherm. Res. 22, 163–197. https://doi.org/10.1016/0377-0273(84)90002-7

Siebert, L., 2002. Landslides resulting from structural failure of volcanoes. GSA Rev. Eng. Geol. 15, 209–235. https://doi.org/10.1130/REG15-p209

Siebert, L., Alvarado, G.E., Vallance, J.W., Van Wyk De Vries, B., 2006. Large-volume volcanic edifi ce failures in Central America and associated hazards. Spec. Pap. Geol. Soc. Am. 412, 1–26. https://doi.org/10.1130/2006.2412(01)

Siebert, L., Begét, J.E., Glicken, H., 1995. The 1883 and late-prehistoric eruptions of Augustine volcano, Alaska. J. Volcanol. Geotherm. Res. 66, 367–395. https://doi.org/10.1016/0377-0273(94)00069-S

Siebert, L., Glicken, H., Kienle, J., 1989. Debris avalanches and lateral blasts at Mount St Augustine volcano, Alaska. Natl. Geogr. Res. 5, 232–249.

Siebert, L., Kimberly, P., Pullinger, C.R., 2004. The voluminous Acajutla debris avalanche from Santa Ana volcano, western El Salvador, and comparison with other Central American edifice-failure events. Spec. Pap. Geol. Soc. Am. 375, 5–23. https://doi.org/10.1130/0-8137-2375-2.5

Siebert, L., Roverato, M., 2021. A Historical Perspective on Lateral Collapse and Volcanic Debris Avalanches, in: Roverato, M., Dufresne, A., Procter, J. (Eds.), Volcanic Debris Avalanches: From Collapse to Hazard. Springer book series advances in volcanology, pp. 11–50.

Silbert, L.E., Ertaş, D., Grest, G.S., Halsey, T.C., Levine, D., Plimpton, S.J., 2001. Granular flow down an inclined plane: Bagnold scaling and rheology. Phys. Rev. E - Stat. Physics, Plasmas, Fluids, Relat. Interdiscip. Top. 64, 14. https://doi.org/10.1103/PhysRevE.64.051302

Smyth, M., 1991. Movement and emplacement mechanisms of the Rio Pita Volcanic Debris Avalanche and its role in the evolution of Cotopaxi Volcano. ProQuest LLC 2014. University of Aberdeen.

Sousa, J., Voight, B., 1991. Continuum simulation of flow failures. Geotechnique 41, 515–538.

Spychala, Y.T., Ramaaker, T.A., Eggenhuisen, J.T., Grundvag, S.-A., Pohl, F., Wroblewska, S., 2021. Proximal to distal grain-size distribution of basin-floor lobes: A study from the Battfjellet Formation, Central Tertiary Basin, Svalbard. Depos. Rec. 0, 1–21.

Stoltman, J.B., 1989. A Quantitative Approach to the Petrographic Analysis of Ceramic Thin Sections 54, 147–160.

Storz-Peretz, Y., Laronne, J.B., 2013. Automatic grain sizing of vertical exposures of

gravelly deposits. Sediment. Geol. 294, 13–26.

Strom, A., 2006. Morphology and internal structure of rockslides and rock avalanches: grounds and constraints for their modelling, in: Landslides from Massive Rock Slope Failure. Springer, pp. 305–326.

Takarada, S., Ui, T., Yamamoto, Y., 1999. Depositional features and transportation mechanism of valley-filling Iwasegawa and Kaida debris avalanches, Japan. Bull. Volcanol. 60, 508–522.

TEIDE GROUP, 1997. Morphometric interpretation of the northwest and southeast slopes of Tenerife, Canary Islands. J. Geophys. Res. Ser. 102, 20–325.

Thompson, N., Bennett, M.R., Petford, N., 2009. Analyses on granular mass movement mechanics and deformation with distinct element numerical modeling: Implications for large-scale rock and debris avalanches. Acta Geotech. 4, 233–247. https://doi.org/10.1007/s11440-009-0093-4

Thompson, N., Bennett, M.R., Petford, N., 2010. Development of characteristic volcanic debris avalanche deposit structures: New insight from distinct element simulations. J. Volcanol. Geotherm. Res. 192, 191–200. https://doi.org/10.1016/j.jvolgeores.2010.02.021

Tischer, M., Bursik, M.I., Pitman, E.B., 2001. Kinematics of sand avalanches using particle-image velocimetry. J. Sediment. Res. 71, 355–364.

Tost, M., Cronin, S.J., Procter, J.N., 2014. Transport and emplacement mechanisms of channelised long-runout debris avalanches, Ruapehu volcano, New Zealand. Bull. Volcanol. 76, 1–14. https://doi.org/10.1007/s00445-014-0881-z

Ui, T., 1983. Volcanic dry avalanche deposits - Identification and comparison with nonvolcanic debris stream deposits. J. Volcanol. Geotherm. Res. 18, 135–150. https://doi.org/10.1016/0377-0273(83)90006-9

Ui, T., 1989. Discrimination Between Debris Avalanches and Other Volcaniclastic Deposits 201–209. https://doi.org/10.1007/978-3-642-73759-6_13

Ui, T., Glicken, H., 1986. Internal structural variations in a debris-avalanche deposit from ancestral Mount Shasta, California, USA. Bull. Volcanol. 48, 189–194. https://doi.org/10.1007/BF01087673

Ui, T., Takarada, S., Yashimoto, M., 2000. Debris avalanches, in: Sigurdsson, H. (Ed.), Encyclopedia of Volcanoes. Academic Press, San Diego, pp. 617–626.

Valentino, R., Barla, G., Montrasio, L., 2008. Experimental analysis and micromechanical modelling of dry Granular flow and impacts in laboratory flume tests. Rock Mech. Rock Eng. 41, 153–177. https://doi.org/10.1007/s00603-006-0126-3

Vallance, J.W., 2000. Lahars. Encycl. volcanoes 601–616.

Vallance, J.W., Iverson, R., 2015. Lahars and Their Deposits, Second Edi. ed, The Encyclopedia of Volcanoes. Elsevier. https://doi.org/10.1016/b978-0-12-385938-9.00037-7

Vallance, J.W., Scott, K.M., 1997. The Osceola Mudflow from Mount Rainier: Sedimentology and hazard implications of a huge clay-rich debris flow. Bull. Geol. Soc. Am. https://doi.org/10.1130/0016-7606(1997)109<0143:TOMFMR>2.3.CO;2

Van Gassen, W., Cruden, D.M., 1989. Momentum transfer and friction in the debris of rock avalanches. https://doi.org/10.1139/t89-075

van Wyk de Vries, B., Delcamp, A., 2015. Volcanic Debris Avalanches, Landslide Hazards, Risks, and Disasters. Elsevier Inc. https://doi.org/10.1016/B978-0-12-396452-6.00005-7

van Wyk De Vries, B., Self, S., Francis, P.W., Keszthelyi, L., 2001. A gravitational spreading origin for the Socompa debris avalanche. J. Volcanol. Geotherm. Res. 105, 225–247.

https://doi.org/10.1016/S0377-0273(00)00252-3

Vezzoli, L., Apuani, T., Corazzato, C., Uttini, A., 2017. Geological and geotechnical characterization of the debris avalanche and pyroclastic deposits of Cotopaxi Volcano (Ecuador). A contribute to instability-related hazard studies. J. Volcanol. Geotherm. Res. 332, 51–70. https://doi.org/10.1016/j.jvolgeores.2017.01.004

Voight, B., 1978. Rockslides and Avalanches. 1. Natural Phenomena. Elsevier, New York.

Voight, B., 2000. Structural stability of andesite volcanoes and lava domes. Philos. Trans. R. Soc. London. Ser. A Math. Phys. Eng. Sci. 358, 1663–1703.

Voight, B., Glicken, H., Janda, R.J., Douglass, M., 1981. Catastrophic rockslide avalanche of May 18 (Mount St. Helens). U.S. Geol. Surv. Prof. Pap. 1250, 347–377.

Voight, B., Janda, R.J., Glicken, H., Douglass, P.M., 1983. Nature and mechanics of the Mount St Helens rockslide-avalanche of 18 May 1980. Geotechnique 33, 243–273. https://doi.org/10.1680/geot.1983.33.3.243

Voight, B., Janda, R.J., Glicken, H., Douglass, P.M., 1985. Reply to Mr Skermer, in Discussion of Voight et al. (1983). Geotechnique 35, 362–369.

Voight, B., Komorowski, J.C., Norton, G.E., Belousov, A.B., Belousova, M., Boudon, G., Francis, P.W., Franz, W., Heinrich, P., Sparks, R.S.J., Young, S.R., 2002. The 26 December (Boxing Day) 1997 sector collapse and debris avalanche at Soufrière Hills Volcano, Montserrat. Geol. Soc. Mem. 21, 363–407. https://doi.org/10.1144/GSL.MEM.2002.021.01.17

Voight, B., Sousa, J., 1994. Lessons from Ontake-san: A comparative analysis of debris avalanche dynamics. Eng. Geol. 38, 261–297. https://doi.org/10.1016/0013-7952(94)90042-6

Walter, T.R., Haghshenas Haghighi, M., Schneider, F.M., Coppola, D., Motagh, M., Saul, J., Babeyko, A., Dahm, T., Troll, V.R., Tilmann, F., Heimann, S., Valade, S., Triyono, R., Khomarudin, R., Kartadinata, N., Laiolo, M., Massimetti, F., Gaebler, P., 2019. Complex hazard cascade culminating in the Anak Krakatau sector collapse. Nat. Commun. 10. https://doi.org/10.1038/s41467-019-12284-5

Walton, O.R., 1993. Numerical simulation of inclined chute flows of monodisperse, inelastic, frictional spheres. Mech. Mater. 239–247.

Wang, Y.F., Cheng, Q.G., Shi, A.W., Yuan, Y.Q., Yin, B.M., Qiu, Y.H., 2019. Sedimentary deformation structures in the Nyixoi Chongco rock avalanche: implications on rock avalanche transport mechanisms. Landslides 16, 523–532. https://doi.org/10.1007/s10346-018-1117-7

Wentworth, C.K., 1922. A Scale of Grade and Class Terms for Clastic Sediments. J. Geol. 30, 377–392. https://doi.org/10.1086/622910

Yang, Q., Cai, F., Ugai, K., Yamada, M., Su, Z., Ahmed, A., Huang, R., Xu, Q., 2011. Some factors affecting mass-front velocity of rapid dry granular flows in a large flume. Eng. Geol. 122, 249–260. https://doi.org/10.1016/j.enggeo.2011.06.006

Yang, Q., Su, Z., Cai, F., Ugai, K., 2015. Enhanced mobility of polydisperse granular flows in a small flume. Geoenvironmental Disasters 2, 12. https://doi.org/10.1186/s40677-015-0019-4

Zernack, A. V., Cronin, S.J., Bebbington, M.S., Price, R.C., Smith, I.E.M., Stewart, R.B., Procter, J.N., 2012. Forecasting catastrophic stratovolcano collapse: A model based on Mount Taranaki, New Zealand. Geology 40, 983–986. https://doi.org/10.1130/G33277.1

Zhang, M., McSaveney, M.J., 2017. Rock avalanche deposits store quantitative evidence on internal shear during runout. Geophys. Res. Lett. 44, 8814–8821.

https://doi.org/10.1002/2017GL073774

Zhang, W., Wang, Q., Chen, J., Li, H., Que, J., Kong, Y., 2015. Grain-size analysis of debris flow alluvial fans in Panxi area along Jinsha River, China. Sustainability 7, 15219–15242.

Zhou, G.G.D., Sun, Q.C., 2017. Study of pore fluid effect on the mobility of granular debris flows. EPJ Web Conf. 140, 1–4. https://doi.org/10.1051/epjconf/201714009046

Appendices

Appendix A

Tenteniguada volcanic debris avalanche study locations

Location	UTM coord. (Zone 28)	Distance from scarp (km)	Illustrated in fig.	Facies and description
1	449414N 3096967N	3.5	-	-
2	449647E 3096571N	3.8	6, 7a, d	**Block facies** with preserved stratigraphic sequence, jigsaw-fractured components and intrablock matrix
3	450030E 3096321N	4.2	9c	**Matrix-rich facies** – mixed, heterolithic, poorly sorted
4	450368E 3096272N	4.5	4	**Block facies** with preserved stratigraphic sequence, jigsaw-fractured components and intrablock matrix
5	450775E 3096174N	4.9	11a	Disaggregated **block facies** with intrablock matrix. Sheared clasts.
6	451571E 3096119N	5.7	5	**Matrix-rich facies** with clastic dike injection in the **block facies, substrate-incorporated block**
7	451726E 3096245N	5.9	2, 10b, c, 11c, d	**Block facies** with preserved stratigraphic sequence, jigsaw-fractured components and intrablock matrix. Normal faults. Large-scale horst and graben.
8	451919E 3096101N	6.1	10a, 11b	Brittle normal faults in **block facies**
9	452526E 3096096N	6.7	7b	Cataclased **block facies**
10	453516E 3096118N	7.7	7c	Cataclased **block facies**
11	454076E 3096909N	8.2	9a, b, 3e	**Matrix-rich facies** – mixed, heterolithic, poorly sorted. Incompletely mixed calsts.

Appendix B

Clast-size analysis in indurated deposits

Extended methodology

Volcanic debris avalanche (VDA), and the non-volcanic equivalent rock avalanche (RA) deposits are poorly sorted with heterogeneous grain-size distributions due to variability in the source rock and heterogeneities in shear stress, fragmentation and comminution distribution during propagation (Tost et al., 2014; Dufresne et al., 2021) depending on factors such as local forces and lithology (Mehl and Schmincke, 1999; Roverato et al., 2015; Dufresne and Dunning, 2017). Deposits commonly contain boulder-sized clasts several meters in diameter as well as clay-sized particles in the matrix (e.g. Glicken, 1996; Tost et al., 2014). VDA deposits (VDADs) are characterised by bimodal to polymodal distributions (Bernard et al., 2017). In order to interpret the deposits, and the mechanisms responsible for their propagation, field investigations need to generate outcrop maps of the distribution of facies, textures, structures and internal sedimentology (Bernard et al., 2017). In addition, for the quantitative examination of the clast-size distribution sampling is required. Determining the clast-size distribution of any indurated sedimentary deposits, as is the case in the Abona VDAD (Ab-VDAD), is a difficult challenge. In fact, the consolidation of the matrix has been suggested to have prohibited the detailed study of the sedimentology of VDA/RA deposits by Tost et al. (2014). To analyse the clast-size distribution of the Ab-VDAD, measurements were carried out using manual photographic grid counting methods on orthophotos generated using photogrammetry with photographs taken in the field. The methodology, its limitation and uncertainties are discussed below.

Structure and facies mapping

Due to the sedimentological heterogeneity in the deposits, it was necessary that detailed facies mapping preceded sedimentological sampling. At different outcrops the structure, stratigraphy, lithology and other features were identified similar to the methodology described by Roverato et al. (2015) and Bernard et al. (2017). Observations were made at different scales regarding the internal architecture and sedimentology. This allows for targeted sampling along the deposit in specific facies. Initially, the mapping allowed the generation of a structural overview (Bernard and van Wyk de Vries, 2017), identifying outcrops to be sampled to offer evidence on clast-size distribution differences as well as their potential longitudinal evolution along the deposit.

Clast-size analysis

Methodology

The large range of clast sizes in VDA/RA deposits means that no single technique can cover the whole range and combinations of techniques have to be used (Casagli et al., 2003; Crosta et al., 2007; Zhang and McSaveney, 2017; Harvey et al., 2022). In cases of weakly cohesive deposits, the disaggregation of material enables sieving and laser diffraction to be employed for the finer spectrum of the size range. However, in indurated cases, such as the Ab-VDAD, samples cannot be disaggregated successfully without producing broken grains. Therefore, analysis by sieving or laser diffraction is not possible (Merico et al., 2020). Clast-size distributions were measured with manual photographic grid sampling exclusively for clasts in the matrix-rich facies at 7 locations to evaluate potential longitudinal evolution and variability of clast sizes and proportion of matrix relative to clasts. Measurements were made at two scales, where permitted by the size of the outcrop, exposures to ensure representation of the coarsest and finest particles.

For VDADs, Glicken (1996) adopted a methodology that was developed for the examination of size distributions in thin sections and adapted it for use at the larger scale of 1 m^2 windows. The original methodology was proposed by Chayes (1956) for the mineral composition of cross sections and is based on an area-volume relationship supporting that:

the ratio of the area occupied by mineral A to the total measurement area is a consistent estimate of the volume percentage of mineral A in the sample (Chayes, 1956, p. 13; Glicken, 1996). Therefore, the relative proportions of measured areas are equivalent to the proportions of volumes for a unit without significant imbrication of ellipsoidal particles (Chayes, 1956). Imbrication of clasts in VDADs is extremely rare (Glicken, 1996). The described photographic method produces frequency-by-area distributions which are different in nature, but theoretically equivalent to the frequency-by-weight output of sieving analysis (Kellerhals and Bray, 1971).

The method used was manual photographic clast-sampling from images of the deposit. This requires sampling the clast-size distribution of an area from scaled photographs or 3D models/orthophotos generated parallel to the surface of an outcrop, or part of it (equivalent methodologies described and employed by Johnson, 1994; Ibbeken et al., 1998; Blair and McPherson, 1999; Casagli et al., 2003; Attal and Lavé, 2006; Crosta et al., 2007; Zhang et al., 2015; Ferraro et al., 2018; Harvey et al., 2022). Image-based clast-size analysis methods are non-intrusive and provide a more efficient way to extract size distributions of non-cohesive material (Detert and Weitbrecht, 2020) and an alternative in cases where sieving is not an option. Additionally, the sieving method produces mass frequency data which are grouped; instead of continuous, in contrast to photographic analysis (Buscombe, 2008). The sieving method also only considers the short or intermediate dimension of the particles, whereas more parameters can be simultaneously measured during photographic analysis (Merico et al., 2020). Manual photographic analysis has been used in the clast-size analysis of VDAs/RAs mainly to incorporate the coarser components (e.g. Siebert et al., 1989; Glicken, 1996; Blair and McPherson, 1999). Additionally, image-based clast-size analysis has been performed for the whole spectrum range of clast sizes encountered in deposits in diverse settings, even of Martian photographs (Detert and Weitbrecht, 2020) and landslide deposits (e.g. Attal and Lavé, 2006).

The sample images were created using photogrammetry to include data from multiple photographs. Where permitted by outcrop scale, photographs were taken at two scales, the first covering the largest possible area (e.g. fig. B.1). These larger scale samples were targeted at sampling the largest of the particles, and therefore cover a large area (<32 m^2). The second scale was of a smaller sample window where smaller particles would be better represented due to the smaller area represented in every pixel of photographs (fig.

Figure B.1: Orthophoto generated from 3D model for the large scale of the outcrop at locality 2. The 3D model was generated with 245 photographs taken in the field and covers an area of 21 m^2, with a resolution of 0.21 mm/pixel.

B.2). These samples achieved resolutions <0.21 mm/pixel and allowed the measurement of particles >0.28 mm (table B.1). Analysis of particles smaller than 0.28 mm was not

Table B.1: Grain size analysis results and properties of the samples used. The final column (total area / largest clast) is a comparison of the area of the sample compared to the area occupied in it by the largest clast.)

Loc./sample	Distance from source (km)	Mean clast size (mm)	Median clast size (mm)	Matrix proportion (%)	Resolution	Min. clast measured (mm)	Clast No. measured (clasts/total grid nodes)	total area / largest clast
10	11.5	162	39	52.4	0.154mm/pixel	0.41	489/1028	95
1	13	102	45	59.1	0.21mm/pixel	0.42	409/999	76
11 upper	15.67	46	19	54.7	0.14mm/pixel	0.28	371/819	92
11 lower	15.67	114	61.5	35.6	0.179mm/pixel	0.64	596/926	50
4	17.71	801	39	52.6	0.176mm/pixel	0.35	418/881	93
9	19.98	118	46	64.9	0.198mm/pixel	0.59	381/1085	462
12	21.46	71	23	50.8	0.14mm/pixel	0.28	466/947	34

possible due to the limitations associated with distinguishing particles in photographs. The original photographs were taken with a DSLR camera at a resolution of 4000x6000 pixels. According to the photographic methodology proposed by Glicken (1996) where necessary the area was cleaned and made as planar as possible, then sprayed with water to enhance the contrast between textures. The locations of the sampling windows were chosen at the interior of the deposit and the middle of each facies to avoid marginal mixing and contamination (Dufresne and Dunning, 2017).

Each sample was generated using photogrammetry, in the commercially available software Agisoft Phtoscan, to combine the information contained in all the photographs into an orthophoto covering the whole area (fig. B.1 and B.2). The orthophotos were scaled using known distances in the sample. However, Glicken (1996), as well as other researchers (e.g. Crosta et al. 2007; Shugar and Clague 2011), have measured all the particles over a threshold size in their samples to predict the area cover of a particular size range as a proxy for the volume percentage (instead of grid-counting), in accordance with the

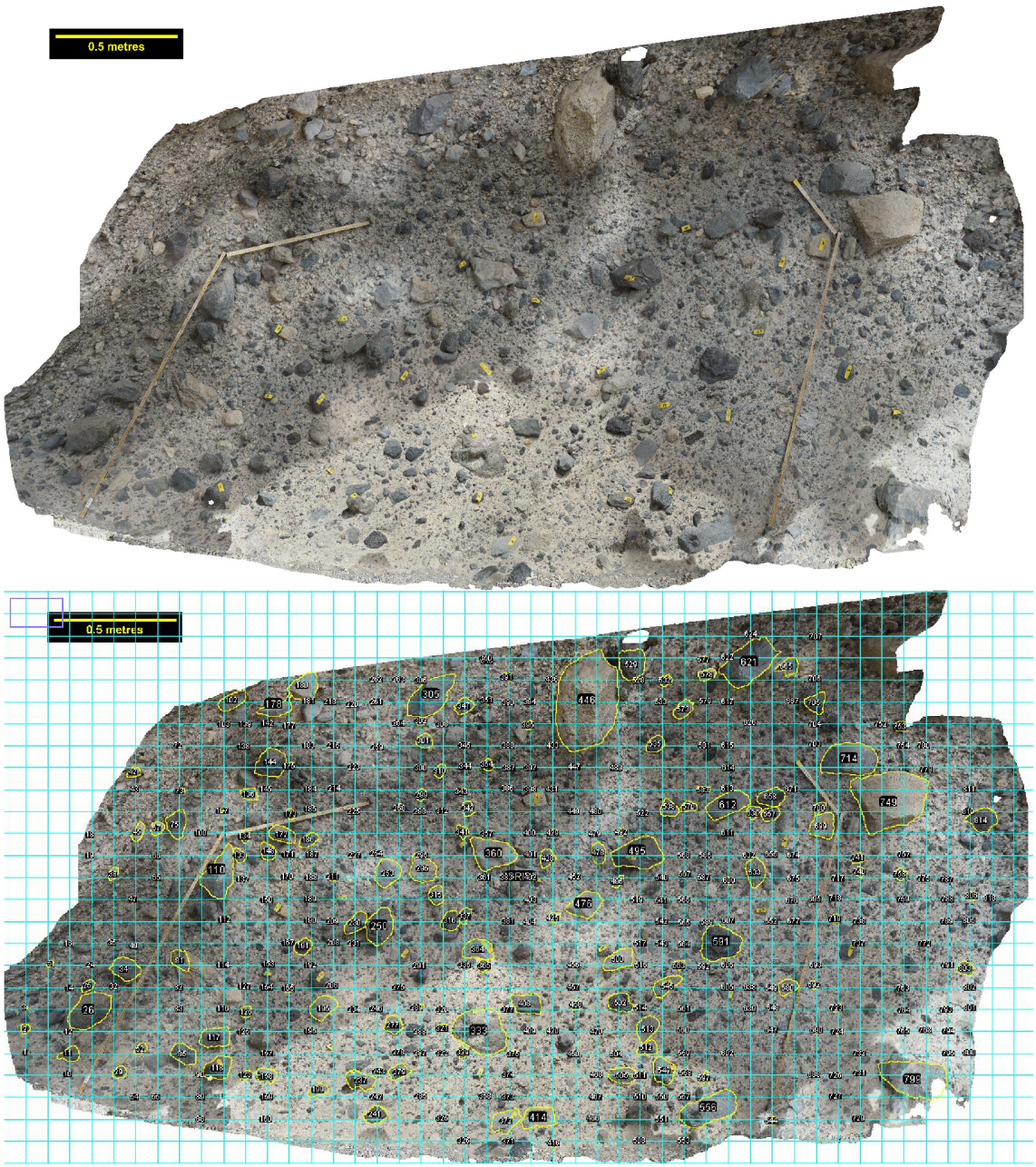

Figure B.2: **TOP**: Orthophoto generated from 3D model for the large scale of sample window at locality 4 (upper). The 3D model was generated with 262 photographs taken in the field and covers an area of 7.5 m^2, with a resolution of 0.14 mm/pixel, allowing clasts > 0.28 mm to be distinguished. **BOTTOM**: The grid has been applied to the orthophoto and particles intersecting its nodes have been outlined for their geometrical parameters to be calculated.

photo-sieving methodology proposed by Ibbeken and Schleyer (1986). In the methodology here described this was impossible due to the large size of the samples. The clast-size distribution was determined by grid-sampling individual clasts and calculating the area occupied by each size range. In the environment of the image analysis software ImageJ the desired grid can be generated and properties of the sampled particles can be automatically calculated (Spychala et al., 2021) when the boundaries of the clasts that intersect the grid

are manually drawn (Berends and Eggenhuisen, 2018). Only the particles intersected by grid nodes were measured. Clasts not entirely included in the photographs were not considered in the sampling, and VDA blocks included in the matrix-rich facies were also excluded. The minimum Feret's diameter, defined as the smallest possible distance between two parallel tangents of an object, was used as the size measurement as it can be considered equivalent to the property by which particles are classified when sieved. However, the data produced are not frequency-by-number as in the case of Blair and McPherson (1999) and Casagli et al. (2003). This is because particles intersected by more than one nodes are counted as many times as they are intersected to account for their higher area occupation in the surface area of the sample. This was done in order to produce a sample strategy that produces frequency-by-area data. Where a node was located over matrix, this was noted in the measurements to allow calculation of the percentage of matrix relative to clasts following the methodology described by Blair (1987). Although particles up to a size of >0.28 mm could generally be measured, for the purposes of this analysis matrix was considered to be composed of all particles of sand size or finer (<2mm). This is for consistency, as the sedimentological term of matrix is scale-dependent rather than assigning a particular size (Vezzoli et al., 2017). Matrix could be composed of different sizes on different occasions within the same deposit as it is defined as an assemblage of smaller particles surrounding coarser particles (Bates et al., 1984). It is also a necessity due to the limitations of the photographic clast-size analysis that has a lower limit. When sampling was carried out on samples from two scales for the same location, results were combined to get the clast-size analysis of the whole size range. The finer clasts were measured in the smaller windows, and the proportion of the coarser clasts was added from the bigger samples. Combining measurements from two samples to incorporate different size ranges and then combining them is typical in clast-size analysis, even with different methodologies (e.g. Casagli et al., 2003; Attal and Lavé, 2006). At the size ranges where there was an overlap there was an approximate agreement between the proportions of the particles and therefore merging the samples was relatively simple.

Sample size and uncertainty

Previous studies have recommended sample sizes for different methods based on coarse fluvial deposits (e.g. Kellerhals and Bray, 1971; Graham et al., 2010; Eaton et al., 2019; Purinton and Bookhagen, 2019). Older literature regarding clast-size analysis (mainly

focused on fluvial gravel) often has empirical recommendations regarding the sample size required (e.g. grid size greater than the largest particle to avoid duplicate measurements - Stoltman 1989), but these methods do not assign a certain level of precision on the findings (Bunte and Abt, 2001). One such recommendation is that the weight of the largest particle should constitute less than <5% of the total weight of the sample (Church et al., 1987). Here, the area equivalent was always fulfilled in terms of the area of the largest particle on the sample. In other literature, it is recommended that the area of the sample is 100-200 times greater than the largest particle in the sample to achieve error margins of <10% (Graham et al., 2010; Storz-Peretz and Laronne, 2013; Eaton et al., 2019; Purinton and Bookhagen, 2019). This was not always achieved here due to the scale of the outcrop exposures (table B.1). In some cases, clasts were so large that the sampling of the whole outcrop was not enough to satisfy this guideline. However, the more quantitative guidelines described below have ensured the reliability of the analysis.

According to the study of Bunte and Abt (2001), the following equations can determine the desired sample size for a clast population for clast counting methodologies after an initial pilot study has been carried out to determine the standard deviation and mean of the population. It should be highlighted that this methodology was initially designed for measuring the size of loose fluvial gravel. In the case that the measurements are made in phi units the equation is:

$$n = \left(\frac{t \times S_1}{e_{\%\phi m} \times \phi_m} \right)^2$$

where n is the sample size, t is the student's t (a statistical numerical value), S_1 is the Inman sorting coefficient, $e_{\%\phi_m}$ the tolerable percentage error around the mean (in phi), and ϕ_m is the median of the population. If the measurements are in mm:

$$n = \left(\frac{t}{\log(1 + e_{\%Dm})} \times S_{g;sq} \right)^2$$

$e_{\%Dm}$ is the tolerable percentage error around the mean (in phi) and $S_{g;sq}$ is the sorting expressed as the logarithmic geometric standard deviation. These equations assume that the population represents a normal distribution. This was only true in phi units and not

in mm, but both these equations are satisfied in the current study so that the sample size is great enough to produce a <5% error around the mean with confidence of >95%.

Limitations

Photographic grain-size analysis implicates several limitations such as photo extent, imbrication, overlap and inconsistency in the axis which is measured (Kellerhals and Bray, 1971; Casagli et al., 2003; Attal and Lavé, 2006; Harvey et al., 2022). All these limitations lead to the underestimation of the coarse component as explained by Harvey et al. (2022). Because of the difficulty in sampling the coarsest of the particles with photographic methods, there are large uncertainties related to their higher percentiles, such as D95 and D99 (Harvey et al., 2022). For example, the methodology proposed by Glicken (1996) uses a $1m^2$ sample window, and therefore, underrepresents coarser clasts (Siebert et al., 2004). This uncertainty can only be increased by increasing the sample size, to include as much of the coarser grains as possible (Guerit et al., 2018; Eaton et al., 2019; Purinton and Bookhagen, 2019; Harvey et al., 2022). However, increasing sample size subsequently results in increased sampling time per site as well as reduced resolution of the sample (Harvey et al., 2022). Generating orthophotos containing information from a large number of photos of the sampled area allowed an increase of the sample size without degradation of the resolution of the sample image to improve this aspect of photographic analysis, solving both problems. An inherent problem of photographic and section analysis is that the image of the clasts is a 2D projection/section through the actual 3D shape of a particle (Glicken, 1996). The standard deviation and sorting of populations of particles obtained from photographic analysis will always be greater than when particles are physically measured, and all their dimensions are available rather than a cross-section of their shape. According to the examination of this effect by Johnson (1994), the difference is greatest when all the particles in a population are of the same size. The effect diminishes linearly as the sorting becomes poorer (Johnson, 1994), and VDADs are characterised by very poor sorting, limiting the effect of this limitation. The clast-size distributions of VDA/RA deposits are wide and multimodal and single clast-size metrics like the median are incapable of meaningfully characterising them (Casagli et al., 2003). A full grain-size range distribution analysis would be required to evaluate processes like comminution and kinetic sieving (Dufresne and Dunning, 2017; Makris et al., 2020; Harvey et al., 2022). However, non-sieving methods, like the one proposed

here, exclude <20% of the finest grains and are thus unable to consider processes where sand and silt-sized particles are affected (Harvey et al., 2022). Manual photo counting also overestimates the D16 value when intended for the whole size range due to the inability of counting the finest particles (Casagli et al., 2003; Harvey et al., 2022). This was limited by enforcing a lower limit to the clasts that were measured, and considering any clast <2mm as part of the matrix. Another limitation of this methodology is that it does not allow lithological component analyis since lithologies cannot be reliably identified in small particles in the photogrphic samples. From this methodology, two additional sources of error can arise. The orientation error depends on the direction that the plane of the exposure (outcrop/polished slab surface direction/thin-section direction) dissects the deposit. This was limited by sampling perpendicular to the sample surface in all cases. The second error is related to the judgement of the operator deciding on the dimensions and the boundaries of the particles whose size will be measured (Spychala et al., 2021). The user bias can lead to low reproducibility for this method (Berends and Eggenhuisen, 2018). The difference in the grain-size distribution characteristics of different samples need to exceed the uncertainties introduced by these errors to indicate significant differences and observations (Spychala et al., 2021). This was not as major as in thin section analysis, in this case, due to the clearly distinctive difference between the clasts and the matrix and the high resolution of the samples allowing observation from different scales. Automated granulometry was considered but the complexity of textures in the samples and the range spanning orders of magnitude made the methodology inapplicable (limitations of this methodology are discussed by Harvey et al. 2022).

Conclusion

Using orthophotos combining data from multiple photographs has allowed enlarging the sample size compared to the methodology originally proposed by Glicken (1996). However, with the increase in sample size, it was not possible to measure the area occupied by every single particle in the frame. Grid counting was therefore employed to sample the area covered by different clast sizes, which is representative of the volume they occupy (Chayes, 1956). Grid-counting methodologies generally aim to avoid repetitive measurements of the same particle, to produce frequency-by-number measurements (Blair and McPherson, 1999; Casagli et al., 2003), which are still theoretically equivalent to

frequency-by-volume (Kellerhals and Bray, 1971). In the current methodology, a denser grid which in some cases had multiple nodes on the same particle allowed for the sampling of the areal coverage of the sample. This produced a frequency-by-area sampling of the area in terms of particle sizes.

Appendix C

Abona volcanic debris avalanche study locations

Sample (prox. to dist.)	UTM coord. (Zone 28)	Distance from scarp (km)	Basal Contact	Marginal areas	Facies	*Description (*Bold text indicates characteristic, repeating features)*
1*	347086E 3115449N	11.5	Abrasive contact with pumice dispersing in Ab-DA		MF	**Heterolithic, very poorly sorted** No preserved blocks Clasts larger compared to other outcrops
2*	346815E 3113205N	13.1			MF	**Heterolithic, very poorly sorted** **Cataclased lave blocks preserved in the MF. Lenticular in shape with diffuse boundaries.**
3	348401E 3114369N	13.4	Variable contact. In areas sharp, abrasive. In areas soil layer preserved under deposit.	Tapered deposit edges	MF	Top section exposed in contact with the overlying pumice
4*	349017E 3111677N	15.7	Sharp, abrasive contact		MF	Higher section free of blocks. Only matrix and clasts.
					EBF	EBF blocks and larger clasts closer to the base and decrease higher up the deposit. Lower section rich in cataclased lava blocks.
5	349877E 3110219N	17.3			EBF	**Elongated, thinned remnant stratigraphy (multiple scorias, lavas) with fluidal features and diffuse boundaries** **Intrablock matrix** **Differential cataclasis of lithologies – e.g. scoria more than lava. Nonetheless, they both form monolithological diamictons.** Shear features – sheared components of jigsaw clasts **Rounded clasts of the softer lithologies**
			Sharp, abrasive contact		MF	Outside of the EBF facies. Lower section of the exposure.
6*	351627E 3111577N	17.7		Tapered deposit edges	MF	**Included cataclased blocks with fluidal features.**
					EBF	**Cataclased blocks and more mixed regions of monolithological diamictons.**
7	351993E 3111334N	18.0	Bulldozing, ploughing, but also undisturbed substrate		MF	**Heterolithic, very poorly sorted** **Majority of clasts of lava lithologies**
8	352491E 3111052N	18.4			EBF	**Elongated, thinned remnant stratigraphy (multiple scorias, lavas) with fluidal features and diffuse boundaries** **Intrablock matrix** **Differential cataclasis of lithologies – e.g. scoria more than lava. Nonetheless, they both form monolithological diamictons.**

						Rounded clasts of the softer lithologies
9	352572E 3111100N	18.6		Tapered deposit edges	MF	*Not examined from close up*
10	352633E 3111044N	19.5	Shallow bulldozing, abrasive sharp sections, soil preserved in undisturbed sections		MF	**Cataclased blocks and monolithological diamictons** **Majority of clasts of lava lithologies**
11*	353202E 3109578N	20.0			MF	**Diffuse boundaries, incomplete mixing of lenticular blocks (lava)** There are areas of the matrix enriched in pumice **Heterolithic, very poorly sorted**
12*	353468E 3108116N	21.5	Abrasive contact, flame injections, penetration of the substrate by MF, bulldozing and also undisturbed substrate		EBF	**Elongated, thinned remnant stratigraphy (multiple scorias, lavas) with fluidal features and diffuse boundaries** **Intrablock matrix** **Differential cataclasis of lithologies – e.g. scoria more than lava.** **Nonetheless, they both form monolithological diamictons.** **Rounded clasts of the softer lithologies**
					MF	**Heterolithic, very poorly sorted** **Clast majority of lava lithology** **Cataclased lenticular blocks and monolithological diamictons** One jigsaw fractured clast
13	353911E 3108334N	21.6			EBF	**Elongated, thinned remnant stratigraphy (multiple scorias, lavas) with fluidal features and diffuse boundaries** **Intrablock matrix** **Differential cataclasis of lithologies – e.g. scoria more than lava** **Nonetheless, they both form monolithological diamictons.** **Rounded clasts of the softer lithologies**
					MF	**Heterolithic, very poorly sorted. Majority of clasts of lava lithologies.** **Cataclased lave blocks preserved**

* Locations where clast-size sampling and analysis was carried out

Appendix D

Abona volcanic debris avalancje deposit - Location 4 outcrop and sample locations

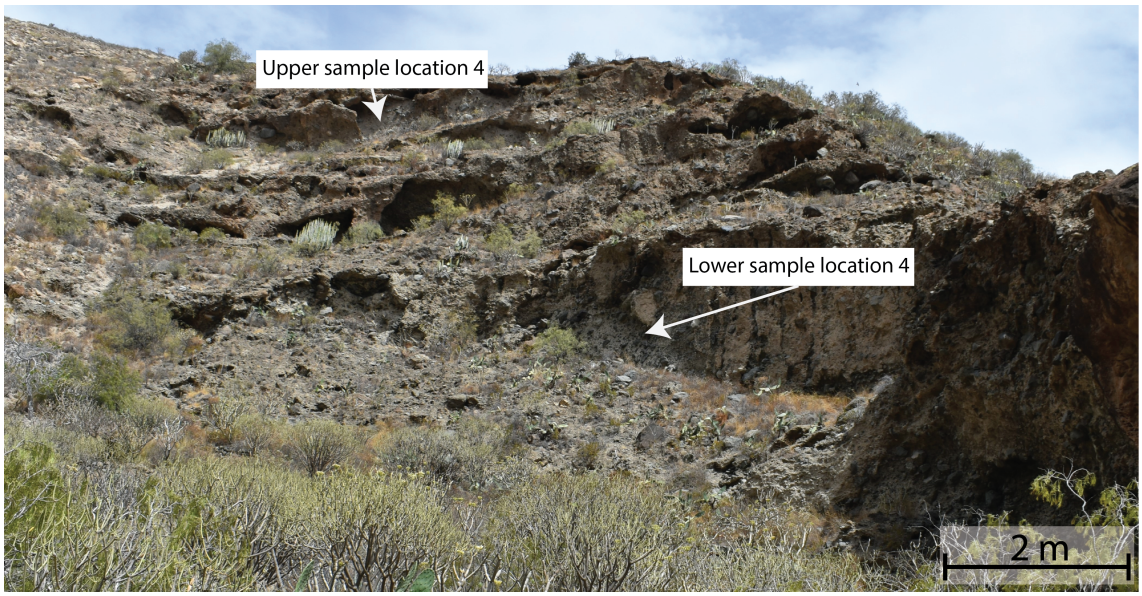

Figure D.1: At location 4 a deep ravine exposes the highest outcrop of the Abona volcanic debris avalanche. Two samples were taken here for clast-size analysis, one at the upper part and one at the lower. Their specific location is indicated.